Biochemical and Molecular Genetic Investigations of Patients with Mitochondrial DNA Disease

Mazhor S. Aldosary

Thesis submitted to Newcastle University in candidature for the degree of Doctoral of Philosophy

Mitochondrial Research Group
Institute for Ageing and Health

June 2010

Abstract

Mitochondria are organelles present in all nucleated cells and are the only location of extra-chromosomal DNA within mammalian cells. They are responsible for the generation of ATP by oxidative phosphorylation (OXPHOS). An extensive range of molecular defects have been identified in the human mitochondrial genome, many associated with well-characterised, progressive neurological syndromes. Diseases due to mutations in the mitochondrial genome (mtDNA) are clinically, genetically and biochemically diverse.

I have investigated the molecular genetic basis of mitochondrial disease in a cohort of patients with biochemical deficiencies, using a range of histochemical, biochemical, molecular genetic and cell biological techniques. Whole genome sequencing results revealed the identification of novel and recurrent pathogenic mutations in different subunits of complex I (m.11453G>A, m.11777C>A, m 13051G>A, m.13513G>A and m.14453G>A). To assign pathogenicity of these identified mutations, several approaches were carried out to distinguish between pathogenic and neutral mtDNA changes. Investigation of different tissues from patients and their relatives explored mtDNA heteroplasmy, and determined whether mutations had a risen sporadically or been maternally-inherited. *Trans*mitochondrial cybrids were established as an *in vitro* model to assess the functional consequences of the m.11777C>A mutation, revealing significant defects in these cells supporting the role of this mutation in causing disease in patient. The m.11777C>A and m.13051G>A mutations were associated with increased reactive oxygen species (ROS) production as a consequence of the effect of these mutations on complex I function. Moreover, the expression of several mitochondrial complex I subunits was differentially affected in fibroblasts from patients based on western blotting analysis.

In addition, 3 novel, pathogenic mt-tRNA mutations were identified; m.618T>G *MTTF* gene mutation, a m.12261T>C *MTTS2* gene mutation and a m.12283G>A *MTTL2* gene mutation. These mutations were shown to be pathogenic as they segregated with the biochemical defect within individual cytochrome *c* oxidase (COX)-deficient fibres. Interestingly, the m.12283G>A mutation was present at very low levels in mature muscle as compared to other mt-tRNA mutations, and exhibited an unusual pattern of segregation in single muscle fibres.

The MitoChip (V2.0) is an oligonucleotide tiling array for the resequencing of the human mitochondrial genome, which has been proposed as an alternative diagnostic screening tool given it is rapid and relatively cheap. A comparative study between conventional dideoxy Sanger sequencing and MitoChip (V2.0) analysis revealed an inability of this technology to detect single nucleotide insertion and deletion mtDNA mutations.

Author’s Declaration

This thesis is submitted to the degree of Doctoral of Philosophy at Newcastle University. The research detailed within this thesis was performed in the Mitochondrial Research Group within the Institute for Ageing and Health and is my own work unless otherwise stated. The research was carried out under the supervision of Professor Robert Taylor and Professor Douglass Turnbull between September 2006 and June 2010.

I certify that none of the material offered in this thesis has been previously submitted by me for a degree or any other qualification at this or any other University.

Acknowledgments

I would like to thank my supervisors Professor Robert Taylor and Professor Douglass Turnbull for accepting me into the Mitochondrial Research Group to pursue my PhD study and for their supervision. I would like also to thank every member in the MRG for their help and support especially Dr. Helen Tuppen for her help and support in doing experiments.

I would like to thank the staff of the NGC Diagnostic Service laboratory for their help and support with preparing and providing me with samples. Also, I would like to thank all patients and their relatives who agreed to provide me with their samples for investigations.

I would like to deeply extend my great thanks to my parents to Professor Robert Taylor and Professor Douglass Turnbull and to my entire family for their support and encouragement.

Finally, I would like to thank the administration of the Research Centre at King Faisal Hospital & Research Centre, Riyadh, Saudi Arabia for giving me this great opportunity to complete my PhD studies.

Abbreviations

ADP	Adenosine diphosphate
ATP	Adenosine-5'-triphosphate
BN-PAGE	Blue native polyacrylamide gel electrophoresis
CoA	Acetyl-coenzyme A
COX	Cytochrome *c* oxidase
Cybrids	Cytoplasmic hybrids
dNTPs	Deoxyribonucleotide triphosphates
FAD	Flavin adenine dinucleotide
H_2O_2	Hydrogen peroxide
HMSN	Hereditary motor and sensory neuropathy
HPRT	Hypoxanthine–guanine phosphoribosyltransferase
HSP	Heavy strand promoter
KSS	Kearns-Sayre syndrome
LSP	Light strand promoter
MDS	mtDNA-depletion syndrome
MnSOD	Manganese superoxide dismutase
mtDNA	Mitochondrial DNA
MTTL2	Mitochondrial $tRNA^{Leu(CUN)}$
mt-tRNA	Mitochondrial transfer RNA

NAD	Nicotine adenine dinucleotide
NCR	Non-coding region
OPA	Optic atrophy
OXPHOS	Oxidative phosphorylation
PBS	Phosphate buffered saline
PCR	Polymerase chain reaction
PGD	Preimplantation genetic diagnosis
PMP22	Peripheral myelin protein 22 gene
PNAs	Peptide nucleic acids
Polg	polymerase-γ
rCRS	revised Cambridge Reference Sequence
RFLP	Restriction Fragment Length Polymorphism
RITOLS	Ribonucleotide Incorporation Throughout the Lagging Strand
ROS	Reactive oxygen species
SDH	Succinate dehydrogenase
TIM	Translocase of the Inner Membrane
TK2	Thymidine Kinase 2 gene
TOM	Translocase of the Outer Membrane

Contents

List of Figures

List of Tables

Chapter 1

Introduction and review of the literature

Chapter 1 : Introduction and review of the literature

This chapter will present an introduction and review of the literature for mammalian mitochondria unless otherwise stated.

1.1 Origin of mitochondria

Mitochondria are ubiquitous cellular organelles present in all nucleated human cells and they are the only location of extra-chromosomal DNA within mammalian cells [1]. The prokaryotic character of the mitochondria suggests that they evolved from bacteria long time ago [2]. According to the endosymbiont hypothesis, eukaryotic cells started out as anaerobic organisms without mitochondria or chloroplasts and then established a stable endosymbiotic relationship with bacteria, which have their own oxidative phosphorylation system [3-5]. Sequence similarity suggests that mitochondria may have descended from a particular type of purple photosynthetic bacterium that had previously lost its ability to perform photosynthesis but had a respiratory chain [2, 3].

Hydrogenosomes and mitosomes are mitochondria-like organelles of eukaryotic organisms originated through endosymbiotic relationship with bacteria [6-8] long time ago [9]. They have some features similar to mitochondria such as the double membrane and pathway of proteins import [10]. However, they lacked mitochondrial DNA [11-14].

1.2 Mitochondrial morphology and structure

Human mitochondria have no fixed size, but typically in hepatocytes and fibroblasts they have a sausage-like shape with dimensions of 3-4μm in length and ~1μm in diameter. The number of mitochondria is different in each cell type and tissues according to the metabolic requirements, so it may range from a single large mitochondrion to thousands of organelles [15]. For example, there are ~800 mitochondria per hepatocyte [16], >100,000 mitochondria in oocytes [17], but only a few in spermatozoa [18].

Mitochondria are found in the cytoplasm of all nucleated mammalian cells [19]. Each mitochondrion contains an inner membrane, outer membrane and matrix (Figure 1-1). The two membranes separate the mitochondrion into two parts: the internal matrix and the intermembrane space [20]. The outer membrane contains many copies of a transport protein named porin, which forms channels through the lipid bilayer [21]. This membrane

functions as a sieve that allows entrance and exit of molecules of 5000 Daltons or less [20, 22, 23]. The inner membrane, which surrounds the matrix, is highly specialized [23]. It is composed of a lipid bilayer with a high proportion of the phospholipid cardiolipin [24, 25], which contains four fatty acids [26] instead of two and may help to make the membrane especially impermeable to ions [27]. In addition, this membrane contains different transport proteins, which make it selectively permeable to small molecules [23, 28] that are metabolised or required by the matrix enzymes. These enzymes include enzymes that metabolize pyruvate and fatty acids to produce acetyl CoA as well as enzyme that oxidise acetyl CoA in the Krebs' cycle. In addition, all enzymes required for respiratory chain reactions are embedded in this membrane [22, 29-32].

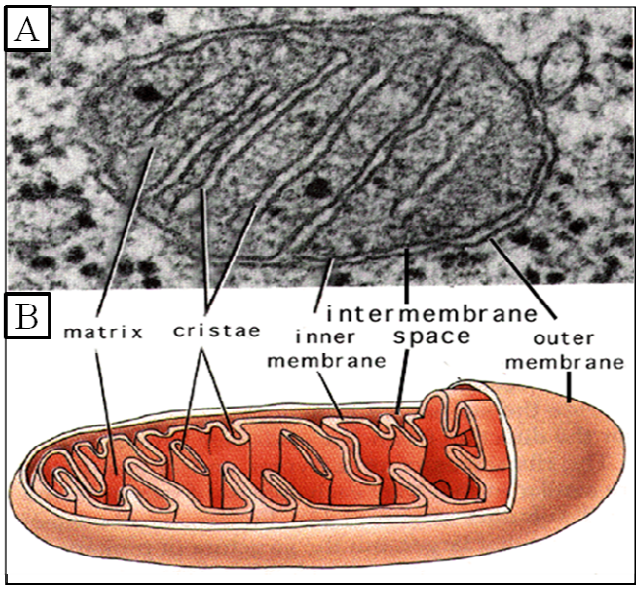

Figure 1-1 The general organisation of a mitochondrion.

Electron microscope image (A) and schematic representation (B) showing the general structure of mitochondria: outer membrane, intermembrane space, inner membrane, cristae, and matrix (taken from http://academic.brooklyn.cuny.edu/biology/bio4fv/page/mito.gif).

In addition to the above, the inner membrane is usually found in a highly convoluted form creating a series of infoldings known as cristae which project into the matrix to increase the surface area of the inner membrane [33]. The number of cristae differs from one mitochondrion to another and may depend on the cellular demand for ATP. For example, the number of cristae is high in the mitochondrion of heart muscle cell [15, 34]. The matrix is a large internal space that contains a mixture of hundreds of enzymes required for oxidation of pyruvate and fatty acids and for the citric acid cycle [35]. It also contains the

mitochondrial DNA, mitochondrial ribosomes, mitochondrial tRNAs, and further proteins required for the expression of mitochondrial genes such as polymerase γ [36].

Moreover, mitochondria are dynamic organelles with dynamic network (Figure 1-2) [37, 38]. The balance between fusion and fission events, which are mediated by specific proteins [39, 40], controls the shape of mitochondria [41] (more details in section 1.16).

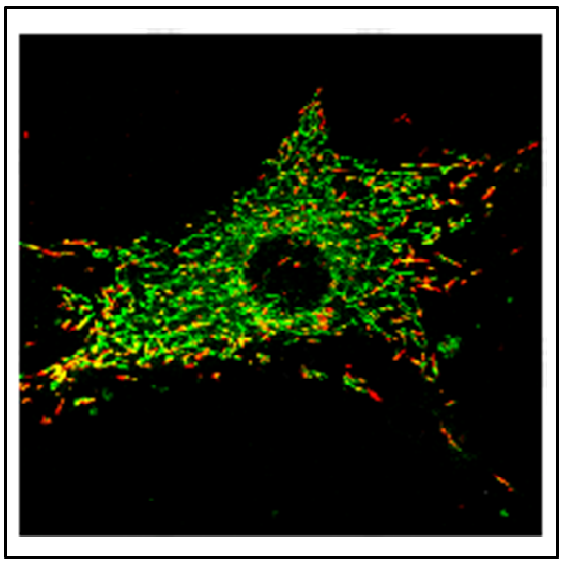

Figure 1-2 The dynamic mitochondrial network.

A 2D image of JC1-stained NIH 3T3 cell (mice fibroblasts), that was excited with the 488 nm line of an Argon laser, shows the mitochondrial network organisation a complex in contact with other cell compartments such as nucleus (black circle in the centre). JC1 undergoes a reversible change in fluorescence emission from green to red as mitochondrial membrane potential increases. Red and green fluorescence emissions were separately recorded and merged (taken from http://www.med.unipg.it/imagelab/mitoch.html).

1.3 Functions of mitochondria

Mitochondria are the main site for ATP generation within most tissues by oxidative phosphorylation (OXPHOS). Without mitochondria, cells would be dependent on anaerobic glycolysis for all of their adenosine triphosphate (ATP) [1, 38]. In addition, mitochondria participate in other cellular activities including intracellular Ca^{2+} regulation, thermogenesis and control of apoptosis. Mitochondria are also the primary site of reactive oxygen species (ROS) production [42]. Functions will be discussed more below.

1.3.1 Mitochondria and thermogenesis

Newborn, cold adapted and hibernating mammals may have the ability to maintain their body temperature in a manner independent of shivering, but secondary to an adrenergic stimulated increase in respiration [43]. This promotes an increase in blood flow to brown adipose tissue which is responsible for non-shivering thermogenesis [44]. Mitochondria within brown adipose tissue behave differently than those in other tissues in terms of limited ATP synthesis, reduced membrane potential and increased rates of respiration [45, 46]. This suggests that inner membranes in these mitochondria have a higher rate of proton permeability. The increase in permeability to protons allows part of the energy stored as membrane potential, generated by the mitochondrial respiratory chain, to be released in the form of heat when protons return to the mitochondrial matrix.

1.3.2 Mitochondria and Ca^{2+} homeostasis

Cytosolic Ca^{2+} levels are maintained at concentrations approximately 10,000 times lower than the Ca^{2+} concentrations in the extracellular medium [47, 48]. This process is controlled mainly by the plasma membrane, endoplasmic reticulum Ca^{2+} ATPases, and by Ca^{2+} exchanges in a process that requires energy. Mitochondria themselves are responsible for providing such energy. They provide cations through the membrane potential to drive the force for Ca^{2+} uptake. For Ca^{2+} efflux, they have a Ca^{2+} release system composed of two transporters: the $Ca^{2+}/2H^{+}$ exchange and the $Ca^{2+}/2Na^{+}$ exchange [42].

1.3.3 Mitochondria and generation of ROS

Under normal conditions, the mitochondrial respiratory chain produces reactive oxygen species as by-products of electron transport [49] . These radicals in the form of either superoxide or hydroxyl radicals are thought to be produced by interaction of molecular oxygen with semi-quinone or -flavone species resulting from transient one electron transfer reactions with the respiratory chain complexes [50, 51]. Because of the antioxidant systems within mitochondria, ROS are removed [52] and do not cause any permanent damage to mitochondria. However, under non-physiological conditions or due to vicious cycles, mitochondrial ROS may lead to both mitochondrial and cellular damage [42]. Both respiratory complexes I and III in mitochondria are the major sources of superoxide and H_2O_2 in mitochondria [53-55]. However, it has been reported that complex I produces most of the ROS generated in intact mammalian mitochondria *in vitro* [56-58] suggesting that

ROS generation by complex III is of limited physiological importance [59, 60]. However, the exact sites for ROS production within complex I *in vivo* or in intact cells are still not fully determined [61]. *In vitro* studies from isolated complex I suggested that the reduced flavin is the source of ROS production [62]. In addition, both NADH and quinone-binding sites are thought to be sites for ROS production within complex I in *Thermus thermophilus* [62].

1.3.4 Mitochondria and apoptosis

Mitochondria play an important role in the regulation of cell death. Two mitochondrial intermembrane-space proteins, cytochrome *c* and the apoptosis inducing factor (AIF), have been shown to migrate from a mitochondrial to a cytosolic location shortly before apoptosis [63, 64]. In addition, mitochondria contain pro-caspase 9, pro-caspase 3 and pro-caspase 2 [65, 66], which initiate the apoptotic cascade. The Bcl-2 family proteins are known to be involved in both anti- and pro-apoptotic activities [42]. Also Smac/DIABLO was identified as a mitochondria-derived pro-apoptotic factor [67]. In addition, other mitochondrial proteins were identified to be involved in apoptosis regulation such as Omi/HtrA2 and EndoG [68].

1.4 Mitochondrial oxidative phosphorylation and respiratory chain

Oxidative phosphorylation (OXPHOS) is so named because this process donates the removal of hydrogen ions from one molecule and gives phosphate molecules to another molecule. Embedded in the inner membranes of the mitochondria are proteins and complexes of molecules that are involved in this process (Figure 1-3). Hydrogen ions or electrons are donated to the two carriers nicotine adenine dinucleotide (NAD) and flavin adenine dinucleotide (FAD) in the Kreb`s cycle. Reduced NAD, NADH, carries energy to complex I and reduced FAD, FADH, carries energy to complex II. As these hydrogens are transferred from one complex to another, the hydrogen protons separate from their electrons and protons are pumped out. NADH binds to complex I through a prosthetic group called flavin mononucleotide (FMN) and is immediately reduced to NAD, which can be recycled, thereby acting as an energy carrier. Upon binding, FMN receives the hydrogen from the NADH and two electrons and also picks up a proton from the matrix. FMN passes the electrons to iron-sulphur clusters, which are part of complex I and also

pumps two protons into the intermembrane space. Electrons cannot travel from complex I without concomitant proton translocation, the two events, must happen together or not at all. Electrons pass from complex I to a carrier, Coenzyme Q, which passes the electrons to complex III, which is associated with another proton translocation event. From complex III, electrons are passed to complex IV through cytochrome *c* and more protons are translocated into the intermembrane space. Finally, complex IV passes two electrons to an oxygen molecule the last electron acceptor within the respiratory chain.

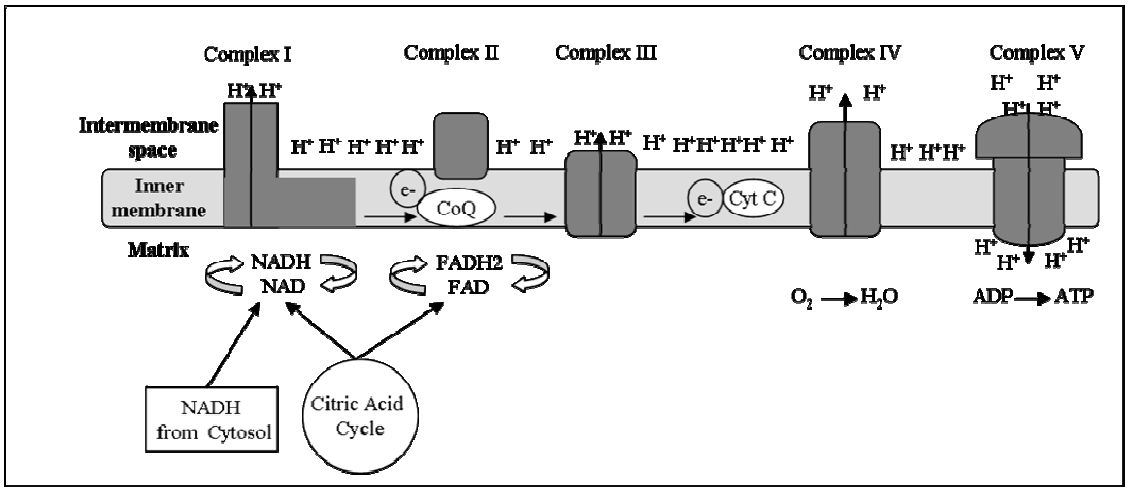

Figure 1-3 Electron transport and oxidative phosphorylation.

The electron transport chain in the mitochondrion is the site of oxidative phosphorylation. The NADH and FADH2, which are generated from citric acid cycle, are oxidized to initiate electron transport through respiratory chain complexes (I-IV). NADH binds to complex I and FADH2 binds to complex II. Electrons pass from complex I to complex III through Coenzyme Q and from complex III to complex IV through cytochrome *c*. Complex IV passes two electrons to oxygen, which is the last electron acceptor within the respiratory chain. During electrons transport more protons are translocated into the intermembrane space generating an electrochemical gradient across the inner membrane. This drives pumping of protons in the matrix through the ATP synthase complex (complex V) and initiates the energy production by phosphorylating ADP molecules to become ATP.

Proton translocation during electron transfer along the respiratory chain generates an electrochemical gradient across the inner membrane which becomes polarized and has ~180mV with negative polarity on the matrix side. As a result, this drives the pumping of protons in the intermembrane space through the ATP synthase (F_oF_1 complex) and initiates the energy production by phosphorylating ADP molecules to become ATP. Finally, the electrons reunite with protons to form hydrogen and the chemical union of the hydrogen and oxygen produces water. The energy carried by ATP is then used for all cellular functions like movement, transport, entry and exit of molecules out of the cytoplasm, and

cell division. Thus, oxygen is the final acceptor in the electron transport system which explains why organisms which respire aerobically. In the absence of oxygen four molecules of ATP energy are produced for each glucose molecule, however, the presence of oxygen makes the Kreb's cycle running to produce many more hydrogen ions which drive the ATP pump and eventually produces 24-28 ATP molecules. In addition, absence of oxygen,which accepts electrons, results in the accumulation of electrons in the respiratory chain complexes therefore blocking ATP production [69].Furthermore, a defect in one or more of these complexes changes the oxidation rate of NADH to NAD (or FADH2 to FAD), which results in an increase in NADH and a decrease in NAD levels. The increased NADH/NAD levels inhibit the conversion of pyruvate to acetyl-CoA leading to an increase in pyruvate levels in both mitochondria and the cytosol. The accumulated pyruvate in the cytosol is metabolized into lactate or converted to alanine. The final result of a complex I deficiency is an intracellular increase of lactate, pyruvate, and alanine as well in the body fluids: blood, urine and in cerebrospinal fluid (CSF) [70].

1.5 Respiratory chain complexes

Mitochondria are the main site for energy production in eukaryotic cells [71]. Within the inner mitochondrial membrane there are five complexes are essential for electron transport and energy transduction. These complexes are: NADH–ubiquinone oxidoreductase (complex I), succinate–ubiquinone oxidoreductase (complex II), ubiquinol–cytochrome *c* oxidoreductase (cytochrome bc_1 complex or complex III), cytochrome *c* oxidoreductase (complex IV), and F_1F_0–ATP synthase (complex V) [71]. Some of these complexes were found to interact with each other to form supercomplexes [71, 72] (more details in section 1.7).

1.5.1 Complex I (NADH: ubiquinone oxidoreductase)

The mammalian complex I is the largest and least understood component of the respiratory chain. It consists of at least 45 different subunits (Figure 1.4) that assemble together into a structure of ~1 MDa [72, 73]. Seven subunits out of the 45 are encoded by the mitochondrial DNA and the other 38 subunits are encoded by nuclear genes, which are imported into the mitochondria after translation. In addition, it initiates the first step in the mitochondrial respiratory chain through the oxidation of NADH as described above.

Despite the availability of the crystal structures for the other OXPHOS complexes, only low resolution 3D structures of complex I are available [74-76]. Electron microscopy revealed that the 45 subunits within complex I assemble together to form an L-shaped [77] structure with a hydrophilic peripheral arm and a hydrophobic membrane-embedded arm (Figure 1-4). Studies from *E. coli* showed that complex I is maintained in a native lipid bilayer as an active enzyme [78]. However, the recent identification of the atomic structure of the hydrophilic peripheral arm of complex I from the thermophilic bacterium *Thermus thermophilus* using X-ray crystallography provided the best current model for mitochondrial complex I structure [79, 80].

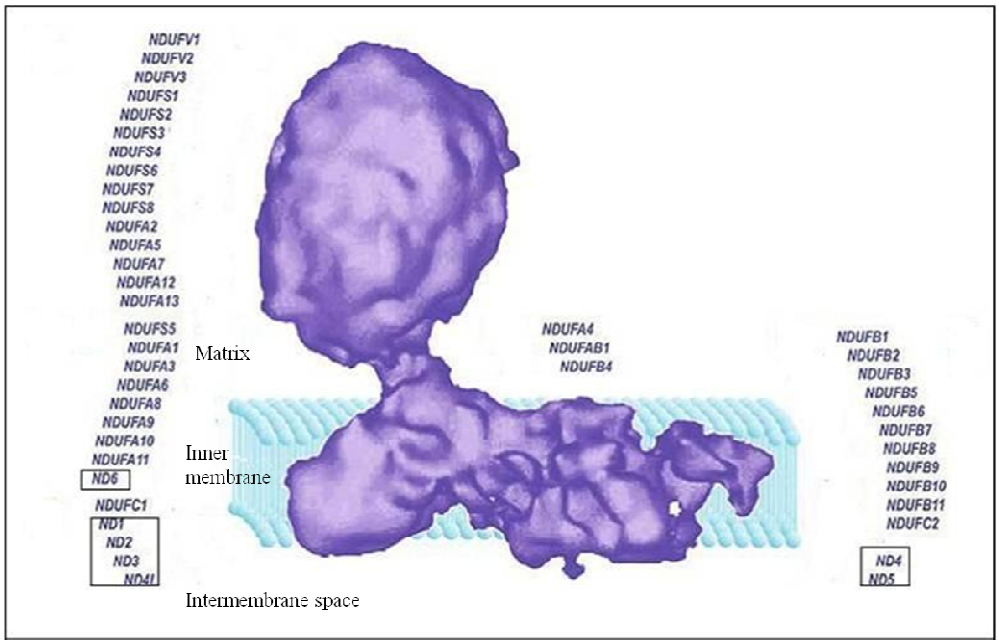

Figure 1-4 Schematic structure showing subunit composition of human complex I.

The mammalian complex I has an L-shaped structure with two arms, a peripheral arm towards the matrix and membrane-embedded arm. The highlighted boxes are the seven mitochondrial encoded subunits of complex I (ND1-6 and ND4L) and the rest are the nuclear encoded subunits (taken and modified from [82]).

The seven mitochondrially encoded subunits of complex I are ND1-6 and ND4L. They are all hydrophobic and in association with ~ 20 other integral membrane proteins they form the membrane arm of the enzyme [81]. Because ND1 has a quinine binding site, it is proposed to be involved in ubiquinone binding [82] as well ND6 [83]. Sequence similarity between ND2, ND4, ND5 and other antiporters subunits such as K+ or Na+/H+ suggests these subunits may be part of the proton translocation machinery [84]. In addition, ND4 and ND5 may also have ubiquinone binding sites [85]. Finally, the ND3 subunit is thought to be involved in proton translocation [83].

1.5.1.1 Assembly of complex I

Although complex I is composed of ~ 45 subunits, which assemble together to form the whole complex. It was reported that nuclear DNA-encoded subunits can integrate rapidly into complex I while mtDNA-encoded subunits first assemble into intermediate complexes that require significant time for their integration into the holoenzyme [86, 87]. The current model for the assembly in mammalian mitochondria is best described by Lazarou *et al*. [72] (Figure 1-5). This model shows the assembly via dynamic cycling between intermediates and fully assembled complex I; however, the exact order of subassembly integration is still not fully understood.

The first step in assembly starts with the subassembly of subunits NDUFS2 and NDUFS7 which is one of the first complex I assembly intermediates formed and additionally contains subunits NDUFS3 and NDUFS8 [88-90].

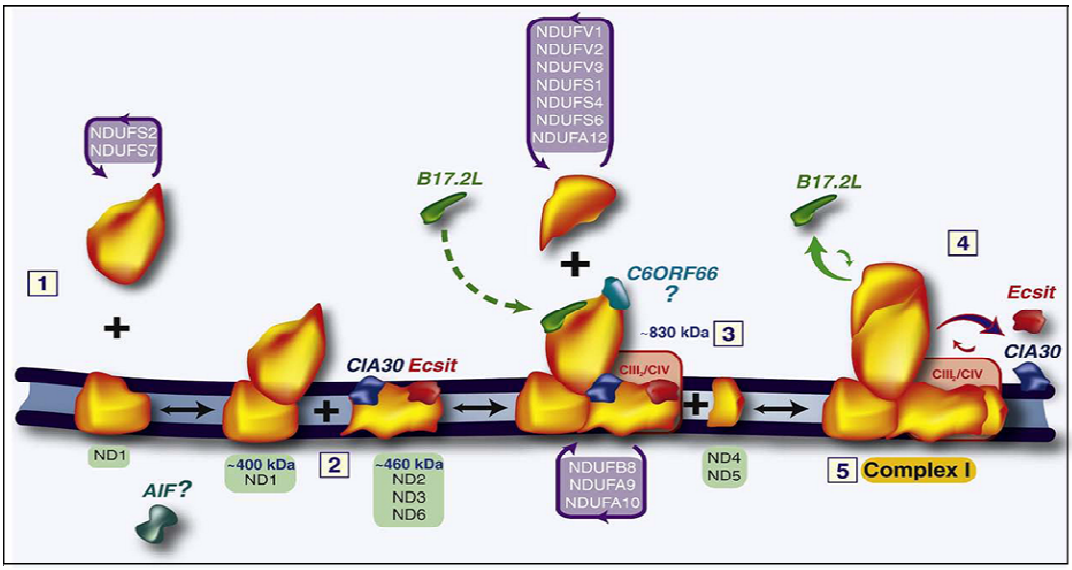

Figure 1-5 Model of human complex I assembly.

Step **1** of complex I assembly involves subassembly of NDUFS2 and NDUFS7 which anchored to the membrane by ND1 and other subunits forming ~ 400 kDa. In step **2**, CIA30, Ecsit, ND2, ND3 and ND6 are assembled forming a ~460 kDa subcomplex. Step **3** involves the combination between the previously formed ~400 kDa and ~460 kDa intermediates to form a stable~830 kDa intermediate that is associated with B17.2L, C6ORF66, complexes III and IV, and other nuclear-encoded subunits. Step **4** involves the addition of other nuclear-encoded subunits, ND4 and ND5. In the last step (**5**), assembly of subunits into the matrix arm of complex I results in the release of CIA30/Ecsit and B17.2L forming the holoenzyme. (Taken from [72]).

Then, the mtDNA-encoded subunit ND1, possibly in conjunction with other subunits, may anchor the subassembly to the inner membrane forming an ~400 kDa intermediate [86].

Secondly, a membrane subcomplex, which contains ND2, ND3 and ND6 (as well as other subunits), is assembled to form a separate ~460 kDa subcomplex via CIA30 [91] in conjunction with Ecsit. Third, the membrane arm intermediates come together to form an ~830 kDa intermediate that is associated with B17.2L and perhaps C6ORF66 then complexes III and IV combine with a complex I intermediate to form a supercomplex. Additionally, subunits such as NDUFA9, NDUFA10 and NDUFB8 are added to the ~830 kDa [86, 92]. Subsequently, the 'cap', which consists of subunits NDUFV1, NDUFV2, NDUFV3, NDUFS1, NDUFS4, NDUFS6 and other subunits, is added to the complex in addition to ND4 and ND5 subunits [86, 91]. Finally, the assembly of subunits into the matrix arm of complex I is associated with the release of CIA30/Ecsit and B17.2L forming the holoenzyme.

1.5.2 Complex II (succinate-ubiquinone oxidoreductase)

Complex II is the simplest complex of all electron transport chain (ETC) complexes since in vertebrates and many bacteria it contains only four subunits [93]: a matrix-exposed FAD-containing subunit that oxidizes succinate to fumarate and an iron-sulfur-containing subunit that is also largely exposed to the matrix, also two integral membrane subunits which provide the binding site, a b-type cytochrome and the quinone-reducing site of the enzyme [94]. This complex is known to be entirely encoded by the nuclear genome and functions to link the Kreb's cycle with the respiratory chain [95-97]. However, this complex does not pump protons across the inner membrane [98].

1.5.3 Complex III (cytochrome *c* reductase)

Complex III is composed of 11 subunits in mammals: 10 subunits are encoded by the nuclear genome, and only one subunit is encoded by the mitochondrial genome which is cytochrome *b*. The most important subunits of this complex are: cytochrome *b*, cytochrome *c1* and the Rieske iron-sulfur protein since they are all involved in electron transport. In addition, this complex contains two reaction centers for ubiquinone, Q_N and Q_P, which are required for proton pumping through Q cycle mechanism to generate a proton gradient and membrane potential for ATP synthesis (Figure 1-6). The Q_N or quinone reduction centre, located on the matrix side of the inner membrane, is involved in the recycling of half of the electrons back into the quinine pool and the uptake of proton from the matrix. The Q_P center, which is located near the outer face of the inner membrane, accepts electrons from

reduced ubiquinone and half of them are recycled and the others are transferred through the iron-sulfur center and cyt c_1 to cytochrome *c*. Thereby, protons are released in the intermembrane space [93].

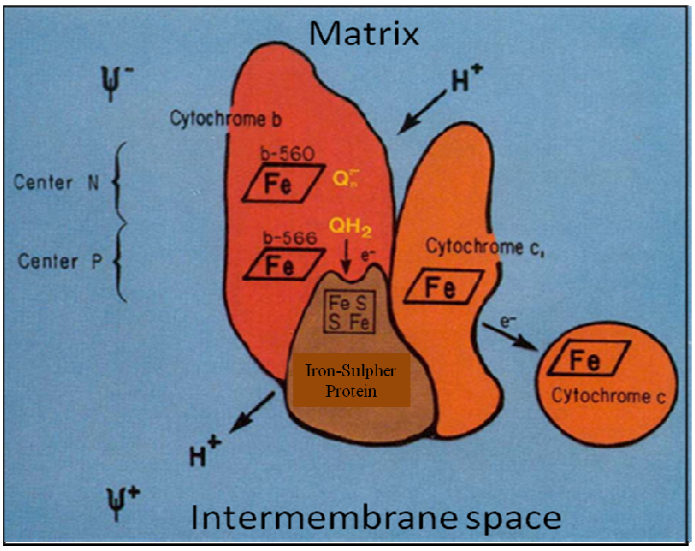

Figure 1-6 The structure of complex III and electrons transfer through the Q cycle.

Complex III is composed of cytochrome *c1* and iron-sulpuur protein, which are located on one side of the membrane. Cvtochrome *b*, with the *b*-566 heme and the *b*-560 heme, is located on the other side of the membrane. The ubiquinol (QH_2) oxidation site, center P, is between the iron-sulphur protein and cytochrome *b*. Q^-_n at centre N is a stable semiqumone radical where cytochrome *b* reduces ubiquinone to ubisemiquinone and ubisemiquinone to utnqumol. Proton uptake and release takes place at centres N and P and electron transfer from cytochrome *c1* to cytochrome *c* (taken and modified from [99]).

1.5.4 Complex IV (cytochrome *c* oxidase)

Complex IV is the final enzyme of the electron transport chain and belongs to the family of heme copper enzymes [100]. It catalyses the four-electron reduction of oxygen to water [101]. Mammalian cytochrome *c* oxidase (COX) is composed of 13 subunits: three large subunits are encoded by the mitochondrial genome, Cox1, Cox2 and Cox3, and all other subunits are encoded by the nuclear genome [102, 103] (Figure 1-7). The Cox1 subunit coordinates heme α and a fused binuclear heme α3-CuB redox center and ligates a sodium ion by a site that also possesses affinity for Ca^{2+} ions [104-106]. In addition, it is the most important subunit both for assembly and function of COX and is involved in proton pumping [100]. Cox2 is the smallest subunit with two transmembrane domains and its function is to dock cytochrome *c* via the CuA center [102]. Cox2 is also involved in the binding of heme α3 in association with Cox1p in humans [107]. The Cox3 subunit is

involved in the folding, action and/or stability of COX [108, 109] but not in proton translocation [102, 110, 111]. The nuclear encoded subunits are involved in the catalytic function of COX in addition to formation of the enzyme [100].

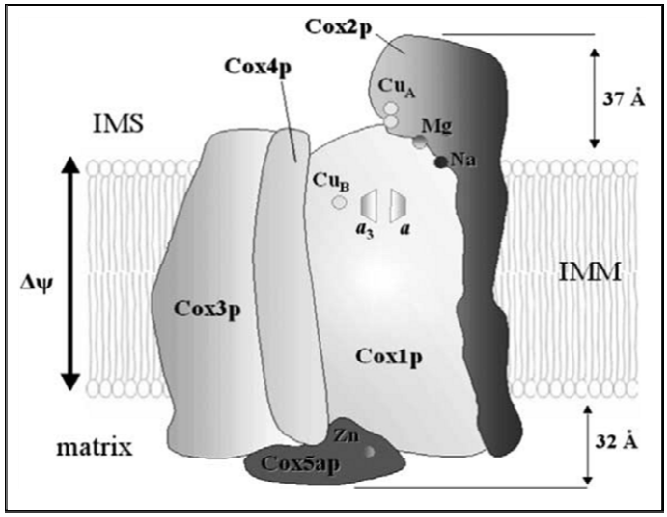

Figure 1-7 A schematic representation of mammalian COX.

This figure shows only the three largest mitochondrial-encoded subunits of COX (Cox1p, Cox2p and Cox3p) and other nuclear- encoded subunits, which are involved in early assembly steps of the enzyme. IMS: inner membrane space (taken from [100]).

1.5.6 Complex V (ATP synthase)

Mammalian complex V is composed of 16 different subunits, two of which are encoded by the mitochondrial genome (subunits 6 and 8) while the rest are encoded by the nuclear genome [112]. Together these subunits form two opposing rotary motors [113]. The F1 motor is composed of the subunits (α3β3γδε) and catalyses ATP synthesis or hydrolysis by a rotary mechanism. The F0 motor catalyses ion translocation across the membrane that is coupled to rotation of the c ring versus the stator subunits α and b2. Both motors are connected by two stalks, a central one containing the γ- and ε-subunits and a peripheral one involving the δ- and b-subunits (Figure 1-8) [113]. The function of this complex is to use the transmembrane proton motive force generated by the electron transport chain to drive the synthesis of ATP from ADP and inorganic phosphate. This is achieved by the flow of protons through the peripheral and central stalks which initiates the c-subunit of F0 to rotate and the energy produced by this rotation is used by F1 to drive ATP synthesis. Each molecule of ATP requires three protons to initiate ATP production, one proton for each active site [114]. In addition, the rotation of the central stalk, which proceeds through 120°, changes the through cycles of ‘open’, ‘loose’ and ‘tight’ states. Three 120° steps in a 360°

cycle take each subunit through all three states, and three molecules of ATP are produced [115, 116].

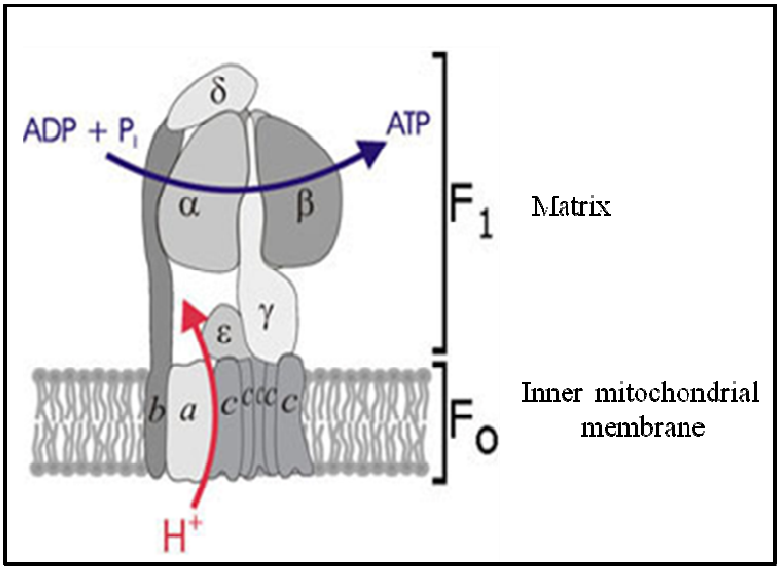

Figure 1-8 Schematic representation of the structure of complex V.

The mammalian complex V is composed of 16 subunits, which assemble together to form the F1F0 ATPase complex. The F1 motor, which catalyses ATP synthesis or hydrolysis, is composed of the subunits (α3β3γδε) and located in the matrix side. The F0 motor, which catalyses ion translocation across the membrane, is composed of c subunits embedded in the inner membrane. Both motors are connected by two stalks, a central one containing the γ- and ε-subunits and a peripheral one involving the δ- and b-subunits. Protons (H^+) pumping intiates the rotation of the two motors in an opposing direction resulting in the production of ATP from ADP and inorganic phosphate (taken from http://www.atpsynthase.info/images/ATP_synthesis1.jpg).

1.6 Control of the OXPHOS

The permeability of the outer mitochondrial membrane and the inner mitochondrial membrane allows entrance of metabolites, such as ADP and ATP. Adenine nucleotide translocase (ANT) has been reported to be involved in the exchange of ADP and ATP on the inner mitochondrial membrane [117]. Generally, the OXPHOS is controlled by two events, the state III and state IV respiration. When concentrations of ADP in the matrix are high and oxygen is consumed by the electron transport chain, ATP is synthesised to restore the electrochemical gradients, this is known as state III respiration. Export of the newly synthesised ATP from the matrix to cytoplasm is coupled with the import of ADP and inorganic phosphate from the cytoplasm into the matrix. However, when the matrix ADP concentrations are low, oxygen consumption is reduced to maintain electrochemical gradients; this is known as state IV respiration. The ratio of state III respiration (maximum

respiration) to state IV respiration (lower respiration) is known as the respiratory control ratio, which indicates the tightness of the coupling between respiration and phosphorylation [15, 118, 119].

1.7 Supercomplexes structure

The respiratory chain complexes as described (section 1.4) were initially identified as random complexes within the inner mitochondrial membrane, with electrons moving between them via the electrons carriers. This model is known as the fluid model [120]. However, other studies have since described another model known as solid model, in which complexes were found to interact and organize into supercomplexes or respirasomes [71, 120-122]. The respirasomes in mammals are found in two forms: the complete respirasome containing complexes I, II and IV in a ratio of 1:2:4 and a second form containing complex III and complex IV in a 2:4 ratio [72]. Complex II was found as a monomer and complex V as a dimer [31, 122]. More recently, the existence of such supercomplexes is thought to have important functional consequences [72]. The use of electron shuttling molecules, such as ubiquinol and cytochrome *c* may not be required [72]. Also, catalytic activity may be enhanced due to reduced diffusion times of substrates [72]. Moreover, the production of damaging molecules such as superoxides [123, 124] may be limited. In addition, the presence of such supercomplexes has shown to be essential for complex I assembly and stability [72, 124].

1.8 Mitochondrial genetics

Each nucleated mammalian cell contains several hundreds to more than a thousand mitochondria and each mitochondrion harbors 2-10 copies of mtDNA. Mitochondrial size, shape and abundance is different in different cell types and may change due to the degree of energy demand and different physiological or environmental conditions [125]. The number of mitochondria within a cell is determined by the biogenesis and division of the mitochondria through the activation of specific transcription factors and signaling pathways [126, 127]. Mitochondria are genetically controlled by both nuclear DNA and the mitochondrial genome [1].

The mitochondrial genome is a multicopy, double-stranded circular DNA molecule, which is 16.6 kb in human. This genome encodes 13 essential proteins for the OXPHOS system

and 24 components of the RNA machinery: 2 rRNAs and 22 tRNAs. MtDNA is intronless and the only non-coding region is the displacement region (D-Loop), a region of 1.1 kb. It contains both the replication origins and the transcriptional promoters (Figure 1-9) [1, 128]. The 13 proteins include seven subunits of NADH dehydrogenase (complex I: ND1, ND2, ND3, ND4, ND4L, ND5and ND6), cytochrome *b* (subunit of complex III), three subunits of cytochrome *c* oxidase or complex IV (COI, COII and COIII) and two subunits of F_0F_1 ATPase (ATPase 6 and ATPase 8); all are encoded by mtDNA and synthesized in the organelle [125, 126]. Complex II or succinate dehydrogenase is entirely encoded by the nuclear genome, as are the remaining subunits of complexes I, III, IV and V. These nuclear encoded proteins are synthesized on cytosolic ribosomes and subsequently transported into the mitochondria [102, 129].

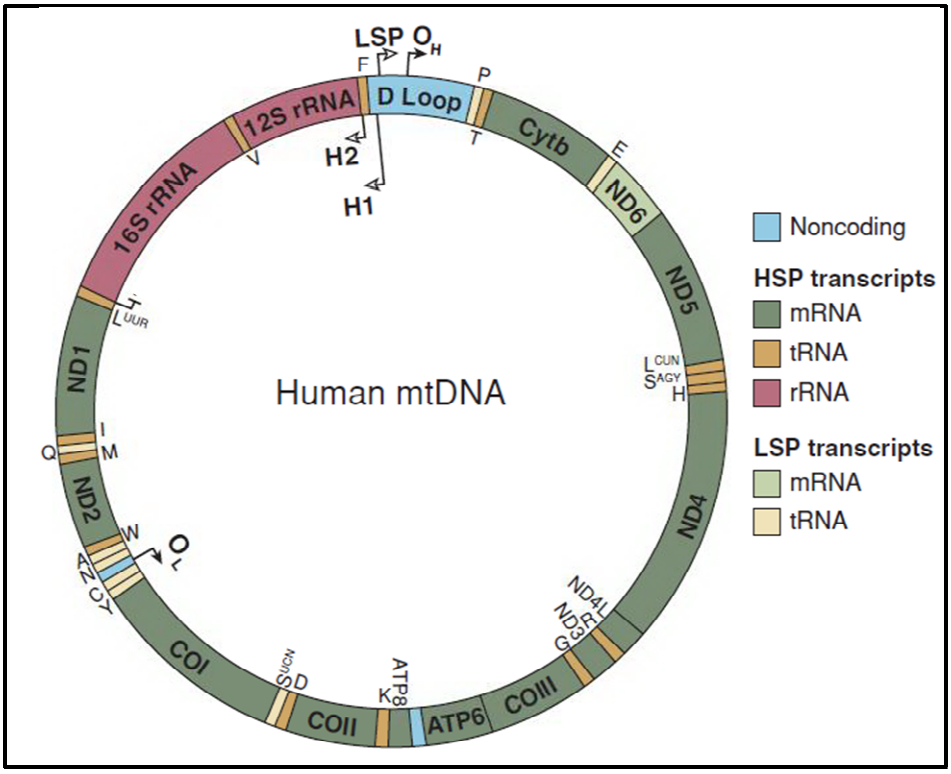

Figure 1-9 The human mitochondrial genome.

The 37 genes entirely encoded by the mitochondrial genome are: the 7 subunits of complex 1 (ND1-6 and ND4L), cytochrome *b* of complex III, the 3 subunits of complex IV (COXI-III), 2 rRNAs (12S and 16S), 2 ATPases (6 and 8), and the tRNA genes, which are denoted by the single letter code of the amino acid they encode. D-loop is the displacement loop or non-coding control region, OH is the origin of heavy-strand replication and OL is the origin of light-strand replication. LSP is the light-strand promoter, H1 and H2 are the heavy-strand promoters (taken from [128]).

Mitochondrial genetics differ from Mendelian genetics in almost every aspect: genome size, number of DNA molecules per cell, number of encoded genes, gene density, lack of introns, mode of inheritance, replication, transcription, and recombination as compared and summarized in Table 1-1.

Table 1-1 Differences between the human mtDNA and nuclear DNA.

Characteristic	**Nuclear genome**	**Mitochondrial genome**
Size	~3.3 x 10^9 bp	16.569 bp
Number of DNA molecules per cell	23 in haploid cells, 46 in diploid cells	Multicopy
Number of encoded genes	~20,000-30,000	37 (13 polypeptides, 22 tRNAs and 2 rRNAs)
Gene density	~1 per 40,000 bp	1 per 450 bp
Introns	In most genes	Absent
Percentage of coding DNA	~3%	~93%
Codon usage	The universal genetic code	AUA codes for methionine, UGA codes for tryptophan instead of termination. AGA and AGG contribute to a −1 frameshift but are not stop codons [130].
Associated proteins	Nucleosome-associated histone proteins and non-histone proteins	No histones; but associated with several proteins (e.g.TFAM) which form nucleoids
Mode of inheritance	Mendelian inheritance for autosomes and the X chromosome; paternal inheritance for the Y chromosome	Only maternal
Replication	Strand-coupled mechanism that uses DNA polymerases α and δ	Strand-coupled and strand-displacement models; only uses DNA polymerase γ
Transcription	Most genes are transcribed individually	All genes on both strands are transcribed as large polycistrons
Recombination	Each pair of homologues recombines during the prophase of meiosis	There is evidence that recombination occurs at a cellular level but little evidence that it occurs at a molecular level

(Modified from Taylor & Turnbull 2005).

1.9 Mitochondrial DNA Replication

The mechanism of mtDNA replication is still not clearly determined since four models of replication have been described. In the first model, mtDNA is replicated from two origins the H-strand (O_H) and the L-strand (O_L). DNA replication is initiated at O_H using an RNA primer generated from the L-strand transcript. Then the H-strand synthesis proceeds two-third of the way around the mt-DNA and displaces the parental H-strand until it reaches the L-strand origin (O_L). This displacement exposes the O_L to allow the accumulation of the transcription machinery to initiate synthesis of the L-strand which proceeds in the opposite direction along the H-strand template (Figure 1-9). Thus, mtDNA replication is bidirectional but asynchronous [131-133].

The second model indicates that the bidirectional replication is initiated at multiple sites across the D-Loop region, which includes the genes for cytochrome *b*, *ND5*, and *ND6*. This bidirectional replication initiation is followed by a subsequent fork arrest near the OH then replication is restricted to one direction only [134, 135].

The third model contradicts the previous models, which described bidirectional and asymmetric mechanisms. In this conventional model, mtDNA replication is initiated at a specific position in the D-Loop (O_H) and the nascent chains starting at this origin do not terminate prematurely at the terminus of the D-Loop but continue along the mtDNA template. This origin is thought to be responsible for mtDNA maintenance under steady-state conditions [136].

Recently, the RITOLS replication model was described which is similar to the strand-asynchronous model of replication but initiation is unidirectional and occurs in the non-coding region (NCR). This model involves the recruitment of RNA on the displaced H-strand rather than the mitochondrial single stranded DNA-binding protein (mt-SSB) thus forming Ribonucleotide Incorporation ThroughOut the Lagging Strand (RITOLS) intermediates [137, 138].

Regardless of the exact mechanism involved in mt-DNA replication, mtDNA replication is achieved by nuclear-encoded factors [139] such as polymerase γ, which consists of a catalytic subunit that has proof reading ability (*POLG1*) and another processing subunit (POLG2) [36], Twinkle [140] and the mitochondrial single stranded DNA-binding protein

(mt-SSB) [139, 141]. All these proteins are associated together with the mtDNA to form mtDNA-protein complexes known as nucleoids, which are believed to be involved in mtDNA transmission, inheritance [1, 142], replication/translation, maintenance, repair, and recombination [143].

1.10 Mitochondrial DNA transcription

MtDNA transcription is initiated from three promoters in the D-Loop, the heavy strand promoter (HSP) and the light strand promoter (LSP) (Figure 1-9) [144].The heavy strand transcript begins first from the HSP and then the light strand transcript begins later from the LSP. Alternatively, transcription of the heavy strand may be initiated either from HSP1, generating a short transcript which terminates at the 16SrRNA, or from HSP2, generating a polycistronic transcript [145]. However, transcription from the mitochondrial promoters produces a polycistronic precursor RNA that is then processed to produce individual tRNA and mature mRNA molecules [1, 132, 146].

The exact mechanisms involved in mtDNA transcription are still not fully understood, however; the understanding of the machinery has improved due to the identification of specific proteins and the availability of *in vivo* experimental system [147]. It is known that mtDNA transcription is different from that of nuclear DNA in some aspects. In mtDNA transcription, the polymerase γ is the only DNA polymerase involved in the process and genes on both strands are transcribed polycistronically, unlike nuclear gene transcription in which most genes are transcribed individually [146]. Interestingly, a recent study showed that the mitochondrial transcription termination factor 3 (MTERF3), which is located in the mitochondria, acts as a negative regulator of mammalian mtDNA transcription. MTERF3 binds at or near the mtDNA promoter regions, HSP1, HSP2 or LSP, to repress transcription, which may be important in regulating oxidative phosphorylation in response to different physiological demands. It may also provide a mechanism to avoid collision between transcription complexes generated by the opposing promoters [148]. More recently, the mitochondrial transcription factor B2 (TFB2M) was reported as a mitochondrial DNA transcriptional activator in a complex with the mitochondrial transcription factor (TFAM) and the RNA polymerase (POLRMT). In addition, the TFBM factors are thought to couple mitochondrial transcription and translation [149].

1.11 Mitochondrial RNA translation

Translation of mt-mRNAs for the 13 mitochondrial-encoded proteins takes place on mitochondrial ribosomes [150, 151] However, initiation and termination of mitochondrial proteins synthesis is not widely understood [152]. The mitochondrial mRNAs were described to lack the 5'-untranslated region, which interacts with 16S rRNA during the initiation of protein synthesis [153], however, 4 RNA species (*MTCO1*, *MTND4*, *MTATP8*, and *MTATP6*) do have the 5'-untranslated region [154]. In addition, the 5` termini of the mtRNAs lack the 7-methylguanylate cap structure that is present in the majority of eukaryotic mRNAs and is essential for recruiting translation initiation factors, which interact with poly(A) binding protein [155]. Although mitochondrial mRNAs harbour initiation codons, the mechanism that guides mitochondrial ribosomal subunits to this region is currently unclear, however, it is possible that the structure of the mRNA alone guides the ribosome to the proper start codon [156]. Many nuclear-encoded factors have been involved in the translation of mtDNA. These include, for example, ribosomal proteins, aminoacyl tRNA synthetases, mt-tRNA modification proteins, mitochondrial initiation factors [157, 158], mitochondrial elongation factors [159, 160], in addition to Pentatricopeptide repeat domain 3 (PTCD3) [161], the ribosome recycling factor mtRRF [162, 163], methionine aminopeptidase (MAP1D) [164], and at least one termination release factor, mtRF1a [165].

The disruption of mitochondrial translation due to mutations in mitochondrial tRNA or ribosomal RNA genes leads to mitochondrial translation defects therefore causing pathology. Mutations in nuclear genes essential for mitochondrial translation, such as the mitochondrial ribosomal protein S16 (MRPS16) [166] and the mitochondrial elongation factor G1 (EFG1) [167], resulted in mitochondrial translation defects [1]. Mutations in the elongation factors Tu (EFTu) [168] and the mitochondrial translation elongation factor Ts (EFTs) were associated with mitochondrial translation defects as well [169]. Recently, a point mutation in the mitochondrial $tRNA^{Met}$ caused a mitochondrial myopathy due to tRNA misfolding leading to defects in translational initiation and elongation [170].

1.12 Mitochondrial protein import

Although mitochondria have their own genome, only 1% of mitochondrial proteins are encoded by the mitochondrial genome. The majority of the mitochondrial proteins are

encoded by nuclear genes and then synthesized as precursors on cytosolic ribosomes. Translocases on the mitochondrial membranes and chaperones direct the import of these proteins into the mitochondria. There are two kinds of mitochondrial precursor proteins. The first are preproteins with positively charged and cleavable targeting signals, termed presequence, at the the N-terminus which interact with mitochondrial import receptors on both outer and inner membranes. These include matrix proteins, some of the intermembrane space proteins, and inner membrane proteins. The second preproteins with various internal targeting signals; these include all outer membrane proteins and other intermembrane and inner membrane proteins [171-173].

There are two translocases involved in mitochondrial protein import. One of these is the translocase of the outer mitochondrial membrane (TOM) complex, which consists of seven different subunits. Only precursors for mitochondrial proteins pass through this complex. The other translocase is located in the inner mitochondrial membrane and includes the TIM22 and TIM23 complexes. The TIM22 complex consists of several subunits including TIM9 and TIM10 involved in precursor transfer to the complex [174]. TIM23 consists of three different subunits [173] in association with TIM50 which transfers precursors from the TOM complex to the TIM complexes [175].

Upon mitochondrial precursor or preprotein synthesis, precursors are directed to receptors on the mitochondrial surface by the help of cytosolic heat shock proteins. The TOM complex is the main gate for import; precursors are then shuttled down one of three different pathways according to their final destination in the mitochondria [171] (Figure 1-10).

Precursors of outer membrane proteins are imported first through the TOM complex and to the intermembrane space. Small TIM proteins within the intermembrane space participate in the transport of these precursors to the sorting and assembly machinery (SAM complex) in the outer membrane [171, 176, 177].

After passing the TOM complex, precursors of many hydrophobic proteins, including metabolite carriers, pass through the carrier translocase (TIM22 complex) and are directed to the inner membrane with the help of chaperone-like components from the intermembrane space [171].

Precursors with a cleavable signal peptide are transferred to the TIM23 complex on the mitochondrial outer membrane, which forms a channel across the outer membrane and associates with both the matrix heat shock protein70 (mtHsp70) and the import motor (PAM) to complete protein transport into the matrix [171]. The signal peptide is then cleaved by an endometallopeptidase.

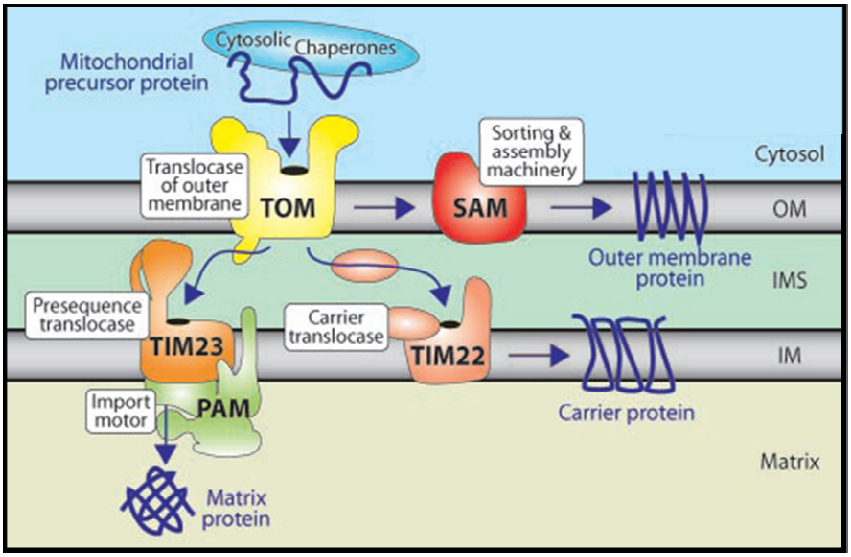

Figure 1-10 Pathways of mitochondrial protein import.

Precursors of mitochondrial proteins are synthesised in the cytosol then imported through the TOM complex with the help of cytosolic chaperones. Precursor proteins are then directed to their destinations according to the targeting signal. Precursors with internal targeting signals, such as precursors of outer membrane (OM) proteins, are directed to the outer membrane through the SAM complex and precursors of the inner membrane, such as carrier proteins, are directed to the inner membrane (IM) through the TIM22 complex and chaperone-like proteins within the inner membrane space (IMS). Precursors with N-terminal signal peptides are directed to the matrix through the TIM23 and PAM complexes (taken from [171]).

1.13 Mitochondrial DNA damage

The human mtDNA is a compact DNA molecule without protection by histones, but instead it is packaged with other proteins such as: mtTFA, mtSSB, Twinkle, and polymerase γ [143, 178]. It replicates rapidly with high mutation rate higher than that observed in nuclear DNA [132]. In addition to the site of the mtDNA, which is attached to the inner mitochondrial membrane [179, 180], all these factors render the mtDNA an easy target for attack by reactive oxygen species (ROS) and free radicals generated as a result of electron leakage from the mitochondrial respiratory chain [181].

The free radical theory suggested that ROS, which are constantly generated through normal mitochondrial metabolism, cause ageing and age-associated degenerative diseases by introducing damage to membranes, proteins and DNA [182]. The mitochondrial theory of aging, which supports the free radical theory, suggests that the accumulation of somatic mutations in mtDNA during an organism`s lifetime results in mitochondrial dysfunction [182-184]. The ROS vicious cycles are believed to account for an exponential increase in oxidative damage during aging, which eventually results in loss of cellular and tissue functions through a combination of energy insufficiency, signaling defects, apoptosis and replicative senescence. This was proved by the presence of pathogenic mutations associated with increased levels of ROS [185]. More recently, some somatic mutations in the mtDNA, which inhibited electron transport, led to increased production of ROS [186-189].

As mentioned above, the mitochondrial DNA has high rate of mutations. T o cope with this high rate if mutations, a DNA repair system is required to maintain the integrity of the mtDNA. However, mtDNA repair may occasionally fail or become limited due to excess of mtDNA damage caused by ROS production resulting in the accumulation of damaged mt DNA leading to diseases [190, 191].

Unlike nuclear DNA, mtDNA repair in mammalian cells is not widely investigated as early studies suggested absence of DNA repair in mitochondria [192]. Several DNA repair pathways have been described in the nucleus including: direct reversal (DR), nucleotide excision repair (NER), base excision repair (BER), mismatch repair (MMR), recombinational repair (RER), and translesion synthesis (TLS) [193]. While the damaged mtDNA can be repaired by the base excision repair pathway, which is well described in mitochondria [194-196], mismatch repair [19], and direct repair [197]. However, the presence of other mtDNA repair pathways is still unclear [191].

1.14 Mitochondrial DNA inheritance

The mammalian egg contains about 100,000 molecules of mtDNA and the sperm contains 100-1500 mtDNAs [17, 198]. When the sperm fertilizes the egg, the sperm mtDNA is actively degraded [199] by an ubiquitin system-driven process [200]. Therefore, the mtDNA is only maternally inherited. However, this model of inheritance has been challenged because the transmission of paternal mtDNA was observed after interspecific

crosses between mouse, but not within species [201]. Further studies showed that the paternal mtDNA was only transmitted after several generations [202]. In humans, only one case was reported of paternal inheritance of an mtDNA mutation, a patient with mitochondrial myopathy due to a novel 2-bp mtDNA deletion in the *MTND2* gene [203, 204]. This case is more likely to be rare because family members were not affected and no trace of mutation was detected in their blood or muscle, which suggest that this mutation arose spontaneously in early embryogenesis or in the paternal germ line [204]. Recent reproduction studies were carried out to further investigate mtDNA paternal inheritance using intracytoplasmic sperm injection (ICSI), which is widely used in cases of severe male infertility. The theory behind these studies was that the mutant mtDNA in the sperm may bypass direct degradation after fertilization thereby increasing the risk of transmitting mtDNA disease to children born by this technique. However, results showed no evidence of paternal mtDNA transmission to offspring or extra-embryonic tissues [205, 206].

1.15 Heteroplasmy and the threshold effect

In contrast to nuclear genes, with one maternal and one paternal allele, mtDNA molecules are present in hundreds or thousands of copies in each cell [199], thus the mitochondrial genome has a polyploid nature which means the mitochondrial genome copies can exist in two forms, homoplasmy or heteroplasmy [1]. Homoplasmy is when all the mitochondrial genome copies are identical and heteroplasmy is when there is a mixture of two or more mitochondrial genotypes.

Deleterious mutations of mtDNA typically affect some but not all genomes. Thus, cells, tissues and individuals may harbor two populations of mtDNA: wild type and mutant (heteroplasmy). In normal subjects, all mtDNAs are identical wild-type copy known as homoplasmy. Non-deleterious mutations of mtDNA (neutral polymorphisms) are typically homoplasmic and the pathogenic mutations are usually but not invariably heteroplasmic [199].

In the presence of heteroplasmy, there is a threshold level of mutation which is important for both the clinical expression of the disease as well as the biochemical defects [1].The phenotypic threshold effect can be observed when the wild-type mtDNA in a single cell can no longer complement the effects of the mutant mtDNAs and eventually leading to mitochondrial dysfunction [207]. The mitochondrial threshold varies according to the

mtDNA mutation type, ranging from 60% for mtDNA deletion mutations to 90% for some tRNA mutations or could be less [133, 208]. For example, high levels of mtDNA deletions were found in Parkinson disease [209]. The threshold levels were 50% in the m.3243A>G mutation [210], 60% in the m.5650G>A mutation [211], and more than 90% in the m.3302A>G mutation [212].

1.16 Mitochondrial division and segregation

Mitochondria are dynamic organelles that actively divide and fuse to mix metabolites and mtDNA copies according to the energy demands of the cell [213]. The copy number and shape of mitochondria are different in different cell types. They can change in the same cell type under different physiological conditions ranging from multiple spherical organelles to a single organelle with a branched structure or reticulum. The number of the mitochondrial genomes inside mitochondrion depends on the degree of fragmentation. In most cells, mtDNA replication is not limited to the S phase of the cell cycle when the nuclear DNA replicates, but occurs independently of the cell cycle. However, during the cell cycle the numbers of mitochondria and their mtDNA have to double and the newly formed organelles have to be segregated to the daughter cells. Mitochondrial fission and fusion (Figure 1-11) events are involved in this complex process because mitochondria are enclosed by a double membrane structure [214].

Large dynamin-related GTPases have been reported to be involved in the balance between mitochondrial fission and fusion. Although the exact mechanism of mitochondrial fission in mammals is not understood, Fis1 and DRP1 have been described to be involved in mitochondrial fission [215-217], by assembling into rings surrounding the mitochondrial outer membrane, in addition to hFIS1 and other unknown cofactors and regulators [40, 218]. hFIS1 is located throughout the outer mitochondrial membrane and it recruits DRP1 from the cytosol to the outer mitochondrial membrane [219]. GTP hydrolysis is thought to cause a conformational change in DRP1 that drives the mitochondrial outer membrane fission event [213].

The fusion event involves both the outer and inner membranes through Mitofusins 1, 2 (Mfn1, 2), which facilitate outer membrane fusion in mammals through *trans* interactions that promote membrane curvature and fusion [37, 220, 221]. Regardless of the exact mechanism, studies showed that the two distinct isoforms of the GTPase OPA1 (optic

atrophy), which is the main mediator of membrane fusion and maintenance of mtDNA in mammals [222-224], are necessary for successful fusion events [225-227].

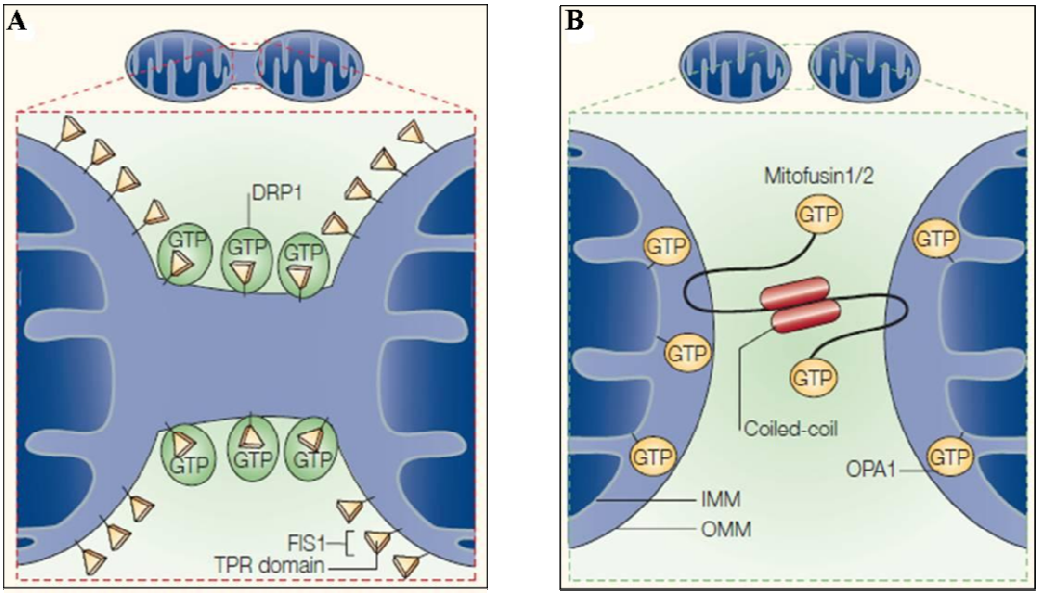

Figure 1-11 Mitochondrial fission and fusion in mammalian cells.

(A) In mitochondrial fission, FIS1 recruits the large GTPase and DRP1 throughout the outer mitochondrial membrane (OMM). (B) Mitochondrial fusion involves both mitofusins 1/2 which are located on the outer mitochondrial membrane (OMM) and OPA1 which is located partially on the inner mitochondrial membrane (taken from [40]).

1.17 Mitochondrial DNA transmission and the genetic bottleneck

Maternal mutant mtDNA is transmitted to offspring with different degrees since the risk depends on the type of mutation and the segregation of mutation in the mother`s tissues. Therefore, a mother carrying a mtDNA mutation may pass it to all her children, but only her daughters will transmit it to their progeny [199]. Homoplasmic mtDNA mutations are transmitted to all maternal offspring. However, not all offspring will develop the disease since nuclear genetics and environmental factors play major roles in the expression of the disease.

The transmission of heteroplasmic mtDNA mutations is more complex since it is controlled by different factors. Not only do nuclear genetic and environmental factors affect the expression of the disease, but also the genetic bottleneck (Figure1-12). In which, the number of mutant mtDNA molecules are reduced during oogenesis thereby decrease

the number of the mutant mtDNA when they are passed from a mother to her offspring [228].

During cell division, the mitochondria and their genomes are randomly distributed to the daughter cells, a process known as replicative segregation. Mitochondria have the ability to fuse, which results in the accumulation of their genomes [229], mitochondria division will result in the random distribution of their genomes. These processes can change the proportion of mutant mtDNA in daughter cells and when the pathogenic threshold changes in a specific tissue, the phenotype can also change. Mitotic segregation explains the differences in the mutation load in different tissues from different members carrying the same pathogenic mutation and the time-related phenotypic differences frequently observed in mtDNA-related disorders [199]. However, mitotic segregation cannot explain changes in non-diving cells such as skeletal muscle and neurons which can be attributed to relaxed replication of mtDNA [230].

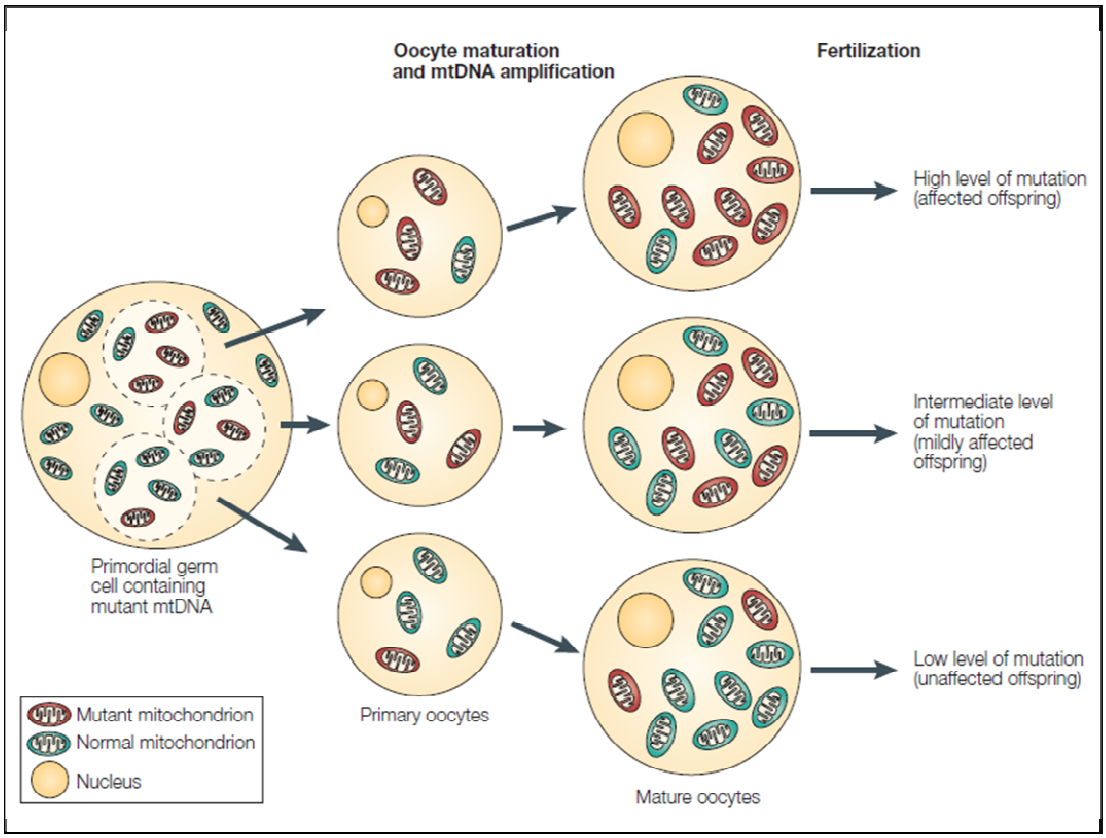

Figure 1-12 The genetic bottleneck.

Selected number of mtDNA molecules is transferred into each oocyte during the production of primary oocytes. Oocyte maturation is associated with the rapid replication of this mtDNA population. Difference in mutation load of the mtDNA between generations is responsible for the variable levels of mutated mtDNA observed in affected offspring from mothers with pathogenic mtDNA mutations (taken from [1]).

1.18 Mitochondrial DNA and mutations

Mitochondrial diseases are estimated to affect 1 in 5000 of the population, although the exact number could be much higher [231]. A study in 2008, in the North East of England, revealed that the prevalence of mitochondrial DNA disease in adults is 9.2 in 100,000 of population [232]. Other studies based on patients with the most common mtDNA mutation, the m.3243A>G mutation, revealed a prevalence of 1 in 200 [233] ; and the m.1555A→G mutation gave a prevalence of 1 in 520 [234]. The mitochondrial diseases are multisystem diseases that mainly affect skeletal muscle, cardiac muscle and the central nervous system [235]. Symptoms range from mild disturbances of eye movement in late adulthood to neonatal death associated with profound lactic acidosis [236]. Several factors increase the rate of mtDNA mutations as mentioned above, such as the lack of a DNA repair system [237], the lack of protective proteins such as histones and the association with the inner mitochondrial membrane which makes the mtDNA a close target for ROS during OXHPHOS [238].

To date, more than 250 pathogenic mtDNA mutations have been reported [190]. Mutations affecting mtDNA can be divided into two groups; mtDNA mutations affecting protein synthesis and mtDNA mutations affecting protein-coding genes [199]. These mutations can also be grouped into base substitution mutations and rearrangement mutations (deletion or duplication). The first group of mutations can change the amino acid thereby the proteins (missense mutation) or rRNAs and tRNAs (protein synthesis mutations). Rearrangement mutations generally involve the deletion of at least one tRNA thereby causing protein synthesis defects [199].

Missense mutations have been linked with different mitochondrial diseases associated with myopathy, optic atrophy, dystonia, Leigh syndrome, ragged-red fibres and subsarcolemmal aggregates of abnormal mitochondria [239]. Diseases resulting from mtDNA rearrangements are invariably heteroplasmic and give rise to phenotypes ranging from adult-onset type II diabetes and deafness, through ophthalmoplegia and mitochondrial myopathy to lethal pediatric pancytopenia [239].

Not every mtDNA mutation leads to the development of mitochondrial disease since some mutations are silent and have no physiological effect. In addition, the mitochondrial genome contains a large number of neutral base changes and insertions or deletions that

have no pathogenic significance, known as neutral polymorphisms [199]. In order to assign pathogenicity to a novel mtDNA mutation, six canonical criteria have been proposed which should be met [199, 240-242].

1.19 Defining pathogenicity of a mtDNA point mutation

Not all sequence changes in the mitochondrial genome are pathogenic since it contains a large number of neutral changes. These changes can be beneficial to anthropological studies and forensic medicine [243, 244]. Defining pathogenicity of mt-tRNA mutations is further complicated because of the clinical and biochemical heterogeneity associated with these mutations. For example there is often little correlation between which mt-tRNA is mutated and the resulting phenotype if we consider the common consequence to be reduction in protein synthesis [118]. To assign pathogenicity of a mtDNA mutation, six canonical criteria were suggested by DiMauro and Schon [199].

1. The mutation must be heteroplasmic (i.e. co-existent wild-type and mutated mitochondrial genomes in the same tissue). However, not only heteroplamic mutations are pathogenic; homoplasmic mtDNA mutations have also been identified to be pathogenic [245-247].
2. The proportion of mutated mtDNA should be higher in tissue from affected individuals than in the same tissue from their unaffected relatives. This is only applicable to heteroplasmic mutations and it is difficult to determine mutation segregation in small families [118].
3. The proportion of mutated mtDNA should be higher in clinically affected tissues. This only applies to heteroplasmic mutations because mutation loads in homoplasmic mutations are 100%.
4. The proportion of mutated mtDNA should segregate with a biochemical defect. This can be clearly seen if the mutation load in the COX-deficient fibres is higher than in the COX-positive fibres to have a direct correlation [248]. However, homoplasmic mutations do not segregate with biochemical defect because mutation load in all fibres will be the same [245, 247, 249, 250].
5. The mutation should occur at an evolutionary conserved site in the mitochondrial genome. However, some pathogenic mutations may not be considered pathogenic because of poor evolutionary conservation in the region [118] such as the pathogenic m.8344A>G in mt-tRNA^{Lys} [248, 251].

6. The mutation should be absent from healthy controls and not reported in the two mitochondrial DNA databases [69, 252].

1.20 Clinical syndromes and features of the human mitochondrial diseases

Syndromes due to mtDNA mutations were widely investigated following the discovery in 1988 of the first two syndromes Kearns-Sayre (KSS) and LHON [253, 254], which were due to pathogenic mtDNA mutations. This led to further investigations for other mtDNA mutations resulting in the identification of hundreds of other mutations. Some classical syndromes, along with the most common clinical phenotypes in patients are summarized in Table 1-2.

The existence of mitochondria in all nucleated cells mean mtDNA associated diseases affect many tissues with different phenotypes [1]. The biochemical and genetic complexity of the respiratory chain system can explain the wide range of clinical phenotypes of mitochondrial disease. It is clear that organs with a high requirement for aerobic respiration, such as brain, heart and skeletal muscle, are more likely to be severely affected by pathogenic mtDNA mutations. Other organs that can be affected include the gastrointestinal tract [255], the liver [256], the kidneys [257] and the endocrine systems [257]. Mitochondrial diseases often show a delayed onset and a progressive course. This is thought to be the result of an age-related decline in OXPHOS function in postmitotic tissues [258] associated with the progressive accumulation of somatic mtDNA rearrangement mutations [259]. The two main features in most mitochondrial disease are respiratory chain deficiency and lactic acidosis. Furthermore, patients with mitochondrial disease often have abnormal subsarcolemmal mitochondria in their muscle shown as ragged-red fibres [260].

Genetically, mitochondrial diseases can be divided into three groups: diseases due to sporadic or maternally inherited mtDNA mutations, diseases due to mutations in nuclear genes, which control mitochondrial and diseases that do not result from mtDNA mutations but are thought on the basis of biochemical findings to be caused by nuclear DNA mutations [261].

Table 1-2 Clinical disorders which are caused by mutations in mtDNA

Mitochondrial DNA disorder	**Clinical phenotype**	**MtDNA genotype**	**Gene**	**Status**	**Inheritance**
Kearns-Sayre syndrome	Progressive myopathy, ophthalmoplegia, cardiomyopathy	Single, large scale mtDNA deletion	Several deleted genes	Heteroplasmic	Usually sporadic
Chronic progressive external ophthalmoplegia (CPEO)	Ophthalmoplegia,	Single, large scale mtDNA deletion	Several deleted genes	Heteroplasmic	Usually sporadic
Pearson syndrome	Pancytopoenia, lactic acidosis	Single, large scale mtDNA deletion	Several deleted genes	Heteroplasmic	Usually sporadic
Mitochondrial myopathy, encephalopathy, lactic acidosis& stroke-like episodes (MELAS)	Myopathy, encephalopathy, lactic acidosis & stroke-like episodes	m.3243A>G, m.3271T>C ; individual mutations	*MTTL1* *MTND1*&*MTND5*	Heteroplasmic	Maternal
Myoclonic epilepsy & ragged-red fibres (MERRF)	Myoclonic epilepsy, myopathy	m.8344A>G, m.8356T>C	*MTTK*	Heteroplasmic	Maternal
Neurogenic weakness, ataxia and retinitis pigmentosa (NARP)	Neuropathy, ataxia, retinitis pigmentosa	m.8993T>G	*MTATP6*	Heteroplasmic	Maternal
Maternally-inherited Leigh syndrome (MILS)	Progressive brain-stem disorder	m.8993T>C	*MTATP6*	Heteroplasmic	Maternal
Maternally-inherited diabetes and deafness (MIDD)	Diabetes, deafness	m.3243A>G	*MTTL1*	Heteroplasmic	Maternal

Mitochondrial DNA disorder	Clinical phenotype	MtDNA genotype	Gene	Status	Inheritance
Leber's hereditary optic neuropathy (LHON)	Optic neuropathy	m.3460G>A, m.11778G>A, m.14484T>C	*MTND1* *MTND4* *MTND6*	Hetero-or homoplasmic	Maternal
Myopathy and diabetes	Myopathy, weakness, diabetes	m.14709T>C	*MTTE*	Hetero-or homoplasmic	Maternal
Sensorineural hearing loss	Deafness	m.1555A>G Individual mutations	*MTRNR1* *MTTS1*	Homoplasmic Hetero-or homoplasmic	Maternal
Exercise intolerance	Fatigue , muscle weakness	Individual mutations	*MTCYB*	Heteroplasmicc	Sporadic
Fatal, infantile encephalopathy, Leigh/Leigh-like syndrome	Encephalopathy, lactic acidosis	m.10158T>C, m.10191T>C	*MTND3*	Heteroplasmic	Sporadic

MTATP6: ATPase 6; MTCYB: cytochrome b; MTND1, 3–6: NADH dehydrogenase subunits 1, 3–6; MTRNR1: 12S ribosomal RNA; MTTE, MTTK, MTTL1, and MTTS1 are mitochondrial tRNAs (modified from [1]).

1.21 Diagnosis of mitochondrial disorders

Diagnosis of a mitochondrial disease is not straightforward. The principal difficulty for clinicians is that patients with mitochondrial disease rarely have a classic phenotype and mtDNA is involved in the differential diagnosis of many common clinical syndromes [1]. For example, mtDNA mutations have been linked to some common metabolic syndromes as reviewed in [262] and [263]. Furthermore, some symptoms of mitochondrial diseases are age-related, while others can present at any age [70], and they often present in specific combination with other clinical symptoms, e.g. mitochondrial diabetes is often accompanied by deafness [264], and stroke-like-episodes usually are associated with migraine-like symptoms [1].

1.22 Investigations of a mitochondrial disorder

1.22.1 Preliminary investigations

Patients suspected to have a mitochondrial disease initially undergo biochemical investigations which include: creatine kinase assay, full blood count, tests of thyroid and liver function and bone chemistry, measurements of resting blood lactate, random blood glucose, and glycated haemoglobin. In addition, investigation should include electrocardiography to determine possible conduction defects or cardiac hypertrophy [265].

1.22.2 Investigation of relevant tissues

Following clinical and laboratory investigations, patients are further investigated by histochemical, biochemical and molecular genetics techniques which provide correct and accurate diagnosis for the majority of patients [265]. These techniques involve the examination of blood or muscle DNA samples, fibroblasts and muscle biopsies.

The biochemical investigations of fibroblasts are necessary for diagnostic purposes if no muscle sample is available, if prenatal diagnosis is required, or to confirm results obtained from muscle investigation. In addition, fibroblasts are suitable for molecular genetic investigations. However, they are less preferred than fresh muscle for investigating respiratory chain disorders since a defect that is present in muscle is not always expressed in fibroblasts [70].

Muscle biopsies are mainly preferred because they are the most diagnostically accessible source of clinically affected tissue [265] and most of the defects are expressed in these tissues [70], however, it is still with some limitations. The biopsy is taken with needle biopsy using local anaesthesia. The size and quality of the investigated muscle biopsy are important. So, it must be free of connective tissue and fatty tissue. Conditions of specimen collection and transport are critical. Also, investigation of a muscle biopsy for diagnostic purposes should be avoided in the first month of life if possible and medication should be avoided before taking the biopsy to avoid false positive diagnosis due to secondary inhibitory effects of medication [70].

Prenatal diagnosis is required, to confirm results obtained in muscle tissues, and if further molecular genetic investigations are required. It can be performed reliably in families if a defect has been confirmed in at least two different tissues. Currently, prenatal diagnosis is performed both in chorionic villi and in amniocytes. However, chorionic villi are preferred because they allow the prenatal diagnosis at earlier stage of the pregnancy (around the 10th week) as compared with amniocytes. Moreover, chorionic villi can be investigated without cultivation, in contrast to amniocytes reducing the time of investigation [70].

1.22.3 Histochemical investigations

The histochemical analysis of muscle biopsy is the most commonly used technique to investigate mitochondrial abnormalities [266]. Gomori trichrome stain is a method used to detect subsarcolemmal mitochondrial accumulation, called ragged-red fibres (RRF) (Figure 1-13-A). However, this method is not fully accurate because it does not evaluate mitochondrial enzyme involvement. The combined succinate dehydrogenase (SDH) and cytochrome *c* oxidase (COX) are widely used to measure activities. The COX reaction (Figure 1-13-B and C) evaluates the mitochondrial myopathies because COX contains subunits encoded by both the mitochondrial and nuclear genomes [240], while the SDH, is only nuclear encoded and the reaction can reveal the subsarcolemmal mitochondrial accumulation (Figure 1-13-D).

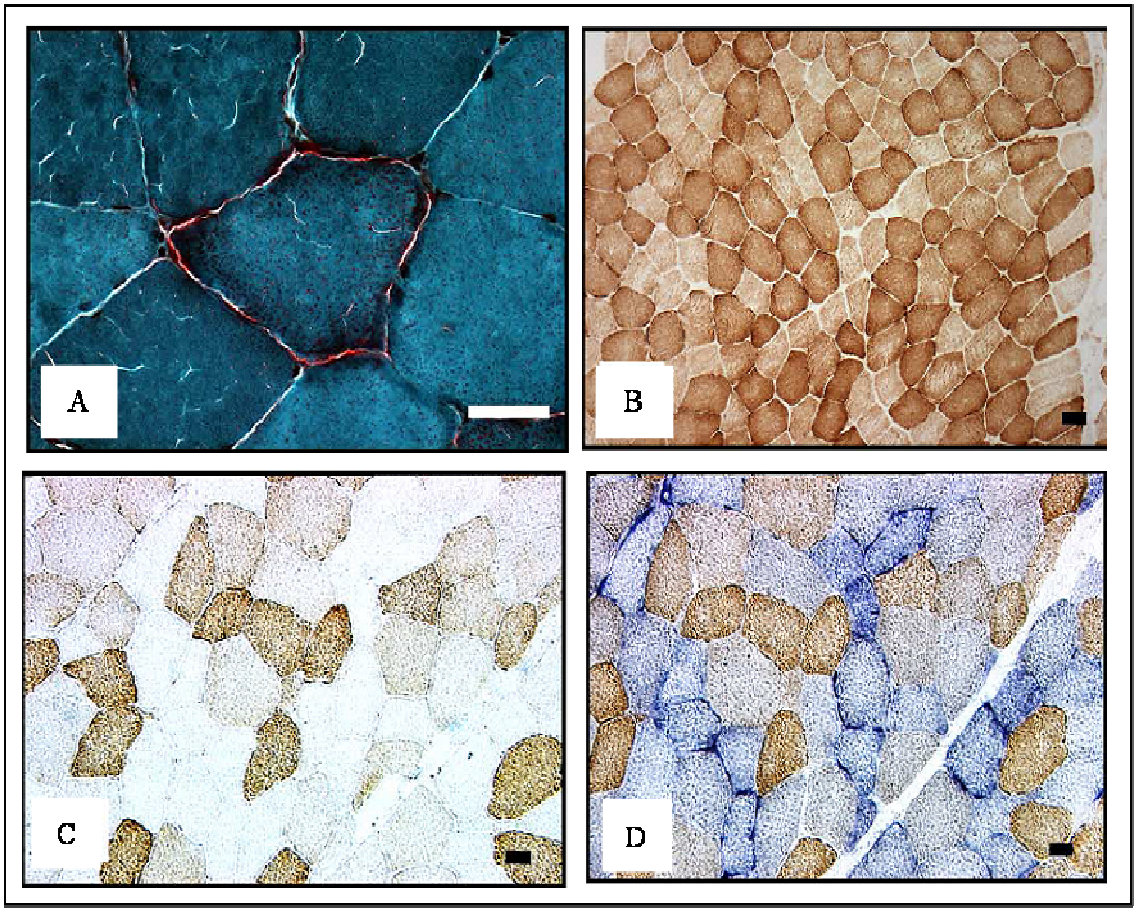

Figure 1-13 Histochemical analysis of muscle fibres.

(A) Classical ragged-red fibres after Gomori trichrome staining showing the subsarcolemmal mitochondrial accumulation. (B) Normal muscle fibres after COX staining (brown). (C) COX-deficient muscle fibres after COX staining alone. (D) COX-deficient fibres stain blue after the combined SDH (blue) and COX staining (taken and modified from [240]).

1.22.4 Biochemical investigations

Measurement of individual respiratory chain enzyme activities for the mitochondrial complexes is the ultimate investigation in the diagnosis of a patient suspected to have a mitochondrial disease because these diseases are caused by deficiencies in one or more of the respiratory chain complexes. This analysis can be performed on both muscle biopsies and fibroblasts. In general, fresh muscle samples are preferred to frozen samples as they contain functionally intact mitochondria, which allows the overall capacity of oxidative phosphorylation and the activity of the respiratory chain enzymes to be measured. A frozen sample can be used for measuring only the individual enzyme activities instead of the complete chain. In addition, other factors have to be considered when dealing with muscle

biopsies to ensure reliable results such as: sample size, quality of the sample, transport conditions, age of the patient at date of biopsy and use of medications [70].

1.22.5 Molecular genetic investigations

The molecular genetic investigations of patients suspected of a mitochondrial disease can be complex. These investigations are normally performed in all patients with abnormal histochemistry or biochemistry and in patients suspected to have a mitochondrial disease but with normal muscle biopsy results [265]. The molecular genetic investigations involve searching for novel and pathogenic mutations through sequencing of the entire mitochondrial genome of patients, or in some cases excluding mtDNA involvement in the disease. Also they involve searching for mitochondrial genome rearrangements which include single deletions, duplications and multiple mtDNA deletions which can be detected by Southern blot [240] or long-range PCR [267].

Furthermore, restriction fragment length polymorphism (RFLP) is one of the molecular genetic techniques often performed to search for common mtDNA point mutations and quantify the mutation load which is clinically significant to correlate genotype with the resulted phenotype in patients [268, 269].

1.23 Animal models of mitochondrial diseases

The inability to transfect mitochondria with exogenous DNAs *in vitro* or *in vivo* is one of the factors that has prevented progress in the study of the relationship between mtDNA genotype and phenotype. However, several trials have been carried out to create animal models carrying heteroplasmic and pathogenic mtDNA mutations to further investigate the pathogenicity of mtDNA mutations.

The first trial involved the microinjection of cytoplasm containing mtDNA into oocytes which resulted in chimeric embryos, but the mutant mtDNA was lost by segregation in early development [270]. Another study involved the introduction of mtDNA mutations into the mouse female germ line by electrofusing cytoplasts derived from NZB or BALB mice zygotes carrying one mtDNA genotype to recipient one-cell embryos of the other type [271-273].

*Trans*mitochondrial chimeric mice with chlorampenicol-resistant mitochondria (CAR^R), resistant to the mitochondrial ribosome inhibitor (CAR), were generated by fusing a

chlorampenicol-resistant cell line with female ES cells. These were then injected into donor blastocysts [273, 274]. Mice with mitochondrial dysfunction were produced by introducing mouse mtDNA carrying a deletion into zygotes [275]. Another group generated mice with pathogenic mtDNA mutations that were transmitted through the germ lines [208].

Advanced studies have moved to create mouse models through the targeting of genes involved in the maintenance or replication of the mtDNA by disrupting the mitochondrial transcription factor A (*Tfam*), which resulted in mitochondria-associated disease phenotypes in different tissues [276-279]. A recent study performed by Trifunovic and colleagues showed that knock-in mice, harboring a mtDNA mutation in the polymerase-γ gene (*PolgA*), resulted in short lifespan and premature ageing phenotypes: weight loss, reduced fat, hair loss, curvation of the spine, osteoporosis, anemia, reduced fertility, and heart enlargement [280, 281].

Although, these trials were successful in generating mice with mtDNA diseases due to mutations in the mitochondrial genome and also showed the involvement of mtDNA mutations in the development of new diseases that were not seen in humans as they died due to renal failure [275], phenotypes and inheritance patterns for some mutations were different from those seen in humans [282]. However, doubts were raised after the premature ageing phenotypes lacked both increased oxidative stress and exponential accumulation of mtDNA mutations. These findings argued against the direct involvement of oxidative stress in the ageing process, contradicting the oxidative stress theory of ageing, and favored the accelerated aging phenotypes to the respiratory chain defect as a primary inducer of premature ageing in those mice [283-285].

To further investigate the relationship between mitochondrial mutations and aging, a quantitative PCR-based approach that relies on PCR amplification of single molecules for mutation detection was carried out. Results showed that mutator mice had increased levels of point mutations in tissues compared to wild-type, which had no obvious features of rapidly accelerated aging. Therefore, results strongly suggest that mitochondrial point mutations do not limit the lifespan of wild-type mice [286].

Despite some doubts raised by previous animal models with mitochondrial mutations, subsequent trials have been performed to further increase our knowledge of the role of mitochondria in diseases. More recently, a mouse model carrying a mutation in the mitochondrial Thymidine Kinase 2 (*TK2*), which is essential for the mitochondrial nucleoside

salvage pathway, was created [287, 288]. Results showed rapid and progressive mtDNA depletion in all studied tissues, which is similar to patients with mtDNA-depletion syndromes (MDS). In addition, a mouse model with two mutations in the mtDNA mutations, in the *MTND6* and *MTCOI* genes, was created [289]. Results showed that the severe *MTND6* mutation was selectively eliminated during oogenesis within four generations, whereas the milder *MTCOI* mutation was retained throughout multiple generations [289]. This is consistent with results from mutator mice which showed strong purifying selection against mutations within mtDNA protein-coding genes [290].

1.24 Cell culture model of mtDNA disease

In order to understand the functional consequences of a point mutation in a specific gene, it is necessary to determine the expression level of this gene, the assembly of the respiratory complexes, and the enzyme activities [207]. *Trans*mitochondrial cytoplasmic hybrids or cybrids are the most widely used approach for these investigations of mtDNA mutations; especially after doubts have been raised against the mtDNA-mutator mice. Cybrids are generated by fusion of enucleated cytoplasts from patient's cells, which harbor a mtDNA mutation, with a human cell line lacking mtDNA (p^0) (Figure 1-12) and growing under specific selection conditions [291]. The p^0 cells are either osteosarcoma or lung carcinoma cells [38], which had been completely depleted of mtDNA by long-term exposure to ethidium bromide and post-fusion are repopulated with the exogenous patient mitochondria [292]. As these Rho^0 cells have no functional respiratory chain and are dependent on pyruvate and uridine for growth, loss of one or both of these metabolic requirements can be used to select for cybrids that have mtDNA [292].

Generally, this system has proved to be useful for the study of the functional and physiological consequence of different levels of heteroplasmy of certain mtDNA mutations [208], for determining the effect of nuclear background on the segregation of pathogenic mtDNA mutations [293], for developing genetic therapies and for investigating heterologous mtDNA recombination in human cells [294].

Although, most cybrid models are established using aneuploid tumour cells (with abnormal number of chromosomes), however, this may affect the stoichiometry of nuclear- and mitochondrial-encoded RC subunits, therefore affecting expression of phenotype [190] . Also, tumour cells are dependent on glycolysis for energy production instead of OXPHOS, while

mtDNA disorders take place in highly aerobic cells. So, this may have an effect on the phenotypic expression of an mtDNA mutation [295]. In addition, both the p^0 cells and cybridisation processes can cause significant and stable up-regulation of many nuclear transcripts involved in OXHOS which can explain why in vivo phenotypes are not always expressed in an *in vitro* cybridsystem [296, 297].

1.25 Approaches to manage and treat mtDNA diseases

Although it has been more than two decades since the identification of the first mtDNA mutation and the subsequent identifications of several others, there is currently no effective treatment for mitochondrial diseases. Only symptom alleviating treatments are available [298]. The increased identification of mtDNA mutations and their involvement in diseases has encouraged researchers to develop several methods to manage mitochondrial diseases. One of the issues, which has hindered the progress to cure these diseases, is the complicated mitochondrial genetics and the varied expressed clinical phenotypes associated with these disorders.

Treatment for the relief of specific symptoms of mitochondrial disorders include drugs, blood transfusions, hemodialysis, invasive measures, surgery, dietary measures and physiotherapy [298]. The administration of different pharmmacological and biochemical agents has shown to be helpful. Those agents include antioxidants such as : co-enzyme Q10, idebenone, vitamin C, and vitamin E. Some agents were used to improve lactic acidosis such as: dichloroacetate and dimethylglycine. Carnitine and creatine were used to correct secondary biochemical defects. Nicotinamide, riboflavin, succinate, and co-enzymeQ10 were used as respiratory chain co-factors in addition to hormones [299]. However, whilst helpful, these approaches are not curative.

The best approach would be to provide a safe and effective treatment to improve patients` lives if cures for the diseases are impossible. Exercise therapy is one of the approaches which has shown great promise for improving physical capacity and quality of life in patients with heteroplasmic mtDNA mutations. This includes endurance training and resistance training. Endurance training means the ability to exert yourself for a long period of time, while resistance training or strength training means training against a specific opposing force. Patients, who undertook 14 weeks endurance training, have shown improved OXPHOS functions but no change in muscle mtDNA mutations levels were detected [300-302].

Resistance training utilizes musculoskeletal loading, such as weight lifting, that is increased in intensity or volume incrementally over time to improve strength and increase muscle mass . It is believed to stimulate muscle regeneration via the satellite cells in response to fibre injury, gave similar results with great improvement in the proportion of heteroplasmic mtDNA mutations. Studies from 12 weeks resistance training in patients with single, large-scale mtDNA deletions have shown increased satellite cell proportion with improvements in muscular strength and oxidative capacity suggesting a change of the mtDNA mutation levels to more wild-type in patients` muscles [303].

Moreover, an *in vitro* trial has been undertaken to manage mitochondrial diseases via gene therapy by shifting the levels of mtDNA mutations to wild-type. This approach was based on the inhibition of mutated mtDNA replication thereby increasing the number of wild-type copies of the mtDNA. This was carried out using selectively targeted sequence-specific nucleic acid derivatives such as peptide nucleic acids (PNAs), which are complementary to human mtDNA templates. The antigenomic PNAs specifically inhibited replication of the mutated mtDNA but not the wild-type mtDNA confirming the success of this approach *in vitro* but the question remains, is it applicable *in vivo*? [304].

Restriction endonucleases approach is another approach capable of distinguishing between the mutated and wild-type mtDNA, however, it is limited to mutations which create a novel cleavage site that is not present in the wild-type mtDNA [190, 305]. Results from mouse models carrying mtDNA mutations, which were injected with transgenes, showed the possibility of manipulating heteroplasmy levels of mtDNA in liver and muscle tissues [305]. A modified approach that targets and the mtDNA in a sequence-specific manner using a chimeric zinc finger methylase was achieved. Results from targeting the m.8993T>G (NARP) revealed the selective methylation of cytosines adjacent to the mutation site confirming the ability to disrupt the mutant mtDNA and maintain the wild-type mtDNA [306].

The recent discovery of the import system of tRNAs, rather than protein import, is another approach to manipulate defective mitochondria by restoring the function of the mutant gene [307]. This can be done by modifying or overexpressing the cognate aminoacyl synthetase of the pathogenic mt-tRNA mutations [190]. Results from overexpressing of the cognate aminoacyl synthetase of the mt-tRNA^{Phe} causing the m.611G>A significantly improved the aminoacylation state of this mutation [308]. Also overexpression of mitochondrial leucyl-

tRNA synthetase [309] and human mitochondrial valyl tRNA synthetase rescued mitochondrial dysfunctions due to mutations in the cognate mt-tRNAs [310].

Another alternative strategy is to prevent the transmission of mtDNA disease. The investigation of prenatal samples such as chorionic villus biopsy or amniocentesis is widely used to detect the presence or absence of mtDNA mutations in such tissues [190]. In addition, preimplantation genetic diagnosis (PGD), which involves screening for mtDNA mutations in unfertilised oocytes or single cells removed from early embryos prior to implantation, is another alternative approach.

Very recently, Craven *et al.* showed that pronuclear transfer from one fertilised human zygote to another enucleated human zygote, with a different mitochondrial genotype, was compatible with development to the blastocyst stage after *in vitro* culturing [311]. Given that maternally inherited mtDNA mutations require high mutation loads to be reached before causing biochemical defects [312] , this approach successfully showed the ability to manipulate human embryos with very low levels of mutation loads, which can not be detected by standard techniques, below the disease threshold. This favours pronuclear transfer with great promise to prevent the transmission of mtDNA disease in humans.

However, some limitations or side effects might arise from such approaches. For example, mtDNA depletion was described to happen during manipulating heteroplasmy levels [305] which may affect results as mtDNA copy numbers known to play a role in defining the expression levels of phenotypes [207, 313]. Also, a very low percentage of carry-over of mutant mtDNA associated with the pronuclear transfer [311].

Despite previously mentioned limitations or side effects; these findings show great promise in preventing the transmission of diseases due to mtDNA defects.

1.26 Aims

This thesis introduces the reader to mitochondria, mitochondrial genetics, basic organellar functions, and biology. I also describe mitochondrial diseases with reference to the variability observed in their clinical phenotypes, and the importance of both mitochondrial DNA (mtDNA)-encoded and nuclear-encoded genes in regulating mitochondrial respiratory chain function. This provides the reader with the necessary information to understand mechanisms

involved in mitochondrial disease pathology, in addition to understanding the functional consequences due to specific defects in mtDNA.

The overall aims of this thesis are several fold:

1] to investigate a cohort of patients either confirmed as having, or suspected to have, a biochemical defect in complex I using a variety of biochemical, histochemical, and molecular genetic approaches to confirm the involvement of mtDNA mutations and prove pathogenicity by assessing several cellular properties;

2] to investigate patients with mitochondrial disease phenotypes with suspected mt-tRNA gene mutations, and demonstrate the pathogenic nature of these novel mtDNA variants;

3] to evaluate whether the MitoChip (V2.0) is a reproducible tool for detecting heteroplasmic, pathogenic human mtDNA mutations which have previously been identified using conventional ABI sequencing protocols.

Chapter 2

Materials and methods

Chapter 2 : Materials and methods

2.1 Materials

2.1.1 Equipment

AlphaImage series 2200 Software for gel imaging	Flowgen
ABI 3130xI Genetic Analyser (SeqScape software)	Applied Biosystems
ABI GeneAMP 9700 Thermal cycler	Applied Biosystems
Autoclave	Astell
Automated Plate reader E1x800	Bio-Tech
AxioCam MR3 digital black and white camera	Zeiss
AxioVision image capture software (Version. 4.6.3.0)	Zeiss
Axiovert 200M fluorescence microscope	Zeiss
Balance: Sartorius Basic	Sartorius
Bench-top centrifuge	Sigma
Bench-top refrigerated centrifuge 5417R	Eppendorf
Binder general purpose incubator	Philip Harris
Cerenkov counter type 6-20	Mini instruments
Cryostat (Cryo-star HM 560M)	Microm International
Dry heat block	Techne
Electrophoresis power supply model 250EX	Life technologies
EPSON Expression 1680 pro (EPSON Scan software)	EPSON
Freezing container	Nalgene

Geiger counter series-900	Mini Instruments
Gel Dryer vacuum system model 543	BioRad
GeneChip CustomSeq® Array 2.0	Affymetrix
GeneChip scanner	Affymetrix
Gradient maker SG series	Hoefer® Inc
Gradient mixer	Hoefer ® Inc
Horizontal agarose gel electrophoresis systems	Amersham
InCu saFe^{TM} CO_2 incubator	Sanyo
Leica laser-microdissection system	Leica
Magnetic stirrer	Fisher
Microflow biological safety cabinet	Bioquell
Mighty Small II SE250	GEHealthcare Life Sciences
NanoDrop ND-1000 spectrophotometer (ND-1000 software)	Labtech International
Partec PAS for flow cytometry	Partec
Peristaltic pump P-1	Pharmacia
PhosphorImager, Storm 860 (Image Quant software)	Molecular Dynamics
Teflon-glass homogeniser (2ml)	Wheaton
UV gel documentation system	Flowgen
Varian cary 300 bio spectrophotometer (WinUV software)	Cary
Zeiss imaging system	Zeiss

2.1.2 Consumables

0.2ml 96 well PCR plates	StarLabs
0.2ml Eppendorf tubes	Biogene
0.5ml Eppendorf tubes	Biogene
1.5ml Eppendorf tubes	Biogene
2.0ml Eppendorf tubes	Biogene
96 well optical bottom plates	Starlabs
Coverslips 22x50mm	Merck
Cellstar disposable Pipettes (5ml, 10ml, and 25ml)	Greiner
Cellstar tissue culture flasks ($25cm^2$, $75cm^2$, and $225cm^2$)	Greiner
Cryo tubes (1.8ml)	Nunc
Falcon tubes (15ml and 50ml)	Costar
Gilson Pipetteman (P2, P10, P20, P200, and P1000)	Anachem
Microscope slides (76x26x1.0-1.2mm)	Merck
Polyethylenenaphthalate (PEN) membrane slide	Leica
SlideRite Mailer™	CellPath
Tissue culture plates (6-well, 12-well, and 24-well)	Cell Star
Whatman paper	Merck
Whatman grade 1 filter paper	Merck

2.1.3 Chemicals and reagents

2.1.3.1 Tissue culture and mitochondrial protein preparations

25% Trypsin /EDTA	Invitrogen
Bromodeoxyuridine (BrdU)	Sigma
Cytochalasin B	Sigma
Dialyzed fetal calf serum	Gibco
Dimethyl sulfoxide (DMSO)	Sigma
Dulbecco`s modified Eagle Medium (DMEM)	Invitrogen
Ethanol Analar	Merck
Fetal Bovine Serum	Invitrogen
Iso-Pentane	Merck
Liquid nitrogen	BOC
MycoAlert® Mycoplasma detection kit	Lonza
Nonidet P-40	BDH
O.C.T. compound	VWR
PEG 1500	Roche
Penicillin and Streptomycin solution (Pen-Strep)	Gibco
Percoll	Amersham
Phosphate Buffered Saline tablets	OXOID
Protease inhibitors	Roche
Polyethylene glycol	Roche

Uridine	Sigma

2.1.3.2 Histological and histochemical reagents

3.3’Diaminobenzidine tetrahydrochloride (DAB)	Sigma
Calcium Chloride	Sigma
Catalase	Sigma
Cytochrome *c*	Sigma
Di-Sodium Hydrogen Phosphate	Sigma
DPX mountant	Sigma
Eosin solution	Merck
Ethanol Analar	Fisher Scientific
Formaldehyde	Merck
Haematoxylin solution	Merck
Histoclear™	National Diagnostics
HRP-Polymer	MenaPath
Liquid stable DAB chromogen	MenaPath
Liquid stable DAB substrate buffer	MenaPath
Nitro Blue Tetrazolium	Sigma
Paraformaldehyde (PFA)	Sigma
Phenazine methosulphate (PMS)	Sigma
Sodium Azide	Sigma

Sodium Dihydrogen Phosphate	BDH
Sodium Succinate	Sigma
Universal probe	MenaPath

2.1.3.3 Extraction, precipitation and purification reagents

3M Sodium acetate pH5.2	Sigma
EZ1 Blood DNA Extraction kit	QIAGEN
Chloroform	Sigma
Ethylenediaminetetracetic acid (EDTA)	Sigma
Hydrochloric acid (HCl)	BDH
Isoamyl alcohol	Sigma
Isopropanol	Sigma
Magnesium Chloride ($MgCl_2$)	Sigma
Phenol	Sigma
Potassium Chloride (KCl)	Sigma
Proteinase K	Invitrogen
Sodium Chloride (NaCl)	BDH
Sodium Hydroxide (NaOH)	BDH
Trizma base	Sigma

2.1.3.4 Gel electrophoresis reagents

1 Kb DNA ladder	Gibco BRL
Agarose MP	Roche

Ammonium Persulphate (AMPS)	Sigma
Bromophenol Blue	Sigma
Butanol	AnalaR
Ethidium Bromide	Merck
Glycerol	Sigma
Hyperladder IV	Bioline
Kaleidoscope Pre-stained standards	BioRad
N,N,N`N`-tetramethylenediamine (TEMED)	Sigma
Sodium dodecyl sulphate (SDS)	BDH
Sodium hydroxide (NaOH)	BDH
Tris-acetate EDTA (10xTAE)	Sigma
Tris-borate EDTA (10xTBE)	Sigma
Trizma base	Sigma
Xylene cyanol	Sigma

2.1.3.5 Polymerase chain reaction and sequencing reagents

10x PCR Buffer	Applied Biosystems
AmpliTaq Gold DNA polymerase	Applied Biosystems
BigDye terminator v3.1 cycle sequencing kit	Applied Biosystems
Dexoynucleotide triphosphates	Roche
DNA oligonucleotide synthesis primers	MWG Biotech UK Ltd

ExoSAP-IT	GE Healthcare
Expand long range	Roche
HiDi	Applied Biosystems
Taq DNA polymerase	New England Biolabs
TaqMan master universal PCR master mix	Applied Biosystems

2.1.3.6 PCR-RFLP reagents

[α-^{32}P]-dCTP (3,000 Ci/mmol)	Amersham Pharmacia
Acrylamide:bisacrylamide 29:1 40%	Amresco
Ammonium Acetate	BDH
AgeI	New England Biolabs
AluI	New England Biolabs
BbsI	New England Biolabs
DraI	New England Biolabs
Fun4HI	New England Biolabs
HaeIII	New England Biolabs
HinfI	New England Biolabs
MaeIII	New England Biolabs
Mn1I	New England Biolabs
Pellet Paint® Co-Precipitant	Novagen

2.1.3.7 Western blot reagents

3-[cyclohexylamino]-1-propanesulphonic acid (CAPS)	Sigma
Acrylamide:bisacrylamide (29:1) 30%	Amresco
Bradford assay kit	Biorad
Dried skimmed milk	Premier Int. Foods Ltd.
ECL-Plus Western detection kit	Amersham
Expand long template PCR system	Roche
Glycine	Sigma
Immobilon transfer membrane	Millipore
Methanol	Fisher Scientific
Mouse anti beta actin antibody	Dako
Mouse anti Complex I subunit GRIM-19	MitoSciences
Mouse anti-OXPHOS complex I -20	MitoSciences
Mouse anti-OXPHOS complex I -30	MitoSciences
Mouse anti-OXPHOS complex II-70	Invitrogen
Poloxyethylenesorbitan monolaurate (Tween 20)	Sigma
β-mercaptoethanol	Sigma
Rabbit anti-mouse horse radish peroxidase	Dako
Rabbit IgG secondary antibody-HRP	Abcam
Rabbit polyclonal IgG Anti-MnSOD	Upstate

2.1.3.8 Blue-Native PAGE reagents

AminoCaporic acid	Sigma
Bis-Tris	Sigma
Digitonin	Fluka
Hydrochloric Acid (HCL)	BDH
Laurylmaltoside (n-Dodecyl β–D-maltoside)	Sigma
Nitro tetrazolium Blue (NBT)	Sigma
Reduced nicotine amide adenine dinucleotide (NADH)	Sigma
Serva Blue G-250	AMS Biotechnology
Tricine	Sigma

2.1.3.9 Respiratory chain complex measurement reagents

Acetyl Coenzyme	Sigma
Albumin bovine serum (BSA)	Sigma
Antimycin A	Sigma
Digitonin	Fluka
2, 6-dichlorophenolindophenol (DCPIP)	Sigma
5, 5`-dithio-bis-(2-nitobenzoic acid) (DTNB)	Sigma
Ethylenediaminetetracetic acid (EDTA)	USB Corp.
Ethyleneglycolbis (β-aminoethyl ether)-N, N, N`, N`-tetraacetic acid (EGTA)	Sigma

4-(2-hydroxyethyl) piperazine-1-(2-ethanesulfonic acid)	
(HEPES)	Sigma
Oxaloacetic acid	Sigma
Potassium Bicarbonate ($KHCO_3$)	Sigma
Potassium Cyanide (KCN)	Sigma
Potassium Chloride (KCL)	Sigma
Potassium phosphate (KH_2PO_4)	Sigma
Rotenone	Sigma
Sodium succinate Triton X-100	Sigma
Sucrose	BDH
Ubiquinone-1	Sigma

2.1.3.10 Flow cytometry reagents

Dihydrorhodamine123 (DHR)	Molecular Probes
(5,5', 6,6'-tetrachloro-1,1', 3,3'- tetraethylbenzimidazolylcarbocyanine-	
iodide (JC1)	Molecular Probes
MitoSOX	Molecular Probes
10-n-nonyl-acridine (NAO)	Molecular Probes

2.1.3.11 The GeneChip human resequencing array 2.0 reagents

GeneChip® Resequencing Assay Kit	Affymetrix
GeneChip® Resequencing Reagent Kit	Affymetrix
LA PCR Kit Ver. 2.1 kit	TaKaRa Bio Inc.

DNA Amplification Clean-Up Kit Clontech

2.1.4 Solutions

Nanopure (18 MegaOhms activity) water was used to prepare the solutions listed below. In some cases, distilled water was used as specified.

Medium B:

120mM KCl,20mM HEPES,5mM $MgCl_2$,1mM EGTA,5mg/ml BSA

DNA loading buffer:

0.25% (w/v) Bromophenol Blue, 0.25% (w/v) Xylene Cyanol, 30% (v/v) Glycerol

Electrophoresis buffer:

100ml 10x TAE, 900ml water, 80µl ethidium bromide

Separating gel (Western blot):

3.75ml of 30% acrylamide (acrylamide:bisacrylamide (29:1)) , 2.81 ml 1M separating buffer, 0.82ml d.H_2O, 37.5µl 20% SDS,75µl 10% AMPS,7.5 µl TEMED

Western blot stacking gel

0.67ml of 30% acrylamide (acrylamide:bisacrylamide (29:1)), 0.25ml 0.5M stacking buffer, 4.05ml d.H_2O, 25 µl 20% SDS, 25 µl 10% AMPS,5 µl TEMED

Lysis buffer:

(170µl of l50mM Tris/HCl, 150mM NaCl, 2mM $MgCl_2$), 28µl of 7x Roche protease inhibitors (1tablet in 1.5ml of d.H_2O), 2µl Nonidet P-40

5% Milk solution in TTBS:

5g skimmed milk powder, 100ml TTBS

1M Phosphate buffer:

Buffer A: 3.12g of Sodium dihydrogen phosphate ($NaH_2PO_4 \cdot 2(H_2O)$) in 50ml d.H_2O

Buffer B: 14.15g of Disodium hydrogen phosphate (Na_2HPO_4) in 250ml d.H_2O

1M Phosphate buffer: 47.5µl of buffer A + 202.5µl of buffer B up to 500ml with d.H_2O.

4% Paraformaldehyde (pH 7.4):

500ml of d.H_2O (65^oC), 40g of Paraformaldehyde, drops of 1M NaOH, 500ml of 1M phosphate buffer

1X Phosphate buffered saline:

1 tablet of Phosphate Buffered Saline in 100ml water

Western blot Running buffer (pH 8.8 with 5M HCl):

3g Trizma base, 14.4g Glycine, 1g SDS, Water up to 1L

Western Blot transfer buffer:

6g Trizma base, 28.8g Glycine, 0.02% SDS, 15% Methanol, Water up to 1L

Western Blot sample buffer:

10ml Stacking buffer, 4ml Glycerol, 4ml 20% SDS, 0.02g Bromophenol blue, 2ml water

Western blot separating buffer (1M Tris-HCl pH, 8.8 with 5M HCl):

60.55g Trizma base in 500ml water

Western blot stacking buffer (0.5M Tris-HCl, pH 6.8 with 5M HCl):

30.275g trizma base in 500ml water

TTBS pH 7.6:

2.42g Trizma base in 1l water, 8g NaCl, 0.1% Tween 20, drops of 1M NaOH

BN-PAGE anode buffer (50 mM Bis-Tris; pH 7.0 with 5M HCl):

19.68g AminoCaproic Acid, 3.1386g Bis-Tris, 100ml water

BN-PAGE cathode buffer A (15mM Bis-Tris; 50mM Tricine; 0.02% Serva Blue G-250; pH 7.0 with 5M HCl):

1.57g Bis-Tris, 4.48g Tricine, 0.1g Serva Blue G-250, 1L water

BN-PAGE cathode buffer B (15 mM Bis-Tris; 50 mM Tricine; pH 7.0 with 5M HCl):

1.57g Bis-Tris, 4.48g Tricine, 1L water

BN-PAGE transfer buffer (25mM Tris, 192mM Glycine, 20% methanol, 0.02% SDS, pH 8.2 with 5M HCl):

5.24g Tris, 14.44g Glycine, 200ml methanol, 1ml 20% SDS, 799ml water

BN-PAGE sample buffer (750mM AminoCaproic acid, 50mM Tricine, 0.5mM EDTA, 0.02% Serva blue G-250, pH 7.0 with 5M HCl):

3.75ml of 2M AminoCaproic acid, 1.0ml of 500mM Bis-Tris, 0.05ml 100mM EDTA, 0.5g Serva Blue G-250, 10ml water

BN-PAGE dissociation solution (1% SDS and 1% β-mercaptoethanol):

0.5ml 20% SDS, 0.1ml β-mercaptoethanol, 10ml water

2.2 Methods

2.2.1 DNA Extraction

Often patient blood, buccal, muscle, and urine DNA samples arrived at the lab already extracted; if not, DNA was extracted. When fibroblasts from patients were provided, DNA was extracted from fibroblasts cultured in 25cm^2 flasks.

2.2.1.1 Total DNA extraction from fibroblasts

Harvested cell pellets were washed twice with 1XPBS and, following the last wash, cells were resuspended in 2ml of 1XPBS and centrifuged at full speed (13000 rpm for 10 minutes). The

resulting pellets were resuspended in 400µl TE/H_2O (25:75) before 50µl of 10% SDS and 50µl of proteinase K (20mg/ml) were added. Samples were then incubated overnight at 37^oC.

The following day one volume (500µl) of Phenol was added to the cell lysate to remove proteins. Samples were vortexed briefly, centrifuged at full speed for 5 minutes at room temperature, and the upper aqueous layer was removed to a clean 1.5 ml eppendorf tube. A mix of 250µl of phenol and 250µl of chloroform: isoamyl alcohol (24:1) was added, vortexed, and the samples centrifuged at full speed again for 5 minutes. Samples were again washed with 500µl chloroform: isoamyl alcohol and centrifuged at full speed for 10 minutes. The aqueous layer, 500µl, was moved to a clean 2ml eppendorf tube and 50µl of 3M NaAc, pH 5.2 and 1ml of absolute ethanol were added, then samples were frozen at -80^oC for more than an hour. Samples were centrifuged at 20817*g* for 10 minutes and the resulting pellets were washed with 70% ethanol. Samples were spun down again for 5 minutes at full speed, the supernatants were removed, and the pellets were allowed to air-dry for 10 minutes. Finally, DNA was resuspended in an appropriate volume of 25:75 TE/H_2O to give a final concentration of ~ 100ng/ml. DNA concentration was quantified by ND-1000 spectrophotometer.

2.2.1.2 Total DNA extraction from blood

EZ1 Blood DNA extraction Kit was used to extract DNA from 5ml blood sample according to the manufacturer's protocol. Extracted DNA was resuspended in an appropriate amount of TE/dH_2O (25:75) according to the pellet size to give a final concentration of 100ng/ml. Samples were stored at -20^oC.

2.2.1.3 Total DNA extraction from hair

Hair follicles were carefully dissected into 1.5ml eppendorf tubes and then 30µl of Tris-EDTA buffer pH 7.4 were added. Samples were centrifuged at 14000rpm for 10 minutes at room temperature. Supernatants were removed and 10µl of DNA extraction buffer (50mM Tris-HCl pH8.5, 1mMEDTA, 0.5% Tween 20 (containing 200µg/ml proteinase K) were added to the pellets. Samples were incubated at 55^oC for 2 hours, during which time samples were centrifuged every 15 minutes. After 2 hours, tubes were centrifuged at 14000rpm for 1 minute at room temperature and incubated at 95^oC to inactivate the proteinase K.

2.2.1.4 Total DNA extraction from single muscle fibres

COX/SDH stained PEN membrane slides were allowed to air dry for 1 hour prior dissecting single-muscle fibres for analysis. Fibres with normal histochemical COX activity (COX positive) and abnormal COX activity (COX deficient) were randomly selected and dissected from the sections using the Leica laser micro-dissection system. To isolate total DNA from single muscle fibres, single cells were cut into separate sterile 0.5ml tubes and centrifuged at full speed for 10 minutes. 10-30µl of cell lysis buffer (0.5M Tris-HCL, pH8.5, 1mM EDTA, 0.5% Tween-20, and 200ng/ml proteinase K) were added to cells, incubated at 55^{o}C for 2 hours followed by 10 minute incubation at 95^{o}C to facilitate proteinase K inactivation.

2.2.1.5 Total DNA extraction from homogenate tissue

A DNAeasy tissue extraction kit was used to extract DNA from ~25mg of homogenate tissue according to the manufacturer's protocol. Extracted DNA was resuspended in an appropriate amount of TE/dH_2O (25:75) according to the pellet size to give a final concentration of ~ 100ng/ µl and stored at -20^{o}C.

2.2.1.6 Total DNA extraction from urine sediment

Phenol/Chloroform extraction was used to extract DNA from urine sediment. Urine samples were centrifuged at 6000rpm for 10 minutes and the supernatant removed. The pellet cells were incubated overnight at 37^{o}C in Proteinase K (0.5mg/ml) diluted in TNES buffer (0.5M Tris-HCl pH 7.4, 1mM EDTA, 0.1M NaCl, 1%SDS).

The following day, one volume (500µl) of Phenol was added to the samples to remove proteins. Samples were vortexed briefly and centrifuged at full speed for 5 minutes at room temperature. The upper aqueous layer was removed to a clean 1.5 ml eppendorf tube and a mix of 250µl of phenol and 250µl of chloroform: isoamyl alcohol (24:1) was added prior to vortexing and centrifugation at full speed for 5 minutes. Samples were again washed with 500µl chloroform: isoamyl alcohol and centrifuged at full speed for 10 minutes. The aqueous layer (500µl) was moved to a clean 2 ml eppendorf tube and 50µl of 3M NaAc, pH 5.2 and 1ml of absolute ethanol were added. Samples were then frozen at -80^{o}C for more than an hour. Samples were centrifuged at 20817*g* for 10 minutes and pellets were washed with 70% ethanol then spun down for 5minutes at full speed. Supernatants were removed and pellets were allowed to air-dry for 10 minutes. Finally, the DNA was resuspended in an appropriate

volume of 25:75 TE/H_2O to give a final concentration of 100ng/ml. DNA concentration was quantified as previously described (section 2.2.1.1).

2.2.2 DNA quantification

A NanoDrop ND-1000 spectrophotometer and ND-1000 software was used to quantify 1µl of the extracted DNA.This software calculates and displays A_{260}/A_{280} ratios to determine both DNA concentration and quality.

2.2.3 Preparation of human muscle tissue

Iso-pentane was pre-cooled to -160^{o}C in liquid nitrogen and muscle tissue was placed on Whatman grade 1 filter paper using OCT as an adhesive. This was then rapidly frozen by immersion in pre-cooled iso-pentane for 15 seconds. Frozen tissue was transported in a liquid nitrogen container and stored at -80^{o}C. To cut sections for histological and histochemical staining, a Cryo-star HM 560M cryostat was used; the internal temperature was set at -19^{o}C and the knife at -21^{o}C.

2.2.4 Tissue culture

A humidified incubator was used to incubate all cells at 37^{o}C with 5% CO_2. All procedures were performed using aseptic techniques, sterile equipment and reagents in a Class II biological cabinet. Periodically, cells were tested for possible Mycoplasma contamination using a MycoAlert® mycoplasma detection kit according to the manufacturer's instructions**.**

2.2.4.1 Cell manipulations

Patients` cultured skin fibroblasts, either frozen in liquid nitrogen or referred for investigation, were grown in Dulbecco's Modified Eagle Medium supplemented with 10% fetal calf serum, 25mg/ml uridine and 1% penicillin-streptomycin.

2.2.4.2 Cell passaging and harvesting

Both medium and trypsin were pre-warmed at 37^{o}C in the incubator prior to use. Cells were washed with 1xPBS. Depending on the size of flask, sufficient trypsin was added to cover the surface of the flask, which was then incubated in 37^{o}C incubator for 1-2 minutes to dislodge the cells from the flask. Complete growth medium was added to prevent further proteolysis by quenching the trypsin**.**

To continue growing the cells, they were split into new flasks, supplemented with complete medium, according to the density of cells. Medium was changed every 3-4 days depending on the speed of cell growth.

Alternatively, cells were harvested at this stage for analysis after washing twice with 1XPBS. Following each wash, cells were pelleted by centrifugation at 1200 rpm for 3 minutes at room temperature and supernatant was aspirated off.

2.2.4.3 Freezing cells

To freeze cells down, they were harvested as previously described and pellets were resuspended in freezing media containing fetal calf serum and 10% DMSO. 1ml of freezing media was added to 90% confluent cells from 75cm^2 flask in 1.8ml Cryo tubes. Aliquots were frozen at -80^{o}C and then transferred to liquid nitrogen for long-term storage the following day.

2.2.5 Generation of cybrids

*Trans*mitochondrial cytoplasmic hybrids (cybrids) were generated by fusing the enucleated patents' fibroblasts (cytoplasts) with the osteosarcoma cell line 143BTK (ρ^o) which was entirely depleted of mtDNA following long-term exposure to low concentrations of ethidium bromide [292].

One day before starting the fusion, 20ml of a 1:1 mix of DMEM (10%FCS, 1% Pen-Strep, 25mg/ml uridine) and Percoll was prepared and allowed to equilibrate at 37^{o}C overnight. Confluent fibroblasts were harvested as previously described (section 2.2.4.2) and enucleated using Percoll isopycnic gradient as described in [314]. Harvested cells were washed in 1xPBS and resuspended in the DMEM/Percoll mix. 80µl of cytochalasin B (5mg/ml in DMSO) were added and samples were centrifuged at 25^{o}C for 70 minutes at 16500 rpm for enucleation. The cytoplast layer was collected, washed with DMEM, centrifuged at 650*g* for 10 minutes and the resulting pellet was resuspended in10ml of DMEM. Confluent ρ^o cells were harvested and resuspended in 5ml DMEM. Then both cytoplasts and ρ^o cells were mixed thoroughly, aliquoted evenly in two 25cm^2 flasks and allowed to attach for 4-5 hours at 37^{o}C. Cells were washed with serum free DMEM twice, 1.5ml of Polyethylene Glycol (PEG) 1500 was added to each flask, agitated for 1 minute, and cells washed again with serum free DMEM three times. 10ml of DMEM were added to each flask and cells were then incubated at 37^{o}C overnight.

The following day, cells were harvested, resuspended in 100ml of DMEM, and evenly aliquoted into four 24-well cell culture plates (1ml/well). The following day, DMEM was removed and replaced with uridine-free selection DMEM containing 10% dialyzed FCS, 100µg/ml BrdU and 1% Pen-Strep to select cybrids (Figure 2-1).

After the appearance of colonies, these were harvested, resuspended in selection medium and aliquoted into 6-well cell culture plates. Finally, the colonies were selected and expanded in 12-well and then 24-well plates.

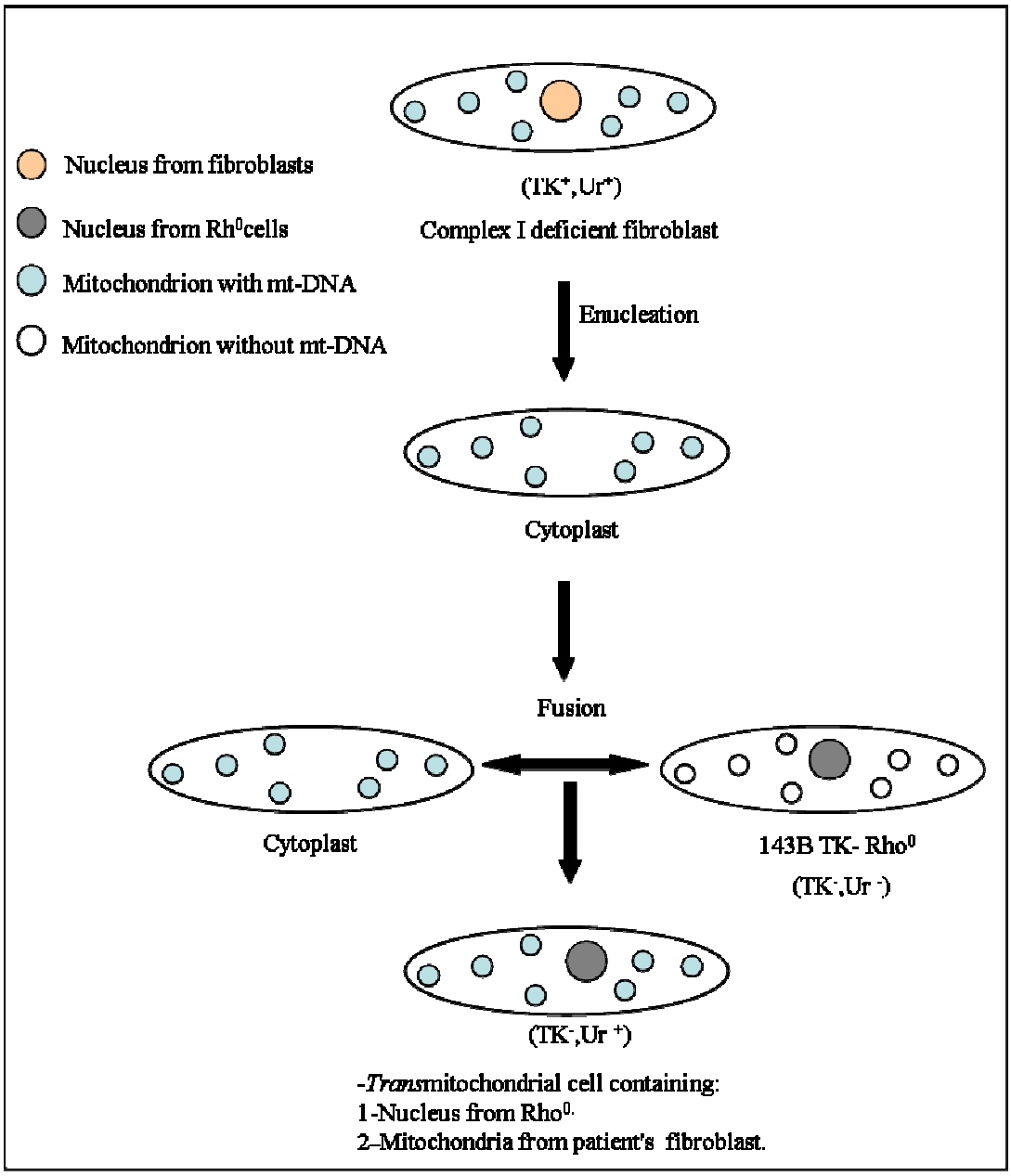

Figure 2-1 The establishment of *trans*mitochondrial cytoplasmic hybrids (Cybrids).

This diagram illustrates the procedure for the isolation of *trans*mitochondrial cell lines. The mitochondrial donor cells, which are thymidine kinase positive (TK^+) and are able to synthesize uridylic acid (UR^+), are enucleated and mixed with the recipient 143B TK- Rho^0 cells, which are TK^- and UR^-. The cytoplasts are fused with Rho^0 cells in the presence of Polyethylene Glycol (PEG) 1500. The *trans*mitochondrial cells are then selected from the resulting populations by their ability to grow in the absence of uridine (to select for mitochondrial function) and in the presence of bromodeoxyuridine (BrdU, to select against cell hybrids and donor cells).

2.2.6 Mitochondrial genome sequencing

DNA from extracted samples was used to amplify the entire mitochondrial genome by PCR. Samples with a DNA concentration lower than 100ng/ul were amplified using two rounds of PCR, while samples with a DNA concentration equal to 100ng/ul or higher were amplified using a second round of PCR amplification.

2.2.6.1 The first round PCR amplification

This PCR was carried out using nine fragments of overlapping primer pairs (Table 2-1), which have an identical annealing temperature (60^{o}C) to avoid any variation in PCR program. Primer sequences were based on the revised Cambridge Reference Sequence (rCRS) [252].

The PCR reactions were performed in total volume of 50µl, containing 2µl DNA as a template, 5µl of 10X dNTPs, 5µl of 10X PCR buffer, 2µl of 25mM $MgCl_2$ solution, 1.5µl of 20µM forward primer, 1.5µl of 20µM reverse primer, and 0.35 of AmpliTaq Gold DNA polymerase. PCR-graded dH_2O was added to make a final reaction volume of 50µl.

The PCR cycling conditions for the amplification included an initial denaturation at 95^{o}C for 10 minutes to activate the polymerase followed by 38 cycles at 94^{o}C denaturation for 45 seconds, 60^{o}C primer annealing for 45 seconds, and 72^{o}C primer extension for 2 minutes. Lastly, final extension at 72^{o}C for 8 minutes was included. In all cases a positive control and a negative control (no DNA) were included. The first round PCR products were diluted 1/3 in sterile water prior to being used as DNA template for the second round PCR amplification.

2.2.6.2 The second round PCR amplification

Amplification was carried out using 36 overlapping pairs of primers with a similar annealing temperature (60^{o}C). In addition, they were engineered to be tagged with universal M13-tails to facilitate sequencing of the PCR products (Table 2-2). The M13 forward primer sequence was 5'-TGTAAAACGACGGCCAGT-3' and the reverse primer M13-tag sequence was 5'-CAGGAAACAGCTATGACC-3'. The PCR products from the first round PCR and other DNA samples for PCR were used as DNA templates for second round PCR.

Table 2-1 First round PCR primer sequences.

Mitochondrial First Round Primer Sequences			
Fragment		Sequence	Position
A	Forward	5’-GCTCACATCACCCCATAAAC-3’	627 - 646
	Reverse	5’-GATTACTCCGGTCTGAACTC-3’	3087 - 3068
B	Forward	5’-ACCAACAAGTCATTATTACCC-3’	2395 - 2415
	Reverse	5’-TGAGGAAATACTTGATGGCAG-3’	4653 - 4633
C	Forward	5’-CCGTCATCTACTCTACCATC-3’	4489 - 4508
	Reverse	5’-GGACGGATCAGACGAAGAG-3’	6468 - 6450
D	Forward	5’-AATACCCATCATAATCGGAGG-3’	6113 - 6133
	Reverse	5’-GGTGATGAGGAATAGTGTAAG-3’	8437 - 8417
E	Forward	5’-TCAATGCTCTGAAATCTGTGG –3’	8167 - 8187
	Reverse	5’-TCGAAGCCGCACTCGTAAG-3’	10103 - 10165
F	Forward	5’-ACTTCACGTCATTATTGGCTC-3’	9821 - 9841
	Reverse	5’-ATAGGAGGAGAATGGGGGATAG-3’	12101 - 12080
G	Forward	5’-ACTGTGCTAGTAACCACGTTC-3’	11866 - 11887
	Reverse	5’-GGTAGAATCCGAGTATGTTGG-3’	13924 - 13904
H	Forward	5’-TATTCGCAGGATTTCTCATTAC-3’	13721 - 13742
	Reverse	5’-GTGCTAATGGTGGAGTTAAAG-3’	15989 - 15969
I	Forward	5’-CCCATCCTCCATATATCCAAAC -3’	15695 - 15680
	Reverse	5’-GGTTAGTATAGCTTAGTTAAAC-3’	868 - 847

Table 2-2 Sequence of the second round PCR primers.

Mitochondrial Second Round primer sequences			
Fragment		Sequence	Base pairs
1	Forward	5`-TGTAAAACGACGGCCAGTTCACCCTCTAAATCACCAG-3`	721 - 740
	Reverse	5`-CAGGAAACAGCTATGACCGATGGCGGTATATAGGCTGAG-3`	1268 - 1248
2	Forward	5`-TGTAAAACGACGGCCAGTTTAAAACTCAAAGGACCTGGC-3`	1157 - 1177
	Reverse	5`-CAGGAAACAGCTATGACCCTGGTAGTAAGGTGGAGTGGG-3`	1709 - 1689
3	Forward	5`-TGTAAAACGACGGCCAGTAACTTAACTTGACCGCTCTGAG-3`	1650 - 1671
	Reverse	5`-CAGGAAACAGCTATGACCATTGGTGGCTGCTTTTAGG-3`	2193 - 2175
4	Forward	5`-TGTAAAACGACGGCCAGTACTGTTAGTCCAAAGAGGAAC-3`	2091 - 2111
	Reverse	5`-CAGGAAACAGCTATGACCTCGTGGAGCCATTCATACAG-3`	2644 - 2625
5	Forward	5`-TGTAAAACGACGGCCAGTCAGTGACACATGTTTAACGGC-3`	2549 - 2569
	Reverse	5`-CAGGAAACAGCTATGACCGATTACTCCGGTCTGAACTC-3`	3087 - 3068
6	Forward	5`-TGTAAAACGACGGCCAGTCAGCCGCTATTAAAGGTTCG-3`	3017 - 3036
	Reverse	5`-CAGGAAACAGCTATGACCGGAGGGGGGTTCATAGTAG-3`	3574 - 3556
7	Forward	5`-TGTAAAACGACGGCCAGTACCATCACCCTCTACATCAC-3`	3505 - 3524
	Reverse	5`-CAGGAAACAGCTATGACCAGAGTGCGTCATATGTTGTTC-3`	4057 - 4037
8	Forward	5`-TGTAAAACGACGGCCAGTTCGCCCTATTCTTCATAGCC-3`	3965 - 3984
	Reverse	5`-CAGGAAACAGCTATGACCGTTTATTTCTAGGCCTACTCAG-3`	4577 - 4556
9	Forward	5`-TGTAAAACGACGGCCAGTACACTCATCACAGCGCTAAG-3`	4518 - 4537
	Reverse	5`-CAGGAAACAGCTATGACCGATTTTGCGTAGCTGGGTTTG-3`	5003 - 4983
10	Forward	5`-TGTAAAACGACGGCCAGTCTCACTCTCTCAATCTTATCC-3`	4932 - 4952
	Reverse	5`-CAGGAAACAGCTATGACCTGTAGGAGTAGCGTGGTAAGG-3`	5481 - 5462
11	Forward	5`-TGTAAAACGACGGCCAGTACCTCAATCACACTACTCCC-3`	5367 - 5386
	Reverse	5`-CAGGAAACAGCTATGACCTAGTCAACGGTCGGCGAAC-3`	5924 - 5906
12	Forward	5`-TGTAAAACGACGGCCAGTAGATTTACAGTCCAATGCTTC-3`	5855 - 5875
	Reverse	5`-CAGGAAACAGCTATGACCATGGCAGGGGGTTTTATATTG-3`	6430 - 6410
13	Forward	5`-TGTAAAACGACGGCCAGTTAGCAGGTGTCTCCTCTATC-3`	6358 - 6377
	Reverse	5`-CAGGAAACAGCTATGACCAAGAAAGATGAATCCTAGGGC-3`	6944 - 6924
14	Forward	5`-TGTAAAACGACGGCCAGTATTTAGCTGACTCGCCACAC-3`	6863 - 6882
	Reverse	5`-CAGGAAACAGCTATGACCCATCCATATAGTCACTCCAGG-3`	7396 - 7376
15	Forward	5`-TGTAAAACGACGGCCAGTGGCTCATTCATTTCTCTAACAG-3`	7272 - 7293
	Reverse	5`-CAGGAAACAGCTATGACCGGCAGGATAGTTCAGACGG-3`	7791 - 7773
16	Forward	5`-TGTAAAACGACGGCCAGTTCCTAACACTCACAACAAAAC-3`	7713 - 7723
	Reverse	5`-CAGGAAACAGCTATGACCTACAGTGGGCTCTAGAGGG-3`	8301 - 8283
17	Forward	5`-TGTAAAACGACGGCCAGTACAGTTTCATGCCCATCGTC-3`	8196 - 8215
	Reverse	5`-CAGGAAACAGCTATGACCGTATAAGAGATCAGGTTCGTC-3`	8740 - 8720
18	Forward	5`-TGTAAAACGACGGCCAGTACCACCCAACAATGACTAATC-3`	8656 - 8676
	Reverse	5`-CAGGAAACAGCTATGACCGTTGTCGTGCAGGTAGAGG-3`	9201 - 9183

Mitochondrial Second Round primer sequences			
Fragment		Sequence	Base pairs
19	Forward	5`-TGTAAAACGACGGCCAGTATCCTAGAAATCGCTGTCGC-3`	9127 - 9146
	Reverse	5`-CAGGAAACAGCTATGACCATTAGACTATGGTGAGCTCAG-3`	9661 - 9641
20	Forward	5`-TGTAAAACGACGGCCAGTCATCCGTATTACTCGCATCAG-3`	9607 - 9627
	Reverse	5`-CAGGAAACAGCTATGACCTAGCCGTTGAGTTGTGGTAG-3`	10147 - 10128
21	Forward	5`-TGTAAAACGACGGCCAGTCAACACCCTCCTAGCCTTAC-3`	10085 -10104
	Reverse	5`-CAGGAAACAGCTATGACCAGGCACAATATTGGCTAAGAG-3`	10649 - 10629
22	Forward	5`-TGTAAAACGACGGCCAGTATCGCTCACACCTCATATCC-3`	10534 - 10553
	Reverse	5`-CAGGAAACAGCTATGACCATGATTAGTTCTGTGGCTGTG-3`	11109 - 11089
23	Forward	5`-TGTAAAACGACGGCCAGTTATCCAGTGAACCACTATCAC-3`	11010 - 11030
	Reverse	5`CAGGAAACAGCTATGACCTAGGTCTGTTTGTCGTAGGC-3`	11605 - 11586
24	Forward	5`-TGTAAAACGACGGCCAGTTCCTTGTACTATCCCTATGAG-3`	11541 - 11561
	Reverse	5`-CAGGAAACAGCTATGACCCGTGTGAATGAGGGTTTTATG-3`	12054 - 12034
25	Forward	5`-TGTAAAACGACGGCCAGTCTCCCTCTACATATTTACCAC-3`	11977 - 11997
	Reverse	5`-CAGGAAACAGCTATGACCGTGGCTCAGTGTCAGTTCG-3`	12545 - 12527
26	Forward	5`-TGTAAAACGACGGCCAGTCTCTTCCCCACAACAATATTC-3`	12478 - 12498
	Reverse	5`-CAGGAAACAGCTATGACCCTGATTTGCCTGCTGCTGC-3`	13009 - 12991
27	Forward	5`-TGTAAAACGACGGCCAGTGCCCTTCTAAACGCTAATCC-3`	12940 - 12959
	Reverse	5`-CAGGAAACAGCTATGACCGGGAGGTTGAAGTGAGAGG-3`	13453 - 13435
28	Forward	5`-TGTAAAACGACGGCCAGTCGGGTCCATCATCCACAAC-3`	13365 - 13383
	Reverse	5`-CAGGAAACAGCTATGACCGTTAGGTAGTTGAGGTCTAGG-3`	13859 - 13839
29	Forward	5`-TGTAAAACGACGGCCAGTACCTAAAACTCACAGCCCTC-3`	13790 - 13809
	Reverse	5`-CAGGAAACAGCTATGACCAGGATTGGTGCTGTGGGTG-3`	14374 - 14356
30	Forward	5`-TGTAAAACGACGGCCAGTATTAAAGTTTACCACAACCACC-3`	14317 - 14341
	Reverse	5`-CAGGAAACAGCTATGACCAAGGAGTGAGCCGAAGTTTC-3`	14857 - 14838
31	Forward	5`-TGTAAAACGACGGCCAGTATTCATCGACCTCCCCACC-3`	14797 - 14815
	Reverse	5`-CAGGAAACAGCTATGACCGGTTGTTTGATCCCGTTTCG-3`	15368 - 15349
32	Forward	5`-TGTAAAACGACGGCCAGTCATCTTGCCCTTCATTATTGC-3`	15295 - 15315
	Reverse	5`-CAGGAAACAGCTATGACCTACAAGGACAGGCCCATTTG-3`	15896 - 15877
D1	Forward	5`-TGTAAAACGACGGCCAGTATCGGAGGACAACCAGTAAG-3`	15758 - 15777
	Reverse	5`-CAGGAAACAGCTATGACCAGGGTGATAGACCTGTGATC-3`	019 - 001
D2	Forward	5`-TGTAAAACGACGGCCAGTCTCAACTATCACACATCAACTG-3`	16223 - 16244
	Reverse	5`CAGGAAACAGCTATGACCAGATACTGCGACATAGGGTG-3`	129 - 110
D3	Forward	5`-TGTAAAACGACGGCCAGTCCTTAAATAAGACATCACGATG-3`	16548 - 16569
	Reverse	5`-CAGGAAACAGCTATGACCCTGGTTAGGCTGGTGTTAGG-3`	389 - 370
D4	Forward	5`-TGTAAAACGACGGCCAGTGCCACAGCACTTAAACACATC-3`	323-343
	Reverse	5`-CAGGAAACAGCTATGACCTGCTGCGTGCTTGATGCTTG-3`	771 - 752

The bold sequence in each primer highlights the relevant M13-tag.

The PCR reactions were performed in total volume of 25µl containing 1µl DNA as template at ~100ng/µl concentration, 2.5µl of 10X dNTPs, 2.5µl of 10X PCR buffer, 1µl of 20µM forward primer, 1µl of 20µM reverse primer, and 0.13µl of AmpliTaq Gold DNA polymerase. PCR-graded dH_2O was added to make a final reaction volume of 25µl.

PCR cycling conditions for the amplification included an initial denaturation at 95^oC for 10 minutes to activate the polymerase followed by 30 cycles at 94^oC denaturation for 45 seconds, 58^oC primer annealing for 45 seconds, and 72^oC primer extension for 1 minute. Lastly, amplification was allowed for final extension at 72^oC for 8 minutes. In all cases a positive and negative control, which had no DNA, were included in the PCR amplification set up.

2.2.7 Agarose gel electrophoresis

Upon amplification, 5µl of PCR products were investigated by running samples on 1.5% agarose gels together with Hyperladder IV to confirm amplification and product size. The 1.5% agarose gel was prepared by mixing 1.5g of agarose and 100ml of 1XTAE buffer containing 5µg/ml ethidium bromide; this was microwaved for around 2 minutes. Agarose was allowed to cool to 60^oC, poured into a sealed casting tray into which well-forming combs were inserted. 1XTAE buffer was added to the tank then 5µl of PCR product and 5µl of Hyperladder IV were individually mixed with 0.5-1µl of 10X loading buffer and loaded into the wells. Gels were electrophoresed at 65-80 Volts, depending on the tank size to allow separation of PCR products. Gels were subsequently examined under a UV light source to visualize bands.

2.2.8 Cycle sequencing

In the cycle sequence stage, 5µl of PCR products were added to the wells of a 96 well-plate and a 2µl of ExoSAP-IT were added while the plate was kept on ice. The plate was covered with a rubber mat, briefly mixed and pulse spun. The plate was incubated in the thermal cycler for 15 minutes at 37^oC followed by 80^oC for 15 minutes. The ExoSAP-IT enzyme functions to remove free dNTPs and any non-specific products such as single stranded DNA molecules to give pure double-stranded PCR products.

To cycle sequence, the following volumes of reagents were added to each sample: 7µl of water, 3µl of 5X sequencing buffer, 1µl of the universal forward primer, and 2µl of Big-Dye v3.1. Then samples were cycle sequenced on the thermal cycler with initial denaturation at

96°C for 1 minute followed by 25 cycles at 96°C for 10 seconds denaturation, 50°C for 5 seconds annealing, 60°C for 4 minutes extension. Finally, samples were precipitated prior to sequencing on an ABI 3130xI genetic analyser.

To precipitate PCR products, 2µl of 125mM EDTA, 2µl of 3M sodium acetate, and 50µl of 100% Ethanol were added to each of the cycle sequenced samples in the 96-well plate. The plate was capped, inverted 4 times to mix the samples and incubated at room temperature for 15 minutes. The plate was centrifuged at 2090*g* for 30 minutes and supernatants were removed by inverting the plate onto a pad of white paper towels and pulse spun at 100*g*. Then 70µl of 70% Ethanol were added to the samples, the plate was spun down at 1650*g* for 15 minutes and supernatants were removed as previous described. The plate was left to air dry at room temperature for 15-20 minutes before adding 10µl of HiDi. Finally, before loading the plate into the machine, the plate was covered and heated to 95°C for 2 minutes in a 9700 PCR block.

2.2.9 Sequence analysis

Sequenced samples were analyzed using Applied Biosystems SeqScape analysis software. The recorded changes were compared to two, web-based human mtDNA sequence databases [69, 252] to see if they were neutral, recurrent or novel changes.

2.2.10 Restriction fragment length polymorphism (RFLP) analysis

Putative pathogenic mtDNA mutations in tissues and/or cells from patients were further investigated to quantify the relative proportion of the wild-type and mutant mtDNA by RFLP as described in [315-318].

PCR reactions were performed as previously described (section 2.2.5.2). The PCR reaction contained 1µl DNA, 5µl 10X PCR buffer, 5µl dNTPs, 1.5µl forward primer, 1.5µl reverse primer, 0.35µl Taq DNA polymerase, and d.H_2O to make a final volume of 50µl. Samples were incubated in the thermal cycler and PCR products were electrophoresed on 1.5% agarose gel to confirm amplification and product size.

Subsequently, PCR products were subjected to an additional (last hot) PCR cycle consisting of 95°C denaturation, 2 minutes annealing at 58°C and extension for 8 minutes at 72°C, following the addition of 0.25µl of α-^{32}P-dCTP, 1µl of forward primer, 1µl of reverse primer

and 0.25ul of Taq polymerase to the reactions. Labelled samples were precipitated in 50µl dH_2O, 2µl pellet paint, 50µl ammonium acetate, and 200µl absolute ethanol. Samples were then left for 1 hour at room temperature followed by centrifugation at 13000 rpm for 10 minutes. Supernatants were removed and the pellets were washed with 100µl of 70% ethanol. Samples were then centrifuged again for 10 minutes at full speed, supernatants aspirated and pellets were allowed to air-dry for 10 minutes.

Radioactivity in each sample was measured using a Cerenkov counter. Pellets were resuspended in dH_2O to give a final concentration of 1000 counts per 17µl. For digestion, 17µl of radiolabelled PCR product, 1µl of restriction endonuclease, and 2µl of enzyme-specific buffer were mixed and incubated overnight at the optimal working temperature for each enzyme. An uncut sample (no digestion enzyme) and a control sample were always included. Finally, 20µl of product were mixed with 3µl of 10X loading dye and loaded onto 12% Polyacrylamide gel electrophoresis.

2.2.11 Polyacrylamide gel electrophoresis

12% polyacrylamide gels were prepared by mixing 12ml of 40% acrylamide (29:1bisacrylamide), 4ml of 10XTBE, 24ml of water, 75µl of 25% ammonium persulfate (APS), and 75µl of N,N,N`,N`-tetramethylenediamine (TEMED). Gels were then poured into a vertical gel cast with a comb to form wells and allowed to polymerize at room temperature. Then 1X TBE buffer was added into the tank and 20µl of digested PCR product mixed with 3µl of 10X loading buffer, were loaded into wells. Gels were electrophoresed at 100V for the first hour and then the voltage was turned up to 150V. Samples were allowed to separate further for approximately 5-6 hours. Gels were transferred onto a Whatman paper, covered with saran wrap and allowed to dry for 1-2 hours at 65^{o}C in a gel dryer. Dried gels were exposed to a PhosphorImager screen overnight and the following day gels were scanned using a Storm scanner. Radioactivity in each band was quantified using ImageQuant software.

2.2.12 Long-range PCR

An expanded long-range PCR system was used to investigate possible mtDNA deletions in patient samples. Muscle DNA was screened for mtDNA rearrangements by 10 or 11 kb long-range PCR assays. The PCR reaction, with a total volume of 50µl, contained 0.5µl of 100ng/µl DNA, 10µl of 1x reaction buffer, 2.5µl of 10mM dNTPs-Mix, 1.5µl of 20pmol of each primer, 1.5µl of 100% DMSO, 0.7µl of the enzyme mix (5U/µl) and 31.3µl of dH_2O.

The PCR conditions for the amplification included initial denaturation at 92^{o}C for 2 minutes to activate the polymerase followed by 10 cycles of denaturation at 92^{o}C for 10 seconds, annealing at 58^{o}C for 15 seconds, and a 68^{o}C primer extension for 11 minutes, followed by 15 cycles at 92^{o}C for 10 seconds, 25 cycles at 58^{o}C for 15 seconds, and 68^{o}C for 11 minutes plus 5 seconds/cycle. A final extension step of 68^{o}C for 7 minutes followed.

5µl of PCR product were mixed with 2µl of 10x loading buffer and loaded onto a 0.7% agarose gel, alongside 5µl of Hyperladder IV. The gel was electrophoresed at 65-80Volts and PCR products were visualized under UV light.

2.2.13 Real time PCR

To quantify the possibility of both mtDNA rearrangements and depletion in patients, a real time PCR assay was used. The PCR primers for ND1 were the forward primer L3485–3504 (5`-CCCTAAAACCCGCCACATCT-3`) and the reverse primer H3532–3553 (5`-GAGCGATGGTGAGAGCTAAGGT-3`). The PCR primers for ND4 were the forward primer L12087–12109 (5`-CCATTCTCCTCCTATCCCTCAAC-3`) and the primer H12140–12170 (5`-GTGTTAGACTACAAAACCAATTTGATATAAA-3`). The fluorogenic probes were for ND1 L3506–3529 (5`-CCATCACCCTCTACATCACCGCCC-3`) and for ND4 L12111–12138 (5`-CCGACATCATTACCGGGTTTTCCTCTTG). The PCR reaction contained: 5µl of cell lysate from a single muscle fibre, 12.5µl of TaqMan Universal PCR Master Mix, 0.5µl of both ND1 and ND4 probes (100nM), 0.75µl of both forward and reverse ND1 and ND4 primers (300nM) and 7.5µl of dH_2O. The PCR amplification conditions were: 2 minutes at 50°C, 10 minutes at 95°C, 40 cycles of 15 seconds at 95°C, and 1 minute at 60°C for probe/primer hybridisation and DNA synthesis.

2.2.14 Measurement of activity of respiratory chain complexes

2.2.14.1 Preparation of mitochondrial fractions from cultured cells

Mitochondrial fractions were prepared from confluent cultured fibroblast cells. Cells were harvested as previously described (section 2.2.4.2), except pellets were resuspended in 1ml of Buffer B (120mM KCl, 20mM HEPES, 5mM $MgCl_2$, 1mM EGTA, 5mg/ml BSA). Cells were transferred to a glass homogeniser and disrupted with 20 strokes of a motor-driven, Teflon plunger on ice. Homogenates were transferred to a new 1.5 eppendorf tube, centrifuged for 10 minutes at 600*g*, and supernatants were kept on ice in 1.5ml tube. Pellets were resuspended in 0.8ml of buffer B, homogenised again and centrifuged for 10 min at 600*g*. Supernatants from

this step were added to the retained supernatants and combined samples were centrifuged for 20 minutes at 20,000*g*. Supernatants were removed, while the resulting pellets containing mitochondria were resuspended in an appropriate volume of buffer B (~ 80µl) according to the pellet size, prior to being stored at -80^{o}C until use.

Measurement of the activities of repiratory chain complexes were carried out in triplicate, at at 30^{o}C and final volume of 1ml, using a Varian Cary 300 Bio spectrophotometer with temperature controller and WinUV software. The mitochondrial fractions of pig heart were used as standard control. All mitochondrial fractions were washed prior to use and diluted 1:5 in a hypotonic buffer, containing 25mM potassium phosphate, 5mM magnesium chloride, pH 7.2, followed by rapid freezing in liquid nitrogen and thawing at 30^{o}C. Measurement of complexes I and II and citrate synthase from mitochondrial fractions were performed individually as described in [235, 319, 320].

2.2.14.2 Complex I (NADH: ubiquinone oxidoreductase) activity

The specific activity of complex I was measured by following the decrease in absorbance due to the oxidation of NADH at 340nm with 425nm as the reference wavelength. 978.5µl of complex I buffer (hypotonic buffer plus 2.5mg/ml of albumin bovine serum (BSA) and 1M KCN), 10µl of 9mg/ml NADH, 2.5µl of 65µM of ubiquinone-1, and 2µl of 1mg/ml of antimycin A were mixed in each cuvette and the absorbance change was recorded for about 20 seconds to ensure that the baseline was stable. Then 5µl of mitochondrial dilution were added and the NADH: ubiqunione oxidoreductase activity was measured for 5 minutes. 2µl of 2µg/ml of rotenone were added and the activity was measured for an additional 4 minutes. Complex I activity is the rotenone-sensitive NADH:ubiqunione oxidoreductase activity.

2.2.14.3 Complex II (Succinate: ubiquinone oxidoreductase) activity

The specific activity of complex II was measured by following the reduction of 2, 6-dichlorophenol-indophenol (DCPIP), which was used as an artificial acceptor, at 600nm.

5µl of diluted mitochondria, 958.5µl of complex II buffer (complex I buffer but without BSA), and 2µl of 1M sodium succinate were preincubated for10 minutes at 30^{o}C prior to use. Then 10µl of 5mM DCPIP, 2µl of antimycin A, and 2µl of rotenone were added to the previous mix and the baseline rate was recorded for 10 seconds. The reaction was started by

adding 2.5µl of ubiqunione$_1$ and the enzyme-catalysed reduction of DCPIP was measured for 4 minutes.

2.2.14.4 Citrate synthase activity

The activity of citrate synthase was assayed by measuring the rate of production of coenzyme A (CoA.SH) from oxaloacetate by measuring free sulfhydryl groups using the thiol reagent 5,5`-dithio-bis-(2-nitobenzoyic acid) (DTNB) which reacts with sulfhydryl groups to produce free 5-thio-2-nitrobenzoate anions with yellow colour that can be detected at 412nm.

967µl of citrate synthase buffer (0.1M Tris-HCl, pH8.0), 3µl of 5mM acetyl Coenzyme, 10µl of 10mM DTNB, 10ul of 10% Triton X-100, and 5µl of mitochondrial dilution were mixed in a cuvette then the baseline rate was recorded for 20 second. The reaction was started by adding 5µl of 50mM oxaloacetate and the activity was recorded for at least 2 minutes.

Citrate synthase is the most commonly used mitochondrial matrix marker enzyme for the integrity of the mitochondria and all activities are referenced to citrate synthase activity [235].

2.2.15 Histological and histochemical analysis

2.2.15.1 Haematoxylin and Eosin (H&E) staining

Muscle sections were cut from muscle biopsies frozen at -80^{o}C using a cryostat. For Haematoxylin and Eosin staining, muscle sections were cut at 12µM onto glass microscope slides and allowed to air dry for an hour. Slides were fixed in formal calcium solution for 15 minutes and washed in tap water until the water ran clear. Sections were immersed for 1 minute in Meyer's Haematoxylin solution (1% (w/v) Haematoxylin, 50% (w/v) Potassium Alum, 0.2% (w/v) Sodium Iodate, 1% (w/v) Citric Acid, and 50% (w/v) Chloral Hydrate). Sections were washed in water for 1 minute. Then sections were immersed for 30 seconds in Eosin solution (1% Eosin, 0.4% (w/v) Erythrosin B and 0.2% (w/v) Phloxin B) and washed in water for 1minute. Stained sections were dehydrated in a graded ethanol series (70%, 95%, 2x100%), and immersed in absolute ethanol for 10 minutes. Finally, sections were mounted in DPX with a glass coverslip and stored at room temperature.

2.2.15.2 Cytochrome *c* oxidase & succinate dehydrogenase staining

To investigate cytochrome *c* oxidase (COX) activity, sections were cut at 12µm onto polyethylenenaphthalate (PEN) membrane slides and allowed to air dry for 1 hour prior to

being stained. For COX staining, sections were incubated for 45 minutes at 37^{o}C in COX media (4mM diaminobenzidine Tetrahydrochloride (DAB), 100mM cytochrome *c*, and 20µg/ml catalase in 0.1M phosphate buffer, pH7.0). Subsequently, sections were rinsed twice in PBS and dried using tissue paper. Finally, sections were dehydrated in a graded ethanol series and allowed to dry. Slides were stored at -20^{o}C in sealed slide mailers until used.

For succinate dehydrogenase (SDH) activity, sections were cut as previously described onto glass microscope slides and allowed to air dry for 1 hour. For staining, slides were incubated for 45 minutes at 37^{o}C in SDH media (1.5mM Nitro Blue Tetrazolium (NBT), 130mM sodium succinate, 0.2mM phenazine methoslphate (PMS), and 0.1mM sodium azide in 0.1M phosphate buffer, pH7.0). Slides were then rinsed twice in PBS, dehydrated as above, and then immersed in absolute ethanol for 10 minutes to remove purple monoformazan reaction product of the SDH reaction. Eventually, sections were dehydrated in a graded ethanol series to dry, and stored at room temperature.

2.2.16 Immunohistochemisry

To investigate protein localization and expression patient tissues, X-Cell-Plus HRP Detection kit and Liquid Stable DAB kit were used. Sections from muscle biopsies were cut at 12µM onto glass microscope slides and allowed to air dry for 1 hour prior to staining. Sections were fixed in 4% Paraformaldehyde in 0.1M for 10 minutes, washed in dH_2O in a fume hood and washed in TBS containing 0.1% Tween 20 for 10 minutes. Sections were then permeablised and endogenous peroxidise activity was inhibited by immersion in a graded methanol series (10% for 10 minutes, 95% + 0.3% H_2O_2 for 10 minutes, absolute methanol for 20 minutes, 95% + 0.3% H_2O_2 for 10 minutes, 10% for 10 minutes and TBST for 5 minutes). Diluted primary antibodies in TBST were then applied to sections for an hour at room temperature. Sections were washed twice with TBS for 5 minutes and once with TBST for 5 minutes. Sections were overlaid with the universal probe for 30 minutes and followed by 2X wash for 5 minutes with TBS and once with TBST for 5 minutes. The HRP polymer was applied to sections and followed with 3X wash with TBS for 5 minutes. After drying the sections, DAB was applied and sections were left at room temperature until a brownish colour appeared. Sections were washed, immersed for 1 minute in Haematoxylin solution and washed in dH_2O. A graded ethanol series (70%, 95%, and 100%) was used to dehydrate the sections before immersing them in Histoclear. Finally, sections were mounted in DPX with a glass coverslip and stored at room temperature.

2.2.17 Bradford assay

This assay was used to quantify protein in whole cell lysates. Two sets of measurements at a final volume of 800µl were made. The first mix contained 1µl of cell lysis, 200µl of Bradford reagent and 799µl of d.H_2O. The second mix contained 5µl of the same sample, 200µl of Bradford reagent, and 795µl of dH_2O. To create a standard curve, different concentration of bovine serum albumin (0µg, 2µg, 5µg, 10µg, 15µg, 20µg) were also prepared. The samples were then loaded in an optical bottom 96-well plate which was loaded into an automated plate reader. Finally, the generated standard curve report was used to calculate protein concentrations.

2.2.18 Western blotting assay
2.2.18.1 Sample preparation

To prepare samples, cultured fibroblasts were allowed to reach confluence before being harvested with trypsin as described (section 2.2.4.2). After the last wash with 1xPBS, 100µl of cell lysis buffer (50mM Tris-HCl pH 7.5, 150mM NaCl, 2mM $MgCl_2$), 28µl of proteinase inhibitor and 2µl of Nonidet P-40 were added to the pellets (from75cm^2 flasks). Samples were then vortexed for 30 seconds and centrifuged at 562*g* for 3 minutes at 4^oC. Supernatant were moved to new 1.5ml eppendorf tubes and equal volumes of buffer containing 10mM Tris-HCl were added. Finally, samples were mixed and quantified by Bradford assay or frozen at -80^oC until use.

2.2.18.2 Gel preparation

Gels were prepared using a minigel system (Mighty Small II SE250) and were cast in gel caster. Prior to pouring the gels, leakage was checked with water. The separating gels (3.75ml 30% acrylamide, 2.81ml 1M Separating buffer, 0.82ml dH_2O, 37.5µl 20% SDS, 75µl 10% AMPS and 7.5µl TEMED) were poured first, overlaid with dH_2O-butanol to give a flat gel and allowed to polymerise for 30 minutes. Gels were washed with dH_2O to remove the d.H_2O-butanol before pouring the stacking gels (0.67ml 30% acrylamide, 0.25ml 0.5M stacking buffer, 4.05ml dH_2O, 25µl 20% SDS,25µl 10% AMPS and5µl TEMED). Combs were inserted and the gels were left to polymerise for 15 minutes.

2.2.18.3 Western blot electrophoresis

After protein quantification, 10-25 µg/µl of protein and 5µl of sample buffer containing 2% β-mercaptoethanol were mixed. Lysis buffer was added to a final volume of 10µl. In addition, 5µl of sample buffer were added to 5µl of Kaleidoscope prestained standard. Samples were denatured at 90°C for 10 minutes in a heat block and were pulse spun prior to loading.

Wells were washed with running buffer before loading the samples. Gels were run at 75V (17mA) for ~ 15 minutes and then the voltage was increased to 150V once the dye front entered the separating gel. Electrophoresis was stopped when the dye ran off the bottom of the gel.

2.2.18.4 Protein transfer

For protein transfer, the blotting sandwich was set up as follows: black side of the cassette, a wet pad, 2x filter papers, the flipped gel, PDVF membrane, 2x filter papers, wet pad and the white side of the cassette. To avoid bubbles between gel and membrane, a glass roller was used to roll over the membrane. Protein transfer was carried out using a Hoefer TE series electrophoresis unit. The assembled cassette was placed into the transfer tank with the black side adjacent to the negative electrode. The transfer tank was filled with a cold transfer buffer containing (25mM Trizma base, 192mM Glycine, 0.02% SDS, and 15% methanol). The transfer was performed at 4ºC by electrophoresis at 65V (300mA) for 3 hours with continual stirring.

2.2.18.5 Membrane immunoblotting

Non-specific binding was blocked by incubating the membrane in 5% milk in TTBS (20 mM Trizma base, 136mM NaCl, pH7.6 and 0.1% Tween 20) for at least one hour at room temperature or overnight at 4ºC on a shaking platform. The membrane was incubated with the primary antibodies for 90 minutes at 4ºC on a shaking platform. The membrane was then washed with TTBS twice for 5 minutes and once for 10 minutes on the shaker at room temperature to remove excess primary antibody. The membrane was incubated with the secondary antibody for 90 minutes as previously described. Eventually, the membrane was washed in TTBS on the shaking platform twice for 5 minutes and once for 15 minutes.

2.2.18.6 Signal detection

To visualise bands, an ECL Plus Western blotting Detection kit was used. The membrane was incubated with 500µl of reagent A and 12.5µl of reagent B for 5-10 minutes. To visualize the fluorescent signals, a Storm 860 PhosphorImager and ImageQuant software were used.

2.2.19 First dimension blue native-PAGE assay

2.2.19.1 Crude mitochondrial purification

Fibroblasts were cultured until they reached confluence and were then washed twice with 1XPBS at room temperature to remove all traces of serum from the culture media. Cells were harvested as described (section 2.2.4.2) by using 1ml of trypsin for < 3 minutes at 37^{o}C and then 9ml of serum containing culture medium were added to inhibit trypsin. Cells were then centrifuged at 1200rpm for 3 minutes at room temperature and pellets were washed twice with cold 1XPBS. The recovered pellets were resuspended in 100µl of cold 1XPBS. Cell suspensions were transferred to new 1.5ml eppendorf tubes on ice and 100µl of (8mg/ml in cold PBS) digitonin were added. Cell suspensions were vortexed, incubated for 10 minutes on ice and centrifuged for 10 minutes at 10,000*g* at 4^{o}C. Supernatants were aspirated and mitochondrial pellets were washed twice in cold 1XPBS and centrifuged as previously described. After the last wash, supernatants were aspirated and mitochondrial pellets were snap frozen in liquid nitrogen to limit the effect of ice crystals prior to being stored at -80^{o}C.

2.2.19.2 Solubilising mitochondria proteins

Mitochondrial pellets were solubilised by vigorously pipetting up and down in 100µl of AC/BT Buffer (2M aminocaprioc acid and 50mM Bis-Tris/HCl adjusted to pH7.0 with HCl) and 20µl of 10% detergent dodecylmaltoside (10% w/v in dH_2O) on ice. Samples were then vortexed and incubated on ice for 5-10minutes. Lastly, they were centrifuged at 20,000*g* for 20 minutes at 4^{o}C and supernatants were transferred to new 1.5ml eppendorf tubes on ice.

A small volume of the supernatants was taken to quantify the mitochondrial proteins by Bradford assay. 10µl of blue native sample buffer (750mM aminocaprioc acid, 50mM Bis-Tris/HCl, pH7.0, 0.5mM EDTA and 5% Coomassie Blue) were added to the mitochondrial suspensions on ice and samples were loaded onto the blue native gels as soon as possible.

2.2.19.3 BN-PAGE gradient polyacrylamide gel preparation

A minigel system (Mighty Small II SE250) was used to carry out the blue native page electrophoresis. The gel sandwich was assembled and placed on the manual casting stand. Prior to pouring gels, leakage was checked using water. The gradient casting set-up (gradient mixer, peristaltic pump, and gel casting stand) was assembled and the gradient mixer outflow tubing was inserted between the glass plates.

The separating (5% & 12%) gel solutions and stacking (4%) gel solution were prepared at $4^{o}C$ to slow down polymerisation (Table 2-3).

Table 2-3 Summary of BN-PAGE gel preparation.

Components	**4% Stacking Gel**	**5% Separation Gel**	**12% Separation Gel**
40% Acryl: bis (29:1)	0.50 ml	0.44 ml	1.05 ml
Gel Buffer	1.67 ml	1.16 ml	1.16 ml
Glycerol	-	-	0.55 ml
dH_2O	2.83 ml	1.9 ml	0.74 ml
Volume	5 ml	3.5 ml	3.5 ml
10% APS	55µl	21µl	21µl
TEMED	5.5µl	2.1µl	2.1µl

Before pouring the 5% separating gel solution in compartment A and the 12% solution in compartment B of the gradient mixer, the connection valve between them was closed, Continual stirring was applied to compartment B, at low speed to avoid air-bubble formation, which can affect gel polymerisation. The 12% gel solution was released first from the gradient mixer, with the peristaltic pump's speed set at 10ml/min and the switch set to 4 for 20 seconds. The connection valve between compartments A and B was then opened to allow the

5% gel solution to mix with the remaining 12% solution and the flow rate was set to 1ml/min and the switch to 8 until both compartments were empty. Gels were then overlaid with dH_2O-Butanol and allowed to polymerise at room temperature. After polymerisation, the dH_2O-Butanol was washed with dH_2O and then the 4% stacking gels were poured. Combs were inserted and the gels were allowed to polymerise at room temperature.2.2.19.4 BN-PAGE electrophoresis

After gel casting and prior to loading the samples, the comb was removed and wells were washed with cathode Buffer A. 10µl of sample buffer was added to 50µg of protein on ice and samples were loaded into the wells as soon as possible. Anode Buffer (50mM Bis-Tris; pH7.0) was added to at positive electrode and cathode Buffer A (15mM Bis-Tris, 50mM Tricine, 0.02% Serva Blue G-250; pH7.0) to the negative electrode. Gels were run at 30V for 30 minutes until the samples started to enter the stacking gel, then the voltage was increased to 80V for 90 minutes. The cathode Buffer A was changed to cathode Buffer B (15mM Bis-Tris, 50mM Tricine, pH7.0) once the dye front had progressed to half or two-thirds of the way through the separating gel. Gels were left to run at 80V for >60 minutes until the dye front ran off the end of the gel.

2.2.19.5 In gel enzyme activity assay

BN-PAGE gels were incubated for one hour at room temperature with complex I activity detecting solution containing 2mM Tris-HCL, pH7.4, 0.1mg/ml NADH and 2.5mg/ml nitrotetrazolium blue (NTB). Gels were then washed with dH_2O and scanned using EPSON Expression 1680 pro scanner and EPSON scan software.

2.2.19.5 Western blot of BN-PAGE

For protein transfer, gels were covered with a dissociation solution (1% of SDS and 1% β-mercaptoethanol) in a fume hood for one hour at room temperature and then excess solution was removed by washing with dH_2O. The blotting sandwich was assembled as follows: black side of the cassette, a wet pad, 2X filter papers, the gel, PDVF membrane, 2X filter papers, wet pad, and the white side of the cassette. To avoid bubbles between the gel and membrane, a glass roller was used to roll over the membrane. Protein transfer was carried out using a Hoefer TE series electrophoresis unit. The assembled cassette was placed into the transfer tank with the black side adjacent to the negative electrode. The transfer tank was filled with

blotting Buffer (25mM Bis-Tris, 192mM glycine, 20% methanol, 0.02% SDS pH8.2) and transfer was performed at 4ºC by electrophoresis at 100V for 1 hour with continual stirring.

2.2.19.5.1 Membrane immunoblotting of BN-PAGE

Non-specific binding was blocked by incubating the membrane in 5% milk in TTBS (20mM Trizma base, 136mM NaCl, pH7.6, 0.1% Tween 20) for at least an hour at room temperature or overnight at 4ºC on a shaking platform. The membrane was then incubated with the primary antibody for 90 minutes at 4ºC on a shaking platform. Later, the membrane was washed with TTBS twice for 5 minutes and once for 10 minutes on the shaker at room temperature to remove excess primary antibody. The membrane was then incubated with the secondary antibody for 90 minutes on a shaking platform at room temperature. Eventually, the membrane was washed twice with TTBS on the shaking platform for 5 minutes and once for 15 minutes.

2.2.19.5.2 Signal detection of BN-PAGE gel

For signal detection, an ECL Plus Western Blotting Detection kit was used. The membrane was incubated with 500µl of reagent A and 12.5µl of reagent B for 5-10 minutes. To visualize the fluorescent signals a Storm 860 PhosphorImager and ImageQuant software were used.

Chapter 3

An Investigation into the role of complex I mtDNA mutations in mitochondrial disease

Chapter 3 : An Investigation into the role of complex I mtDNA mutations in mitochondrial disease

3.1 Introduction

Mitochondria are the main site for energy production in the form of ATP generation by oxidative phosphorylation. This task is achieved by five multi-protein complexes embedded in the inner mitochondrial membrane. OXPHOS disorders are the most frequent causes of metabolic diseases in paediatric neurology [321] with an incidence of 1:5000 live births [231, 322]. They are heterogeneous and range from fatal encephalomyopathies of early childhood to severe diseases of adulthood [323]. They can affect different organs, tissues, or be multisystemic, however, tissues which require more energy such as the brain, heart, and skeletal muscles are more likely to be affected [82]. The OXPHOS system contains ~ 85 proteins, the majority of them are encoded by nuclear DNA; the remaining 13 proteins are encoded by the mitochondrial genome. OXPHOS diseases are therefore associated with a variety of different clinical phenotypes [324]. Such disorders can affect mitochondrial membrane potential, ATP synthesis, ROS production, and calcium homeostasis [324].

Complex I is the largest and least understood of the respiratory chain complexes, as described earlier in chapter 1. Mitochondrial energy metabolism disorders due to deficiencies in complex I are the most frequently seen cases. Only ~20% of those disorders seen in children are due to mutations in the mtDNA suggesting that the majority of such disorders are due to mutations in nuclear genes [324, 325]. Most of the clinical phenotypes due to mutations in the nuclear subunits of complex I occur in infancy and early childhood, whereas, clinical phenotypes due to mutations in the mitochondrial subunits present between both childhood and adulthood [82].

Mitochondrial DNA mutations causing isolated complex I disease have been reported in all of the seven subunits of complex I [323]. Mutations in the ND1 subunit have been associated with encephalopathy [326], MELAS [327], and sudden infant death [328]. Mutations in the ND2 subunit have been linked to encephalomyopathy [329], Leigh syndrome [330], and LHON [331]. Mutations in the ND3 subunit resulted in LHON [332] and Leigh syndrome [333]. Mutations in the ND4 subunit have been linked to MELAS [334] and LHON [335]. Several diseases have been linked to mutations in the ND5 subunits such as LHON [336], MELAS [337], optic neuropathy/retinopathy [338-340], MELAS/Leigh disease [339], ataxia,

and PEO [341]. Finally, mutations in the ND6 subunit result in LHON [342], MELAS [343], Leigh disease [341], and myopathy [344]. Interestingly, mutations in the mt-tRNA$^{Leu(UUR)}$ (the m.3302A>G) [212, 345] and the mt-m.3243A>G [346] also caused isolated complex I defects.

In addition, defects in one or more of complex I subunits may give rise to defects or instability of its assembly suggesting that integrity of this complex is essential for its function. Several patients have been reported with mutations in the mitochondrial genome or the nuclear genome had a defect in complex I assembly (Table 3-1). At least half of all observed cases of complex I deficiency are caused by defects in the assembly of the complex [82]. Mutations in complex I assembly chaperones reduce both the activity of complex I and the assembly of the holoenzyme [72]. A mutation in complex I intermediate associated protein (CIA30), termed NDUFAF1, caused a cardioencephalomyopathy, reduced levels and activity of complex I [89, 91]. Also, a mutation in the complex I assembly chaperone B17.2L caused progressive encephalopathy and reduced complex I assembly [89, 347]. Recently, a mutation in the chromosome 6 open reading frame 66 gene (C6ORF66) caused infantile mitochondrial encephalomyopathy, antenatal cardiomyopathy, and reduced assembly of complex I [325]. Furthermore, a defect in the apoptosis-inducing factor (AIF) reduced both complex I enzymatic activity and assembly [348-350]. Lastly, mutations in other genes that interact with the complex I assembly chaperones resulted in complex I assembly defects. For example, the evolutionarily conserved signaling intermediate in Toll pathways protein (Ecsit), which is essential for the inflammatory response and embryonic development [351, 352] impaired complex I assembly and disturbed mitochondrial function [353].

As mentioned previously in Chapter 1, mitochondrial complex I is the first step in the electron transport oxidizing NADH to NAD^+ and transferring electrons to coenzyme Q10. During glycolysis, pyruvate is produced from glucose in the cytoplasm of the cell. Pyrvate can be converted into lactate by lactate dehydrogenase (LDH), under anaerobic conditions or transported into the mitochondria and converted into acetyl-coenzyme A (CoA) by the pyruvate dehydrogenase (PDH) complex. The PDH complex is regulated by two enzymes: pyruvate dehydrogenase phosphatase and pyruvate dehydrogenase kinase in addition to the ratio of both NADH/NAD^+ and acetyl-CoA/CoA. Increases in these ratios inhibit the PDH complex. Acetyl-CoA and fatty acids are oxidized in the citric acid cycle, producing NADH and $FADH_2$. Complex I oxidizes NADH to NAD+ and complex II oxidizes $FADH_2$ which together initiate the electron transport chain (Figure 3-1). A defect in complex I or other

OXPHOS complexes results in a disturbed oxidation ratio of NADH to NAD+ leading to mitochondrial disease [70]. In addition, the NADH to NAD^+ ratio and concentrations have been shown to regulate the production of ROS in studies from isolated mitochondria [62, 354], which can explain the involvement of ROS production in some OXPHOS disorders.

Table 3-1 List of mutations in patients reported to affect complex I assembly.

Human Gene	References
mtDNA	
MTND1	[316, 355]
MTND2	[330]
MTND3	[242, 333]
MTND4	[356, 357]
MTND5	[315, 358]
MTND6	[359, 360]
Nuclear	
NDUFA1	[361]
NDUFS1	[362, 363]
NDUFS2	[364]
NDUFS4	[365, 366]
NDUFS6	[367]
NDUFS7	[368]
NDUFS8	[369, 370]
NDUFV1	[347, 362]
Assembly proteins	
NDUFAF1	[91]
NDUFA12L	[347]
C6orf66	[325]
C20orf7	[371]
C3orf60	[372]

(Taken and modified from [72]).

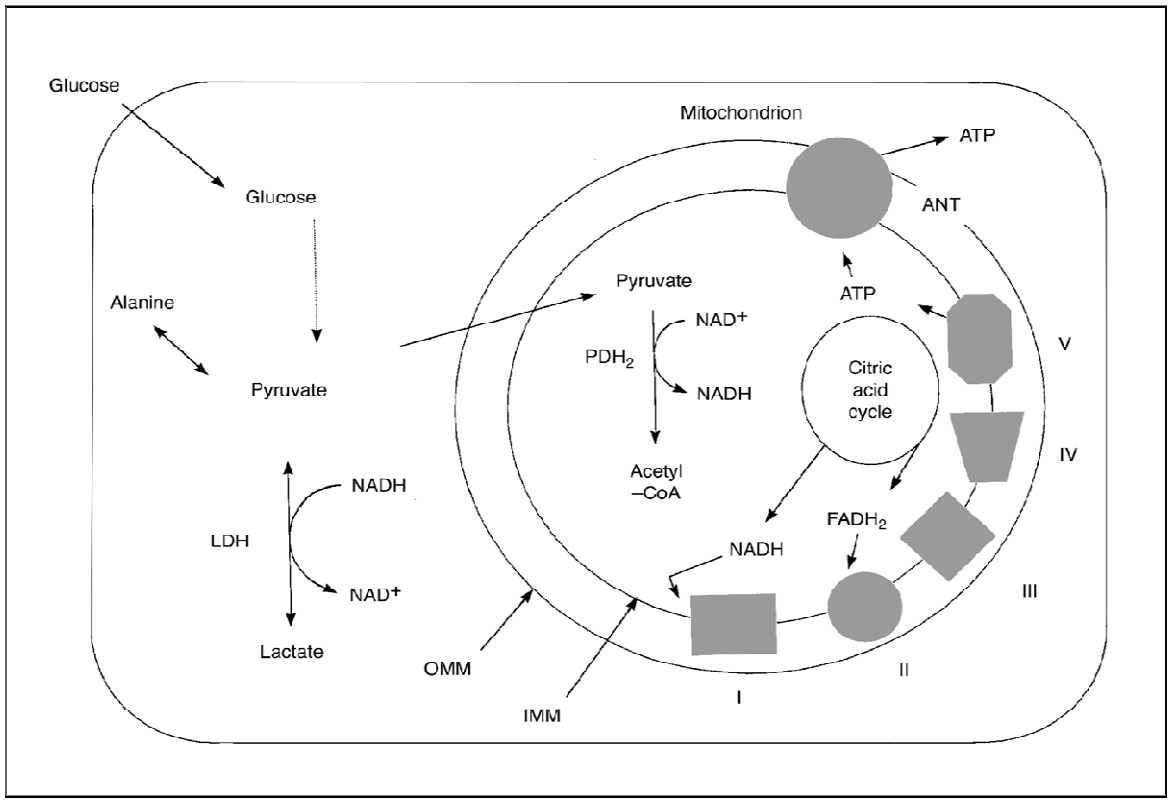

Figure 3-1 Schematic representation of ATP synthesis through the oxidation of pyruvate.

In the cytoplasm of the cell, pyruvate is produced from glucose and either converted into lactate by lactate dehydrogenase (LDH). Alternatively, pyruvate is transported into the mitochondria and converted into acetyl-coenzyme A by the pyruvate dehydrogenase (PDH2) complex through pyruvate dehydrogenase phosphataise, pyruvate dehydrogenase kinase, and NADH/NAD^+ ratios. NADH and $FADH_2$, which are produced from citric acid cycle, initiate the electron transport chain by binding to complex I and II respectively to produce ATP. CoA: coenzyme A, OMM: outer mitochondrial membrane, and IMM: inner mitochondrial membrane, I: complex I, II: complex II, III: complex III, IV: complex IV, and V: complex V (taken from [70]).

3.2 Aims

This chapter will present the clinical, biochemical, and molecular genetic investigations in a cohort of patients. Some of the patients were already confirmed to have a defect in complex I based on initial biochemical investigations including direct measurements of complex I activity by spectophotometry or BN-PAGE. Some others were suspected to have a defect in complex I due to the expression of clinical phenotypes previously-related to complex I deficiency. Although this Chapter describes patients with complex I, also it describes another patient with a mutation in Complex IV. This patient was referred based on clinical phenotypes related to complex I deficiency.

3.3 Summary of clinical presentations

All clinical phenotypes and other information related to the investigated patients are summarized in Table 3-2.

Table 3-2 Summary of clinical phenotypes and other related information for investigated patients.

Patients	**Age**	**Clinical phenotypes**	**Biochemical investigations**	**Identified mt-DNA mutations**
Canadian patients (4)	adults	-	Complex I deficiency	No pathogenic mtDNA mutations identified
Japanese patients (7)	children	Congenital lactic acidosis, cardiomyopathy	Complex I deficiency	No pathogenic mtDNA mutations identified
1	11	Seizure, weakness, strokes, lactic acidosis.	COX deficient fibres, Isolated complex IV defect in muscle	m.7023G > A *MTCO1*
2	42	LHON- like optic neuropathies.	Normal complex I activity	m.11453G>A *MTND4*
3	14	Ataxia, bulbar palsy, extensive progressive deterioration, and white matter changes on MRI	Complex I deficiency	m.11777C>A *MTND4*
4	10	Leigh syndrome phenotypes: delayed milestones, deafness, ataxia, bilateral basal ganglia changes on MRI; and high levels of lactate in CSF	Normal respiratory chain enzymes	m.13051G>A *MTND5*
5	4	Leigh syndrome phenotypes: developmental delay, acquired microcephaly, microcephaly, left ventricle hypertrophy, and high blood and CSF lactate.	Complex I deficiency in muscle	m.13513G>A *MTND5*

6	8	Spasms, pigmentary retinopathy, encephalopathy, increased blood lactate, and changes in basal ganglia on MRI ,	Complex I deficiency in muscle	m.14453G>A *MTND6*
7	10	Hypotonia, failure to thrive, elevated blood and CSF lactate, and abnormal MRI	Isolated complex I defect	m.7792C>G *MTCO2* m.12055A>G *MTND4* (silent changes)
8	-	General body ache and weakness	-	m.10632T>C *MTND4* (silent change)
9	4	Fever, acute deterioration in consciousness; high blood and CSF lactates; left ventricular hypertrophy;and white matter changes on MRI	Normal COX activity and low complex I and IV activity;	m.12645C>T *MTND5* (silent change)
10	46	CPEO	COX deficient fibres	m.13095T>C *MTND5* (silent change)
11	35	Unusual multiple sclerosis presentation with optic atrophy	Normal biochemistry in muscle	No pathogenic mtDNA mutations identified
12	8 months	Hypertrophic cardiomyopathy	Reduced complex I and IV activities COX defect	No pathogenic mtDNA mutations identified
13	17	Myoclonic epilepsy, diabetes, and learning difficulties	Many pale staining COX fibres Rreduced complex I activity	No pathogenic mtDNA mutations identified

3.4 Materials and methods

3.4.1 Patients` samples preparation

Upon arrival of the patient samples in the lab, the DNA was extracted from the different tissues (blood, buccal, fibroblasts, hair, and urine) as previously described (section 2.2.1).

3.4.2 Mitochondrial DNA sequencing

The entire mitochondrial genome from total muscle homogenate, blood, or fibroblasts was performed as described (section 2.2.6) to search for mtDNA point mutations or rearrangement leading to the disease.

3.4.3 Generation of cybrids

To establish the pathogenic role of the identified mtDNA mutations, *trans*mitochondrial cytoplasmic hybrids (cybrids) were generated by fusing cytoplasts from patient carrying the m.11777A>C with the osteosarcoma cell line 143BTK$^-$ and were grown under selection conditions as previously described (section 2.2.5).

3.4.4 PCR-RFLP analysis

PCR-RFLP analysis was carried on DNA samples from different tissues from patient and relatives where available to quantify mutation load in investigated tissues and to determine whether the mutation is sporadic or maternally transmitted. Table 3.3 summarises details for this analysis such as primer position, sequences, restriction endonuclease enzymes, and annealing temperatures. All restriction fragments were separated on a 12% polyacrylamide gel as previously described (section 2.2.11).

3.4.5 Measurement of activity for respiratory chain complexes

The specific activities of complex I, II, and citrate synthase were measured in these patients as previously described (section 2.2.14).

3.4.6 Flow cytometry

Flow cytometry was used to assess different cellular properties of fibroblasts from the patient with the identified mtDNA. This included measuring ROS production levels, membrane potential, and mitochondrial mass. Statistics were performed using SigmaStat

3.5 software (Systat Software Inc, USA) and two-sample unpaired Student t-tests between each patient and control sample were carried out to determine statistical significance. This part was done in association with Dr.Gabriele Saretzki (International centre for Life, bioscience Centre).

3.4.6.1 Cells preparation

Cells were grown until confluent using serum supplemented DMEM and then were harvested as described (section 2.2.4.2). Cells (~200,000) were transferred to 15ml Falcon tubes for centrifugation at 1200rpm for 3 minutes at room temperature. Supernatants were removed by aspiration and replaced with the specific probe solution.

3.4.6.2 MitoSOX staining

The working concentration for MitoSOX was 5µM **(**1µl stock solution/1ml serum-free DMEM). To measure mitochondrial superoxide levels, cells (~200,000) were resuspended in MitoSOX solution (200µl of solution/sample), mixed well and incubated for 15 minutes at 37^{o}C. Cells were then centrifuged at 1200rpm for 3 minutes at room temperature and supernatants were aspirated. Finally, cells were resuspended in 3ml of DMEM without serum and FL3 median fluorescence intensity was measured by flow cytometry.

3.4.6.3 DHR staining

The working concentration for DHR was 30µM (15ul stock solution/5ml serum-free DMEM). Cells (~200,000) were resuspended in DHR solution (2ml of solution/sample), mixed well and incubated for 30 minutes at 37^{o}C in the dark. Cells were then centrifuged at 1200rpm for 3 minutes at room temperature and supernatants were aspirated. Finally, cells were resuspended in 3ml of DMEM containing serum to analyse samples by flow cytometry.

3.4.6.4 JC1 staining

To measure mitochondrial permeability transition, a JC1 probe (1µg/1ml PRMI media) was used. Cells (~200,000) were resuspended in 500µl of JC1 solution, mixed well and incubated for 30 minutes at 37^{o}C. Cells were then centrifuged at 1200rpm for 3 minutes at room temperature and supernatants were aspirated. Cells were washed twice with cold

1XPBS and after the second wash pellets were resuspended in 3m 1XPBS. Finally, cells were resuspended in 3ml of DMEM without serum to analyse samples by flow cytometry.

3.4.6.5 NAO staining

Fluorescent dye 10-n-nonyl-acridine orange (NAO) probe (10mML NAO/1ml DMEM free serum) was used to measure mitochondrial mass. Cells (~200,000) were resuspended in 1ml of NAO solution, mixed well, and incubated for 10 minutes at 37°C. Cells were then centrifuged at 1200 rpm for 3 minutes, supernatants were aspirated, and pellets were resuspended in 3ml of DMEM without serum to analyse samples by flow cytometry.

3.4.7 Western blot

To assess the pathogenicity of identified mtDNA mutations, fibroblasts from patients were collected and subjected to Western blot analysis as previously described (section 2.2.18).

3.4.8 First dimension blue native-PAGE assay

BN-PAGE was used to assess the pathogenicity of identified mtDNA mutations by investigat whether the mutations can affect complex I activity and assembly. This approach was carried out as previously described (section 2.2.19).

Table 3-3 Summary of PCR-RFLP analysis.

Mutation	Primer Position	Primer Sequence	Primer Annealing Temperature (°C)	Enzymes and Digestion site	Digest Temperature (°C)	Uncut product (bp)	Wild-type products (bp)	Mutant products (bp)
m.11453G>A	L11343 H11498	5`-TATGACTAGCTTACACAATAGC-3` 5`-TGAGGCGTATTATACCATAGC-3`	60	*Fun4HI* (GC/NGC)	37	156	112+22+22	134+22
m.13051G>A	L12947 H13104	5`-TAAACGCTAATCCAAGCCTC-3` 5`-TCCT GCTACAACTATAGTGC-3`	56	*HaeIII* (GG/CC)	37	158	34+72+52	34+124
m.13513G>A	L13491 H13663	5`-CCTCACAGGTTTCTACTCCGAA-3` 5`-TGTTAGTAAGGGTGGGGAAGC-3`	57	*BbsI* (GAAGACN(2)/N(6)	37	173	146+27	173
m.11777C>A	M13-L11754 H12038	5`-tgtaaaacgacggccagt CAAACTACGAACGCACTCA**G**AG-3` 5`-TTCTCGTGTGAATGAGGGTTT-3`	57	*HinfI* (G/ANTC)	37	323	176+38+109	14+109
m.14453G>A	L14425 H14613	5`-CCCCCATGCCTCAGGATACTCCTCA**G**TA-3` 5`-TCTAAGCCTTCTCCTAGTTA**C**GGG-3`	58	*MaeIII* (GTNAC)	37	189	168+21	25+143+21

3.5 Results

3.5.1The m.7023G>A mutation

3.5.1.1 Mitochondrial DNA sequencing

Sequencing of the entire mitochondrial genome from a muscle sample from patient #1, who presented with seizure, weakness, aphasia, multiple infarcts and learning difficulties resulted in the identification of the pathogenic m.7023G>A mutation. This transition changes the amino acid at position 374 from valine to methionine in the COX1 subunit of complex IV (Figure 3-2). All other sequence changes identified in this patient are summarized in Table 3.4.

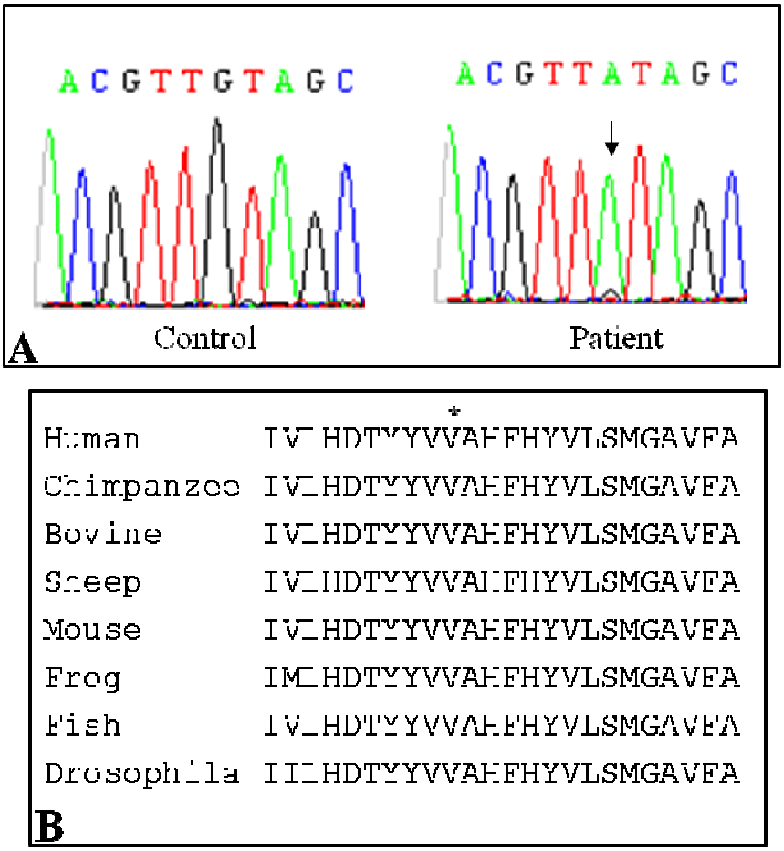

Figure 3-2 Conservation of the nucleotide at position m.7023.

(A) Sequence chromatogram showing the m.7023G>A transition in the patient (indicated by arrow) and compared to control. (B) Alignment of amino acids sequences at position 374 (as indicated by asterisk) within COX1 showing the high conservation in different species.

Table 3-4 Sequence changes identified in the patient carrying the m.7023G>A mutation.

Sequence change	**Previously reported as a SNP or pathogenic? Mitomap or mtDB**	**Amino acid change**	**Location**
m.73A>G	Yes	-	D-Loop
m.152T>C	Yes	-	D-Loop
m.263A>G	Yes	-	D-Loop
m.TC310ins	Yes	-	D-Loop
m.310T>C	Yes	-	D-Loop
m.750A>G	Yes	-	12SrRNA
m.C3106ins	Yes	-	16SrRNA
m.1438A>G	Yes	-	12SrRNA
m.4769A>G	Yes	NO	*ND2*
m.6776T>C	Yes	NO	*CO1*
m.7023G>A	**No**	**Val374Met**	***CO1***
m.7034C>T	No	NO	*CO1*
m.8860A>G	Yes	Thr112Ala	*ATPase6*
m.13404T>C	Yes	NO	*ND5*
m.13404T>C	Yes	NO	*ND5*
m.14125C>T	No	NO	*ND5*
m.15326A>G	Yes	Thr112Ala	*Cytb*
m.15326A>G	Yes	Thr194Ala	*Cytb*
m16239C>G	Yes	-	D-Loop
m.16519T>C	Yes	-	D-Loop

3.5.1.2 The m.7023G>A mutation is pathogenic

DNA muscle sample from patient #1, who presented with a MELAS-like syndrome was referred to our lab to carry out full genome sequencing. After we identified the pathogenic m.7023G>A mutation, the investigations to support the role of this mutation in pathogenicity was carried out in Dr. Brian Robinson`s lab.

The m.7023G>A mutation is a strong candidate for causing disease in this patient for several reasons. It was heteroplasmic with high levels in muscle and low in different tissues (buccal, blood, and fibroblasts). It was not found in normal individuals and not reported in the two mitochondrial DNA databases [69, 252]. It caused a biochemical defect in complex IV activity as measured in both muscle and fibroblasts. This defect associated with a clear decrease in protein expression level in subunits of COX IV in the patient when compared to controls (Figure 3-3).

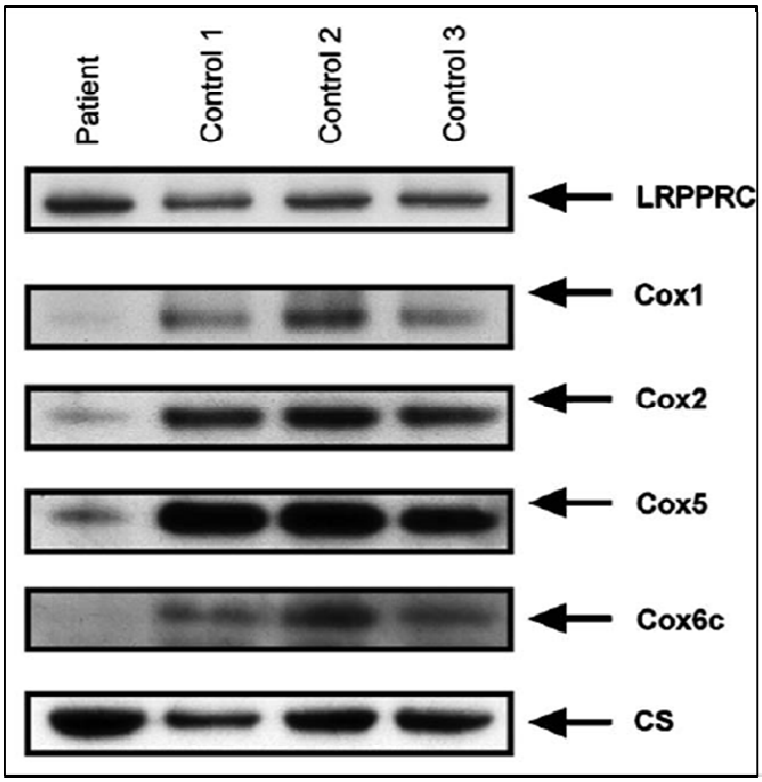

Figure 3-3 Immunoblot of patient and control COX subunit.

Protein expression levels were decreased in all COX IV subunits in samples from patient`s muscle. LRPPRC is the Leucine-rich PPR motif-containing protein and CS is citrate synthase (taken from [373].

The m.7023G>A affects the amino acid valine at position 374, which is found in helix 17 of subunit I, within the close packed interior of the complex (Figure 3-4). This mutation

results in adding more methionine residue affecting the tertiary structure formation of COX1 and its ability to interact normally with heme a, therefore, this will affect the quaternary complex formation [373].

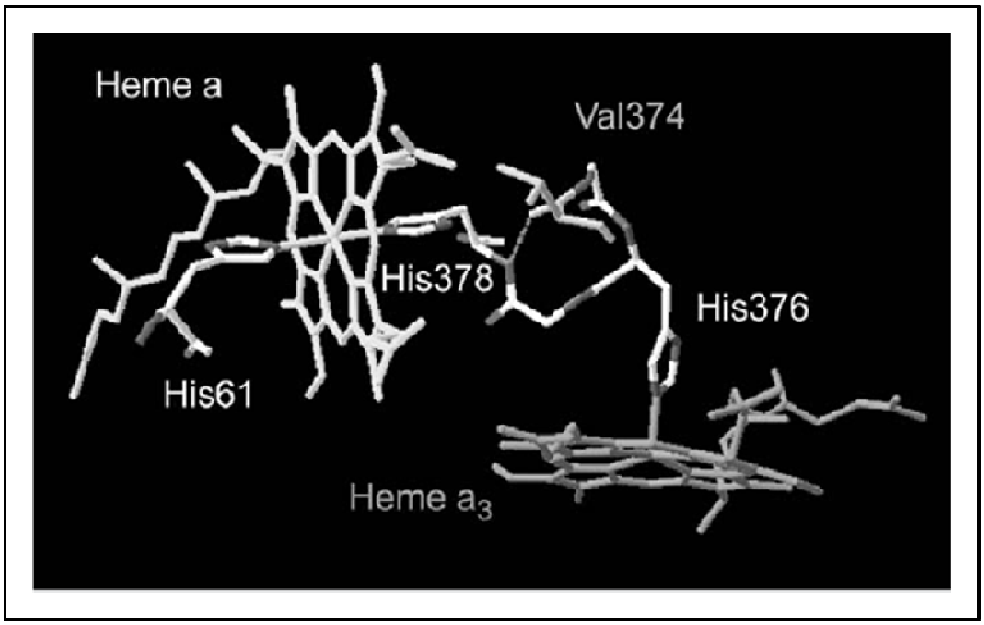

Figure 3-4 The crystal structure of cytochrome *c* oxidase in *B.taurus*.

In addition to Val374, this structure contains His61, His376, and His 378 which interact with Heme. The m.7023G>A affects Valine 374 tertiary formation of COX1 and its interaction with Heme a, by disturbing existing hydrogen bonds (taken from [373].

The existence of the m.7023G>A mutation in a heteroplasmic state in tissues from the patient, together with the absence of mutation in tissues from the mother and brother who showed no symptoms, strongly suggests that this mutation is pathogenic and occurred *de novo.*

Because the investigations were done in another diagnostic lab, further information relating to this mutation can be found in the following article [373].

3.5.2 The m.11453G>A mutation

3.5.2.1 Mitochondrial DNA sequencing

Sequencing of the entire mitochondrial genome from a blood sample from patient #2, who presented with LHON, resulted in the identification of a novel m.11453G>A variant. This transition changes the amino acid at position 232 from alanine to threonine in the ND4 subunit of complex I. In addition; it affects a strictly conserved amino acid of the protein

(Figure 3-5). All other sequence changes identified in this patient are summarized in Table 3-5.

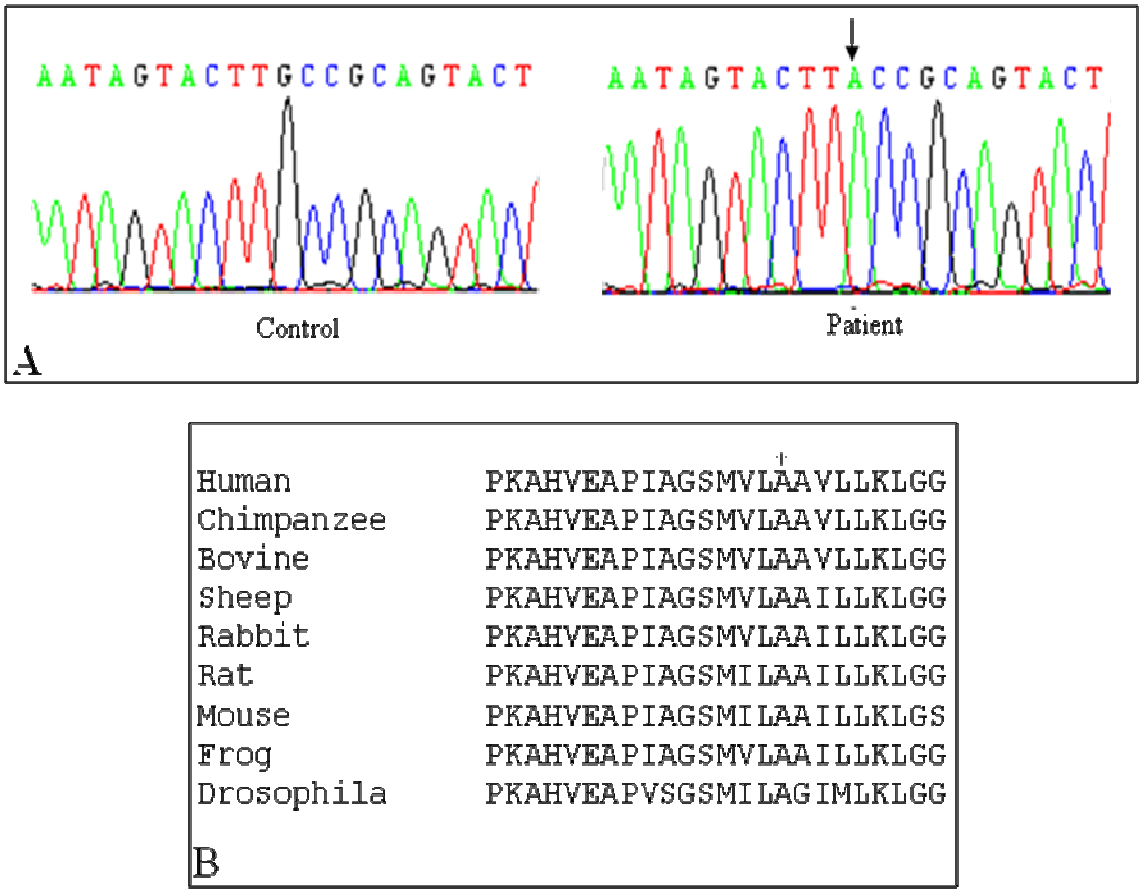

Figure 3-5 Conservation of the nucleotide at position m.11453G>A transition.

(A) Sequence chromatogram showing the m.11453G>A transition in the patient (indicated by arrow) and compared to control. (B) Alignment of amino acids sequences at position 232 (as indicated by asterisk) within MTND4 showing the high conservation in different species.

3.5.2.2 PCR-RFLP analysis of the m.11453G>A mutation

PCR-RFLP analysis was carried out to quantify mutation load in tissues from patient and mother using different primers and endonuclease. The m.11453G>A mutation causes the loss of *Fun4HI* recognition site (GC/NGC) in the mutant mtDNA. This endonuclease cuts wild-type mtDNA into 112 bp and duplicate 22 bp products, while it cuts the mutant mtDNA into 134 bp and 22 bp products. Results revealed the presence of the m.11453G>A in all the investigated tissues (Figure 3-6). The existence of the m.11453G>A mutation in tissues from mothers confirms that this mutation was transmitted to the patient.

Table 3-5 Sequence changes identified in the patient carrying the m.11453G>A mutation.

Sequence change	Previously reported as a SNP or pathogenic? Mitomap or mtDB	Amino acid change	Location
m.73A>G	Yes	-	D-Loop
m.93A>G	Yes	-	D-Loop
m.150C>T	Yes	-	D-Loop
m.152T>C	Yes	-	D-Loop
m.263A>G	Yes	-	D-Loop
m.295C>T	Yes	-	D-Loop
m.CT309 ins	Yes	-	D-Loop
m.310T>C	Yes	-	D-Loop
m.,489T>C	Yes	-	D-Loop
m.750A>G	Yes	-	12S rRNA
m.1438A>G	Yes	-	12S rRNA
m.2404T>C	Yes	-	12S rRNA
m.2706A>G	Yes	-	12S rRNA
m.3107C del.	Yes	-	16S rRNA
m.4216T>C	Yes	Tyr-304>His	*MTND1*
m.4769A>G	Yes	No	*MTND2*
m.5633C>T	Yes	-	*MTTA*
m.6962G>T	Yes	No	*MTCOX1*
m.7028C>T	Yes	No	*MTCOX1*
m.7211G>A	Yes	No	*MTCOX1*
m.7476C>T	Yes	-	*MTTS1*
m.8860A>G	Yes	Thr112Ala	*MTATP6*
m.10172G>A	Yes	No	*MTND3*
m.10389T>C	Yes	No	*MTND3*
m.10398A>G	Yes	No	*MTND3*
m.11251A>G	Yes	No	*MTND4*
m.11453G>A	**No**	**Ala232Thr**	***MTND4***
m.11719G>A	Yes	No	*MTND4*
m.12612A>G	Yes	No	*MTND5*
m.13708G>A	Yes	Ala458Thr	*MTND5*
m.14766C>T	Yes	Ile7Thr	*MTCYB*
m.15257G>A	Yes	Asp171Asn	*MTCYB*
m.15326A>G	Yes	Thr194Ala	*MTCYB*
m.15452C>A	Yes	Leu236Ile	*MTCYB*
m.15812G>A	Yes	Val356Met	*MTCYB*
m.16069C>T	Yss	-	D-Loop
m.16126T>C	Yes	-	D-Loop
m.16193C>T	Yes	-	D-Loop
m.16519T>C	Yes	-	D-Loop

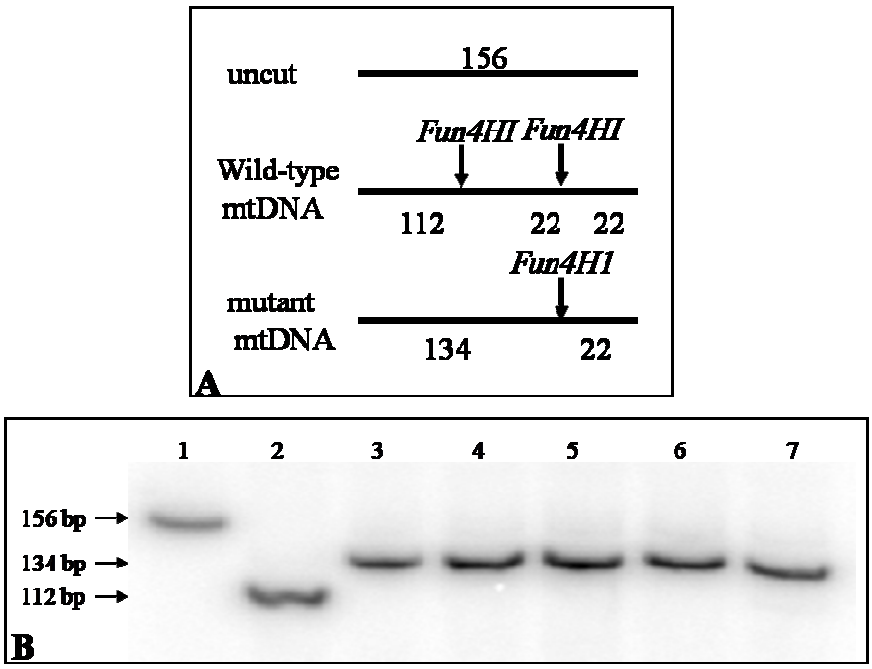

Figure 3-6 PCR-RFLP analysis of the m.11453G>A mutation in patient and mother.

(A) Schematic diagram showing sizes of PCR products after digestion with the restriction endonuclease (*Fun4HI*). (B) Quantification of mutation load in different tissues: lane 1 is an uncut sample; lane 2 is a negative control DNA sample; lanes 3 is DNA from patient`s fibroblasts sample; lane 4 is DNA from patient`s blood sample; lane 5 is DNA from mother`s blood sample, lane 6 is DNA from mother's urine sample; and lane 7 is DNA from mother's buccal sample.

3.5.2.3 Measurement of respiratory chain complexes activity

Measurement of the activity of the individual respiratory chain complexes I and II and the matrix marker citrate synthase in patient fibroblasts appeared to show a minor decrease in complex I activity (patient, 0.101 nmols NADH oxidized.min^{-1}.unit citrate synthase^{-1} (CI/CS); controls, 0.197±0.034 nmols NADH oxidized.min^{-1}.unit citrate synthase^{-1} (CI/CS) (mean±SD, *n*=8). However, the ratio of complex I:II activities showed no apparent abnormality (patient, 0.819 (CI/CII); controls, 0.58-0.90 (CI/CII)). Given I could not demonstrate a complex I deficiency by both these criteria that are routinely used within our diagnostic laboratory; I felt that I could not equivocally show that the patient fibroblasts reliably demonstrated an observable biochemical defect involving complex I.

3.5.2.4 Measurement of ROS levels and mitochondrial mass in fibroblasts from the m.11453G>A patient

To assess the pathogenic role of the m.11453G>A, ROS levels and mitochondrial mass were investigated in fibroblasts from the patient. Results showed a slight increase in ROS levels (with no significance, *n*=6) and no change in mitochondrial mass (*n*=4) as compared to fibroblasts from three different control samples: control 1 (C1) is a healthy neonatal, control 2 (C2) is a pediatric, and control 3 (C3) is embryonic lung fibroblasts (MRC5) (Figure 3-7).

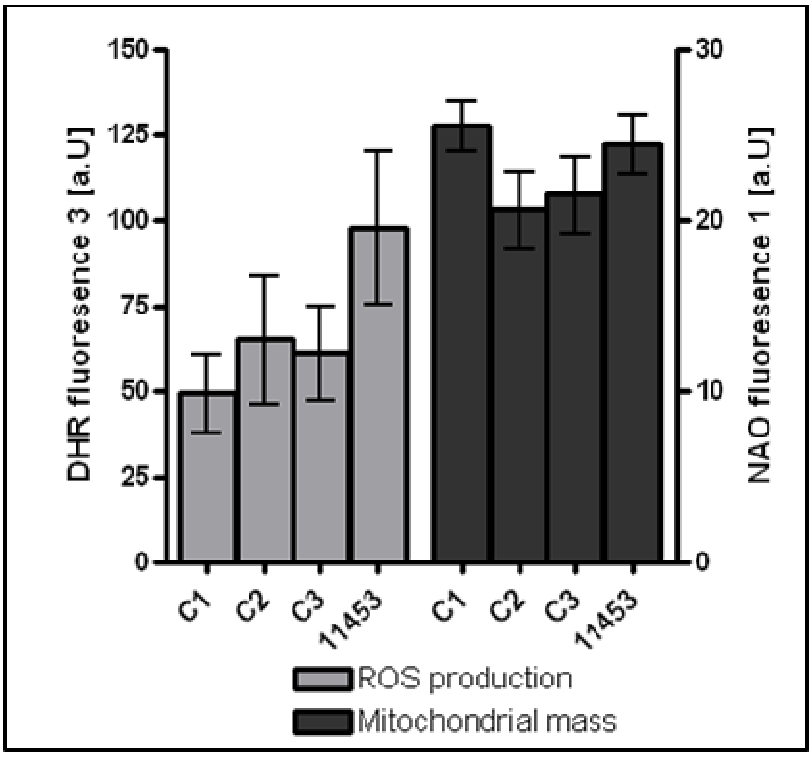

Figure 3-7 Measurement of ROS production levels and mitochondrial mass in fibroblasts from patient with the m.11453G>A mutation.

This figures shows a slight increase in ROS production without any significance and no change in mitochondrial mass as compared to control samples. C1 is a healthy neonatal, C2 is a healthy pediatric, and C3 is embryonic lung fibroblasts (MRC5). Error bars represent SEM.

3.5.2.5 Western blot analysis and protein expression levels in fibroblasts from the m.11453G>A patient

Western blot analysis was carried out to investigate whether this mutation affects protein expression levels in fibroblasts from the patient. Three monoclonal antibodies were used. Complex I subunit NDUFB8 (20kDa) protein expression levels were shown to be

increased in the patient fibroblasts. Also, MnSOD (24kDa) protein levels showed a slight increase. However, the increase in both cases was not statistically significant when compared to controls. The monoclonal antibody against complex II subunit (70kDa) was used as control for loading (Figure 3-8).

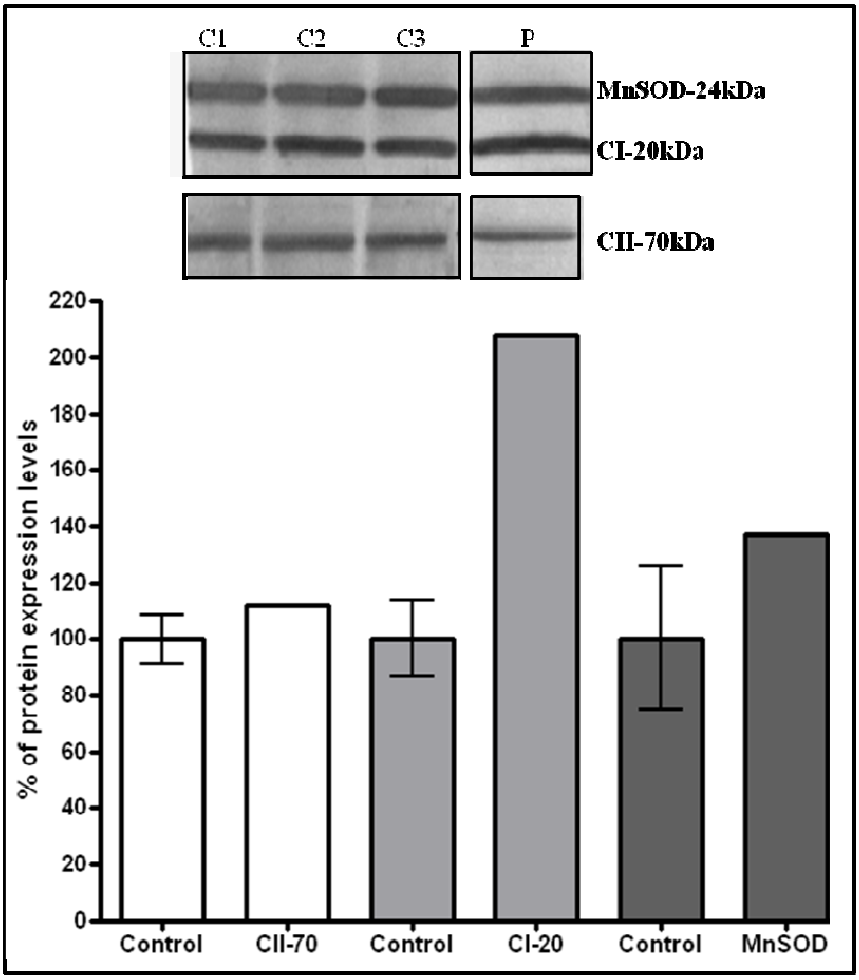

Figure 3-8 Western blot analysis for the m.11453G>A mutation.

A high increase in CI-20kDa (NDUFB8) protein expression levels was seen, while MnSOD levels showed a slight increase when compared to CII-70kDa subunit. C1, C2, and C3 represent healthy control samples. The graph represents quantification of bands intensity and error bars represent SEM.

3.5.2.6 Is the m.11453G>A mutation pathogenic?

Leber's hereditary optic neuropathy (LHON) is a maternally inherited disease leading to bilateral visual loss and the majority of cases are caused by three primary pathogenic mutations (m.3460G>A *MTND1*, m.11778G>A *MTND4* and m.14484T>C *MTND6*) [374]. Blindness is due to optic nerve degeneration and visual loss usually occurs between the ages of 20 and 40 [190].

Patient #2 presented with a LHON-like phenotypes but full genome sequence analysis of the patient`s DNA sample did not reveal any of the primary LHON mutations. Instead, mutation in *MTND4*, the m.11453G>A, was identified. This mutation is homoplasmic and is present at high levels in blood and fibroblasts from the patient. In addition, it affects a highly conserved sequence in the *MTND4* gene in different species (Figure 3-5-B). Moreover, this mutation was not found in normal individuals.

The existence of the m.11453G>A mutation in a homoplasmic state in the carrier mother can be explained by several factors which can affect expression of LHON phenotypes in different members of the same family. First, environmental factors such as: medications, industrial toxins, alcohol drinking, and smoking [250, 375-377]. Second, some mtDNA polymorphisms can influence the expression of phenotypes in individuals with the same mtDNA mutation [378]. Third, the nuclear genetic background can also influence the phenotype [379, 380].

This mutation was present at homoplasmic levels in all investigated tissues from the patient`s healthy mother. The finding of this mutation in the mother without expressing LHON phenotypes suggests she is asymptomatic. Several mtDNA mutations, identified as homoplasmic, have been confirmed to be pathogenic [69] and some individuals with such mutations have remained asymptomatic [246]. The existence of the mutation in a homoplasmic state does not exclude its involvement in pathogenicity as LHON is usually found as a homoplasmic disease [381] and inherited from carrier females to all offspring but affecting 50% of males and only 10% of females [190, 254, 382]. All together these data suggest that this mtDNA mutation may be related to the clinical presentation in this patient.

3.5.3 The m.11777C>A mutation

3.5.3.1 Mitochondrial DNA sequencing

Sequencing the entire mitochondrial genome from a blood sample in patient #3 resulted in the identification of the pathogenic m.11777C>A mutation. This transversion changes the amino acid at position 340 from arginine to serine in the ND4 subunit of complex I. In addition, it affects a highly conserved sequence of the protein, which is part of the transmembrane region (Figure 3-9). All other sequence changes that were found in the patient are summarised in Table 3-6.

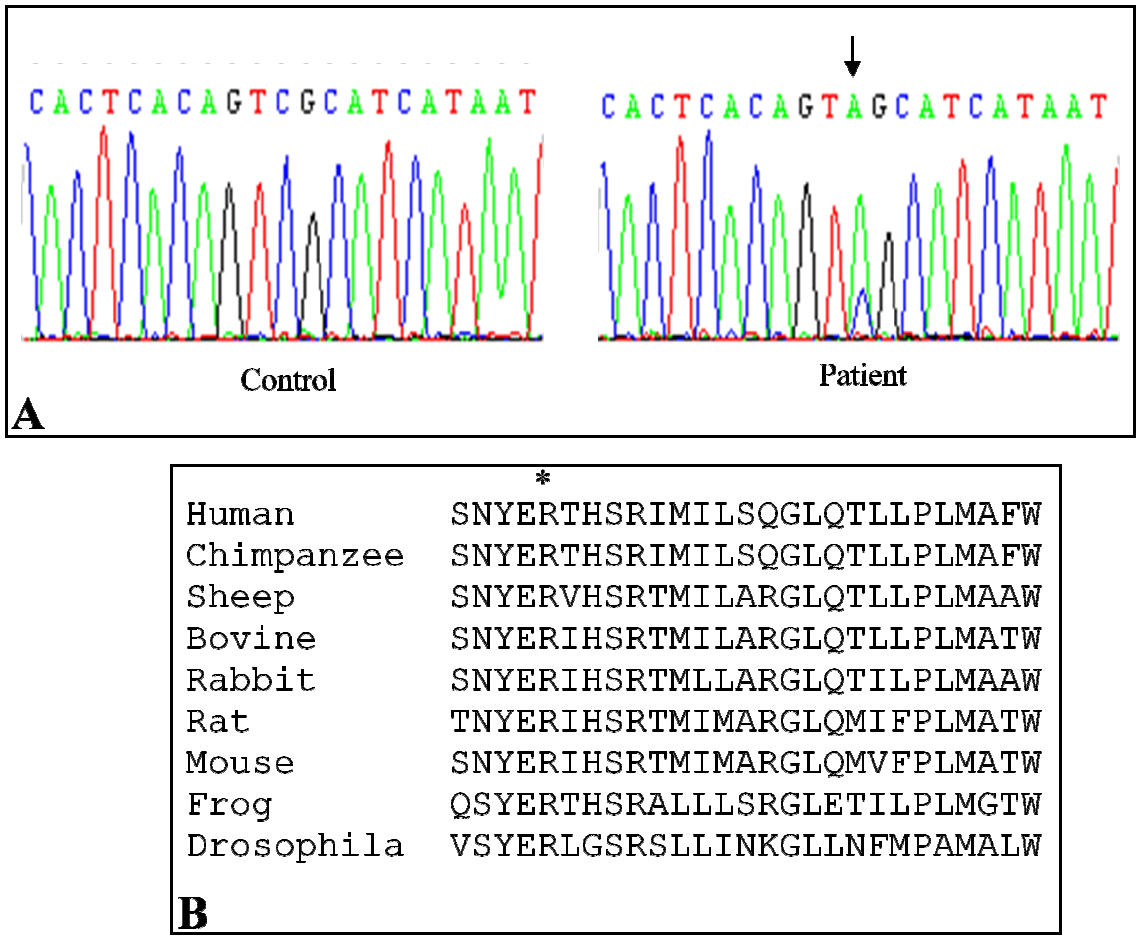

Figure 3-9 Conservation of the nucleotide at position m.11777C>A transversion.

(A) Sequence chromatogram showing the m.11777C>A transversion in the patient (indicated by arrow) and compared to control. (B) Alignment of amino acids sequences at position 340 (as indicated by asterisk) within MTND4 showing the conservation in different species.

3.5.3.2 PCR-RFLP analysis of the m.11777C>A mutation

PCR-RFLP was used to correlate the genotype with the expressed phenotype in the patient and also to quantify the mutation load in different tissues. In this experiment, the forward primer was designed to have a mismatch base to create an extra *HinfI* site (G/ANTC). So mutant mtDNA is cut into 214 bp and 109 bp products while wild-type mtDNA is cut into 176 bp, 109 bp, and 38 bp products (Figure 3-10). Results showed high levels of mutant mtDNA in muscle (78%), blood (64%), and fibroblast DNA (52%) samples.

Subsequent RFLP analysis in tissues from patient's mother and sister confirmed the presence of this mutation in all investigated tissues. In the mother the mutation load was 16% in blood, 36% in buccal epithelia and 17% in urine. However, the mutation load was greater in the sister`s tissues at 30%, 43.5% and 36.35 % in blood, buccal and urine

Table 3-6 Sequence changes identified in the patient carrying the m.11777C>A mutation.

Sequence change	Previously reported as a SNP or pathogenic? Mitomap or mtDB	Amino acid change	Location
m.73A>G	Yes	-	D-Loop
m.150C>T	Yes	-	D-Loop
m.263A>G	Yes	-	D-Loop
m.C311C ins.	Yes	-	D-Loop
m.750A>G	Yes	-	12S rRNA
m.896A>G	Yes	-	12S rRNA
m.1438A>G	Yes	-	12S rRNA
m1721C>T	Yes	-	16S rRNA
m.2706A>G	Yes	-	16S rRNA
m.3106C del.	Yes	-	16S rRNA
m3197T>C	Yes	-	16S rRNA
m.4732A>G	Yes	Asn88Ser	MT ND2
m.4769A>G	Yes	No	MT ND2
m.7028C>T	Yes	No	MT COX1
m.7768A>G	Yes	No	MT COX2
m.8860A>G	Yes	Thr112Ala	MT ATP6
m.9477G>A	Yes	Val91lle	MT COX3
m.11467A>G	Yes	No	MT ND4
m.11719G>A	Yes	No	MT ND4
m.11777C>A	**Yes**	**Arg340Ser**	**MT ND4**
m.12308A>G	Yes	-	MT TL2
m.12372G>A	Yes	No	MT ND5
m.13617T>C	Yes	No	MT ND5
m.13637A>G	Yes	Gln434Arg	MT ND5
m.14182T>C	Yes	No	MT ND6
m.14766C>T	Yes	Lle7Thr	MT CYB
m.15326A>G	Yes	Thr194Ala	MT CYB
m.15511T>C	Yes	No	MT CYB
m.16185C>T	Yes	-	D-Loop
m.16192C>T	Yes	-	D-Loop
m.16270C>T	Yes	-	D-Loop
m.16311T>C	Yes	-	D-Loop
m.16250C>T	Yes	-	D-Loop
m.16252A>C	Yes	-	D-Loop
m.16270C>T	Yes	-	D-Loop
m.16311T>C	Yes	-	D-Loop

respectively (Figure 3-11). The presence of the mutation in different tissues from patient`s mother and sister suggests that this mutation was transmitted from the mother to her offspring.

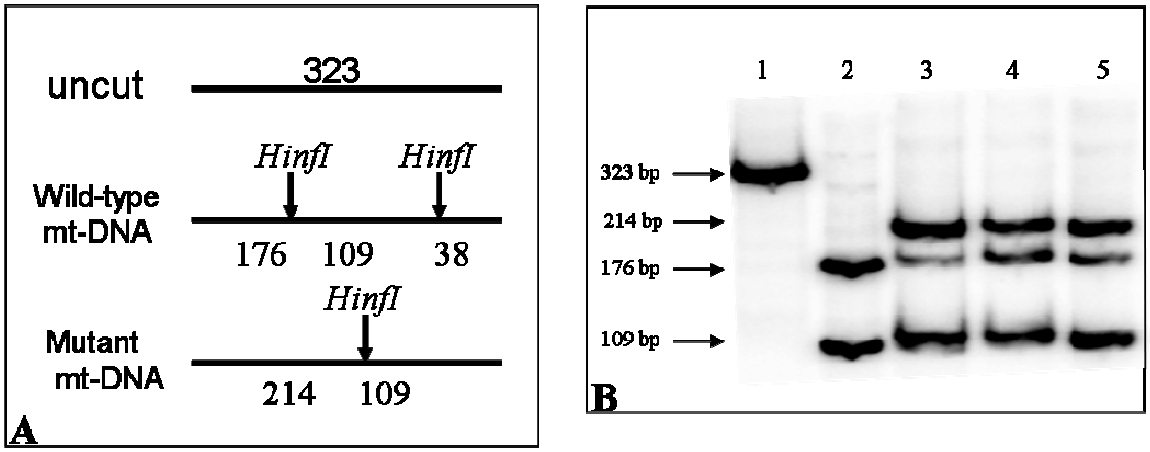

Figure 3-10 PCR-RFLP analysis of patient with the m.11777C>A mutation.

(A) Schematic diagram showing the sizes of PCR products after digestion with the restriction endonuclease (*HinfI*). (B) Quantification by PCR-RFLP of mutation load in different tissues from patient: lane 1 is uncut DNA sample, lane 2 is DNA from a negative control, lanes 3, 4, and 5 show DNA samples from patient muscle (78% mutant), blood (64% mutant) and fibroblasts (52% mutant), respectively.

In addition, these results were consistent with previous results found in two patients in unrelated cases with the same mutation. Both patients showed a high mutation load in affected tissues such as muscle, blood and fibroblasts [357].

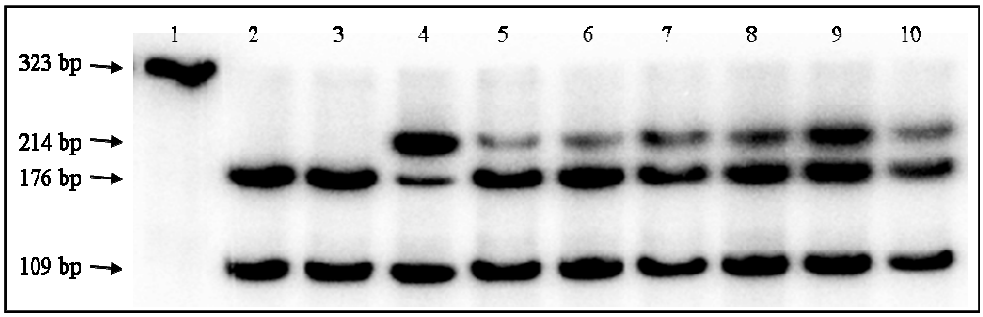

Figure 3-11 PCR-RFLP analysis of the m.11777C>A in patient's family.

Lane 1 is uncut DNA sample, lanes 2 and 3 are DNA from negative control samples, lane 4 is patient's muscle DNA with the m.11777C>A mutation (positive contro)l, lanes 5, 6 and 7 are DNA from mother's blood (16% mutant), buccal (36% mutant), and urine (17% mutant) samples, respectively. Lanes 8, 9 and 10 are DNA from the patient`s sister`s blood (30% mutant), buccal (43.5% mutant) and urine (36.35% mutant) samples, respectively.

3.5.3.3 Measurement of respiratory chain complexes activity

Measurement of the individual of respiratory chain complexes I and II and of the citrate synthase from patient's fibroblasts showed a significant decrease in complex I activity (0.306 (CI/CII)) and (0.1054 nmols NADH oxidized.min^{-1}.unit citrate synthase^{-1} (CI/CS)) as opposed to the normal complex I activity in human fibroblasts (0.58-0.90 (CI/CII)) and (0.197±0.034 nmols NADH oxidized.min^{-1}.unit citrate synthase^{-1} (CI/CS)) (mean ± SD, *n*=8) (Figure 3.12). These results confirm and support the involvement of this mutation in the previously isolated complex I defects in muscle. In addition, measurement of complex I activity in other unrelated case, which patient had the m.11777C>A mutation, revealed complex I deficiency which suggests the involvement of the m.11777C>A mutation in pathogenicity [357].

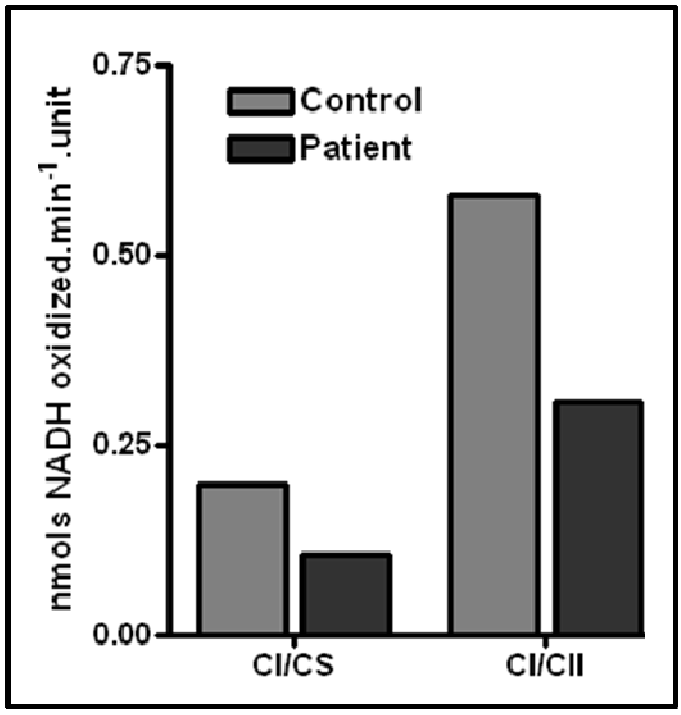

Figure 3-12 Measurement of respiratory chain complex activity in patient's fibroblasts carrying the m.11777C>A mutation.

This figure shows a significant decrease in complex I activity (CI/Cs and CI/CII) in fibroblasts from patient when compared to fibrblasts from control.

3.5.3.4 Generation of cybrids

To further confirm pathogenicity of the 11777C>A mutation, cytoplasts from patient`s fibroblasts carrying this mutation were fused to the 143BTK$^-$ cell line. Within 4-5 weeks, cybrid cells started to appear as a new generation that morphologically differed from the

input cells. Cells were harvested when they reached confluence and subjected to PCR-RFLP analysis to quantify mutation loads in the resulting cybrid clones. Results showed the successful generation of 11 cybrid clones with mutation loads (Figure 3-13).

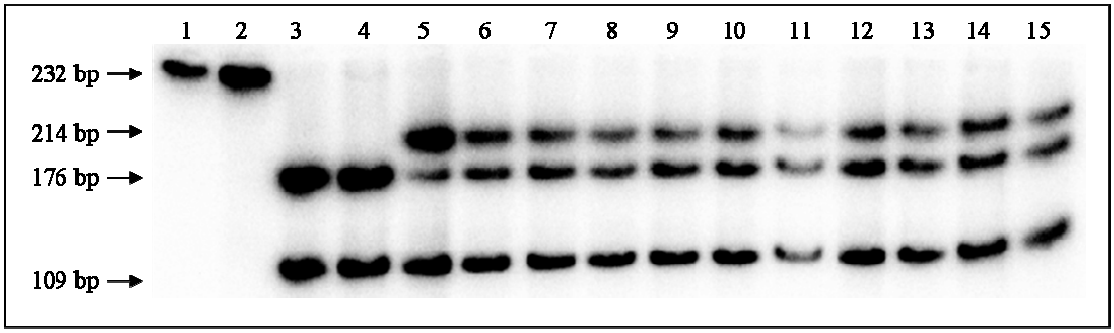

Figure 3-13 PCR-RFLP analysis of cybrid clones carrying the m.11777C>A mutation.

Lanes 1 and 2 are uncut DNA samples. Lanes 3 and 4 are DNA from negative control samples. Lane 5 is DNA from patient`s blood sample with the m.11777C>A mutation (positive control), Lanes 6-15 are DNA from different cybrid clones.

To confirm that the 143BTK p^o cells had no mitochondrial DNA, cells were treated with either selection media, which has BrdU but lacks uridine, or normal media, which has uridine but no BrdU. Upon treatment with selection media, we expected the death of 143TK p^o cells and only cells with mtDNA to survive. As expected, treatment with selection media led to morphological changes in 143TK p^0 cells, which started to shrink. Moreover, the cells eventually died (Figure 3-14).

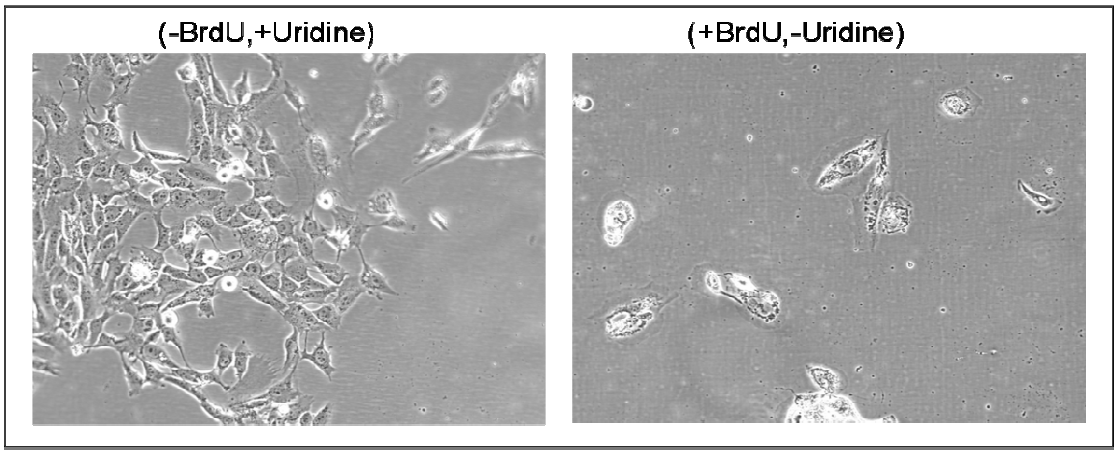

Figure 3-14 Treatment of the 143BTK p^o cells.

143BTK p^o cells were treated with normal media (-BrdU, +uridine) and selection media (+Brdu, -uridine) to test the presence of any mtDNA. Treatment with normal media showed normal growth (left panel), while treatment with selection media led to morphological changes and death of cells due to lack of mtDNA (right panel).

In addition, to exclude the possibility of any mtDNA contamination in the p^o cell, DNA was extracted as described (section 2.2.1.1). Four random primer sets specific to mtDNA were used as described (section 2.2.6.2 and 2.2.7). Results showed absence and presence of mtDNA in some lanes (Figure 3-15). However, the presence of some mtDNA in the p^o cells could be due to similar nuclear DNA sequences or mitochondrial pseudogenes, which are common in eukaryotes.

Upon successful generation of cybrids, 2 clones (lane #6 and lane #11 from Figure 3-13) were further expanded to obtain different subclones varying in their mutation loads. RFLP analysis was carried out and results showed that presence of this mutation with varying mutation loads ranging between 63% (subclone #6) and 81% (subclone #11) (Figure 3-16). Mutation loads in all the different subclones are summarised in Table 3-7.

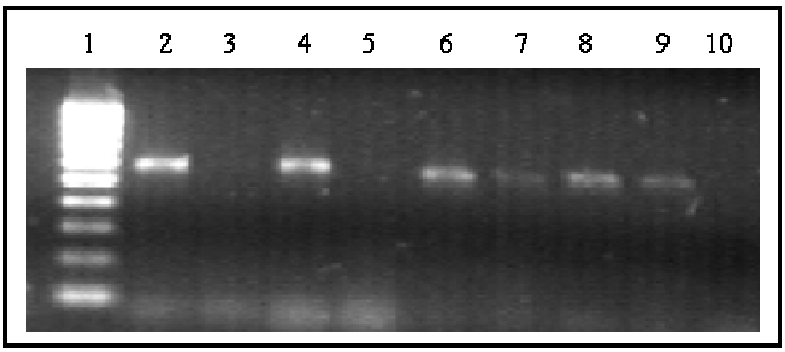

Figure 3-15 PCR analysis to test the 134B-p^o cell contamination with mt-DNA.

Lane 1 is Hyperladder IV; lanes 2, 4, 6, and 8 are PCR products from control samples containing mtDNA. Lanes 3, 5, 7, and 9 are PCR products from 143B-p^0 cells. Lane 10 is a negative control (water). Lanes 2 and 3 are PCR products amplified by primer specific for fragment 2. Lanes 3 and 4 are PCR products amplified by primer specific for fragment 6. Lanes 6 and 7 are PCR products amplified by primer specific for fragment 15. Lastly, lanes 8 and 9 are PCR products amplified by primer specific for fragment 18.

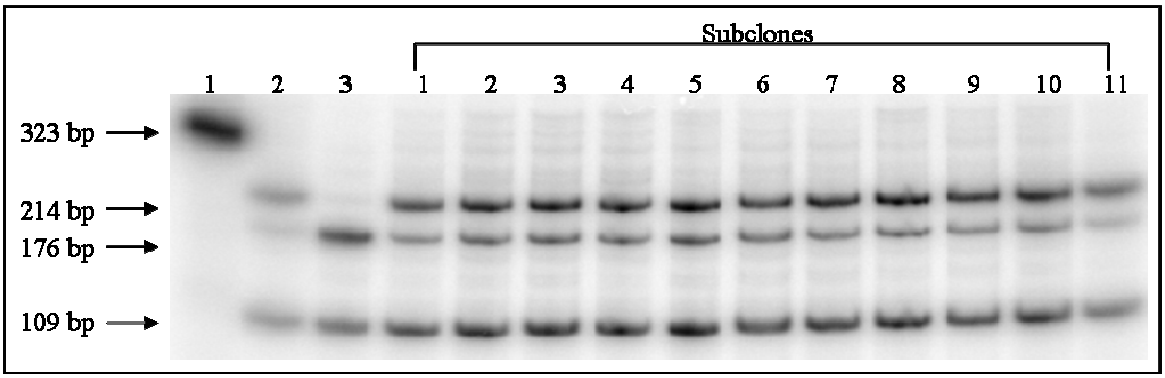

Figure 3-16 PCR-RFLP analysis of subclones from cybrids with the m.11777C>A mutation.

Lane1 is an uncut DNA sample; lane 2 is DNA from patient`s blood DNA sample with the m.11777C>A mutation (positive control); lane 3 is DNA from a negative control sample. The remaining lanes are DNA from the obtained subclones labelled from 1-11.

Table 3-7 Summary of both mutant and wild-type mtDNA percentages in all subclones.

Subclone #	% of mutant mtDNA	% of wild-type mtDNA
1	71	29
2	68	32
3	66	34
4	70	30
5	68	32
6	63	37
7	74	26
8	77	23
9	77	23
10	76	24
11	81	19

3.5.3.5 Measurement of ROS levels and mitochondrial mass in fibroblasts from patient with the m.11777C>A mutation

To further support the pathogenicity of the m.11777C>A mutation, ROS levels in fibroblasts from the patient was assessed. Results showed a significant increase in the ROS levels (P<0.001, *n*=5) when cells were stained with DHR when compared to fibroblasts from three different control samples (section 3.5.1.4). In addition, the increase in ROS correlated with a significant increase in mitochondrial mass (P<0.00, *n*=4) when cells were stained with NAO and compared to previous controls (Figure 3-17).

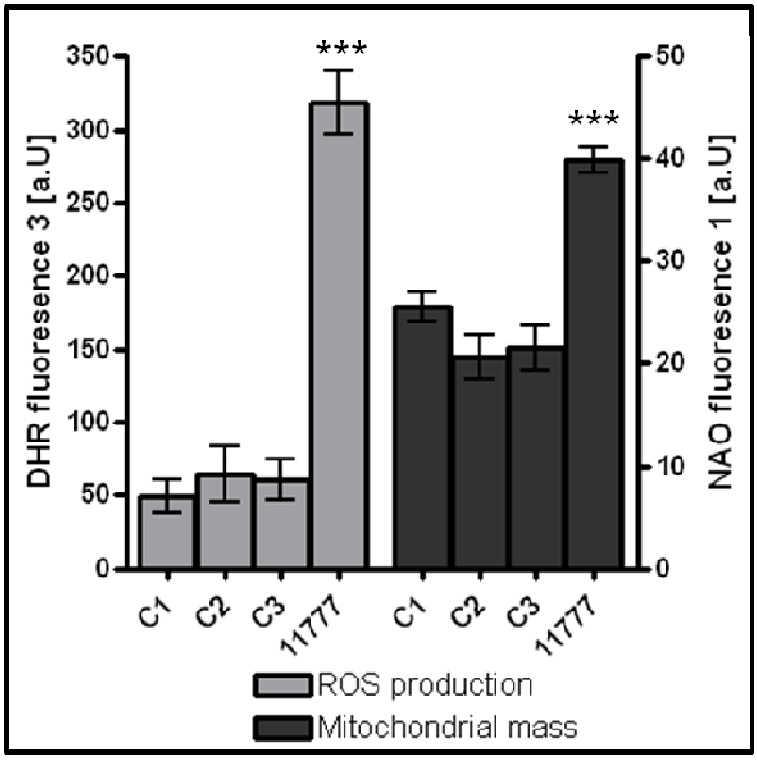

Figure 3-17 Measurement of ROS levels and mitochondrial mass in fibroblasts from the m.11777C>A patient.

Patient cells showed a significant increase in both ROS levels and mitochondrial mass when compared to the three healthy control samples. C1 is a healthy neonatal, C2 is a healthy pediatric, and C3 is embryonic lung fibroblasts (MRC5). Error bars represent SEM.

3.5.3.6 Western blot analysis and protein expression levels in fibroblasts from the m.11777C>A patient

Western blot analysis was carried out to investigate whether this mutation affects protein expression levels in fibroblasts from the patient. Complex I subunit NDUFB8 (20kDa) protein expression levels were slightly increased. MnSOD (24kDa) were also slightly

upregulated, likely due to increased levels of ROS production. The monoclonal antibody against complex II subunit (70kDa) was used as a control for loading (Figure 3-18).

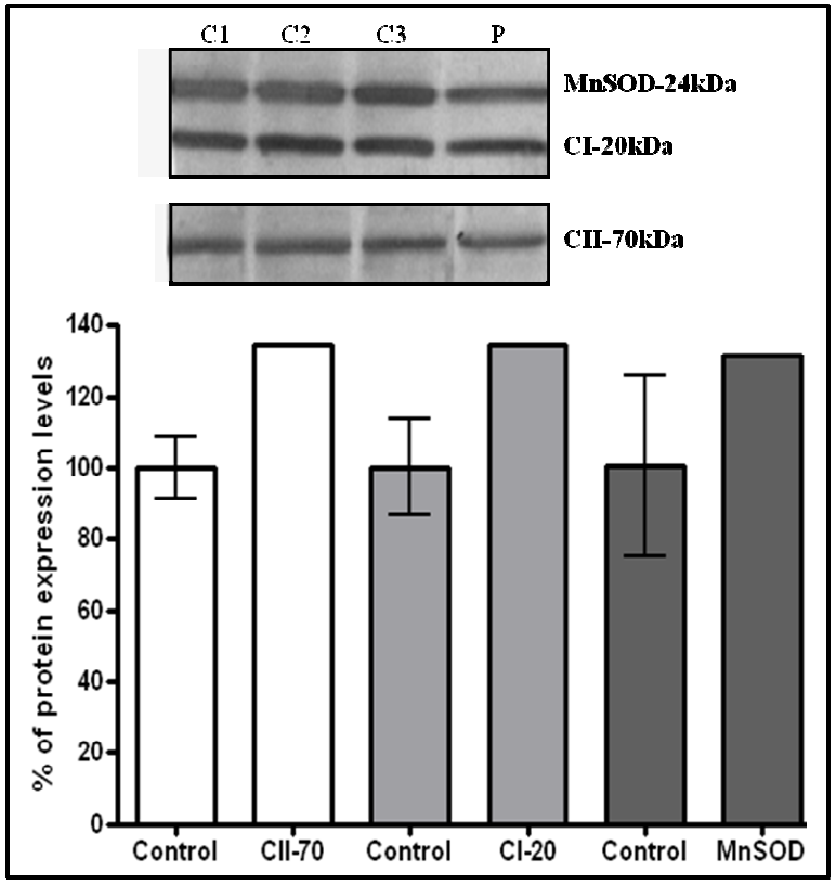

Figure 3-18 Western blot analysis in the m.11777C>A patient fibroblasts.

Both protein expression levels were slightly increased to almost the same levels as probed by antibody against CI-20 subunit and antibody against MnSOD when compared to control (CII-70kDa subunit). C1, C2, and C3 are healthy controls and error bars represent SEM.

3.5.3.7 Measurement of ROS production and mitochondrial mass in cybrids from the m.11777C>A patient

ROS production and mitochondrial mass were analysed in two subclones, subclone #6 which showed the lowest percentage of heteroplasmy and subclone #11 which showed the highest. Results from MitoSOX probe staining, DHR staining, and NAO staining showed neither changes in ROS production nor mitochondrial mass when subclones #11 and #6 compared to control ($n = 3$) (Figure 3-19).

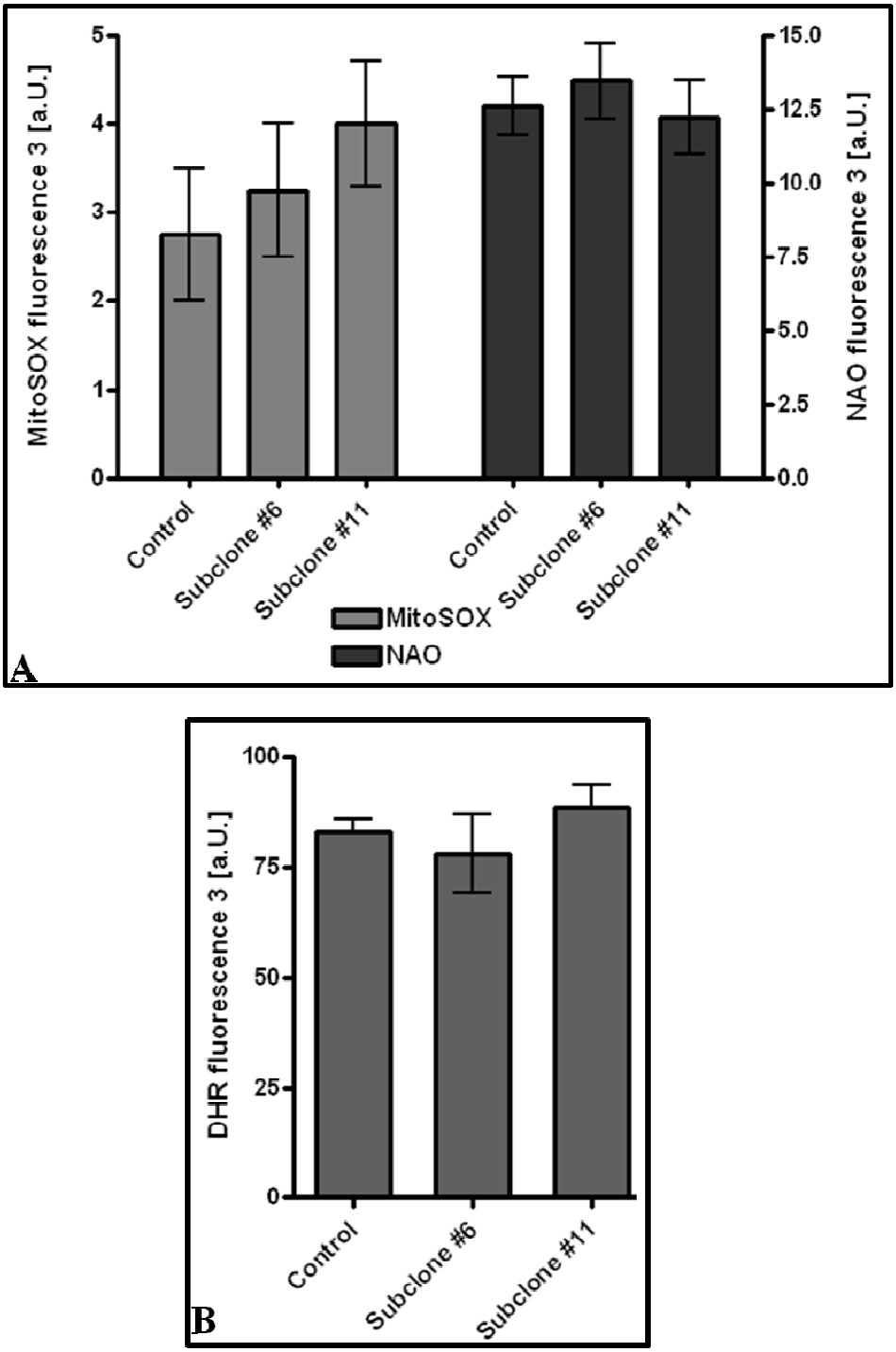

Figure 3-19 Measurement of ROS levels and mitochondrial mass in cybrid subclones carrying the m 11777C>A mutation.

Measurement of mitochondrial superoxides using MitoSOX probe, mitochondrial mass using NAO probe (A), and intracellular peroxides using DHR probe (B) showed normal levels. Error bars represent SEM.

3.5.3.8 Western blot analysis and protein expression levels in cybrid subclones carrying the m.11777C>A mutation

Western Blot analysis showed an almost similar decreased in NDUFB8 (CI-20kDa) protein expression levels in both subclones, but no change in the levels of MnSOD (Figure 3-20).

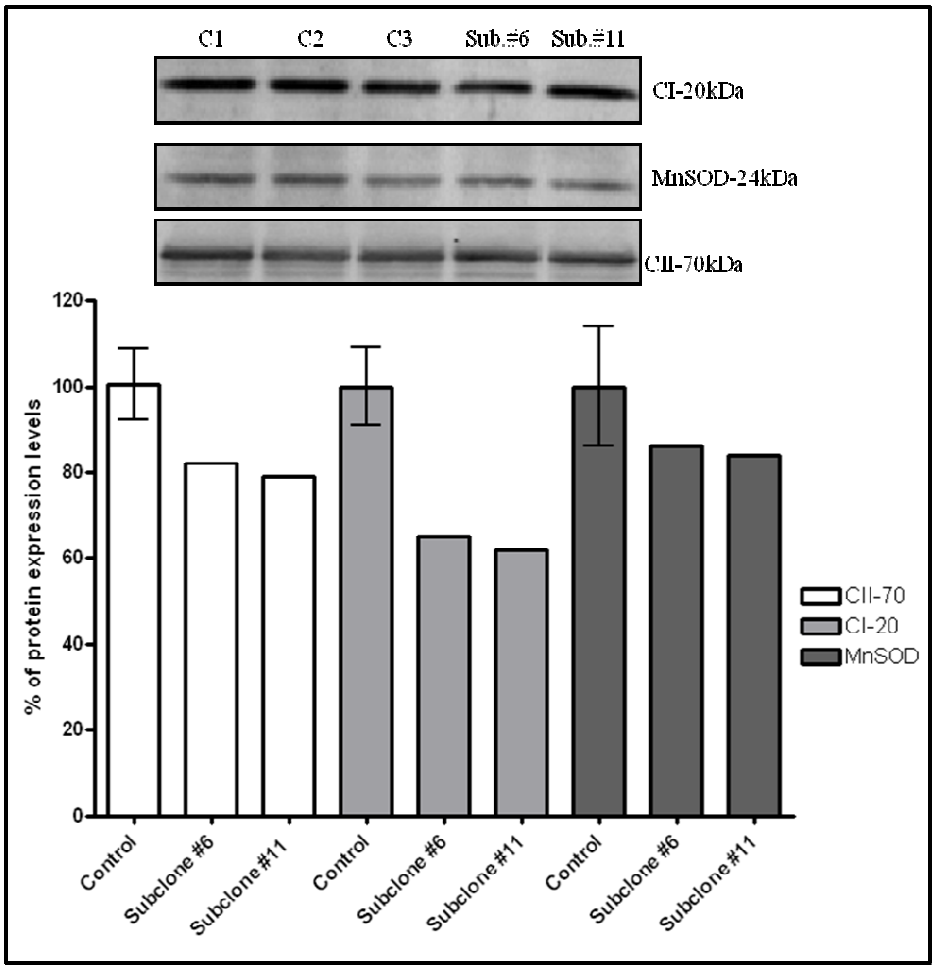

Figure 3-20 Western blot analysis of cybrid subclones carrying the m.11777C>A mutation.

NDUFB8 (CI-20kDa) protein expression levels in both subclones were decreased similarly whilst the levels of MnSOD expression in these subclones were normal compared to the 143B parental control cell line (Ctr.1, 2 and 3). Samples were loaded in triplet and error bars represent SEM.

3.5.3.9 BN-PAGE analysis of Cybrids

This analysis was carried out to assess the effect of the m.11777C>A mutation on complex I assembly and further support reduced activity. Three cell lines were used: 143B parental cell line as a control, cybrids carrying the m.11777C>A mutation with 63% heteroplasmy (subclone #6) and cybrids with 80% heteroplasmy (subclone #11) as in Figure (3-16). In-gel enzyme activity revealed no change in complex I activity between control (143B

parental) and subclone #6 (lane #1) and subclone #11(lane #2) (Figure 3-21-A). In addition, Western blot analysis of 1D BN-PAGE showed, in a similar manner, no change in fully assembled complex I, which was visualised with an antibody against complex I subunit NDUF3 (30kDa), when compared to control (Figure 3-21-B). An antibody against complex II-70kDa was used as a control for loading. This showed reduced loading for subclone #11 (Figure 3-21-B lane #2). However, a repeat of experiment showed no change in complex I activity and a slight decrease in fully assembled complex I, which was visualised with NDUF3 (CI-30kDa) (Figure 3-21-C). However, because the results were not consistent and experiment was repeated only twice, due to time limit, it was difficult to give a clear-cut interpretation for these results.

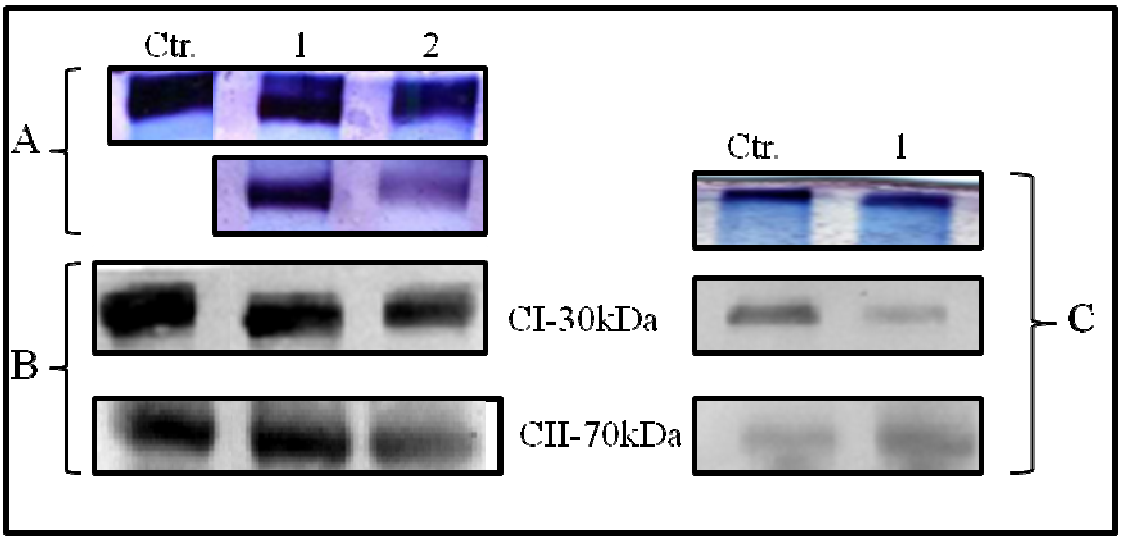

Figure 3-21 BN-PAGE analysis.

(A) In-gel enzyme activity showing the activity of complex I in control (Ctr.) and cybrids with different heteroplasmy levels of the m.11777C>A mutation. Lanes 1 is subclone #6 (with 63% heteroplasmy) and lane 2 is subclone #11 (with 80% heteroplasmy) (duplicate). (B) Western blot of BN-PAGE showing the fully assembled complex (~ 900kDa) in control (Ctr.), subclones #6 (lane #1), and subclone #11 (lane #2). (C) Repeat of both in-gel enzyme activity and Western blot for samples from control (lane #1) and subclone #11 (lane #2).

3.5.3.10 The m.11777C>A mutation is pathogenic

Full genome sequencing results from patient #3, who presented with ataxia, bulbar palsy, extensive progressive deterioration, white matter changes and complex I deficiency in both muscle and fibroblasts revealed the identification of the m.11777C>A in *MTND4*. Several lines of evidence suggest this mutation is pathogenic and is the main cause of the disease. First, this mutation is heteroplasmic and was found to affect different tissues in the patient

and relatives. Second, it changes the amino acid arginine to serine at position 340, which is highly conserved in different species (Figure 3-9-B). Third, measurement of respiratory chain complex activities revealed isolated complex I deficiency in both muscle and fibroblasts from the patient. Fourth, measurement of ROS levels in fibroblasts from the patient showed increased levels of ROS. Interestingly, fibroblasts from this patient showed an increase in mitochondrial mass, a possible compensatory response to defect in the mitochondrial respiratory chain system or the mutant mtDNA.

ROS production levels and mitochondrial mass can increase as a consequence of mitochondrial defect. It has been demonstrated that ROS production can be increased as a consequence of respiratory chain defects caused either by mtDNA mutations or inhibition of the respiratory chain [324, 383]. This is consistent with the increase in ROS production levels in the m.11777C>A case, which showed a defect in OXPHOS.

In addition, mitochondrial mass has been shown to be increased in fibroblasts exposed to oxidative stress through a feedback mechanism compensating for a defective respiratory chain or mutant mtDNA [384, 385]. This can be achieved by increasing mitochondrial proliferation and/or mtDNA copy number [386]. Similarly, this can explain the increase in mitochondrial mass in fibroblasts from the m.11777C>A patient who showed a defect in complex I activity.

Previous studies have shown that mRNA levels of several respiratory chain subunits [387] and many nuclear encoded proteins involved in mitochondrial biogenesis [384] are upregulated in cells with mtDNA depletion. In addition, the import and expression of transcription factors, such as that of transcription factor A (Tfam), were increased as well in response to mitochondrial DNA defects [388]. Those findings are consistent with the slight increase of protein expression levels in both CI-20 and MnSOD in fibroblasts from patient but not cybrids. Also, the expression levels of MnSOD in cybrids carrying the m.11777C>A mutation showed no significant change despite the increase in ROS production. This is not entirely unexpected as other patients with complex I deficiency have shown variable levels of MnSOD expression, ranging from high to low in response to increases in ROS [383, 389].

3.5.4 The m.13051G>A mutation

3.5.4.1 Mitochondrial DNA sequencing

Sequencing of the entire mitochondrial genome from a blood sample in patient #4, who presented with Leigh syndrome, resulted in the identification of the potentially pathogenic m.13051G>A mutation. This transition changes the amino acid from glycine to serine at position 239 in the ND5 subunit of complex I. In addition, it affects a region of the membrane protein spanning toward the matrix, which is highly conserved in different species (Figure 3-22). All other sequence changes found in the patient are summarised in Table 3-8.

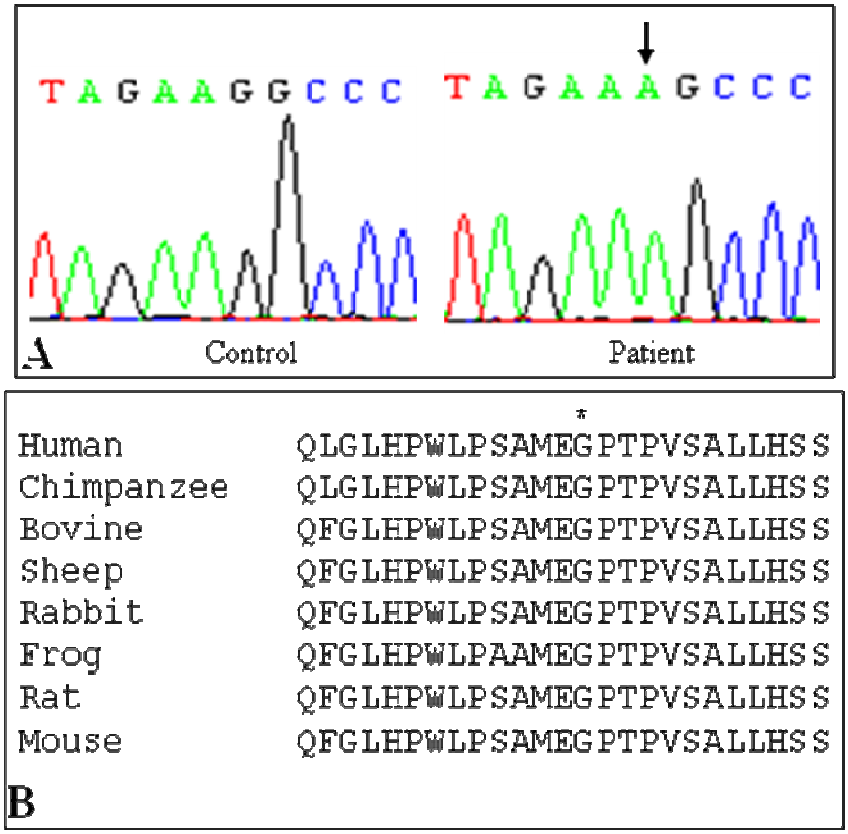

Figure 3-22 Conservation of the nucleotide at position m.13051G>A transition.

(A) Sequence chromatogram showing the m.13051G>A transition in the patient (indicated by arrow) and compared to control. (B) Alignment of amino acids sequences at position 239 (as indicated by asterisk) within MTND5 showing the conservation in different species.

3.5.4.2 PCR-RFLP analysis of the m.13051G>A mutation

To quantify mutation load in tissues from patient and related family members, including mother, sister and grandmother, PCR-RFLP was carried out. This mutation leads to the loss of one site for a recognition site for the *HaeIII* endonuclease (GG/CC).

Table 3-8 Sequence changes identified in the patient carrying the m.13051G>A mutation.

Sequence change	Previously reported as SNP or pathogenic? Mitomap or mtDB	Amino acid change	Location
m195T>C	Yes	-	D-Loop
m.207G>A	Yes	-	D-Loop
m.263A>G	Yes	-	D-Loop
m.303CC ins.	Yes	-	D-Loop
m.311C ins.	Yes	-	D-Loop
m.750A>G	Yes	-	12S rRNA
m.961T>G	Yes	-	12S rRNA
m.1438A>G	Yes	-	12S rRNA
m.3106C del.	Yes	-	16S rRNA
m.4769A>G	Yes	-	*MTND2*
m.8448T>C	Yes	Met28Thr	*MTATP8*
m.8860A>G	Yes	Thr112Ala	*MTATP6*
m.13051G>A	**Yes**	**Gly239Ser**	***MTND5***
m.13759G>A	Yes	Ala475Thr	*MTND5*
m.14361A>G	No	Trp105Arg	*MTND6*
m.15326A>G	Yes	Thr194Ala	*MTCYB*
m.16293A>G	Yes	-	D-Loop
m.16311T>C	Yes	-	D-Loop

The enzyme therefore cuts mutant mtDNA into 124 bp and 34 bp products, while it cuts wild-type mtDNA into 72 bp, 52 bp and 34 bp products (Figure 3-23). Results showed

almost homoplasmic levels of the m.13051G>A mutation in the patient's blood and buccal epithelia and high levels of heteroplasmy (88%) in the patient`s hair sample. In addition, high levels of mutation were observed in the mother's blood (65%) and almost homoplasmic levels in the grandmother's muscle sample (98%). The presence of the mutation in tissues from the grandmother and mother confirms this mutation was transmitted to the patient.

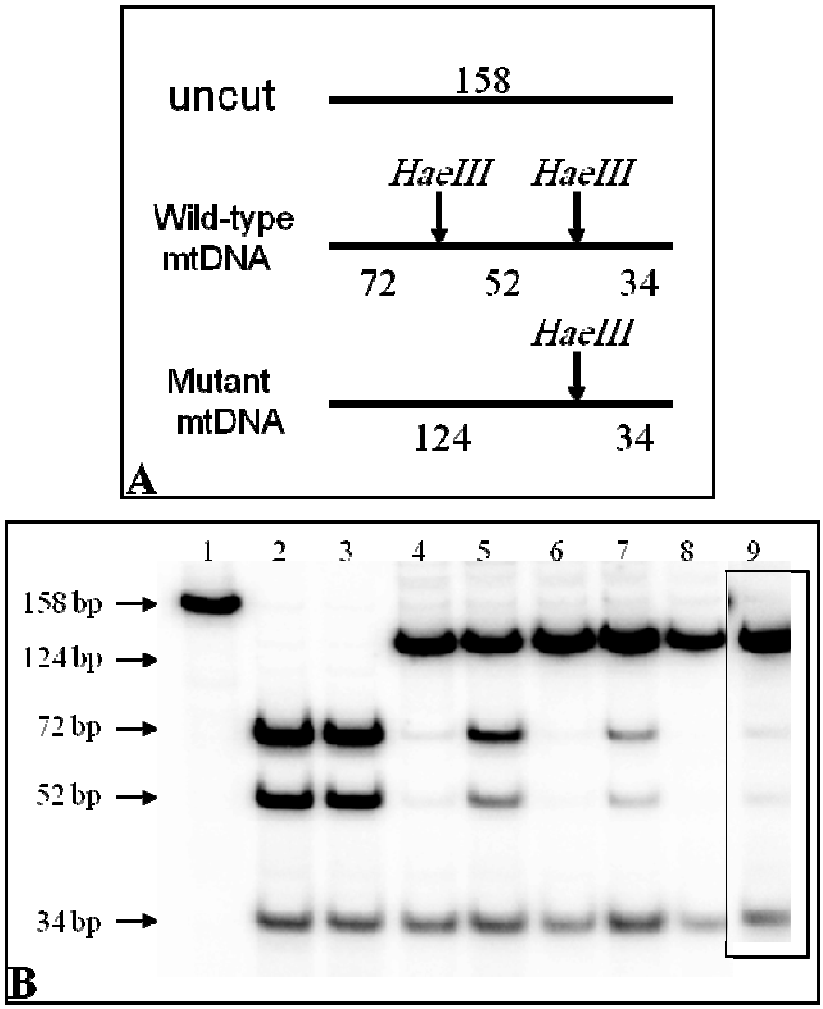

Figure 3-23 PCR-RFLP analysis in patient with the m.13051G>A mutation.

(A) Schematic diagram showing the sizes of the PCR products after digestion with the restriction endonuclease (*HaeIII*). (B) Quantification of mutation load in different tissues from patient and relatives: lane 1 is an uncut DNA sample; lanes 2 and 3 are DNA from negative control samples; lane 4 is DNA from Dutch patient blood DNA sample with 77% heteroplasmy level (positive control); Lane 5 is DNA from mother's blood sample (65% mutant); lane 6 is DNA from patient's blood sample (homoplasmic); lane 7 is DNA from patient hair's sample (88% mutant); lane 8 is DNA from patient's buccal sample (homoplasmic); and lane 9 is DNA from grandmother's muscle sample (98% mutant). Boxed lane was taken from another experiment.

3.5.4.3 Measurement of respiratory chain complex activity

Measurement of the activity of the individual respiratory chain complexes I and II and of citrate synthase from patient's fibroblasts showed no biochemical defect in complex I activity (1.2 (CI/CII)) and (447 nmols NADH oxidized.min^{-1}.unit citrate synthase^{-1} (CI/CS)) as opposed to the normal complex I activity in human fibroblasts (0.58-0.90 (CI/CII)) and (0.197±0.034 nmols NADH oxidized.min^{-1}.unit citrate synthase^{-1} (CI/CS)) (mean ± SD, *n*=8). However, these values are still slightly above normal values and this can be attributed to the quality of the cells.

3.5.4.4 Measurement of ROS production and mitochondrial mass in fibroblasts from the m.13051G>A patient

Results from measuring ROS production in the patient`s fibroblasts, stained with DHR probe, showed a significant increase in ROS production (P<0.001, *n*=5) as compared to control samples. This was accompanied by a significant increase in mitochondrial mass (P <0.001, NAO probe, *n*=4) (Figure 3-24).

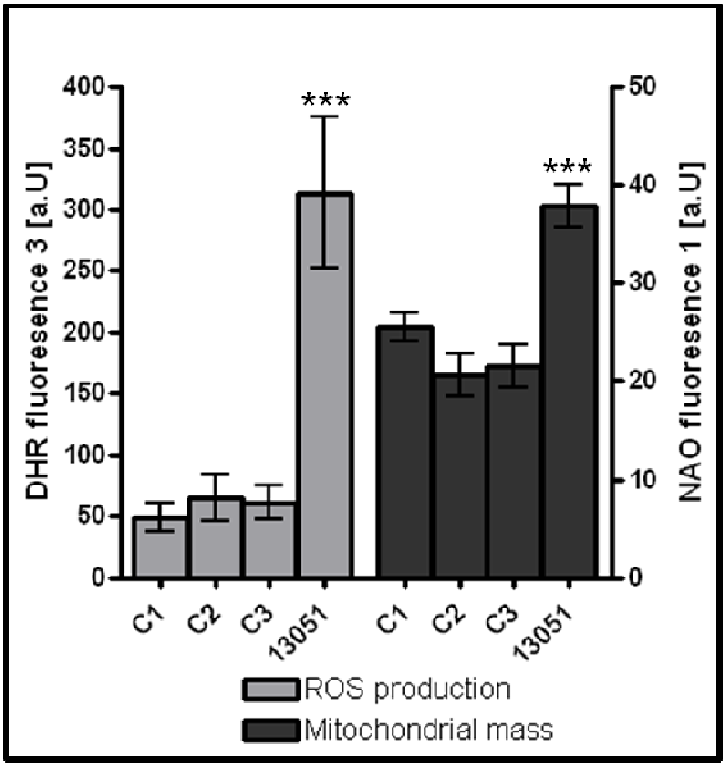

Figure 3-24 Measurment of ROS levels and mitochondrial mass in fibroblasts from the m.13051G>A patient.

A significant increase in both ROS levels and mitochondrial mass was observed when compared to control samples (C1 is a healthy neonatal, C2 is a healthy pediatric, and C3 is embryonic lung fibroblasts (MRC5). Error bars represent SEM.

3.5.4.5 Western blot analysis and protein expression levels in fibroblasts from the m.13051G>A patient

Results from Western blot analysis showed a slight increase in the CI-20kDa protein expression levels and a greater increase in MnSOD levels consistent with the increased levels of ROS (Figure 3-25).

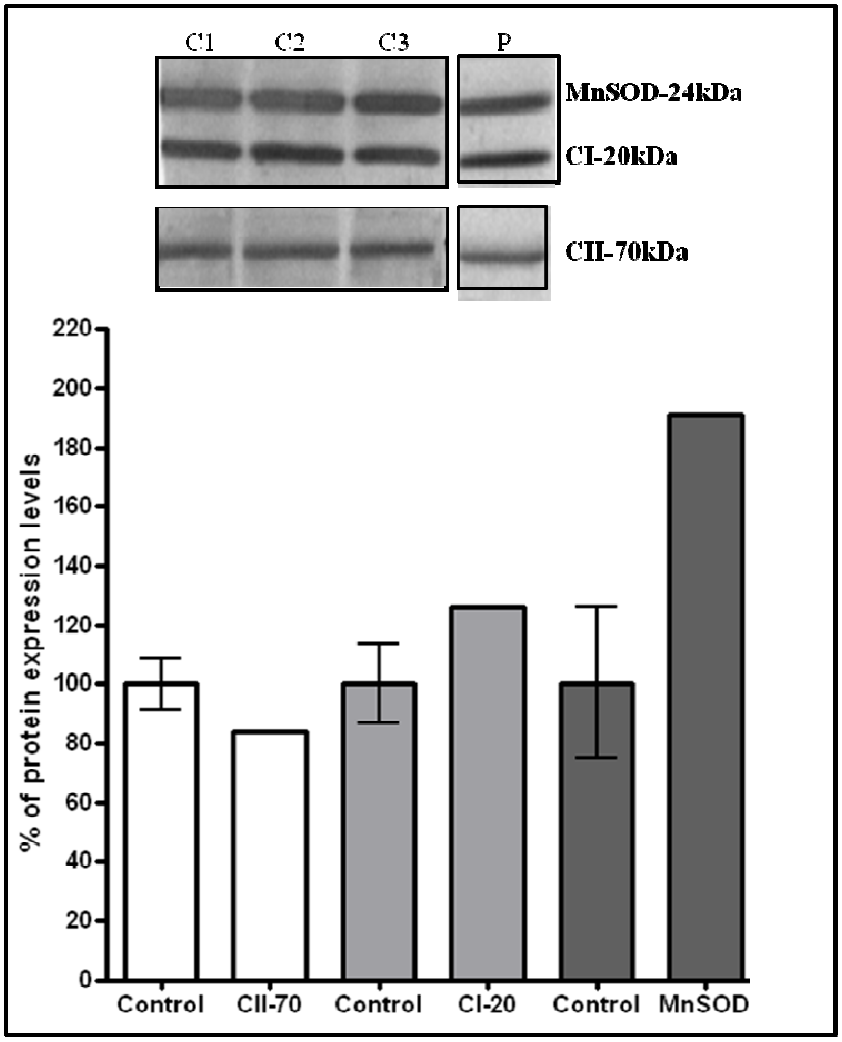

Figure 3-25 Western blot analysis of the m.13051 G>A.

This figure shows a slight increase in the CI-20 protein expression levels and more increase in MnSOD levels. Error bars represent SEM.

3.5.4.6 Is the m.13051G>A mutation pathogenic?

Leigh syndrome is a heterogeneous progressive neurodegenerative disease that affects infant and adults, It is associated with defects in mitochondrial energy production [390]. It mainly affects the central and peripheral nervous systems in children as well as adults due to mutations in either the nuclear or mitochondrial genomes [391]. Deficiencies in the

respiratory chain complexes I, II, IV or V have been seen in patients with Leigh or Leigh-like syndrome [392].

Full mitochondrial genome sequencing of DNA from patient #3, who presented with Leigh syndrome and normal respiratory chain enzymes activities, identified the m.13051G>A mutation in the subunit ND5 of complex I. This mutation was present in all investigated tissues from patient, mother and grandmother. It was almost homoplasmic in the patient's samples, with the exception of the patient`s hair sample, and the grandmother`s muscle. High levels of heteroplasmy were identified in the mother's blood sample. In addition, it affected a highly conserved sequence in the *MTND4* gene in different species (Figure 3-22-B), which resulted in the substitution of serine instead of glycine with serine at position 239. Moreover, this mutation was not found in healthy individuals and other patients with mitochondrial disorders.

As mentioned previously (section 1.5.1) ND5 may be involved in proton machinery [84] and ubiquinone binding [85]. The m.13051G>A mutation within this gene had not effect on complex I activity in this patient which makes it difficult to explain the role of this mutation in causing the observed clinical phenotype. However, this does not exclude a pathogenic role for this mutation in this patient. Moreover, the statistically significant increase in both ROS levels and mitochondrial mass in fibroblasts from this patient supported the involvement of the mutation in the disease pathogenesis. However, it is not clear what caused the increased levels of ROS production and mitochondrial mass in this patient who had normal energy production.

3.5.5 The m.13513G>A mutation

3.5.5.1 Mitochondrial DNA sequencing

Sequence analysis of patient #5 with Leigh syndrome, identified the potentially pathogenic m.13513G>A mutation. This mutation changes the highly conserved aspartic acid to an asparagine at residue 393 of the ND5 subunit of complex I (Figure 3-26). In addition to this pathogenic mutation, other sequence changes were identified as summarized in Table 3-9.

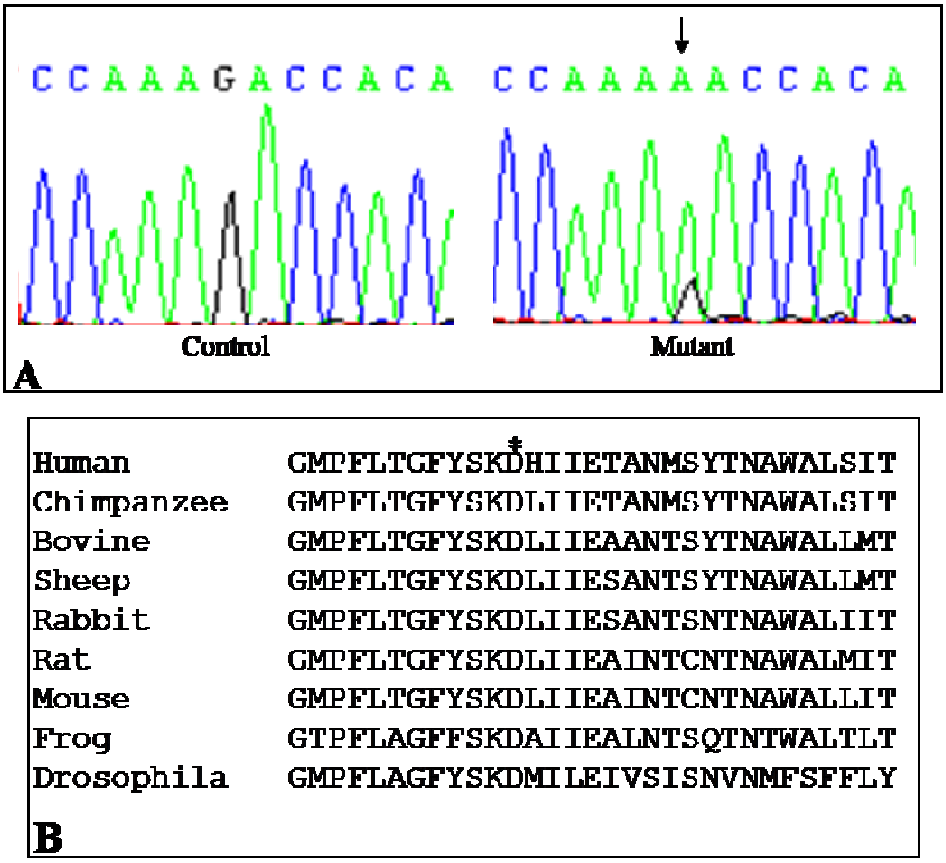

Figure 3-26 Conservation of the nucleotide at position m.13513G>A transition.

(A) Sequence chromatogram showing the m.13513G>A transition in the patient (indicated by arrow) and compared to control. (B) Alignment of amino acids sequences at position 393 (as indicated by asterisk) within MTND5 showing the high conservation in different species.

3.5.5.2 PCR-RFLP analysis of the m.13513G>A mutation

PCR-RFLP analysis was carried out to quantify mutation load in a skeletal muscle sample from patient. A mismatch forward primer was designed to introduce a recognition site for the endonuclease *BbsI* (GAAGACN(2)). This endonuclease leaves the uncut and mutant mtDNA as 173bp products, while it cuts the mutant mtDNA into 147bp and 27bp products (Figure 3-27). Results showed ~ 50% of mutation load levels in patient muscle sample.

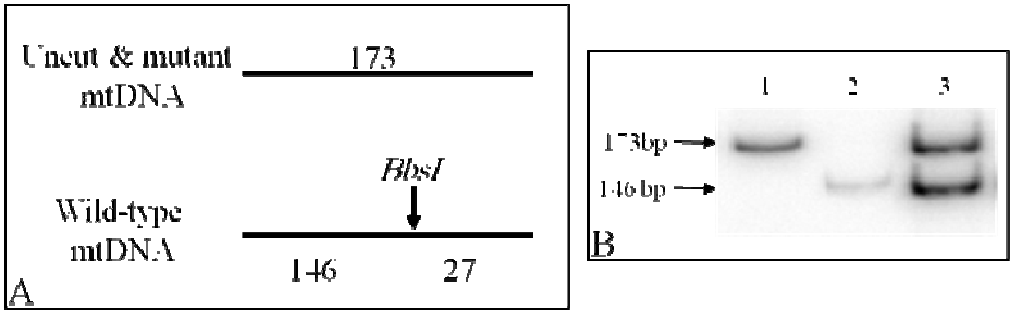

Figure 3-27 PCR-RFLP analysis of patient with the m.13513G>A mutation.

(A) Schematic diagram showing the sizes of the PCR products after digestion with the restriction endonuclease (*BbsI*). (B) Quantification of mutation load; lane 1 is an uncut sample; lane2 is a control sample; and lane 3 is a skeletal muscle sample from the patient (50% heteroplasmy).

Table 3-9 Sequence changes identified in the patient carrying the m.13513G>A mutation.

Sequence change	**Previously reported as a SNP or pathogenic? Mitomap or mtDB**	**Amino acid change**	**Location**
m.309CT ins.	Yes	-	D-Loop
m.310T>C	Yes	-	D-Loop
m.750A>G	Yes	-	12S rRNA
m.1438A>G	Yes	-	12S rRNA
m.3106C del.	Yes	-	16S rRNA
m.4769A>G	Yes	No	*MTND2*
m.8860A>G	Yes	Thr112Ala	*MTATP6*
m.11016G>A	Yes	Ser86Asn	*MTND4*
m.13513G>A	**Yes**	**Asp393Asn**	***MTND5***
m.15326A>G	Yes	Thr194Ala	*MTCYB*
m.16519T>C	Yes	-	D-Loop

3.5.5.3 Measurement of respiratory chain complex activity

Measurement of the activity of the individual respiratory chain complexes I and II and of citrate synthase from the patient's muscle sample revealed a biochemical defect in complex I activity (0.062 nmols NADH oxidized.min^{-1}.unit citrate synthase^{-1} (CI/CS)) and (0.334 (CI/CII) as opposed to the normal complex I activity in human muscle (0.104±0.036 nmols NADH oxidized.min^{-1}.unit citrate synthase^{-1} (CI/CS)) and (0.52-0.95 (CI/CII)) (mean ± SD, *n*=25).

3.5.5.4 Measurement of ROS levels and mitochondrial mass in fibroblasts from the m.13513G>A patient

Patient fibroblasts, stained with DHR probe, showed an increase in ROS levels relative to controls but without statistical significance (*n*=5). Fibroblasts stained with NAO probe showed no change in mitochondrial mass as compared to controls (*n*=4) (Figure 3-28).

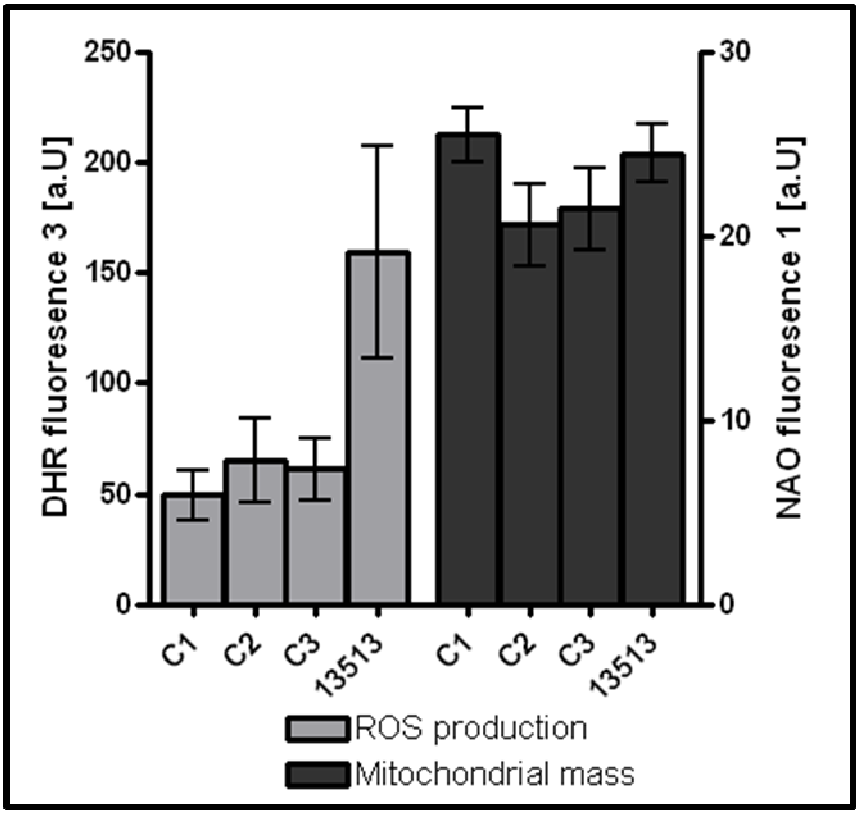

Figure 3-28 Measurement of ROS levels and mitochondrial mass in fibroblasts from the m.13513G>A patient.

DHR staining showed an increase in ROS levels but NAO staining showed no change in mitochondrial mass. C1 is a healthy neonatal, C2 is a healthy pediatric, and C3 is embryonic lung fibroblasts (MRC5). Error bars represent SEM.

3.5.5.5 Western blot analysis and expression of protein levels in fibroblasts from the m.13513G>A patient.

CI-20kDa protein expression levels were highly increased in this patient. MnSOD levels were markedly upregulated, which could be as a response to the increase in ROS production (Figure 3-29).

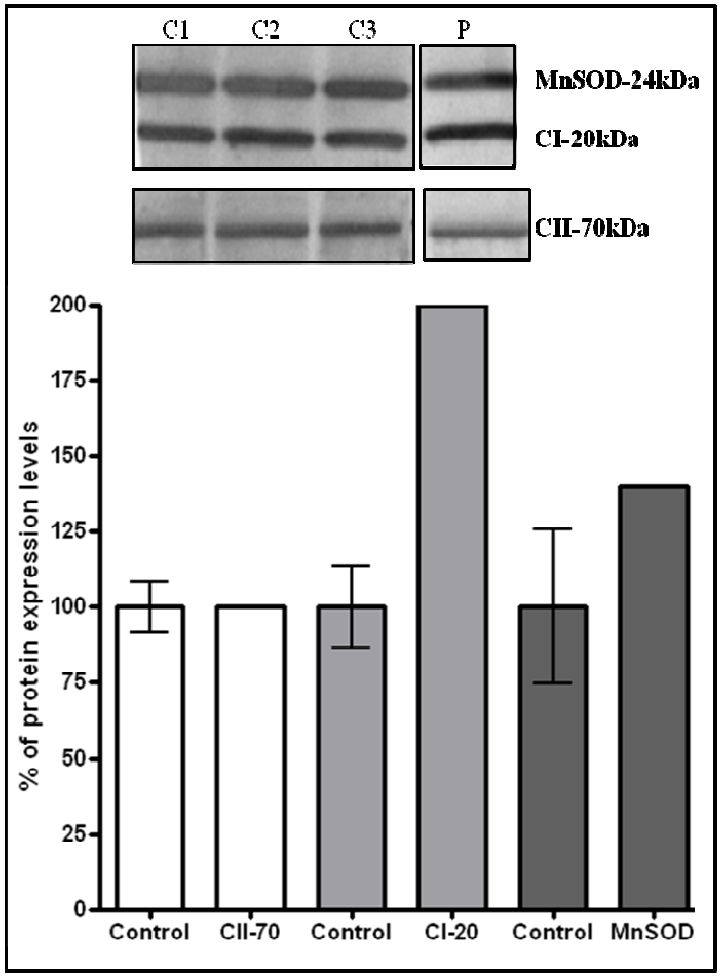

Figure 3-29 Western blot analysis in fibroblasts from patient with the m.13513G>A mutation.

A high increase of protein expression levels was seen in CI-20, while a sligh increase of protein expression levels was seen in MnSOD. C1, C2, and C3 are healthy controls and error bars represent SEM.

3.5.5.6 Is the m.13513G>A mutation pathogenic?

The m.13513G>A mutation was identified in patient #5, who presented with Leigh syndrome and had a biochemical defect in complex I in muscle. Sequence chromatogram (Figure 3.26.A) showed that this mutation was heteroplasmic with high levels. This mutation affects an evolutionary conserved nucleotide and leads to the change of an aspartic acid to asparagine at amino acid position 393 in the ND5 (Figure 3-26-B). It

caused a biochemical defect in the patient`s muscle sample. This mutation was not found in normal individuals and other patients with mitochondrial disorders.

The 13513G>A in this patient was not novel since the same mutation was reported in at least 16 other cases most of which presented with Leigh or Leigh-like syndrome [393]. Initially, m.13513G>A was associated with MELAS [337]. Subsequently, other cases were reported and associated with LHON/MELAS overlap syndrome [394], MELAS [395], mitochondrial encephalomyopathy [395] and Leigh syndrome [315, 392]. More recently, this mutation was reported, in our lab, in a child who was referred with a suspected with mitochondrial disorder. PCR-RFLP analysis using the endonuclease *BbsI* (Table 3-3) revealed ~ 60% mutation load in urinary epithelia cells from this child. In addition, this mutation was absent in tissues from the mother suggesting the mutation is sporadic (Figure 3.30).

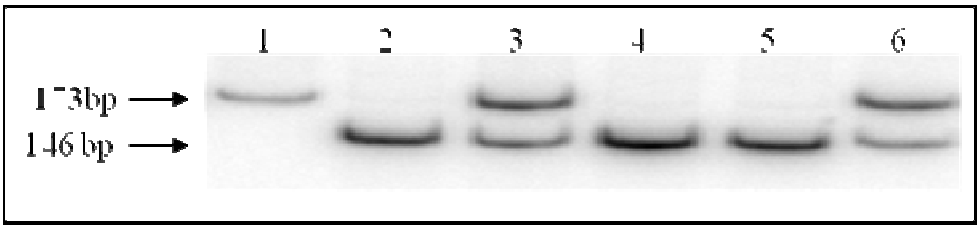

Figure 3-30 PCR-RFLP analysis of the m.13513G>A mutation in a recent patient and mother.

Lane 1 is an uncut DNA sample; lane2 is DNA from a negative control sample; lane 3 is DNA from patient`s muscle DNA sample with the m.13513G>A mutation (positive control); lane 4 is mother's blood DNA sample; lane 5 is mother's DNA urine sample; and 6 is patient`s DNA urine sample (60% mutation load levels).

Finally, all previous reasons make the m.13513G>A mutation in the *MTND5* gene of complex I a strong candidate for causing the disease in this patient. In addition, this mutation should be considered in individuals suspected with Leigh or Leigh-like phenotypes associated with complex I deficiency.

Although the m.13513G>A mutation affects the nucleotide directly next to the m.13514A>G, which was described in two patients with MELAS, it does not result in the same change in amino acid, aspartic acid to glycine with m.13514A>G. This indicates that the amino acid at position 393 is likely to be highly important for complex I structure and function [395] since both mutations are believed to change the secondary structure of the protein [315, 396]. Moreover, the 393 position within complex I is thought to be involved

in ubiquinone binding, therefore this mutation may disrupt this binding, therefore leading to a defect in mitochondrial oxidative phosphorylation [85]. However, the defect in complex I activity in muscle from this patient and other cases with the m.13513G>A mutation could also be attributed to the change of charge in the peptide disrupting the whole complex activity [337].

3.5.6 The m.14453G>A mutation

3.5.6.1 Mitochondrial DNA sequencing

Sequencing of the entire mitochondrial genome from a blood sample from patient #6, who presented with spasms, pigmentary retinopathy, encephalopathy, increased blood lactate, and changes in basal ganglia resulted in the identification of the pathogenic m.14453G>A mutation. This transition changes the amino acid at position 47 from alanine to valine in the ND6 subunit of complex I, which is thought to be part of the single membrane-spanning domain now considered a hot spot for mutations [397]. In addition; it affects a highly conserved sequence of the protein (Figure 3-31). All other sequence changes identified in this patient are summarized in Table 3-10.

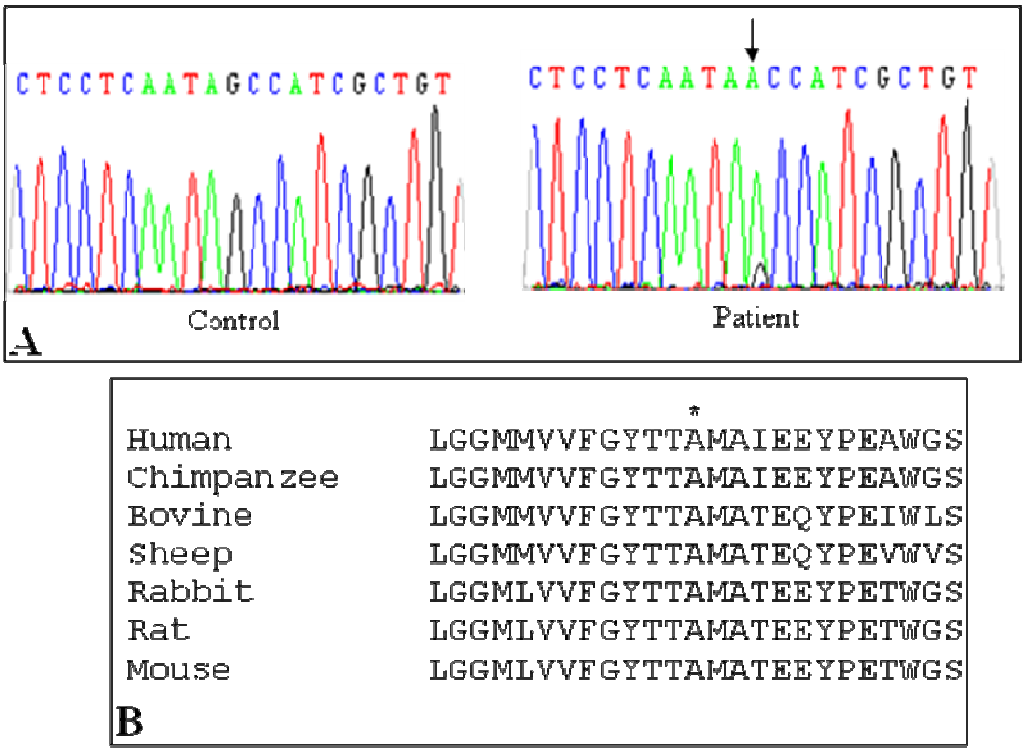

Figure 3-31 Conservation of the nucleotide at position m.14453G>A transition.

(A) Sequence chromatogram showing the m.14453G>A transition in the patient (indicated by arrow) and compared to control. (B) Alignment of amino acids sequences at position 74 (as indicated by an asterisk) within MTND6 showing the high conservation in different species.

Table 3-10 Sequence changes identified in the patient carrying the m.14453G>A mutation.

Sequence change	**Previously reported as a SNP or pathogenic? Mitomap or mtDB**	**Amino acid change**	**Location**
m.311C ins.	Yes	-	D-Loop
m.263A>G	Yes	-	D-Loop
m.750A>G	Yes	-	12S rRNA
m.1438A>G	Yes	-	12S rRNA
m.3106C del.	Yes	-	16S rRNA
m.4769A>G	Yes	No	*MTND2*
m.6776T>C	Yes	No	*MTCO1*
m.7148T>C	Yes	No	*MTCO1*
m.8860A>G	Yes	Thr112Ala	*MTATP6*
m.11914G>A	Yes	No	*MTND4*
m.12681T>C	Yes	No	*MTND5*
m.14020T>C	Yes	No	*MTND5*
m.14453G>A	**Yes**	**Ala47Val**	***MTND6***
m.15326A>G	Yes	Thr194Ala	*MTCYB*
m.16519T>C	Yes	-	D-Loop

3.5.6.2 PCR-RFLP analysis of the m.14453G>A mutation

PCR-RFLP analysis using mismatched primers, to introduce an additional *MaeIII* site (GTNAC), was carried out to quantify the mutation loads in different tissues from the patient and mother. This endonuclease cut wild-type mtDNA into 168 bp and 21 bp products, while it cuts mutant mtDNA into 143 bp, 25 bp, and 21 bp products (Figure 3-32). Results showed high levels of mutation in the patient`s muscle (65%) but low levels in fibroblasts (39%). The mutation was not found in investigated tissues from the mother suggesting this occurred as a sporadic mutation in the patient.

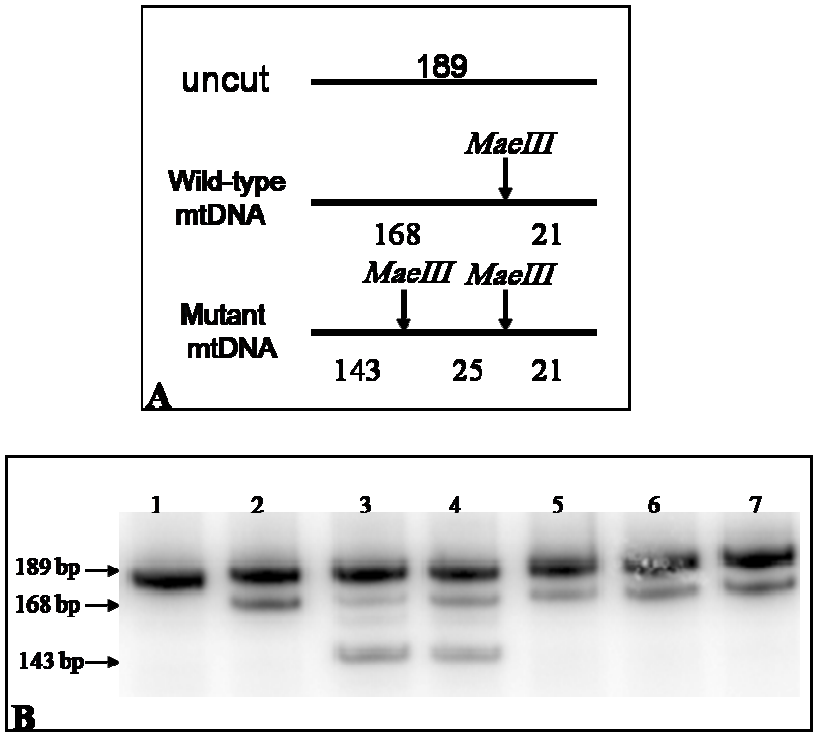

Figure 3-32 PCR-RFLP analysis in patient with the m.14453G>A mutation.

(A) Schematic diagram showing the sizes of the PCR products after digestion with the restriction endonuclease *MaeIII* (B) Quantification of mutation load in different tissues: lane 1 is an uncut DNA sample; lane 2 is DNA from a negative control sample; lane 3 is DNA from patient's muscle (65% mutant); lane 4 is DNA from patient's fibroblasts (39% mutant). Lanes 5, 6, and 7 are DNA from mother's blood, buccal and urine samples, respectively.

3.5.6.3 Measurement of respiratory chain complex activity

Measurement of the activity of the individual respiratory chain complexes I and II and of citrate synthase from patient's fibroblasts showed no biochemical defect in complex I activity (0.334 nmols NADH oxidized.min^{-1}.unit citrate synthase^{-1} (CI/CS)) as opposed to

the normal complex I activity in human fibroblasts (0.197±0.034 nmols NADH oxidized.min^{-1}.unit citrate synthase^{-1} (CI/CS)) (mean ± SD, *n*=8). However, this patient showed complex I deficiency in muscle as initially investigated prior to referral.

3.5.6.4 Measurement of ROS levels and mitochondrial mass in fibroblasts from the m.14453G>A patient

Patient fibroblasts stained with DHR probe showed a high increase in ROS levels with no statistical significance when compared to each control (*n*=6), however, fibroblasts stained with NAO probe showed no change in mitochondrial mass (*n*=4) (Figure 3-33).

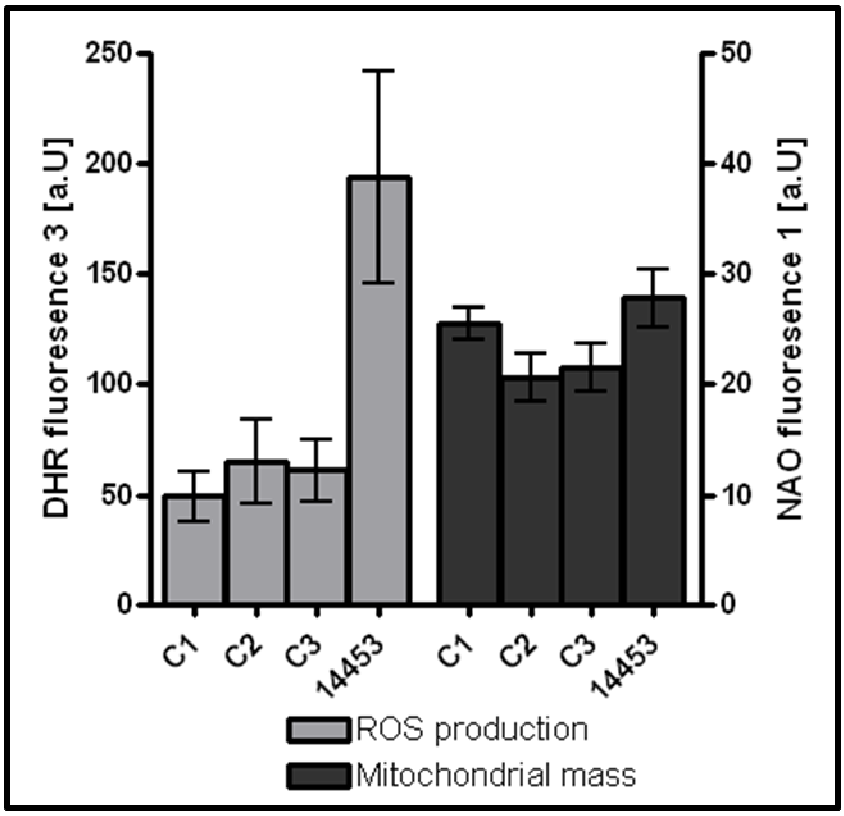

Figure 3-33 Measurement of ROS levels and mitochondrial mass in fibroblasts from patient with the m.14453G>A mutation.

A high increase in ROS levels with no statistical significance was observed in patient sample, while no change in mitochondrial mass when compared to control samples. C1 is a healthy neonatal, C2 is a healthy pediatric, and C3 is embryonic lung fibroblasts (MRC5). Error bars represent SEM.

3.5.6.5 Western blot analysis and expression of protein levels in fibroblasts from the m.14453G>A patient

Results from Western blot analysis showed an increase in CI-20kda protein expression levels and no change in MnSOD levels as compared to controls (Figure 3-34).

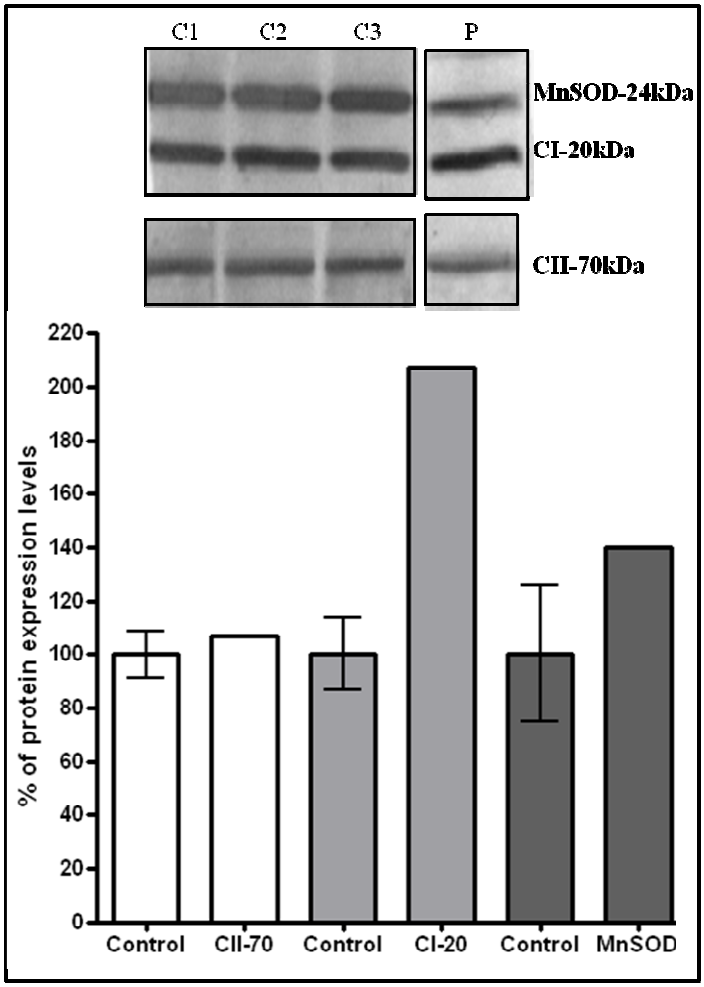

Figure 3-34 Western blot analysis in fibroblasts from the patient with the m.14453G>A mutation.

A high increase of protein expression levels was seen in CI-20 and a slight increase in MnSOD levels were observed when compared to control. C1, C2, and C3 are healthy controls and error bars represent SEM.

3.5.6.6 The m.14453G>A mutation is pathogenic

Full genome sequencing of DNA samples from patient #6, who presented with spasms, pigmentary retinopathy, encephalopathy, increased blood lactate, changes in basal ganglia, and defect in complex I activity in muscle, identified the m.14453G>A mutation in ND6 subunit of complex I. This mutation is believed to be the main cause of the disease for several reasons. First, it is a heteroplasmic mutation that changes the amino acid at position 47 from alanine to valine. This is a highly conserved nucleotide in the ND6 subunit of complex I (Figure 3-31-B). Several mutations have previously been reported within this region of the N-terminus of this subunit, which is thought to be a hot spot for mutations [397]. Second, the mutation was present in all investigated tissues from this patient, with a high mutation load in muscle and a low load in fibroblasts. Third, it caused a biochemical defect in complex I activity in muscle.

PCR-RFLP analysis revealed high levels of mutation load in patient's muscle and low levels in fibroblasts. This is consistent with results from respiratory chain enzyme activity measurement, which showed a biochemical defect in complex I activity in muscle but not in fibroblasts. The maintenance of complex I activity in fibroblasts can be attributed to the low levels of mutation in these cells, which suggests it is still below the threshold to cause a defect.

Lastly, the presence of this mutation in tissues from patient and the absence in mother's tissues confirms that the m.14453G>A has arisen *de novo* and is only restricted to the patients' tissues. In conclusion, all given data confirms the involvement of the m.14453G>A mutation in causing the disease in this patient.

3.3 Discussion

Those identified complex I mtDNA mutations in patients are main candidates to cause pathogenicity in investigated patients because they fulfill the canonical criteria for pathogenicity. They are heteroplasmic except the m.11453G>A mutation, which was homoplasmic. Those transitions change the amino acids in subunits of complex I. In addition, they affect a highly conserved sequence of the protein. They are present in investigated samples from patients with variable mutation loads.

To further support the roles of those mutations in pathogenicity, other cellular properties were investigated such as ROS levels, mitochondrial mass, membrane potential, and protein expression level.

The m.11777G>A and the m.13051G>A mutations were the only mutations which showed significant results as both revealed increases of in both ROS levels and mitochondrial mass in fibroblasts, while the remaining mtDNA mutations showed no significant changes from controls. In addition, measurement of membrane potential in fibroblasts from all patients revealed no statistically significant changes (Figure 3-35).

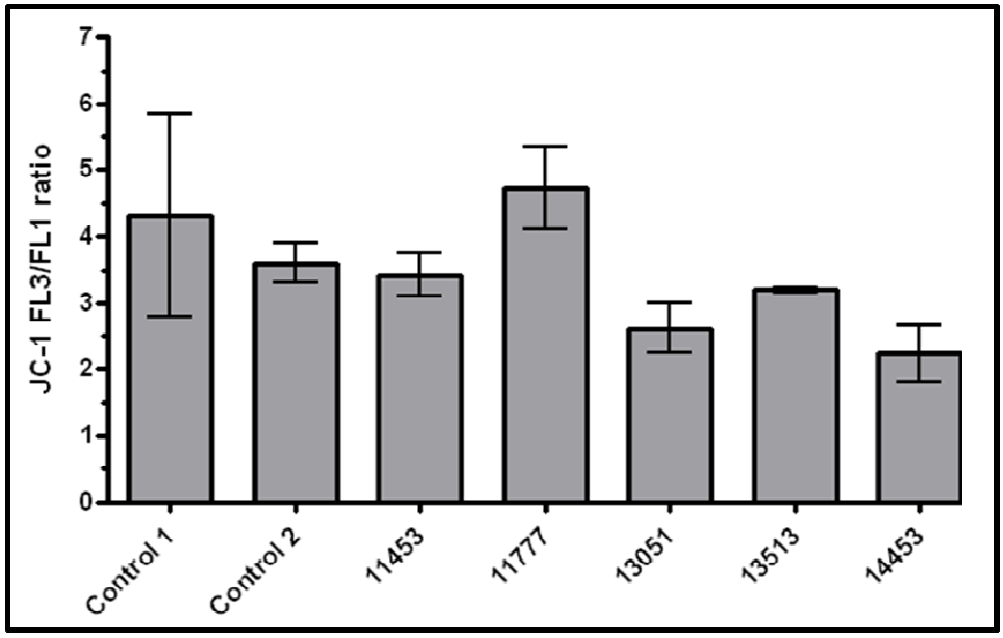

Figure 3-35 Membrane potential measurement in fibroblasts from investigated patients.

Results from measurement of membrane potential in patient`s cells using JC-1 probe showed no significance change when compared to contol samples as values still within the control values (*n*=2). Control 1 is a healthy control and control 2 is a healthy neonatal. Error bars represent SEM.

The increase of ROS level can be explained as a consequence of the respiratory chain defect due to mtDNA mutation, which caused a respiratory chain defect in patient #2 who carries the m.11777C>A mutation. The biochemical defect in complex I activity mimics inhibition of complex I activity by rotenone. In the process of electron transport through the complex, rotenone prevents the electrons from leaving complex I preventing electrons from transport. This results in the increase of electrons concentration and their availability to produce more ROS [62], which can explain the observed increased levels of ROS in this patient. However, it is not clear what caused the increased levels of ROS in patient #3 who has the m.13051G>A mutation but has normal OXPHOS. The normal levels of ROS production in the other patients could be explain by that those mutations did not cause structural modifications of complex I, which may play a crucial role in ROS production process when they affect the specific sites to cause ROS production [62]. Also, phosphorylation of mitochondrial proteins, which protect mitochondria against dysfunction, may affect levels of ROS production [398].

Mitochondrial mass also was increased in fibroblasts from both patients (#2 & #3). This increase results from a feedback mechanism to compensate for defective respiratory chain. Similarly, this can explain the increase of mitochondrial mass in patient with the

m.11777C>A mutation, who showed a defect in complex I activity. It is still not known what causing the increase of mitochondrial mass in the patient with the m.13051G>A mutation. However, mitochondrial mass does not increase in all pathogenic conditions due to mutations in the mtDNA [399].

Because the increase of mitochondrial mass may increase protein expression levels, we checked this by western blotting; however, measurement of protein expression levels in all patients showed no significance since fibroblasts from patients (2 & 3) showed low levels when compared to the other patients which revealed high levels of expression. The expression levels of MnSOD revealed no significant change in the m.11777G>A and the m.13051G>A patients even with the observed increase of mitochondrial mass.

Together, results from biochemical and molecular genetic investigations revealed that these mutations fulfilled the canonical criteria for pathogenicity, which make these mtDNA mutations in complex I strong candidates in causing the disease in the investigated patients.

Chapter 4

Identification of two novel and pathogenic mt-tRNA mutations

Chapter 4 : Identification of two novel and pathogenic mt-tRNA mutations

4.1 Introduction

An extensive range of molecular defects have been identified in the human mitochondrial genome, many associated with well-characterised, progressive neurological syndromes. These mutations may affect mitochondrial protein synthesis such as mtDNA deletions or single nucleotide substitutions, which predominantly affect mitochondrial transfer RNA (mt-tRNA) genes [1, 400]. A recent survey of an adult population with mtDNA disease has shown that mt-tRNA mutations are the most prevalent genetic defect, accounting for approximately 50% of all genetically-diagnosed cases [232]. Those mutations are either homoplasmic (all copies of the mtDNA are mutated) or heteroplasmic (a mixture of mutated and wild-type genomes in the same cell or tissue). Heteroplasmic mutations are most frequently observed in patients, with variation in levels of heteroplasmy contributing to the major differences in clinical phenotypes [401] .

To date, more than 250 mt DNA mutations have been associated with human diseases [402]. Mutations in the mitochondrial tRNA genes were identified after the discovery and characterization of the MERRF mutation (m.8344A>G) and MELAS mutation (m.3243A>G), respectively, in the late 1980s and early 1990s [403-405]. Some of the mutations in the tRNA genes are correlated with specific phenotypes and the clinical phenotypes can be different from mild to severe or even lethal [118]. Interestingly, there is considerable overlap in many cases in which mutations in the same mt-tRNA gene can give rise to different clinical phenotypes and conversely the same clinical phenotype can be caused by mutations in different mt-tRNA genes (Figure 4-1). Notably, although mt-tRNA genes represent ~10% of the mtDNA genome, almost 75% of mtDNA–related diseases are caused by mutations in these genes [406].

Mutations in the mitochondrial tRNA genes usually cause generalised impairment of mitochondrial protein synthesis. Individual mutations may affect mt-tRNA function by different mechanisms, including inhibition of aminoacylation [407], impairment of mt-tRNA stability [408], altered processing of the mt-tRNA [409], modification of wobble-bases [410, 411], reduced association of mt-tRNA with the ribosome [412] or a combination of these mechanisms. These mutations generally cause a ‘loss-of-function’ of

the affected mt-tRNA and are considered functionally recessive, as it is only when they affect most mtDNA molecules in a cell (70–90%) that a biochemical phenotype is observed [207]. However, this concept was recently challenged with the identification of an mt-tRNA mutation found to cause a biochemical defect at low levels of heteroplasmy [402, 413]. Initially, mt-tRNA mutations have been associated with multisystem syndromes, but they also have been observed in patients with tissue-specific disorders. Almost 50% of these mutations occur in only three mt-tRNA genes (mt-tRNA$^{Leu(UUR),}$ mt-tRNA^{Lys}, and mt-tRNA^{Ile}. The greater susceptibility of these mt-tRNA genes to mutagenesis than others can be explained by the weak stabilised tertiary structure of mt-tRNA$^{Leu(UUR)}$ and mt-tRNA^{Lys} [414] and the high content of A-U base-pairs in mt-tRNA ^{Ile} [415]. In addition, this can explain as well why one mt-tRNA mutation, such as m.3243A>G, can cause such a broad spectrum of clinical phenotypes while different mutations can be associated with the same clinical phenotype as explained by Giuseppe Attardi and colleagues [412].

Sequence changes in the mt-tRNA genes can be either pathogenic or polymorphic. Some of these genes are known to be hotspots for polymorphisms: mt-tRNA^{Thr}, mt-tRNA^{Asp}, mt-tRNA^{Arg}, mt-tRNA^{Cys}, mt-tRNA^{Gln} and mt-tRNA^{His}. Conversely, some are known to be hotspots for pathogenic mutations: mt-tRNA$^{Leu(UUR),}$ mt-tRNA^{Lys}, and mt-tRNA^{Ile}. Sequence changes are randomly distributed throughout the different structural domains of the mt-tRNAs that, suggests that all domains are equally prone to mutagenesis [118, 416]. However, the mt-tRNA$^{Leu(UUR)}$ gene was shown to have the greatest pathogenic mutation to neutral changes ratio and the mt-tRNA ^{Pro} gene had the least changes with only one pathogenic change. Almost 73% of mutations occurred in the stem structures and ~ 94% of the pathogenic mutations that occurred in stem structures disrupted Watson–Crick base pairing, while ~44% of neutral changes occurred in the stem structures and only 57% disrupted Watson–Crick base pairing [248]. Only a few mutations have been identified in the anticodon triplet region, which is known to be highly conserved in all mt-tRNAs. These are the m.12298T>C polymorphism in mt-tRNA$^{Leu(CUN)}$ [417], the m.15990G>A pathogenic mutation in mt-tRNA^{Pro} [418] , and the m.5545C>T pathogenic mutation in mt-tRNA Trp [402].

Finally, although some of mt-tRNA mutations exhibit maternal transmission within families, sporadic cases are rare [419]. The mt-tRNA mutation selection in a rapidly

replicating tissue such as blood is an important factor in determining whether this mutation is transmitted to offspring. Recent results showed that sporadic mt-tRNA mutations with low levels of mutation load in blood cells are likely to be inherited [420].

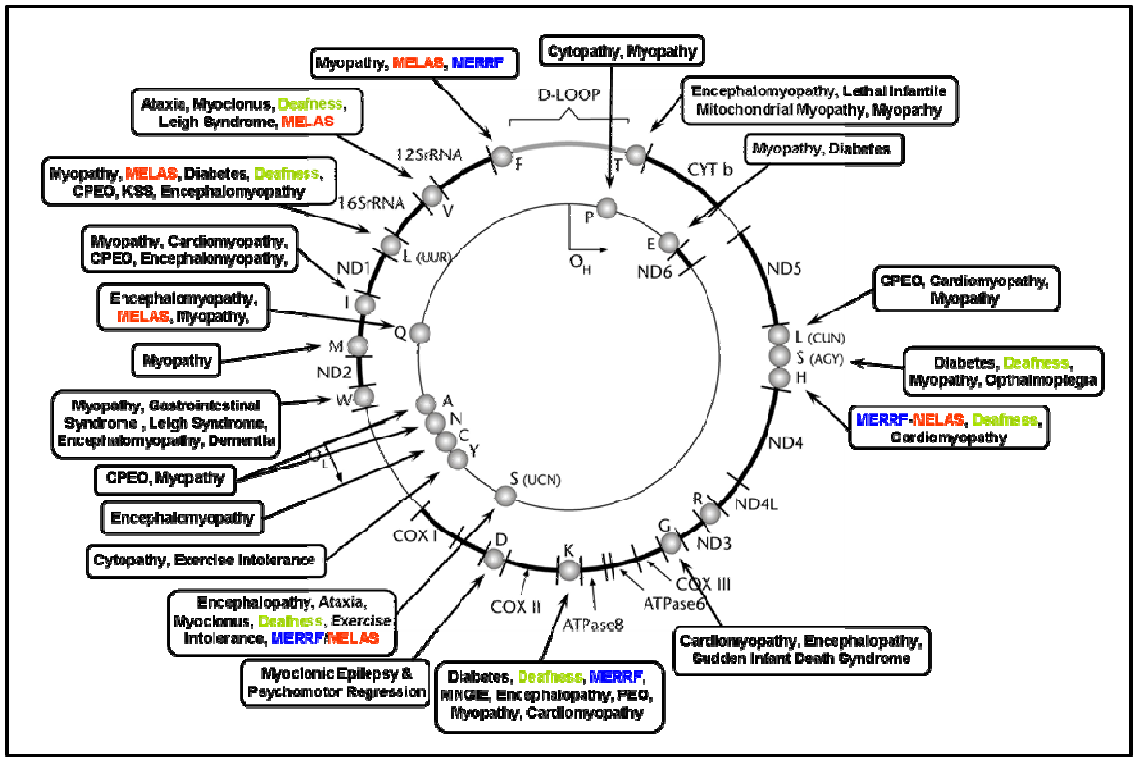

Figure 4-1 Association between mt-tRNA point mutations and clinical presentations.

The majority of mtDNA–related diseases are caused by mutations in mt-tRNA genes, which represent the minority of the mtDNA genome. In many cases, overlap was observed between mutations and clinical phenotypes. Associated clinical phenotypes and syndromes are shown. CPEO, chronic progressive external ophthalmoplegia; MELAS, mitochondrial myopathy, encephalopathy, lactic acidosis, and stroke-like episodes; MERRF, myoclonic epilepsy and ragged red fibres; PEO, progressive external ophthalmoplegia; MNGIE, mitochondrial neurogastrointestinal encephalopathy syndrome; KSS, Kearns-Sayre syndrome (modified from a Figure courtesy of Dr. Helen Swalwell).

4.2 Aims

In this chapter, I will describe the histochemical, biochemical, and molecular genetic investigation of two patients. The first patient (NCL-1) was investigated because she developed a clear clinical phenotype related to a mitochondrial biochemical defect. The second patient (Portland-4) was from a cohort of 6 patients (Table 4-1) who were referred on the basis of their clinical phenotypes for mitochondrial DNA investigations, their muscle biopsies revealed biochemical or histochemical defects.

Table 4-1 Summary of the clinical presentations and other related investigations in the studied cohort of patients.

Patient	**Age**	**Clinical phenotypes**	**Biochemical and histochemical investigations**	**Identified mtDNA mutations**
Portland-1	24	Learning disability, seizures, hearing loss, and stroke	COX negativity with ragged red fibres. -Mild COX deficiency.	m.6299A>G, *MTCOX1* silent change
Portland-2	34	Recurrent muscle cramps and exercise fatigue	- Ragged red fibres without COX negativity.	m.6794A>G, *MTCOX1* silent change
Portland-3	62	Severe fatigue, exercise intolerance, progressive ataxia,peripheral neuropathy	-Decrease Complex I and COX activities. -High percentage of COX negativity but no ragged red fibres.	No pathogenic mtDNA mutation identified
Portland-4	28	Some developmental delay, motor and speech delay, hearing loss. Grand mal seizures, vision loss and retinitis pigmentosa	-Mild complex I deficiency. - Many ragged red fibres and some COX deficient fibres.	**m.12261G>A, *MTTL2***
Portland-5	71	Muscle pain with weakness, ptosis, chest pain, and decreased attention span and memory	- COX deficient fibers but no ragged red fibres. - Mild complex I deficiency.	m13497A>G, *MTND5* silent change
Portland-6	74	Muscle weakness, CPEO, ptosis, and retinitis pigmentosa	-Numerous ragged red fibres and scattered COX deficient fibres.	m.5450C>T, MTND2 silent change

4.3 Material and methods

4.3.1 Needle muscle biopsy analysis

Sections from frozen muscle biopsies were cut using a cryostat to perform routine histological analysis. Haematoxlyin and eosin (H&E) staining was carried out as described (section 2.2.15.1). In addition, combined COX/SDH staining was carried out as decribed (section 2.2.15.2).

4.3.2 Long-range PCR analysis

Long-range PCR analysis was carried out as described (section 2.2.12) to screen for large-scale mtDNA rearrangements in total muscle DNA.

4.3.3 Mitochondrial DNA sequencing

Entire mitochondrial genome sequencing from total muscle homogenate or blood was performed as described (section 2.2.6) to search for mtDNA point mutations.

4.3.4 PCR-RFLP analysis

Table 4.2 summarises details for this analysis such as primer position, sequence, restriction endonuclease enzyme, and annealing temperatures in investigated patients.

Table 4-2 Summary of PCR-RFLP analyses for the m.618T>G and m.12261T>C mutations in NCL-1 ansd Portland-4 patients.

Mutation	**Primer Position**	**Primer Sequence**	**Primer Annealing Temperature (^{o}C)**	**Enzymes and Digestion site**	**Digest Temperature (^{o}C)**	**Uncut PCR product (bp)**	**Wild-type products (bp)**	**Mutant products (bp)**
m.618T>G	L503 H639	5`-GCACACACACACCGCTGC-3` 5`-GGGTGATGTGAGCCCGT**T**TAA-3`	61	Mismatch reverse primer to introduce a *DraI* site (TTT/AAA)	37	127	108 + 19	127
m.12261T>C	L12221 H122468	5`-GAACTGCTAACTCATGCCC-3` 5`-AAAGGTGGATGCGACAATGG-3`	58	Mutation creates another *Mn1I* site (CCTC(N))	37	248	192+56	141+56+51

4.4 The m.618T>G mutation case

4.4.1 Summary of clinical representations for the m.618G>A case

The NCL-1 patient is a 50-year old female who presented at age 25 with left sided ptosis that became bilateral. She had limb and respiratory weakness. In addition, she had CPEO, myopathy, diplopia, dysphagia, and exercise intolerance. Initial results from long-range PCR appeared to show multiple mtDNA deletions; however, no evidence of mutations in the three major mtDNA maintenance genes (*POLG*, *SLC25A4*, and *PEO1*) was noted. Combined COX-SDH histochemical analysis showed ~25% COX deficiency in her muscle biopsy (Figure 4-2).

She had two daughters. The first (NCL-2) is 28-years old and clinically asymptomatic. However, muscle biopsy analysis revealed ~ 3% COX deficiency, which is abnormal at this age although no evidence of mtDNA deletions was detected on long-range PCR.

Her other daughter (NCL-3) is 27-years old. She presented with deafness and a stroke-like episode at the age of 19. A CT scan showed that she had had two mini strokes. Muscle biopsy investigations showed no evidence of mtDNA deletions and biochemical assessment of respiratory chain activity was normal. In addition, histochemical and histological analyses showed normal results.

4.4.2 Results

4.4.2.1 Histochemical analysis

The combined COX/SDH staining of the patient`s muscle biopsy showed ~ 25% COX deficiency with several fibres showing evidence of subsarcolemmal mitochondrial accumulation typical of ragged-red changes which are suggestive of an underlying mitochondrial genetic abnormality (Figure 4-2).

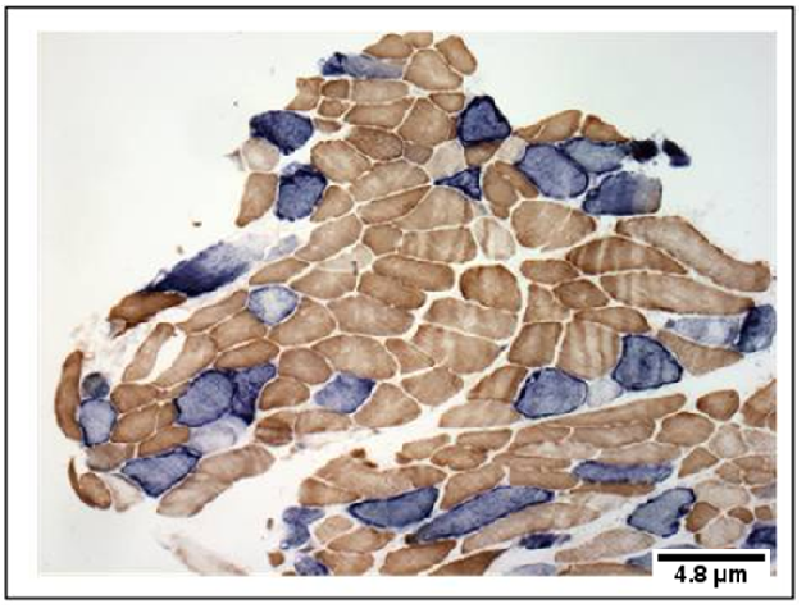

Figure 4-2 Histological and histochemical analysis of muscle biopsy from patient with the m618T>G.

The figure shows the combined COX/SDH staining in muscle biopsy from patient, which revealed ~25% of COX deficiency in the patient. COX-positive fibres are brown and COX-deficient fibres are blue.

4.4.2.2 Long-range PCR analyses

Total muscle DNA was assessed for large-scale mtDNA rearrangements. In addition to the full-length wild-type 10kb amplicon, a number of faint, smaller products were also amplified, which were initially suggestive of multiple mtDNA deletions (Figure 4-3) although a great proportion of mtDNA deletions were expected given the marked histochemical changes seen in muscle.

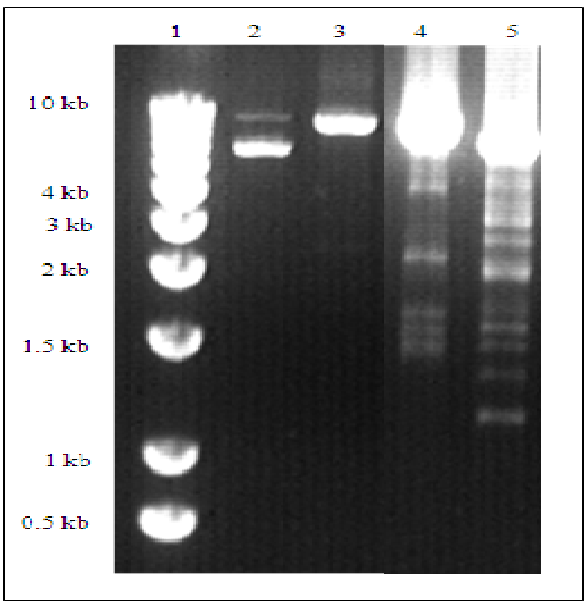

Figure 4-3 Long-range PCR analysis of muscle biopsy from patient NCL-1.

Lane 1 is a 10 kb DNA ladder, lane 2 is a PCR product from a patient who has a single mtDNA deletion (positive control), lanes 3 is a PCR product from a person who has no mtDNA deletion (control), lane 4 is the resultant PCR product from NCL-1 muscle DNA sample, and lane 5 is a PCR product from a patient who has multiple mtDNA deletions (positive control).

4.4.2.3 Real- time PCR analysis

Real-time PCR was carried out as described (section 2.2.13) to further investigate the molecular basis of the COX deficiency in individual muscle fibres. DNA was prepared from laser-microdissected COX-positive (*n*=13) and COX-deficient fibres (*n*=15). Specific sets of primers and probes were used to quantify the amount of mtDNA. These were located in the *MTND1* gene, which is rarely deleted in patients and the *MTND4* gene, which is deleted in the majority of patients. However, results revealed no evidence of mtDNA deletion in the *MTND4* gene since all values are below the known threshold levels for mtDNA deletion, which is about 65% [421] (Figure 4-4).

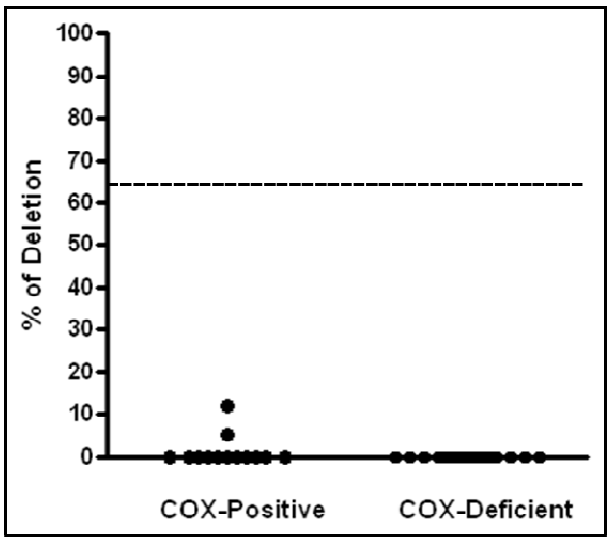

Figure 4-4 Real-Time PCR analyses of individual muscle fibres from NCL-1 patient to assess mtDNA deletion.

This figure shows no evidence of mtDNA deletion in the investigated COX-positive and COX-deficient fibres as levels of mutation load fall below threshold levels of mtDNA deletion.

4.4.2.4 Whole mitochondrial genome sequencing

To further investigate the COX-deficient fibres, which we had proven were devoid of mtDNA deletion, whole mitochondrial genome sequencing was carried out on skeletal muscle DNA. Results showed the identification of the heteroplasmic m.618T>G mutation in the *MTTF* gene (mt-tRNA^{Phe}) (Figure 4-5) in addition to other changes (Table 4-3), all previous reported in the main mitochondrial databases [69, 252]. The *MTTF* mutation disrupts a highly conserved base pairing in the anticodon stem of the mt-tRNA Phe (Figure 4-6). A mutation at the same location was previously reported as novel and pathogenic but the change observed was m.618 T>C [422].

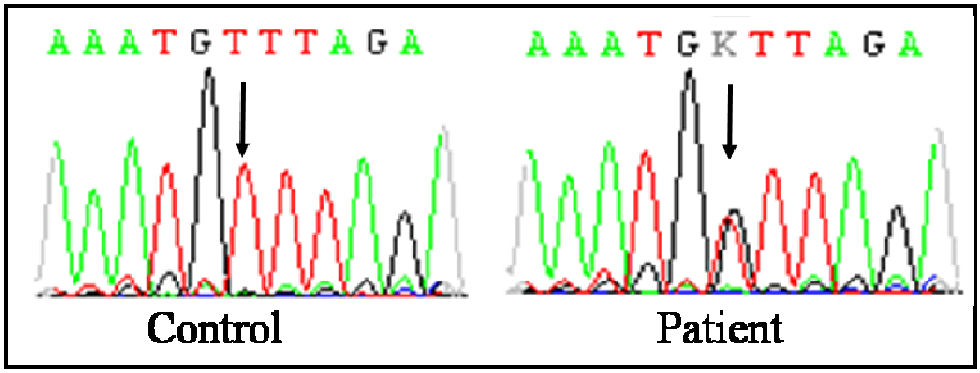

Figure 4-5 Sequence chromatogram showing the m.618T>G transversion in patient NCL-1.

Position of the m.618 is shown in both control and patient (indicated by arrow).

Table 4-3 Sequence changes identified in patient NCL-1.

Sequence change	**Previously reported as a SNP or pathogenic? Mitomap or mtDB**	**Amino acid Change**	**Location**
m.263A>G	Yes	-	D-Loop
m.303C ins.	Yes	-	D-Loop
m.414T>C	Yes	-	D-Loop
m.618T>G	**No**	-	***MTTF***
m.750A>G	Yes	-	12S rRNA
m.1438A>G	Yes	-	12S rRNA
m.3107delC	Yes	-	16S rRNA
m.4769A>G	Yes	No	*MTND2*
m.5663C>T	Yes	-	*MTTN*
m.8860A>G	Yes	Thr112Ala	*MTATP6*
m.14470T>C	Yes	No	*MTND6*
m.15326A>G	Yes	Thr194Ala	*MTCYB*
m.16519T>C	Yes	-	D-Loop

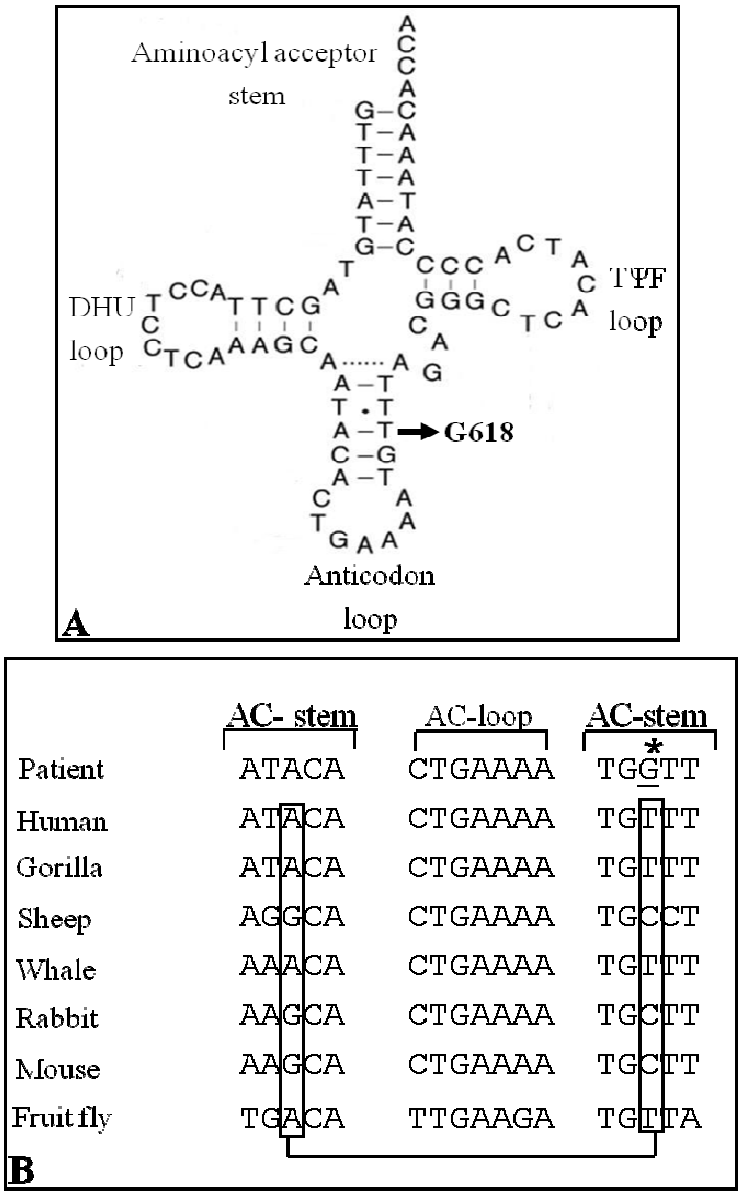

Figure 4-6 Conservation of the nucleotide at position m.618T>G.

(A) Schematic representation of the mt-tRNA^{Phe} cloverleaf structure showing the position of the mutation in the anticodon stem (taken and modified from http://mamit-trna.u-strasbg.fr/mutations.asp?idAA=20). (B) Phylogenetic conservation of this region of the *MTTF* gene sequence in different species showing the highly conserved base pairing (boxes).

4.4.2.5 PCR-RFLP analysis

A mismatch reverse primer was designed to introduce a *DraI* site (TTT/AAA) in the wild-type mtDNA. The endonuclease *DraI* cuts wild-type into 108bp and 19bp, while the mutant mtDNA and uncut samples result in 127bp products (Figure 4-7-A). Results showed high levels of m.618T>G in skeletal muscle from the patient as high (as high as

76%) but the mutation was absent in the patient's blood and urine samples. In addition, the m.618T>G was absent in skeletal muscle, blood, and urine samples from two daughters (Figure 4-7-B).

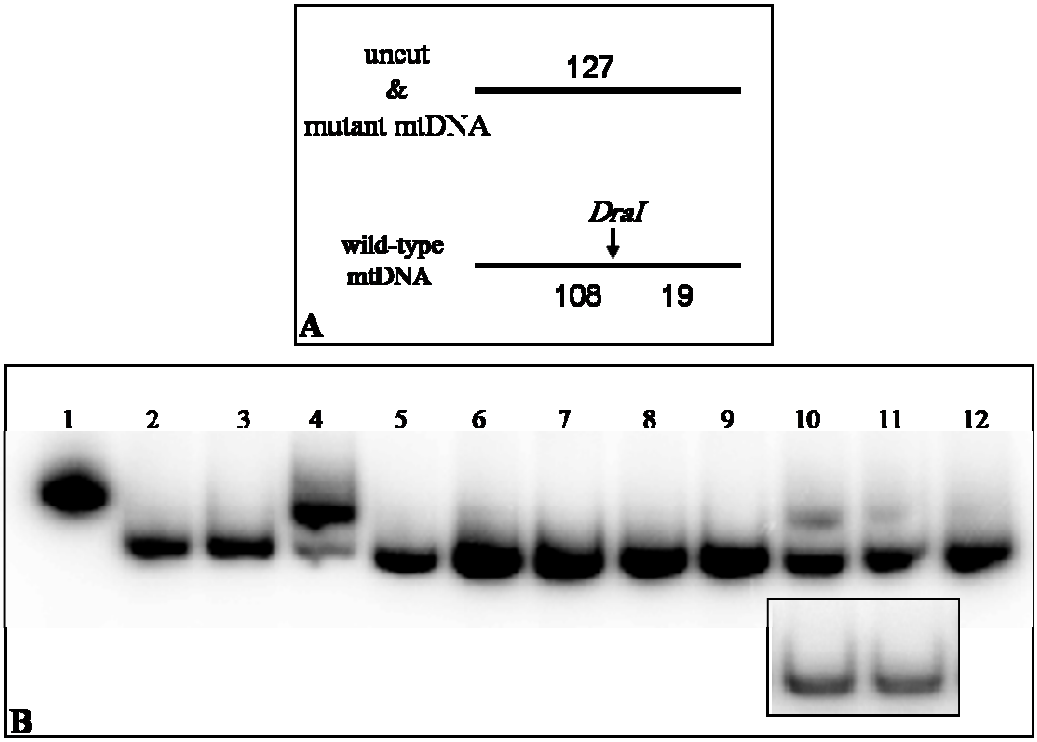

Figure 4-7 PCR-RFLP analysis of the m.618T>G mutation in patient NCL-1.

(A) Schematic diagram of PCR-RFLP analysis showing the sizes of the products after digestion with restriction endonuclease DraI. (B) PCR-RFLP analyses to quantify the m.618T>G levels in different tissues from the patient and her daughters. Lane 1 is an uncut DNA sample, lanes 2 and 3 are DNA samples from negative controls, lane 4 is a patient's muscle (76% mutant), lanes 5 6 is patient's blood, and lane 6 is patient`s urine. Lanes 7-9 are NCL-2 patient`s muscle, blood, and urine. Lanes 10-12 are NCL-3 patient`s muscle, blood, and urine. The boxed lanes are a repeat of the two samples to confirm absence of mutation.

To determine whether the m.618T>G mutation segregates with the biochemical defects in individual cells. DNA was prepared from laser-microdissected COX-positive (*n*=20) and COX-deficient fibres (*n*=18). Results showed that the higher levels of the m.618T>G mutation were detected in COX-deficient fibres (96.56 ± 11.77%) than in the COX-positive fibres (22.35 ± 33.61%) (P<0.0001), confirming segregation of the m.618T>G genotype with respiratory chain dysfunction (Figure 4-8).

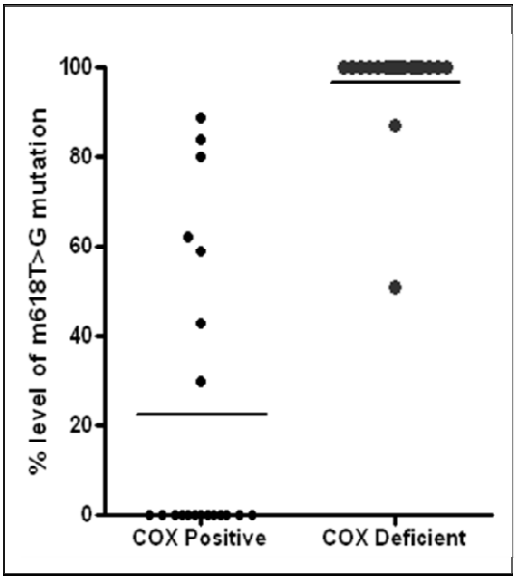

Figure 4-8 Graphical representation of single PCR-RFLP analysis of the m.618T>G.

This graph shows the mean percentage and SE values of PCR-RFLP analysis of COX-positive and COX-deficient fibres. COX-positive (*n*=20, 22.35 ± 33.61%), COX-deficient fibres (*n*=18, 96.56 ± 11.77%) and P<0.0001 confirming segregation of the m.618T>G genotype with respiratory chain dysfunction.

4.4.3 The m.618T>G mutation is pathogenic

Many pathogenic mtDNA mutations have been identified in association with a wide spectrum of clinical phenotypes. The majority of these mutations are found in mt-tRNA genes, resulting in translational defects and subsequent mitochondrial respiratory chain dysfunction [423, 424]. Patients with extraocular muscle involvement (CPEO) usually have pathogenic mtDNA rearrangements [236], while patients with myopathy, proximal limb weakness, myalgia , and exercise intolerance usually have an mtDNA point mutation in a protein-encoding gene [1, 236]. Pathogenic point mutations in the mt-tRNA genes are usually associated with COX deficiency and abnormal proliferation of mitochondria in muscle tissue [419].

This patient was described to have CPEO and weakness in respiratory muscles and both limbs. Histochemical analyses of the patient's muscle biopsy showed COX negativity in muscle fibres with ragged red fibres, which suggest mitochondrial accumulation. The identified m.618T>G mutation within mt-tRNA^{Phe} in this patient appeared to be the pathogenic mutation causative of the disease for several reasons. This mutation is not a neutral polymorphic variant and has not been reported in either of the mitochondrial genome databases [69, 252]. It is a heteroplasmic change present at high levels in muscle tissues but absent in other tissues. Furthermore, it affects and disrupts a highly conserved

base pairing within the $tRNA^{Phe}$ anticodon stem suggesting this nucleotide has an important function and its loss may be harmful (Figure 4-6-B), Finally, higher mutation load was observed in the COX-deficient fibres as compared to the COX-positive fibres confirming segregation of the mutation with the biochemical defect.

In summary, the m.618T>G mutation was present in high levels in DNA samples from skeletal muscle of the patient and absent in DNA samples from blood and urine. Also, it was absent from DNA samples in different tissues (muscle, blood, and urine) from her two daughters. This strongly indicates that the m.618T>G is sporadic and not transmitted. However, it is still not known what is causing COX negativity in her daughter (NCL-2) as PCR-RFLP analysis showed absence of the m.618T>G and long-range PCR revealed no evidence of mtDNA deletion.

4.5 The m.12261T>C *MTTS2* mutation

4.5.1 Summary of clinical presentations for Portland-4 patient

As mentioned before (section 4.2), Portland-4 patient was from a cohort of six patients, whose their samples were sent to be investigated. The patient is a 28-year old male who presented with some developmental delay. He had motor and speech delay and hearing loss at the age of 6 years. At 12 years of age, he had grand mal seizures, vision loss, and retinitis pigmentosa, which are features of Noonan syndrome. His father had a history of migraines, sarcoidosis, and joint pain. His mother had migraines, heart problems, fatigue, and aerobic exercise intolerance. All observed clinical phenotypes and other related information for this patient and the other patients from the cohort are summarised in Table 4-1.

4.5.2 Results

4.5.2.1 Mitochondrial DNA sequencing

Full mitochondrial genome sequencing of muscle homogenate DNA from all patients identified mostly silent changes or non-pathogenic mutations (Table 4-4). The only pathogenic mutation identified was in portland-4 patient, which was a transition mutation at nucleotide m.12261T>C in the *MTTS2* gene, mt-$tRNA^{Ser(AGY)}$ (Figure 4.9). The m.12261T>C sequence change was not previously reported in either of the mitochondrial genome databases [69, 252]. This mutation resides in a highly conserved position in the aminoacyl acceptor stem and disrupts a Watson-Crick base pairing (Figure 4-10).

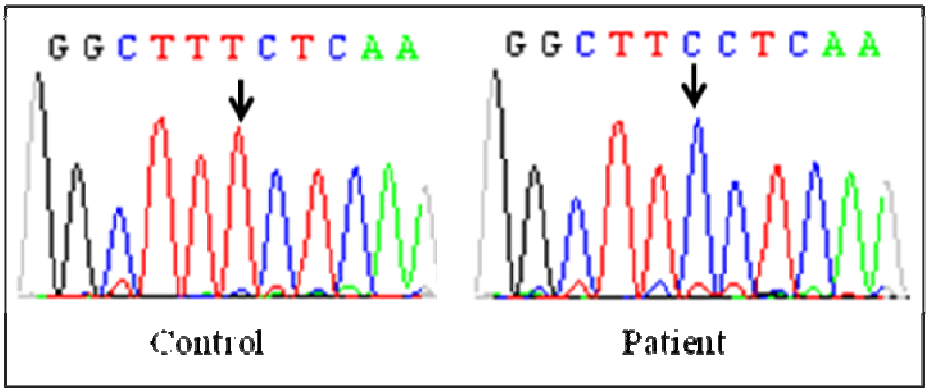

Figure 4-9 Sequence chromatogram showing the m.12261T>C transition in Portland-4 patient.

Position of the m.12261 nucleotide is shown in both control and patient (indicated by arrow).

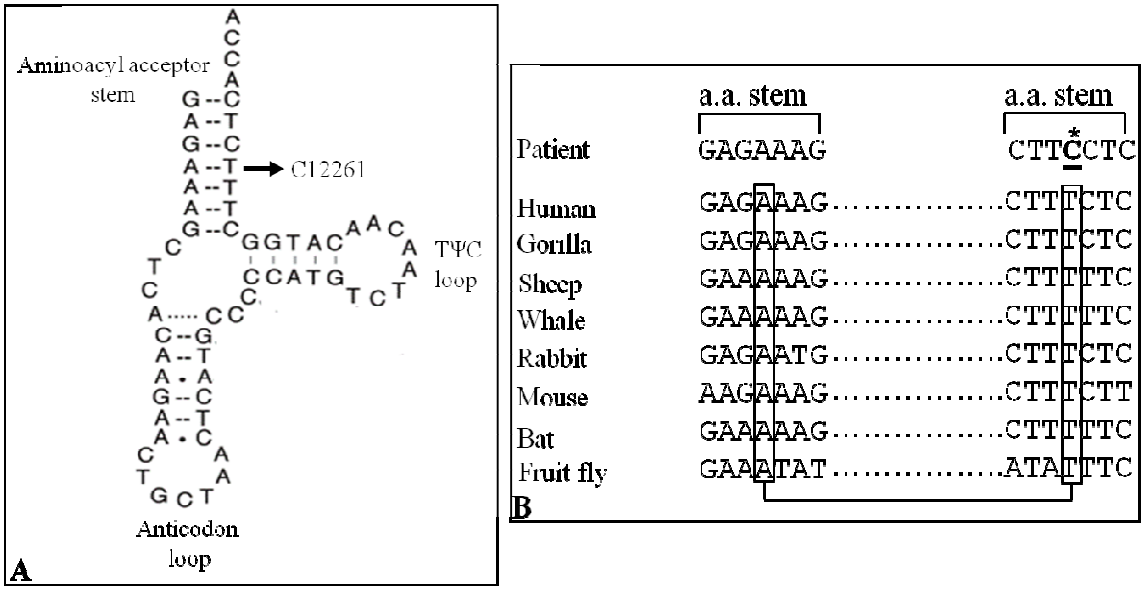

Figure 4-10 Conservation of the nucleotide at position m.12261.

(A) Schematic representation of the mt-tRNA $^{Ser(AGY)}$ cloverleaf structure showing the position of the mutation in the aminoacyl acceptor stem (taken and modified from http://mamit-trna.u-strasbg.fr/mutations.asp?idAA=22). (B) Phylogenetic conservation of this region of the *MTTS2* gene sequence in different species showing the highly conserved base pairing (boxes).

Table 4-4 Sequence changes identified in Portland-4 patient.

Sequence change	Previously reported as a SNP or pathogenic? Mitomap or mtDB	Amino acid change	Location
m.73A>G	Yes	-	D-Loop
m.263A>G	Yes	-	D-Loop
m.1438A>G	Yes	-	12S rRNA
m.1811A>G	Yes	-	16S rRNA
m.2352T>C	Yes	-	16S rRNA
m.2706A>G	Yes	-	16S rRNA
m.3106C ins.	Yes	-	16S rRNA
m.3720A>G	Yes	No	*MTND1*
m.4733T>C	Yes	No	*MTND2*
m.4769A>G	Yes	No	*MTND2*
m.5390A>G	Yes	No	*MTND2*
m.5426T>C	Yes	No	*MTND2*
m.6045T>T	Yes	No	*MTCOX1*
m.6152T>C	Yes	No	*MTCOX1*
m.7028C>T	Yes	No	*MTCOX1*
m.8860A>G	Yes	Thr112Ala	*MTATP6*
m.10876A>G	Yes	No	*MTND4*
m.11467A>G	Yes	No	*MTND4*
m.11719G>A	Yes	No	*MTND4*
m.12261T>C	**No**	-	***MTTS2***
m.12308A>G	Yes	-	*MTTL2*
m.12372G>A	Yes	No	*MTND5*
m.13020T>C	Yes	No	*MTND5*
m.13734T>C	Yes	No	*MTND5*
m.15326A>G	Yes	Thr194Ala	*MTCYB*
m.15907A>G	Yes	-	*MTTT*
m.16051A>G	Yes	-	D-Loop
m.16189T>C	Yes	-	D-Loop
m.16129G>C	Yes	-	D-Loop
m.16182A>C	Yes	-	D-Loop
m.16183A>C	Yes	-	D-Loop
m.16189T>C	Yes	-	D-Loop
m.16362T>C	Yes	-	D-Loop
m.16519T>C	Yes	-	D-Loop

4.5.2.2 PCR-RFLP analysis

The m.12261T>C mutation leads to the creation of an additional endonuclease *Mn1I* site (CCTC(N)) in the mutated mtDNA resulting in three products: 141bp, 56bp, and 51bp, while the restriction enzyme only cuts the wild-type mtDNA into two products: 192bp and 56bp (Figure 4-11-A). Results showed high levels of the m.12261T>C in the patient that ranged from 13%-94% in analysed tissues (Figure 4-11-B). However, mutation load was very low (<1%) in different tissues from relatives (Figure 4-11-C).

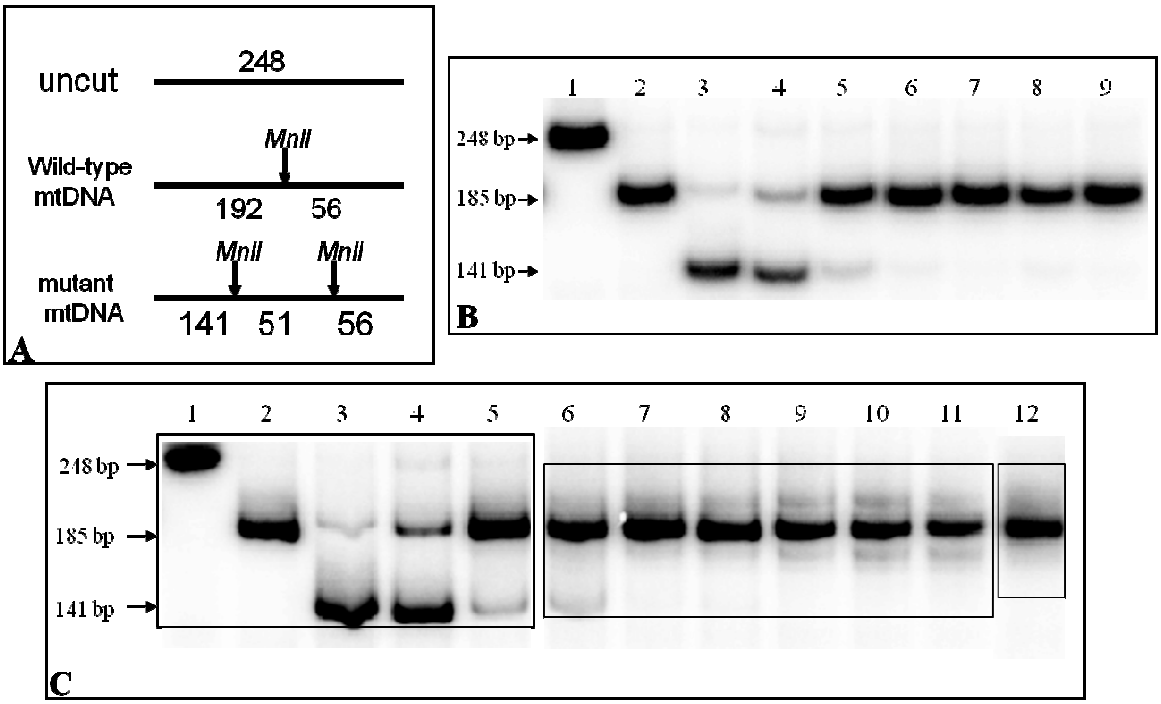

Figure 4-11 PCR-RFLP analysis of the m.12261T>C mutation.

(A) Schematic diagram of PCR-RFLP analysis showing the sizes of the products after digestion with restriction endonuclease *MnlI*. (B) PCR-RFLP analysis to quantify the m.12261T>C levels in different tissues from patient and relatives. Lane 1 is an uncut DNA sample, lane 2 is DNA sample from a negative control, lane 3 is patient`s muscle DNA sample (94% mutant), lane 4 is patient's urine DNA sample (78% mutant), and lane 5 is patient's buccal DNA sample (15% mutant). Lane 6 is mother's urine DNA sample, and lane 7 is mother's buccal DNA sample. Lane 8 is grandmother's urine DNA sample, and lane 9 is grandmother's buccal DNA sample. (C) Levels of the m.12261T>C in blood DNA samples from patient and relatives. Lane 1 is an uncut DNA sample, lane 2 is DNA sample from a negative control, lane 3 is DNA from patient`s muscle with the m.12261T>C mutation (positive control, 94% mutant), and lane 4 is patient`s blood DNA sample (13% mutant). Lane 5 is mother `s blood DNA sample, lane 6 is grandmother's blood DNA sample, lanes 7 & 8 are patient's brothers blood DNA samples, and lanes 9 & 10 are patient`s sisters blood DNA samples. Boxed lanes are taken from another experiment.

To determine whether the m.12261T>C mutation segregates with the biochemical defects in individual cells, DNA was prepared from laser-microdissected COX-positive (*n*=11) and COX-deficient fibres (*n*=10). Although high levels of mutation load (up to 94%) were seen in DNA sample from muscle, a significant difference between the percentage of the mutant mtDNA in the COX-positive and COX-deficient fibres was seen. Results showed that higher levels of the m.12261T>C mutation were detected in COX-deficient fibres (97.10 ± 1.101%) than in COX-positive fibres (85.82 ± 16.59%) (P<0.0001), confirming segregation of the m.12261T>C genotype with respiratory chain dysfunction (Figure 4-12).

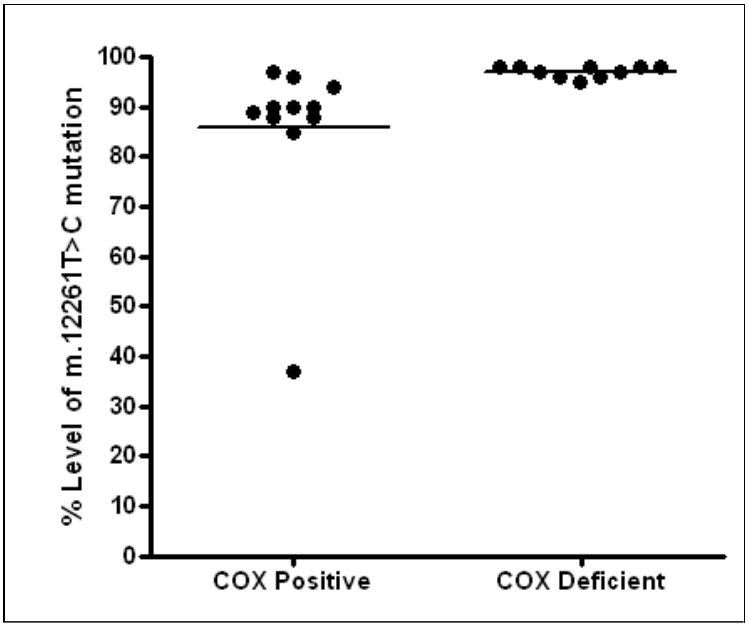

Figure 4-12 Graphical representation of single PCR-RFLP analysis of the m.12261T>C mutation.

This graph shows the mean percentage and SE values of PCR-RFLP analysis of COX-positive and COX-deficient fibres: COX-positive (*n*=11, 85.82 ± 16.59%), COX-deficient fibres (*n*=10, 97.10 ± 1.101), and P<0.0001 confirming segregation of the m.12261T>C genotype with respiratory chain dysfunction.

4.5.2 The m.12261T>C mutation is pathogenic

Portland-4 patient was described to have developmental delay, motor and speech delay and hearing loss. In addition, he had seizure, vision loss and retinitis pigmentosa. Initial analysis of patient's muscle biopsy showed COX negativity in muscle fibres and many ragged red fibres, which suggest mitochondrial accumulation. Moreover, biochemical analysis showed a mild defect of the respiratory chain complex I. The identified mt-tRNA$^{Ser(AGY)}$ sequence variant in this patient was demonstrated to be the pathogenic mutation, causative of the observed clinical presentations. This mutation fulfilled the canonical criteria for pathogenicity of mtDNA mutations [199]. It is not a neutral

polymorphic variant and has not been reported in either of the mitochondrial genome databases [69, 252]. It is a heteroplasmic change with higher levels in postmitotic muscle than mitotic cells and affects a highly conserved nucleotide within the tRNA structure. In addition, it disrupts a Watson-Crick base pair in the aminoacyl acceptor stem (Figure 4-8). Finally, this mutation showed high levels of mutation load in COX-deficient fibres as compared to COX-positive fibres confirming segregation with the biochemical defect. All these given data provide a strong evidence that the m.12261T>C mutation is causative of the disease.

Not only did this mutation show different levels of heteroplasmy in different tissues from the patient, but it was also present in different tissues from mother and grandmother with low levels of heteroplasmy, which suggests transmission of the mutation to patient. The presence of this mutation with low levels in both mother and grandmother explains why they are asymptomatic, while the presence of this mutation in the patient but not in the other siblings can be attributed to mtDNA segregation.

Further conclusions from the analysis of the two patients investigated in this Chapter will be discussed in the General Discussion (Chapter 7).

Chapter 5

Neuromuscular disease presentation with three genetic defects involving two genomes

Chapter 5 : Neuromuscular disease presentation with three genetic defects involving two genomes

5.1 Introduction

Mutations in the human mitochondrial genome (mtDNA) have been shown to cause progressive neurological syndromes [1]. These commonly include mutations that affect mitochondrial protein synthesis such as single, large-scale mtDNA deletions and single nucleotide substitutions affecting mitochondrial transfer (mttRNA) genes [400]. The majority of mt-tRNA mutations are heteroplasmic, with clinically-affected tissues such as skeletal muscle exhibiting high mutation loads, leading to a respiratory chain defect. This is best illustrated in individual muscle fibres with cells exhibiting a mutation load above a critical threshold, typically ~90% for most mt-tRNA mutations, lacking demonstrable histocytochemical cytochrome *c* oxidase (COX) activity [317, 425, 426]. However, the pathogenic threshold may be influenced by several factors, including mitochondrial morphology and dynamics. Also the situation may be different in replicating cells compared with that of non-dividing muscle fibres [402].

The recent description of a patient with a multisystem presentation due to a novel mt-tRNA^{Trp} (*MTTY*) gene mutation that was present at low mutant loads in clinically-affected tissues has challenged the accepted dogma that all mt-tRNA mutations are "functionally-recessive". The m.5545C>T mutation within the mt-tRNA^{Trp} caused a severe multisystemic disorder and marked respiratory chain deficiency even at low levels of heteroplasmy (<25%) in affected tissues. The pathogenic threshold for the mutation in cybrids was between 4 and 8%, confirming a dominant mechanism of action regardless of the precise mechanism [402]. Two hypotheses were proposed to better understand this phenomenon. First, the central base (A<u>C</u>U) of the anticodon triplet of the mt-tRNA^{Trp} at position 5545 interacts with the central base (G) of the codon triplet (UGA) and (UGG) in the mRNA and is essential to determine tRNA specificity. However, the m.5545C>T changes the anticodon from ACU to AUU which makes the mutated mt-tRNA decode UAA or UAG, which are termination codons. So the mutated mt-tRNA^{Trp} may cause a read-through of the mRNA adding one Trp residue at the position of the stop codon followed by the incorporation of a tail of lysine residues specified by the poly-A sequence at the end of the transcript. Second, since the third base of the codon in the mitochondrial genome is usually

not essential to determine tRNA specificity [427], the mutated tRNA could recognize UGC and UGU codons and incorporate tryptophan in the place of tyrosine [402] (Figure 5-1).

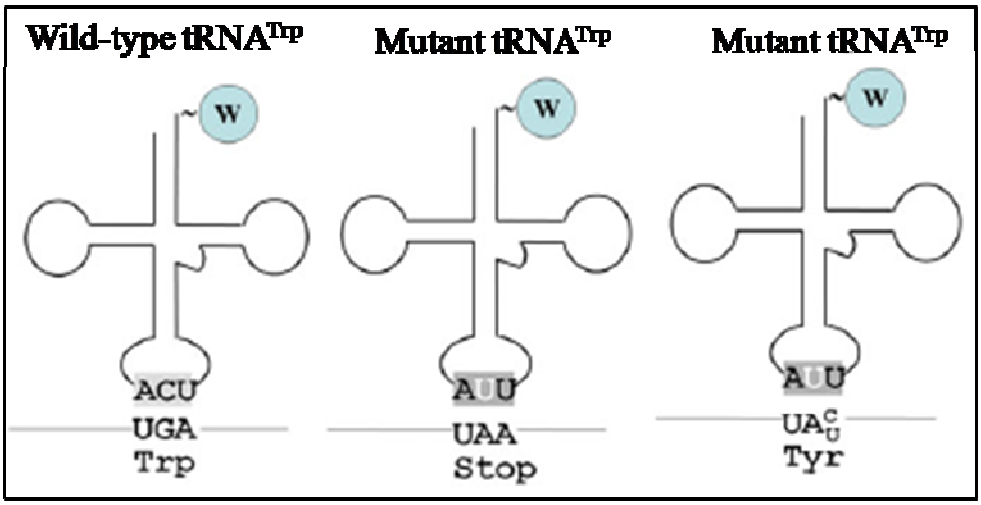

Figure 5-1 Schematic representation showing the structure of the mt-tRNA^{Trp}.

This figure shows structure of the wild-type mt-tRNA^{Trp}, mutant mt-tRNA^{Trp}, and the possible effect of mutation on codon recognition. The wild-type mt-tRNA^{Trp} anticodon (ACU) recognises the (UGA) codon on the mRNA that encodes the mt-tRNA^{Trp}. However, the m.5545C>T mutation changes the anticodon from ACU to AUU which makes the mutated mt-tRNA decodes UAA or UAG, which are stop codons, or could recognize UGC and UGU codons and incorporate tryptophan in the place of tyrosine (taken and modified from [402]).

This chapter presents the m.12283G>A mutation within the mt-tRNA$^{Leu(CUN)}$ (*MTTL2*), which is another mutation present at low levels that clearly segregates with a functional, biochemical defect as measured by COX activity in individual muscle fibres. Interestingly, this novel mtDNA mutation represents only one of three, confirmed genetic abnormalities in this patient.

The identification of such mutations has led to a rethink about the way to diagnose some pathogenic mtDNA mutations since these mutations may easily escape detection by standard diagnostic screening methods. Indeed, failure to identify the m.12283G>A mutation the first time I sequenced muscle homogenate mtDNA from this patient was due to mutation load levels, which were below detection threshold levels. Investigation of this patient has highlighted that such mutations may only be detected by performing full genome sequencing on biochemically-affected individual muscle fibres (COX-deficient).

5.2 Aims

This chapter will present the clinical, histochemical, biochemical and molecular genetic investigations in a patient with a neuromuscular disease presentation due to three genetic defects involving two genomes.

5.3 Clinical presentations

The patient is a thirty-one year old gentleman who first presented to a specialist mitochondrial clinic for investigation of progressive bilateral ptosis, chronic progressive external ophthalmoplegia and increasing difficulties with walking but who has an extensive past medical history going back to childhood. He had always been poor at running and jumping at school and at the age of eleven was investigated for drooping eyelids, difficulty holding a pen and difficulty with walking. He was found to have a demyelinating polyneuropathy on neurophysiological testing and HMSN type 1A was confirmed genetically by the demonstration of duplication of the *PMP22* gene on the short arm of chromosome 17 at another diagnostic centre.

At the age of 25 years he developed gout and presented in acute renal failure at the age of 30 years. He was found to have a grossly elevated plasma urate level of 1.35mmols/L (normal < 420µmol/L) and was subsequently investigated for a possible *HPRT* mutation. Direct sequencing at another diagnostic Centre revealed a c.481G>T mutation predicting a missense mutation (p.A161S) in a recognised mutation hotspot of the gene. His mother was later confirmed as being a carrier of this X-linked recessive mutation.

His ptosis had progressed to the point that he had required bilateral eyelid elevation surgery earlier in the year. At that time he had been noted to have external ophthalmoplegia but described no diplopia. He had weak grip in both hands, required a stick to walk, and found that his legs often gave way. He has bilateral ptosis despite the previous surgery. Eye movements are restricted in all directions to less than 30^0. There is reduced muscle bulk in his limbs and power was reduced to MRC grade 4/5 in both proximal and distal muscles. Deep tendon reflexes were absent throughout and there was impaired sensation to pin prick, light touch and joint position sense to above the ankles. His father and paternal grandfather were described as ‘shaky’. The patient’s youngest son had recently developed difficulty walking.

5.4 Methods

5.4.1 Needle muscle biopsy analysis.

Sections from a frozen muscle biopsy were cut using a cryostat to perform routine histological analysis. Hematoxlyin and eosin (H&E) staining was carried out as described (section 2.2.15.1) followed by electron microscopy to identify any structural changes within the muscle. In addition, combined COX/SDH staining was carried as decribed (section 2.2.15.2).

5.4.2 Long-range PCR analysis

Long-range PCR analysis was carried out as described (section 2.2.12) to screen for large-scale mtDNA rearrangements in total muscle DNA.

5.4.3 Mitochondrial DNA sequencing.

The entire mitochondrial genome of both total muscle homogenate and individual laser-captured single fibres mtDNA was performed as described (section 2.2.6) to search for point mtDNA mutations.

5.4.4 Real time PCR analysis

MtDNA from individual laser-captured COX-positive and COX-deficient fibres was assessed for any possible mtDNA copy number depletion or deletions [428] by real-time PCR as described (section 2.2.13).

5.4.6 PCR-RFLP analysis

PCR-RFLP analysis was carried out from DNA samples from muscle homogenate, individual single fibres, and other tissues as described (section 2.2.10). Table 5-1 summarises details for this analysis such as primer position, sequence, restriction endonuclease enzyme, and annealing temperatures.

Table 5-1 Summary of PCR-RFLP analysis of patient with the m.12283G>A mutation.

Primer Sequence	**Primer Annealing Temperature (^{o}C)**	**Enzyme and Digestion site**	**Digest Temperature (^{o}C)**	**Uncut PCR product (bp)**	**Wild-type products (bp)**	**Mutant products (bp)**
Forward-L12177 5`-ACAACAGAGGCTTACGACC-3` Reverse-H12336-5`-TACTTTTATTTGGAGTTGCACC-3`	59	*Alu1* (AG/CT)	37	160	70+53+37	123 +53

5.5 Results
5.5.1 Histochemical analysis

H&E staining showed a minor variation in fibre size (21–96 μm). Fibres had splits and there was some fat and connective tissue replacement but only minor inflammator changes (Figure 5-2-A). In addition, occasional internal nuclei and agonal fibres were observed (not shown in the Figure 5-2-A). The combined COX/SDH staining showed ~ 15% COX negativity with several fibres showing evidence of subsarcolemmal mitochondrial accumulation typical of ragged-red changes, which are suggestive of an underlying mitochondrial genetic abnormality (Figure 5-2-B).

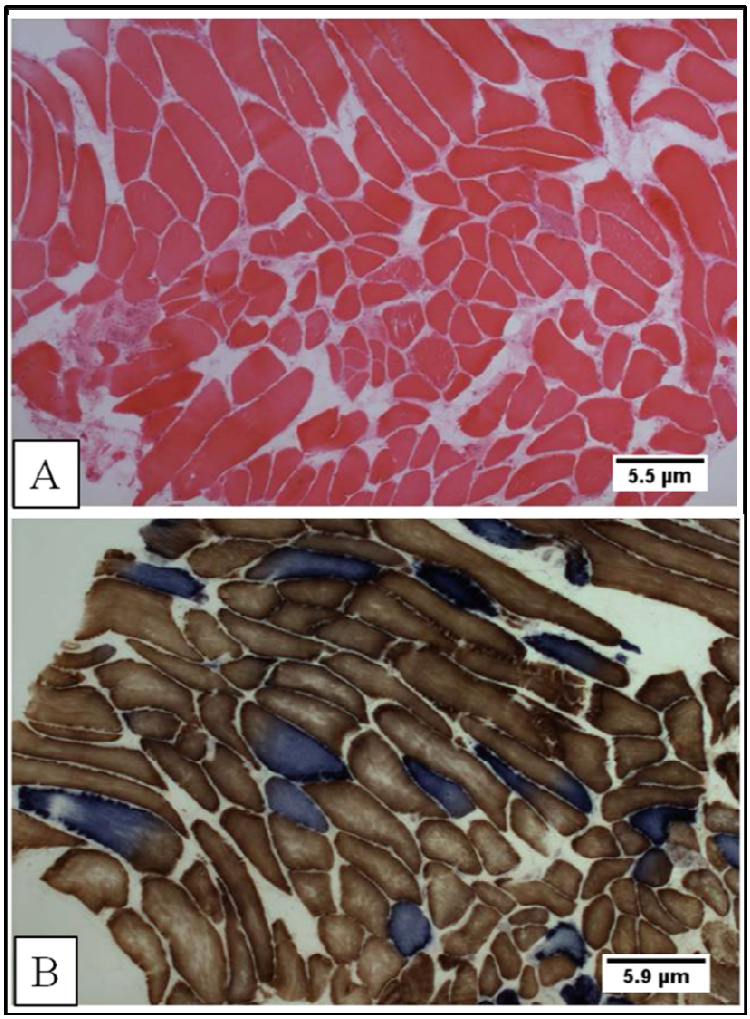

Figure 5-2 Histochemical analysis of muscle biopsy from patient with the m.12283G>A mutation.

(A) H&E staining of patient muscle showing different sizes in fibres, splits, and minor inflammatory changes. (B) COX/SDH staining showed some COX negativity (blue-stained fibres), COX-positive fibres (brown), and mitochondrial proliferation.

5.5.2 Long-range PCR analysis:

Total muscle DNA was assessed for large scale mtDNA rearrangements using 11-kb and 16-kb primers. However, results showed no signs of mtDNA abnormality (Figure 5-3).

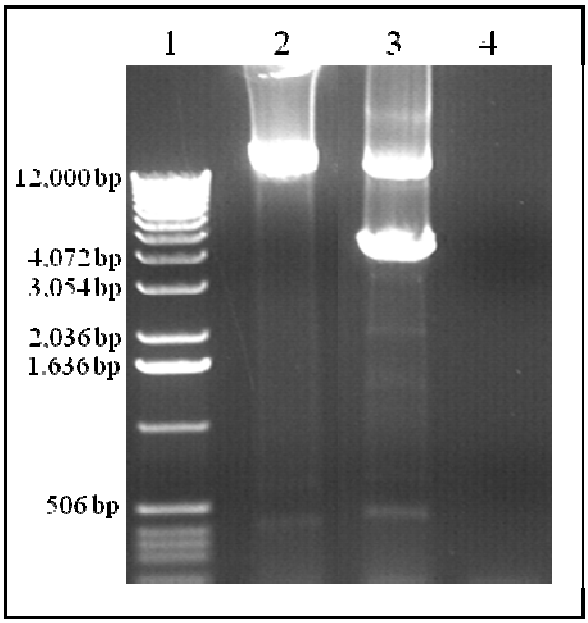

Figure 5-3 Long-range PCR analysis for the m.122813G>A.

Lane 1 is a 1kb ladder, lane 2 is the resultant PCR product from patient`s muscle DNA, lane 3 is the resultant PCR products from a patient who has a single mtDNA deletion (positive control), lane 4 is a negative control (water).

5.5.3 Initial screen for mtDNA point mutations.

DNA from muscle homogenate from patient was initially screened for any mtDNA changes by sequencing the whole mitochondrial genome. Results showed failure to detect any novel mtDNA point mutation could cause the disease. However, reanalysis was carried out as described (section 5.5.5).

5.5.4 Real time PCR analysis

Real time PCR was carried out to further investigate the molecular basis of the COX negativity within the COX-deficient muscle fibres. This was carried out because the patient had a mutation in the *HPRT* gene, which is involved in the purine salvage to provide nucleosides for *de novo* DNA synthesis. Mutations in various enzymes involved in nucleoside salvage within mitochondria have been shown to cause a defect in mtDNA maintenance, manifesting as mtDNA depletion leading to COX deficiency [429-432]. On

this basis, mtDNA copy number was measured in individual, laser-captured COX-positive and COX-deficient fibres. In addition, the same technique was used to quantify mtDNA deletions within individual cells, however, results showed neither mtDNA depletion nor mtDNA deletion (Figure 5-4). The latter results supported the previous results obtained from long-range PCR data.

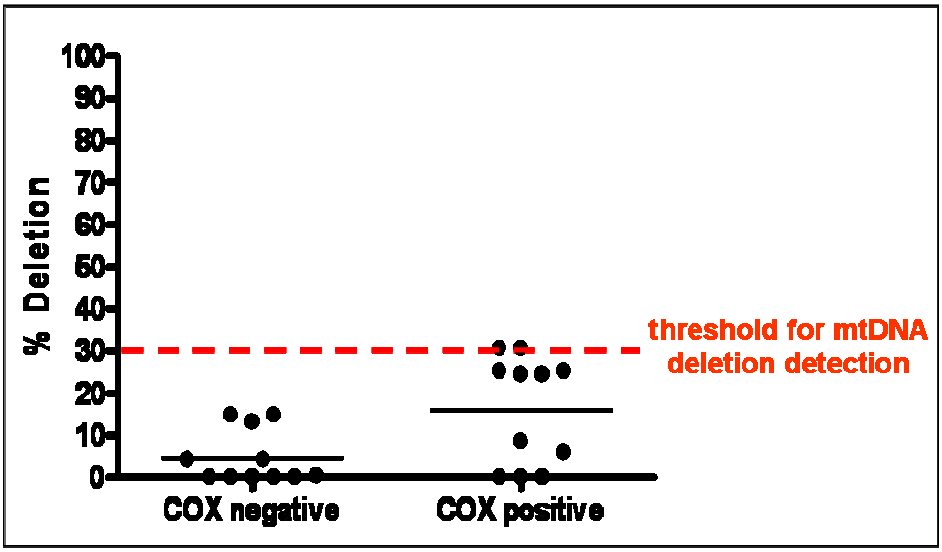

Figure 5-4 Real-time PCR analysis of individual muscle fibres to assess mtDNA deletion.

Results showed no mtDNA deletion because all values from analysed COX-positive and COX-deficient fibres were below the threshold for mtDNA deletion detection.

5.5.5 Whole mitochondrial genome sequencing

To further investigate the COX-deficient fibres, whole genome sequencing was carried out on DNA samples from three random COX-deficient fibres. Results showed the identification of the novel m.12283G>A mutation in the *MTTL2* (mt-tRNA$^{Leu(CUN)}$) gene at high levels in two COX-deficient fibres (Figures 5-5-A and 5-5-B), but was absent in the COX-positive fibres. In addition, other previously reported changes, listed in the two mitochondrial DNA databases [69, 252], were identified (Table 5-2). Reanalysis of the muscle homogenate sequencing chromatogram revealed the m.12283G>A mutation, which was initially determined as ‘‘wild-type” due to low levels of heteroplasmy at this site (Figure 5-5-C), which explain why it was missed in the initial analysis of the sequence as described earlier (section 5-5-3).

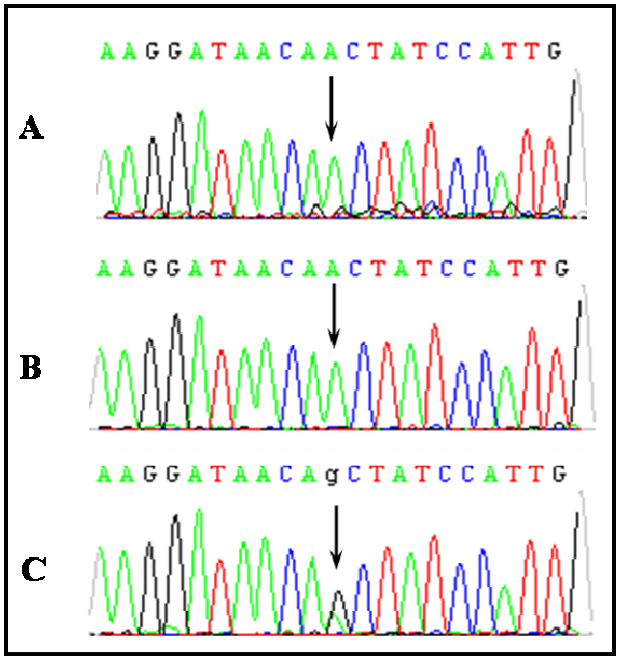

Figure 5-5 Sequencing electropherograms showing the m.12283G>A transition.

This mutation was present at high levels of mutation load in individual COX-deficient fibres from the patient (A & B), while low levels of mutation load were seen in muscle homogenate sample (C).

Table 5-2 Sequence changes identified in single fibres from the patient with the m.12283G>A mutation.

Sequence change	**Previously reported as a SNP or pathogenic? Mitomap or mtDB**	**Amino acid change**	**Location**
m.73A>G	Yes	-	D-Loop
m.185A>G	Yes	-	D-Loop
m.189A>G	Yes	-	D-Loop
m.263A>G	Yes	-	D-Loop
m.309C ins.	Yes	-	D-Loop
m.310T>C	Yes	-	D-Loop
m.311C ins.	Yes	-	D-Loop
m.334T>C	Yes	-	D-Loop
m.513G>A	Yes	-	D-Loop
m.750A>G	Yes	-	D-Loop
m.1438A>G	Yes	-	12S rRNA
m.3010G>A	Yes	-	16S rRNA
m.3107C del.	Yes	-	16S rRNA
m.4769A>G	Yes	No	*MTND2*
m.5460G>A	Yes	Ala331Thr	*MTND2*
m.8251G>A	Yes	No	*MTCOX2*
m.8860A>G	Yes	Thr112Ala	*MTATP6*
m.11914G>A	Yes	No	*MTND4*
m.12283G>A	**No**	**-**	***MTTL2***
m.15326A>G	Yes	Thr194Ala	*MTCYB*
m15936A>G	Yes	-	*MTTT*
m.16148C>T	Yes	-	D-Loop
m.16519T>C	Yes	-	D-Loop

This mutation at this position affects a nucleotide that resides within the variable DHU loop of the mt-tRNA Leu (CUN) structure but does not disrupt Watson-Crick base pairing. Sequence comparison has shown that this nucleotide is strictly conserved in different species suggesting it is of functional importance (Figure 5-6).

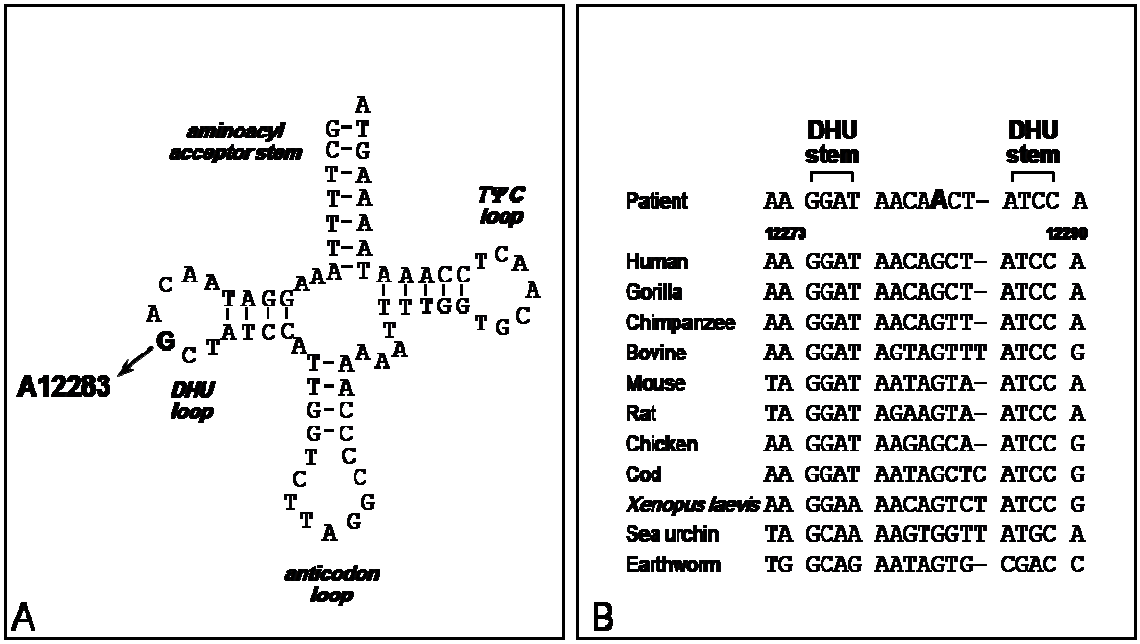

Figure 5-6 Conservation of the nucleotide at position m.12283.

(A) Schematic representation of the mt-tRNA$^{Leu(CUN)}$ cloverleaf structure, illustrating the position of the mutation which affects a nucleotide within the DHU loop structure (taken and modified from http://mamit-trna.u-strasbg.fr/mutations.asp?idAA=17). (B) Phylogenetic analysis of this region of the *MTTL2* gene confirms that this nucleotide at position m.12283 is strictly conserved throughout species, providing compelling evidence for pathogenicity (taken from [413]).

5.5.6 PCR-RFLP analysis

The m.12283G>A mutation leads to the loss of *AluI* restriction site, allowing the detection of wild-type mtDNA (cut into three bands of 70, 53 and 37 bp) from mutated mtDNA (cut into two bands of 123 and 37 bp) (Figure 5-7-A). Results showed high levels of the m.12283G>A mutation load in COX-deficient fibres (>90%) and 18% in muscle homogenate (Figure 5-7-B). Mutation load was quantified in additional tissues from the patient and his mother to assess segregation of mutation. The mutation load was 8% in DNA from patient's fibroblasts, 4% in urinary epithelia cell sediment, and absent in buccal epithelia. In addition, this mutation was absent in all tissues from mother (blood, buccal, and urine) (Figure 5-7-C).

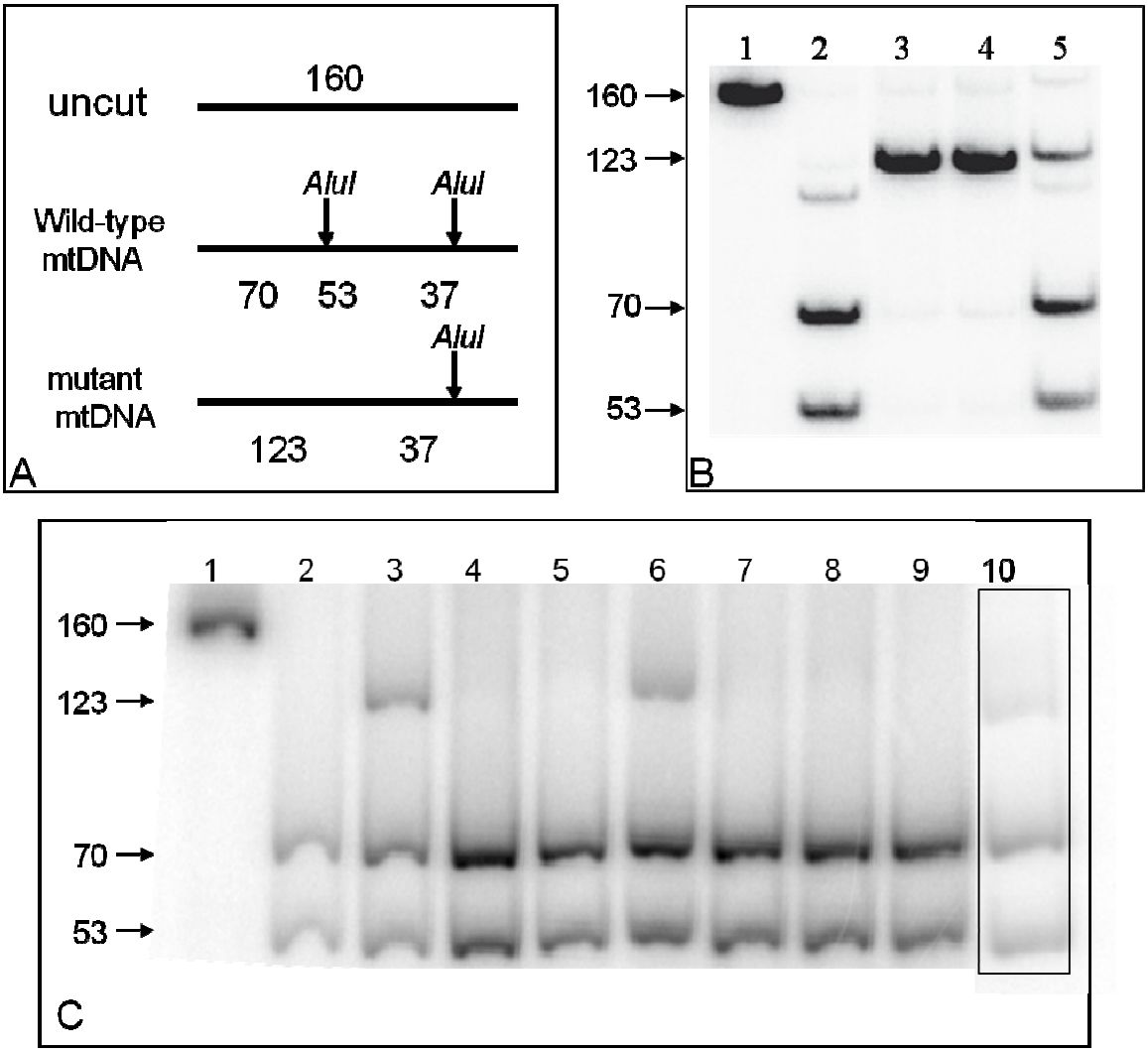

Figure 5-7 PCR-RFLP analysis of the m.12283G>A in tissues from patient and mother.

(A) Schematic diagram shows sizes of PCR products after digestion with the restriction endonuclease. (B) Quantification of mutation load in the COX-deficient fibres and muscle homogenate. Lane 1 shows the uncut DNA sample as 160 bp. Lane 2 shows a negative control DNA sample as 70bp and 53bp products. Lanes 3 and 4 show high levels of mutation load in DNA from COX-deficient fibres. Lane 5 shows low levels of heteroplasmy in muscle homogenate DNA sample. (C) PCR-RFLP analysis to quantify mutation load in tissues from patient and mother. Lane 1 is an uncut DNA sample, lane 2 is DNA sample from a negative control, and lane 3 is DNA muscle sample from a patient with 18% mutation load levels (positive control). Lanes 4, 5, 6, and 10 are blood, buccal, urine DNA samples (4% mutant), and fibroblasts (8% mutant) from patient, respectively. Lanes 7, 8, and 9 are mother's DNA samples from blood, buccal, and urine respectively. The 37bp bands are not shown in panel B and C because of the trimming of the gel. The boxed lane is taken from another experiment.

To determine whether the m.12283G>A mutation segregated with the biochemical defect in individual cells. DNA was prepared from laser-microdissected COX-positive (*n*=14) and COX-deficient fibres (*n*=15). Results showed higher levels of the m.12283G>A mutation

were detected in COX-deficient fibres (98.14 ± 1.35%) than in the COX-positive fibres (1.38 ± 0.44%) (P < 0.001), confirming segregation of the m.12283G>A genotype with respiratory chain dysfunction (Figure 5-8) with a remarkable skewing of mutation load between the two groups.

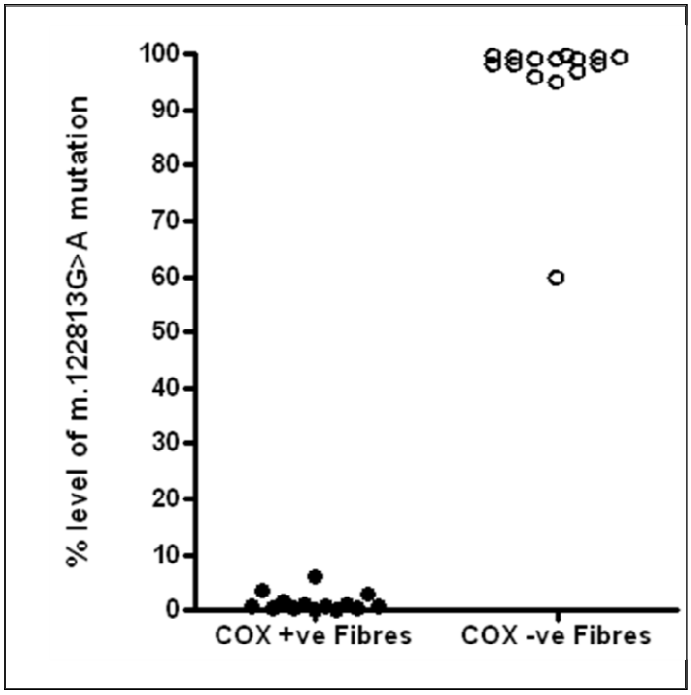

Figure 5-8 Single fibre PCR-RFLP analysis of the m.12283G>A mutation.

This figure shows that both COX-positive and COX-deficient fibres confirmed segregation of the mutation with biochemical defect as a significance difference between both groups was detected. The mean percentage and SE values of PCR-RFLP analysis of COX-positive and COX-deficient fibres as follow: COX-positive (*n*=14, 1.38 ± 0.44%), COX-deficient fibres (*n*=15, 98.14 ± 1.35%), and P<0.0001 confirming segregation of the m.12283G>A genotype with respiratory chain dysfunction.

5.6 The m.12283G>A mutation is pathogenic

In this patient with a neuromuscular phenotype we have identified three distinct genetic diseases, all contributing to the clinical picture: a dominant *PMP22* gene duplication responsible for his demyelinating polyneuropathy, an X-linked recessive *HPRT* gene mutation leading to a grossly elevated level of urate in plasma and gout, and a sporadic, mitochondrial *MTTL2* gene mutation which we show is responsible for the COX-deficient fibres in his muscle biopsy and therefore the mitochondrial CPEO phenotype. Although, the m.12283G>A mutation was present at low levels in muscle homogenate, several lines of evidences have proven this mutation to be pathological and to contribute to the neurological phenotype in this patient. The m.12283G>A variant is not a recognised

neutral polymorphic variant and it is not represented in either of the large, publically-available databases of human mtDNA sequences [69, 252]. In addition, this mutation affects a highly conserved nucleotide, which resides within the variable DHU loop of the mature mt-tRNA$^{Leu(UCN)}$ structure and does not disrupt Watson–Crick base pairing (Figure 5-6). Moreover, results from single muscle fibre analysis clearly demonstrated that the m.12283G>A mutation segregated with COX-deficient fibres, which harboured significantly higher levels of mutated mtDNA than COX-positive fibres. Interestingly, there was a very clear skewing of the segregation of mutated mtDNA since all the COX-positive fibres showed very low levels of the mutation and all the COX-deficient fibres showed high mutation levels close to 100%. This pattern was not observed previously in the majority of pathogenic mt-tRNA mutations in which mutation levels in COX-positive fibres can approach the critical threshold and may often exceed 90% mutated mtDNA [317, 425, 426].

Because this patient developed CPEO, IT WAS initially hypothesised that he had either a mtDNA point mutation or mtDNA rearrangements. This was supported by the identification of the pathogenic mtDNA mutation, m.12276G>A, which like the previously reported mt-tRNA$^{Leu(CUN)}$ mutation, m.12283G>A, was located in *MTTL2* and caused CPEO with low levels of mutation load (18%) [433]. However, initial full genome sequence and long-range PCR results from muscle homogenate in this patient failed to detect neither mtDNA point mutation nor mtDNA rearrangements.

This patient was identified with a mutation in the nuclear-encoded *HPRT* gene, which is known to salvage and recycle purine nucleotides during DNA synthesis, converting hypoxanthine to inosine monophosphate (IMP) and guanine to guanosine monophosphate (GMP) [434]. In view of the known role of several nucleotide salvage enzymes (e.g.TK2) in mtDNA maintenance [432], two hypotheses were suggested. First, are the COX-deficient fibres a secondary phenomenon to the *HPRT* defect leading to a depletion of mt DNA copy number in these cells, similar to the tissues of patients harbouring mutations in the *TK2* gene [435-437]? Second, do the COX-deficient fibres exhibit mtDNA depletion or mtDNA rearrangements? Given that these results showed that the COX-deficient fibres had neither mtDNA depletion nor deletion, it is possible that the *HPRT* mutation is influencing mtDNA segregation. In summary, all presented evidence points towards the

m.12283G>A mutation being a strong candidate in the development of the clinical phenotypes related to the mitochondrial defect in this patient.

Chapter 6

GeneChip resequencing array 2.0

Chapter 6 : GeneChip resequencing array 2.0

6.1 Introduction

To date, more than 250 pathogenic mtDNA mutations have been identified within the mitochondrial genome in association with diseases [69]. Given the highly polymorphic nature of the mitochondrial genome, it is necessary to distinguish between pathogenic mtDNA mutations and the common polymorphic variants or SNPs. To facilitate the identification of cases caused by pathogenic mtDNA mutations, accurate and rapid techniques, which can reduce time and cost are required. In addition, these techniques must be able to detect both single nucleotide changes and small rearrangement (single nucleotide deletion or insertion) mutations, or possibly mtDNA inversions [438, 439].

Currently, several techniques have been developed to detect single nucleotides substitutions or deletion/insertion mutations within the mitochondrial genome. Single-stranded conformational polymorphism (SSCP) uses the electrophoretic separation of single-stranded nucleic acids based on a single base pair, which results in a different secondary structure and hence an altered mobility of the PCR product through a gel. The SSCP method was first used in 1989 and applied to a range of DNA polymorphisms and sequence variations. This method has been described as an inexpensive, convenient, and sensitive to detect genetic variation [440], although false negative results have been reported [441]. It is sensitive to electrophoresis temperature, buffer concentration and gel concentration [442], and limited to small and selected DNA mtDNA regions [443].

Denaturing gradient gel electrophoresis (DGGE) is another technique that has been applied to identify single nucleotide changes. It is based on the electrophoresis of PCR-amplified fragments through polyacrylamide gels containing a linearly increasing gradient of denaturants, so when DNA enters the gradient gel, double-stranded DNA molecules become partially melted, and their gel-electrophoretic mobility decreases [444]. DGGE is a sensitive method to detect single-base changes in amplified DNA fragments, heteroduplexes, and does not involve the use of any radioactivity. UV is used to visualise fragments after staining with ethidium bromide [445]. However, this method is only limited to small DNA fragments [443], costly, and is not quantitative [446].

Denaturing high-performance liquid chromatography (DHPLC) allows the detection of single base substitutions and small insertions and deletions, and has been applied to to the

study of the mitochondrial genome. DHPLC is based on mismatches between amplified DNA fragments resulting in the formation of heteroduplices. The formed heteroduplices, which are thermally less stable than homoduplices, are then separated by liquid chromatography at elevated column temperatures [447]. DHPLC has been has been used to screen the entire mitochondrial genome [448], providing an automated, accurate and rapid method [449]. It can be applied to genotyping, loss of heterozygosity and gene expression analysis [447], although it is still sensitive to temperature [447] and is not considered to be a cost effective method [450].

Pyrosequencing technology has also been applied to the detection and estimation of heteroplasmic mtDNA point mutations [451]. This technology offers a real-time, minimal sequencing method for the analysis of short to medium length DNA sequences [452] and uses the detection of pyrophosphate release when nucleotides are incorporated into the extending template [451]. Pyrosequencing has shown to be rapid, accurate, quantitative and provided 100% sensitivity and specificity[451], whilst it is also relatively cheap and does not take a lot of time to runit is [453]. On the other hand, pyrosequencing still has a number of disadvanteges: it is limited to short sequences, unable to determine the correct number of incorporated nucleotides and the occasional occurrence of nonsynchronized extension of some sequences due to minus or plus frameshifting, which limits the length of obtained reliable and correct sequences [452, 454, 455].

Conventional Sanger di-deoxy sequencing is routinely used to detect sequence changes within the entire mitochondrial genome, which can be PCR-amplified using pairs of overlapping primers. It is preferred because it provides quick, accurate results and allows the researchers to identify all changes within a genome; it can also be applied to the study of somatic mtDNA point mutation in single cells [456, 457]. Although it is able to detect point mutations and small mtDNA rearrangements, it is relatively costly and mutations present at low heteroplasmic level (20% or below) may easily escape detection [448, 458].

Surveyor Nuclease has been used to detect heteroplasmic mtDNA mutations [459]. It uses mismatch-specific DNA endonuclease, named Surveyort Nuclease, which cleaves DNA heteroduplexes formed by the hybridisation of PCR products from wild-type and mutant mtDNA [460, 461]. This method provided the ability to sequence the entire mitochondrial genome. It is able to detect heteroplasmic mtDNA mutatons but noted to be time-

consuming [459]. However, a drawback of this technology is that it is not able to detect homoplasmic mtDNA mutations [461].

More recently, suspension array technology has been used to detect both heteroplasmic and homoplasmic mtDNA point mutations. The suspension array analysis is based on the use of multi-microspheres combined with multiple sequence-specific oligonucleotide (SSO) customized probes and flowmetry [462]. This technique has been described as rapid detection system with a detection limit of approximately 2%, mtDNA heteroplasmy levels, is suitable for screening large numbers of samples, and the analysis is relatively cheap as compared to conventional sequencing [463]. However, the detection system in this method is currently limited to mtSNPs of Japanese ethnicity only [463].

The complexity and limitations associated with previous methods have led to the development of the Affymetrix oligonucleotide-based array MitoChip, which allows the analysis of 29 mitochondrial genomes per day [464]. The Affymetrix MitoChip (V2.0) is an oligonucleotide tiling array for the resequencing of the human mitochondrial genome.

The first generation of MitoChip, MitoChip (V1.0), was developed early in 2004. It was not capable of sequencing the non-coding D-loop region of the mitochondrial genome [465] [466], so a second chip, the MitoChip (V2.0) was developed in 2006; this contains probes that match the revised Cambridge Reference Sequence (rCRS) [467]. In addition to tiling of sequences for the most common haplotypes including single-nucleotide changes, insertions and deletions, it contains segments of the control region allowing sequence of the entire mitochondrial genome [464, 466]. The MitoChip system is based on the use of a standard chip, which is 1.28 cm x 1.28 cm in size. On each chip there are over 6.5 million sections known as features or squares, with each feature containing millions of identical DNA probes. A probe is a 25 base pair (25-mer) length piece of DNA that is attached to the chip and only differs in SNP at position #13 (Figure 6-1). Each base of the mitochondrial genome is interrogated by hybridization of fluorescent- labeled DNA fragments. A comparison study between both MitoChip versions carried out by Zhou et al., revealed that MitoChip (V2.0) gave 99.99% reproducibility. In addition, 31 variations in the D-loop region, which were not detected by (V1.0), were successfully detected in the (V2.0) chips.

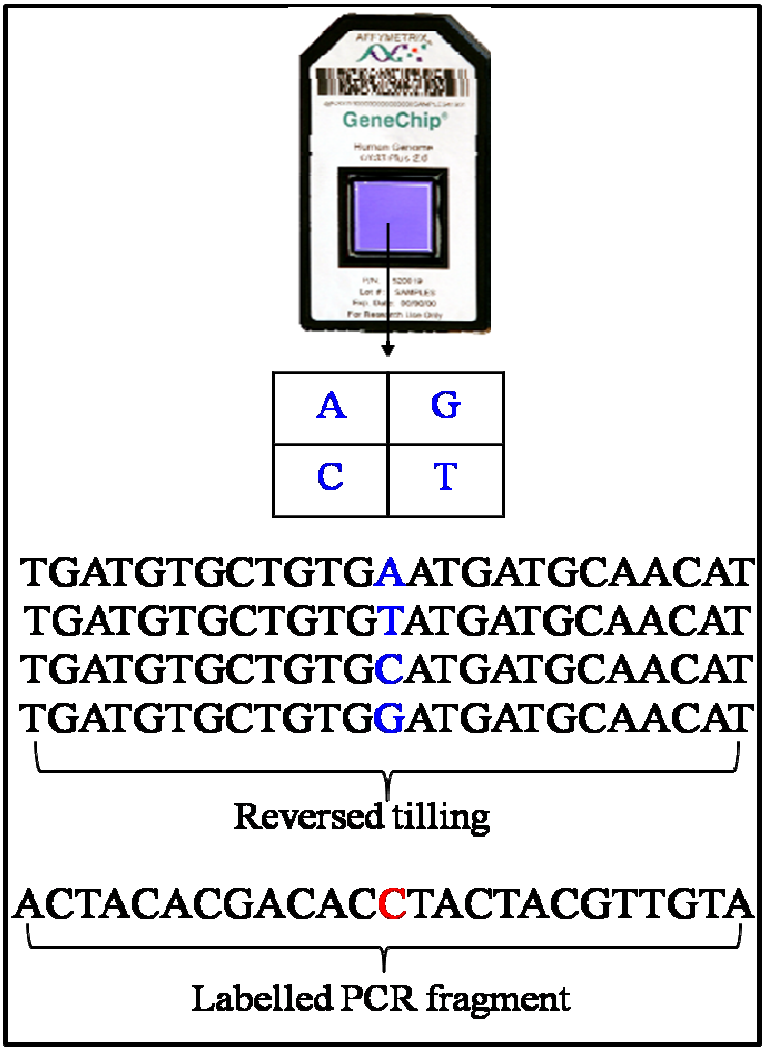

Figure 6-1 Shwoing the structure of GeneChip used in the MitoChip V2.0 Technique.

For simplicity one square is shown, which contains millions of identical probes that differ only in nucleotide at position #13 known as reversed tilling. The Biotin labelled PCR fragments bind to the complimentary revised tilled probe (modified from Dr. Tony Sierra, Affymetrix).

The high sensitivity of the MitoChip (V2.0) makes it a suitable tool to be applied for early detection and clinical screening of mtDNA changes in human tumours [468, 469] and population genetics [464]. The existence of polymorphisms within the mtDNA [470] allows the MitoChip to be used in forensic applications [464]. Sequencing the entire mitochondrial genome on the MitoChip involves only three reactions, reducing both the time, labour and cost involved in analysing human mtDNA. On the other hand, the MitoChip (V2.0) is unable to detect mitochondrial inseretion and deletion mutations. It does not cover the whole genome sequence for all haplogroups and not quantitative. It may give miscalls and often results need to be validated by conventional sequencing.

6.2 Aims

The aim of this chapter is to investigate the reliability of detecting pathogenic human mtDNA mutations in nine of our patients with mtDNA disease, previously identified in our lab, using the MitoChip (V2.0) and to compare the results obtained from both the conventional sequencing and the MitoChip to evaluate whether the MitoChip is a reproducible tool in a diagnostic setting. All information related to the investigated patients is summarised in Table 6-1.

Table 6-1 Summary of related information to the patients investigated by MitoChip (V2.0).

Sex	Age	Tissue	mtDNA mutation	Gene
F	53	muscle	m.12315G>A	*MTTL2*
M	38	blood	m.11453G>A	*MTND4*
M	13	muscle	m.11777C>A	*MTND4*
M	9	muscle	m.14709T>C	*MTTE*
M	5	muscle	m.14453G>A	*MTND6*
M	10 months	muscle	m.13513G>A	*MTND5*
M	4	fibroblast	m.13513G>A	*MTND5*
M	53	muscle	m.13042G>A	*MTND5*
F	-	muscle	m.7472Cins	*MTTS1*

6.3 Material and Methods

This project was undertaken in association with Dr. Andy Duncan and Dr. Shamima Rahman, Institute for Child Health, London) using the GeneChip® Resequencing Assay Kit and the GeneChip Human Mitochondrial Resequencing Array (V2.0) from Affymetrix according to the manufacture's protocol or as described in [466] . Data were analysed and compared with the rCRS [252]. Briefly, this method includes long-range PCR amplification, PCR products pooling, fragmentation, labelling, and hybridization, washing and staining (Figure 6-2).

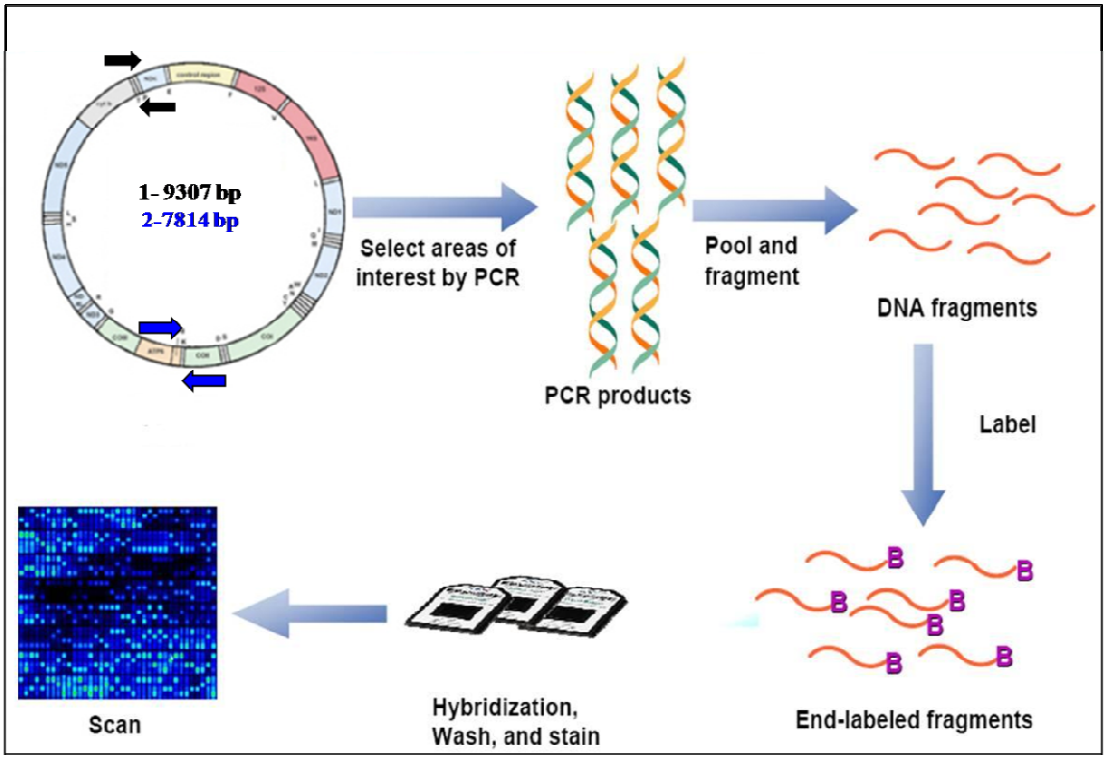

Figure 6-2 Summary of the methods in the MitoChip (V2.0) analysis.

After amplification of the human mitochondrial genome using 45 overlapping primer pairs, the PCR products were subjected to two runs of long-range PCR using 2 overlapping primer pairs to generate 9307bp and 7814 bp PCR products. The amplified PCR products were then pooled and fragmented using a fragmentation reagent. Fragmented DNA was labelled with biotin to allow visualisation. DNA fragments were then hybrodized to the chip followed with washing and staining prior to loading in the system and scanning.

6.3.1 Long-range PCR

The entire mitochondrial DNA sequence was amplified using two pairs of long PCR primers, each containing 50ng of genomic DNA, in a 96-well plate using LA PCR Kit Ver. 2.1 kit. The Mito3 forward primer sequence 5'-TCA TTT TTA TTG CCA CAA CTA ACC TCC TCG GAC TC-3' and the Mito3 reverse primer 5'-CGT GAT GTC TTA TTT AAG GGG AAC GTG TGG GCT AT-3' were used to amplify 7814 bp. The Mito1-2 forward primer sequence 5'-ACA TAG CAC ATT ACA GTC AAA TCC CTT CTC GTC CC-3' and the Mito1-2 reverse primer 5'-ATT GCT AGG GTG GCG CTT CCA ATT AGG TGC -3' were used to amplify 9307 bp. The total PCR reaction volume was 50µl and thermal cycling conditions were as follows: 95°C for 2 minutes, 95°C for 15seconds, 68°C for 7 minutes, 29 cycles, and final extension for 12 minutes.

6.3.2 Quantitation and pooling of PCR products

The amplified PCR products were analysed for quality and quantity and were cleaned up using a DNA Amplification Clean-Up Kit.

6.3.3 Fragmentation and labelling

The pooled DNA fragments were digested with Affymetrix fragmentation reagents and then incubated at 95°C for 15 minutes to inactivate DNase I. Fragmented DNA was labelled by adding 2µl of GeneChip DNA labelling reagent and 3.4µl of 30U/µl terminal deoxynucleotidyl transferase according to the manufacture's protocol.

6.3.3 Hybridization, staining and washing

Prehybridization, hybridization and washing were carried out according to the Affymetrix CustomSeq Resequencing protocol. The chips were prehybridized for 15 minutes in 80µl of a solution containing 3 mol/L tetramethylammonium chloride, 0.1% Tween 20, and 10 mmol/L Tris, pH 7.8. Next, they were hybridized for 16 hours at 48°C at 60 rpm rotation in a hybridization solution containing: 3 mol/L tetramethylammonium chloride, 100µg/ml herring sperm DNA, 500µg/ml bovine serum albumin, 10 mmol/L Tris, pH 7.8, 0.01% Tween 20, and 200 pmol/L control oligo. Eventually, chips were washed and stained on the GeneChip fluidics station using the pre-programmed CustomSeq Resequencing wash and stain protocol.

6.3.4 Microarray data analysis

Arrays were scanned on a GeneChip scanner that measures the fluorescence intensity for all positions. Data were analysed using two software programs: the GeneChip operating software (GCOS v1.4) and GeneChip sequence analysis software (GSEQ v4.0). Sequences were compared to the rCRS.

6.4 Results

6.4.1 Long-range PCR

Two PCR proucts were amplified using the Mito-3 primers as a 7184 bp (Figure 6-3) and the Mito1-2 primers as a 9307 bp (Figure 6-4).

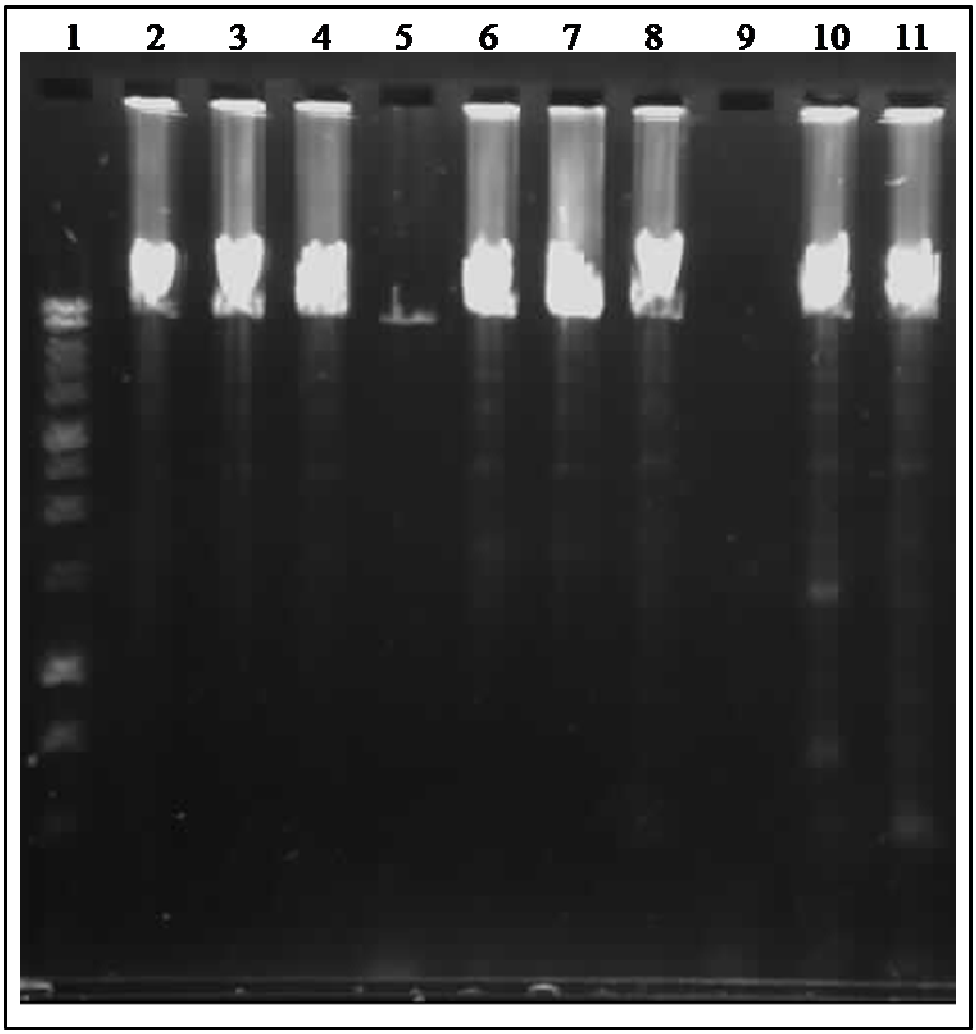

Figure 6-3 First long-range PCR for the MitoChip analysis.

The first long-range PCR results in the amplification of 7184 bp products. Lane 1 is a 1kb DNA ladder; lane 2 is PCR products from patient with the m.14453G>A mutation; lane 3 is PCR products from patient with the m.12351G>A mutation; lane 4 is PCR products from patient with the 13513G>A mutation; lane 5 is PCR products from patient with the 14709T>C mutation; lane 6 is PCR products from patient with the m.13042G>A; lane 7 is PCR products from patient with the 11453G>A mutation; lane 8 is PCR products from patient with the m.13051 G>A, lane 9 is a negative control (water) , lane 10 is PCR products from patient with the m.7472Cins mutation, and lane 11 is PCR products from patient with m.11777C>A mutation.

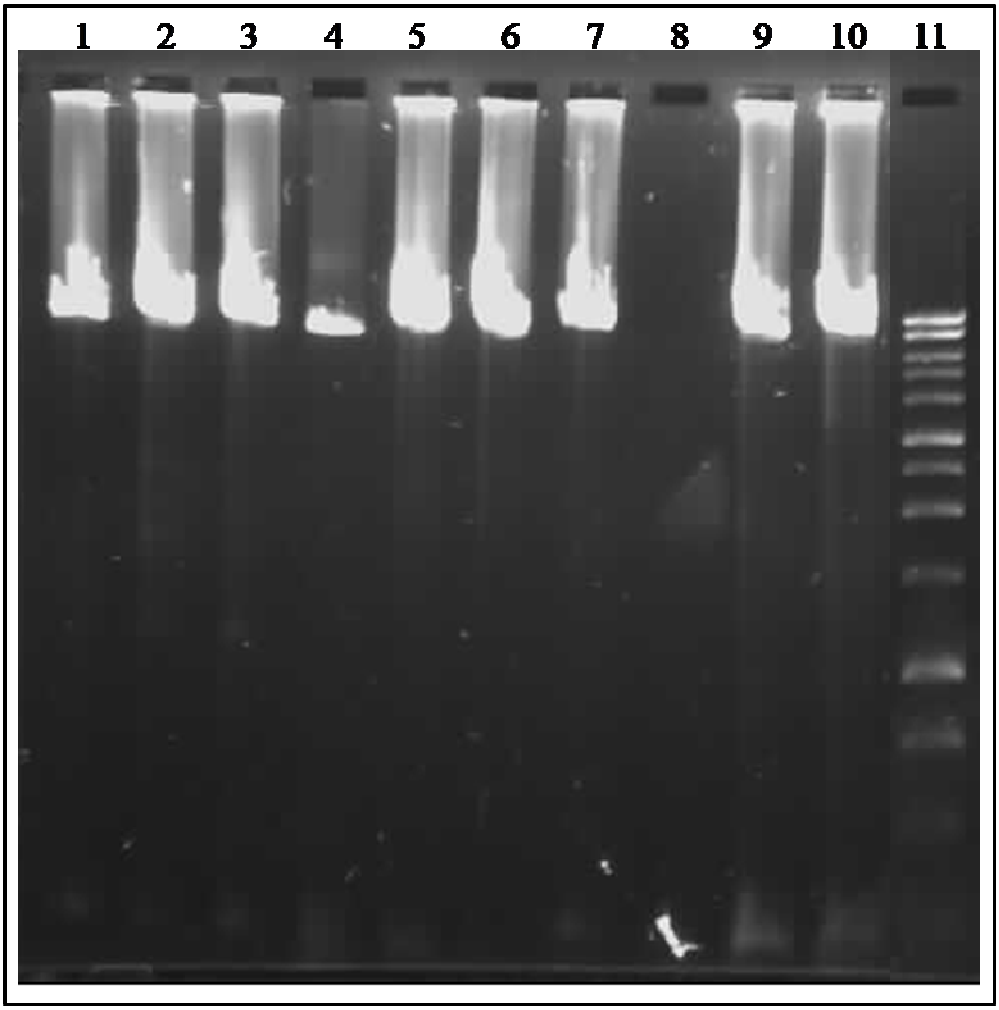

Figure 6-4 Second long-range PCR for the MitoChip analysis

The second long-range PCR results in the amplification of the 9307 bp products. Lane 1 is PCR products from patient with the m.14453G>A mutation; lane 2 is PCR products from patient with the m.12351G>A mutation; lane 3 is PCR products from patient with the 13513G>A mutation; lane 4 is PCR products from patient with the 14709T>C mutation; lane 5 is PCR products from patient with the m.13042G>A; lane 6 is PCR products from patient with the 11453G>A mutation; lane 7 is PCR products from patient with the m.13051 G>A, lane 8 is a negative control (water), lane 9 is PCR products from patient with the m.7472Cins mutation, lane 10 is PCR products from patient with m.11777C>A mutation; and lane 11 is 1kb DNA ladder.

6.4.2 Microarray data analysis

All information for investigated patients are summarised in Table 6.1, which included eight samples with single nucleotide changes and one sample with a single nucleotide insertion (m.7472Cins). Results showed the ability of the MitoChip to pick up all single nucleotide changes (Figures from 6-5 to 6-12). However, because the mutation detection set up in the Mitochip does not support identification of insertions or deletions, the m.7472insC mutation was not detected by the MitoChip (Figure 6-13).

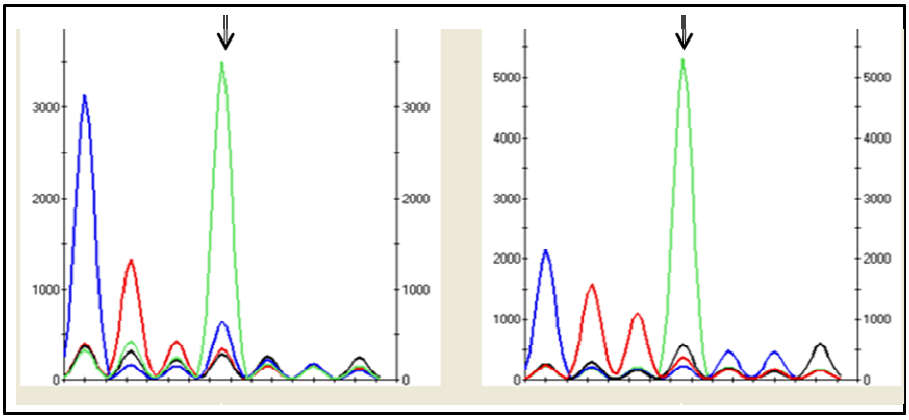

Figure 6-5 Sequence chromatogram showing the m.11453G>A mutation.

Forward (right panel) and reverse (left panel) strands.

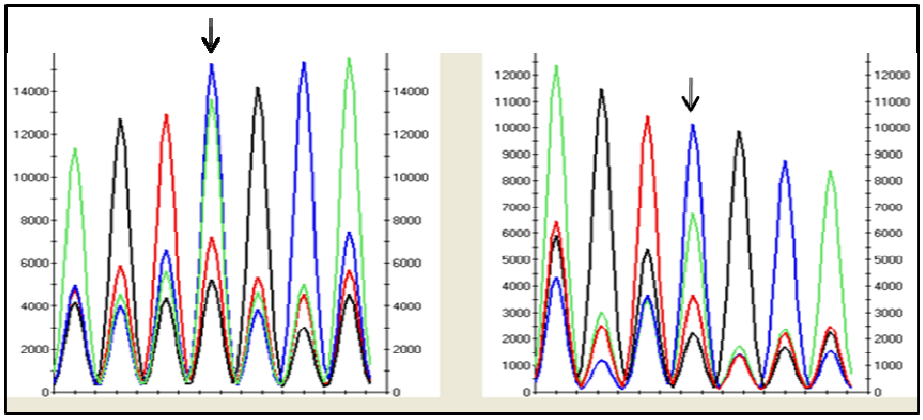

Figure 6-6 Sequence chromatogram showing the m.11777C>A mutation.

Forward (right panel) and reverse (left panel) strands.

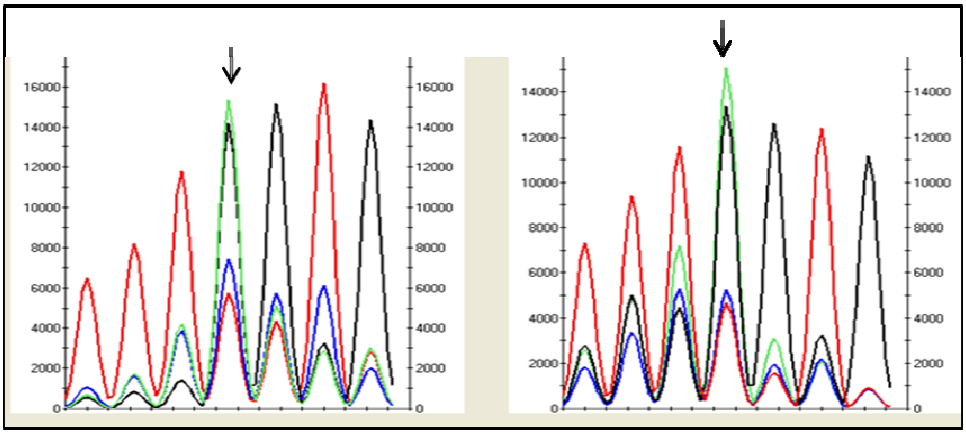

Figure 6-7 Sequence chromatogram showing the m.12315G>A mutation

Forward (right panel) and reverse (left panel) strands.

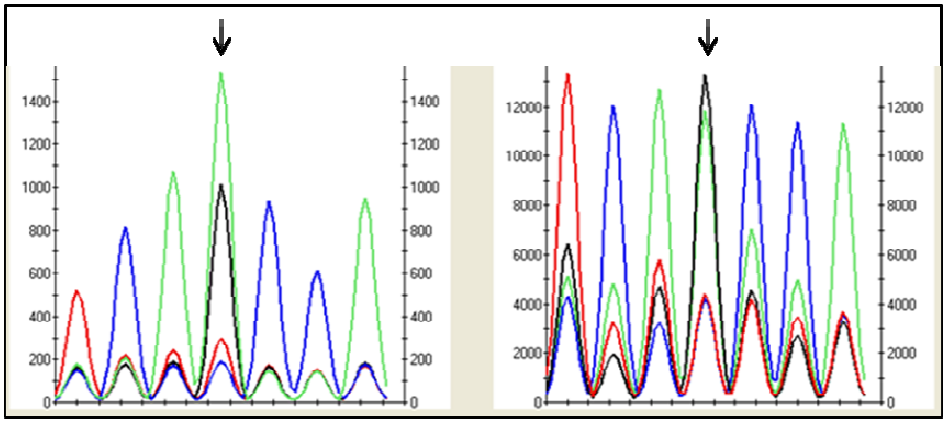

Figure 6-8 Sequence chromatogram showing the m.13042G>A mutation.

Forward (right panel) and reverse (left panel) strands.

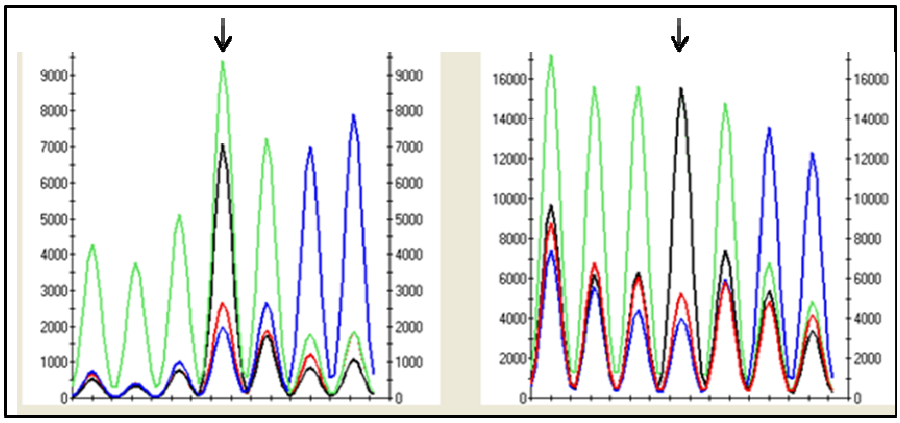

Figure 6-9 Sequence chromatogram showing the m.13051G>A mutation.

Forward (right panel) and reverse (left panel) strands.

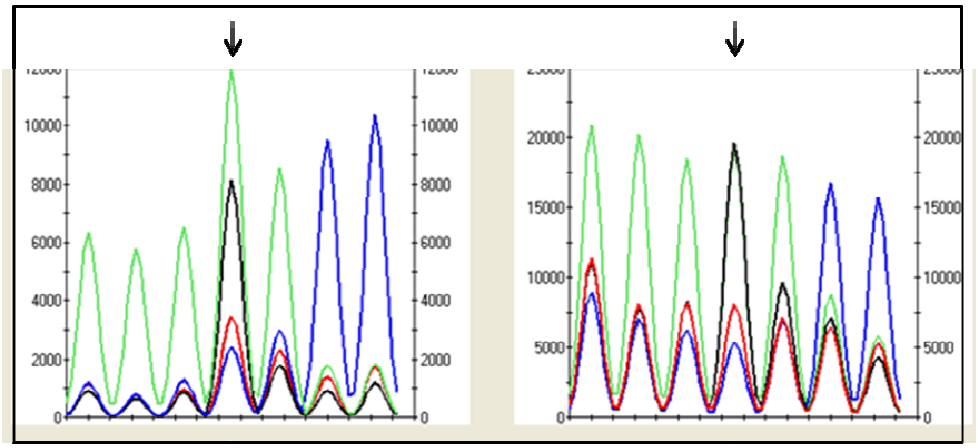

Figure 6-10 Sequence chromatogram showing the m.13513G>A mutation.

Forward (right panel) and reverse (left panel) strands.

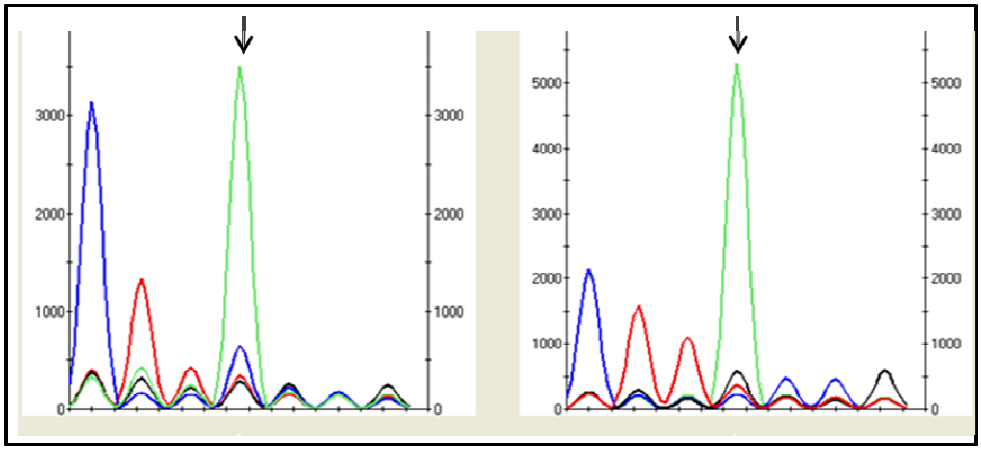

Figure 6-11 Sequence chromatogram showing the m.14453G>A mutation.

Forward (right panel) and reverse (left panel) strands.

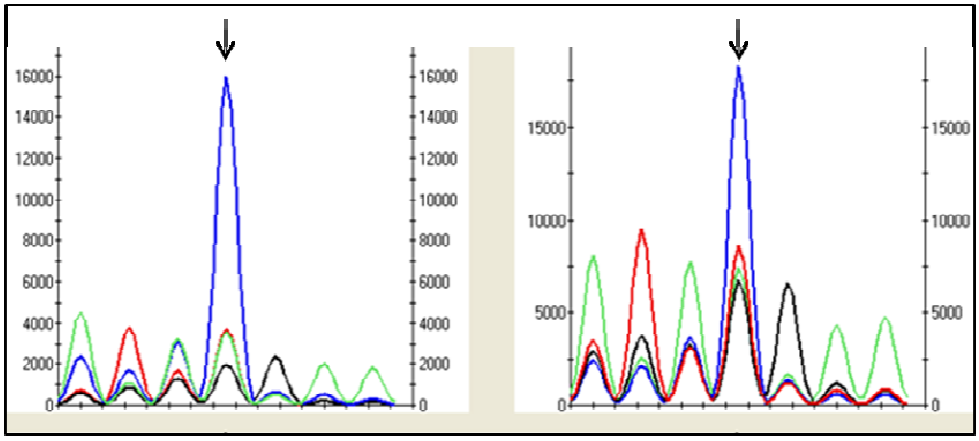

Figure 6-12 Sequence chromatogram showing the m.14709T>C mutation.

Forward (right panel) and reverse (left panel) strands.

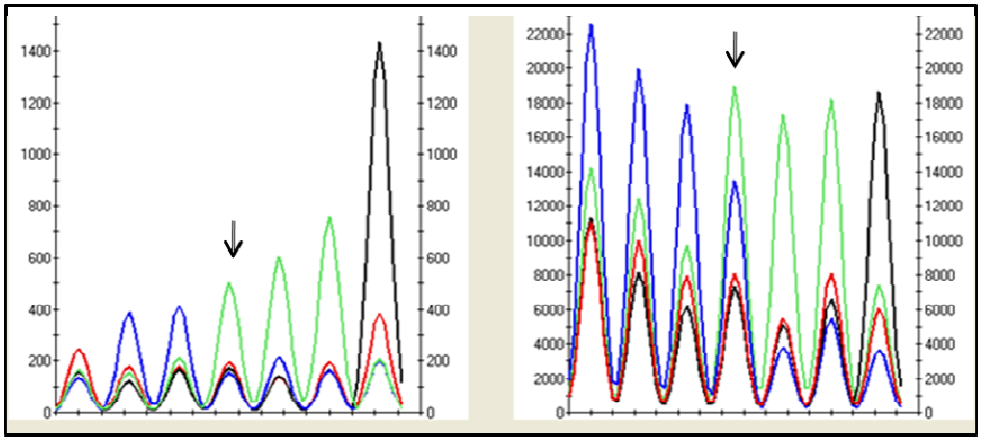

Figure 6-13 Sequence chromatogram showing the inability to detect the m.7472Cins mutation.

Forward (right panel) and reverse (left panel) strands.

6.5 Discussion

With the increase identification of pathogenic mtDNA, several techniques have been developed and applied in a diagnostic setting; however, some of them are still with limitations as previously described (section 6.1). In this associated project, the MitoChip array (V2.0) has been to evaluate whether this method is reproducible and accurate in detecting mtDNA mutations. This project involved the investigation of DNA samples from 40 patients in total who has been referred to the diagnostic centre at Queen Square and UCL in London. Nine of these samples, which were provided from our lab, had previously been identified as harbouring heteroplasmic, pathogenic mtDNA mutations to test the ability of the MitoChip (V2.0) to detect these mutations.

Several reasons make the MitoChip (V2.0) valuable tool in the diagnostic setting. It has the ability to sequence the whole mitochondrial genome in a short time and can be applied to a range of different applications (medical analysis, forensics and population genetics, rather than the simple detection of pathogenic mtDNA mutations. It gave an accuracy and reproducibility greater than 90% and is able to detect mtDNA mutations with low level of heteroplasmy down to a threshold level of 2% mutated mtDNA [466].

On the other hand, MitoChip (V2.0) has some features that could be considered disadvantageous. Although, it is capable of detecting mtDNA single nucleotides polymorphisms (SNPS), however, it cannot detect mtDNA insertion and deletion mutations, this is because the detection method relies on labelled DNA binding to the 25-mer sequence on the chip. In some cases, non-specific binding may occur causing miscall of the nucleotide. The Mitochip (V2.0) has been improved for detecting D-loop region mutations but cannot detect mutations from Asian mtDNA, because it is based on the revised Cambridge reference sequence [467] which belongs to the European haplogroup H2 [463]. During data analysis, the first nucleotide called in the mitochondrial genome is the nucleotide at position 13, because all probes, which are tilled on the chip, are identical in the sequence except nucleotide #13. Because mtDNA at nucleotide position 3107 is not tiled on the chip therefore all bases after this position are shifted 1 base, which does cause some problems with the analysis.

The inability of the MitoChip to detect insertion and deletion mtDNA mutations, is perhaps the main issue with this method. According to MitoMAP website, there are more than 250

mtDNA mutations have been reported. Simple insertion mtDNA mutations only represent ~ 2.4% of these reported mutations, which is relatively very small. The inability of the MitoChip (V2.0) to detect simple insertion mtDNA mutations, as compared to large-scale mtDNA rearrangements that can be identified by other techniques, means simple mtDNA rearrangements can be missed when using the MitoChip (V2.0) to detect mtDNA mutations and would remain unidentified.

Although there is similarity in mtDNA sample preparations for sequencing between cycle sequencing and MitoChip, the MitoChip is substantially cheaper than cycle sequencing and more time-saving when considering running more than one chip at the same time. In conclusion, the human MitoChip (V2.0) is a high-throughput tool for mtDNA mutation detection but with some limitations. The understanding is that the London lab has reverted to the analysis of patient samples by conventional sequencing, and for the time being Newcastle Diagnostics are continuing to do the same. The advent of next-generation sequencing technologies [471-474], in particular for the mitochondrial genome [475, 476], may influence the Newcastle Diagnostics decision again in the near future.

Chapter 7
General Discussion

Chapter 7 : General Discussion

Mitochondria are ubiquitous cellular organelles present in all nucleated cells and they are the only organelles, which contain DNA within mammalian cells [1]. They are the main site for ATP generation within most tissues by oxidative phosphorylation (OXPHOS) [1]. Mitochondrial diseases are multisystem disorders exhibiting clinical, genetical and biochemical variability [477, 478]. Several factors increase the rate of mtDNA mutations: the lack of efficient DNA repair systems [237], a lack of protective proteins such as histones and the association with the inner mitochondrial membrane which makes the mtDNA a target for ROS-induced damage via OXHPHOS [238].

The work presented in this thesis aims to investigate patients with specific mtDNA mutations and to understand the role of these mutations in causing a phenotype using biochemical and molecular genetic techniques.

7.1 Investigations of patients with complex I mitochondrial DNA mutations

As mentioned in Chapters 1 and 3, complex I is the largest and least understood of the respiratory chain complexes. Mitochondrial energy metabolism disorders due to deficiencies in complex I are the most frequently seen cases. Approximately 20-30% of those disorders seen in children are due to mutations in the mtDNA. Although this suggests that the majority of such disorders are due to mutations in nuclear genes [325] [324], mtDNA mutations represent an important cause of complex I deficiency. In this work, patients were identified with novel and recurrent mtDNA mutations in complex I. To confirm pathogenicity of these mutations several investigations were carried out on different tissues from patients.

Patient #2 presented with LHON-like phenotypes but was negative for any of the primary LHON mutations. The m.11453G>A mutation was considered to cause the disease for several reasons. It was heteroplasmic, it affected blood and fibroblasts tissues from the patient with high levels of mutation, it affected a highly conserved sequence in the *MTND4* gene and it was not found in normal individuals.

LHON was previously reported in a patient who had the m.11778G>A mutation within the ND4 subunit of complex I and this mutation compromised complex I activity [479, 480].

All the primary LHON mutations are distributed within complex I subunits and they all cause a biochemical defect in complex I. Measurement of respiration rate revealed that these mutations affected this rate differently. The m.3460G>A mutation reduced the rate 20–28%, the m.11778G>A mutation 30–36% and the 14484T>C mutation 10–15% [356]. Conversely, the m.11453G>A mutation, which resides within the same complex and affects a highly conserved nucleotide within the same subunit, did not affect complex I activity. As described in section 3.5.15, the m.11778G>A mutation disrupts complex I binding with ubiquinone, thereby compromising respiratory chain function. However, the maintenance of complex I activity and the normal levels of ROS in this patient make it difficult to explain the role of the m.11453G>A mutation in causing the disease in this patient. One possibility is that the m.11453G>A mutation may cause LHON in this patient by affecting either the NADH/NAD ratio or OXPHOS by a different pathway than complex I; other mtDNA mutations caused a defect in complex I activity but did not cause LHON. Another possibility is that the defect may only be seen in the target cells such as retinal or optic nerve cells, and not in fibroblasts [481].

Patient #3 was presented with clinical phenotypes related to a mitochondrial disorder. The m.11777C>A mutation was identified in this patient and is considered the main cause of the disease since it met canonical criteria for pathogenic mtDNA mutations. It is heteroplasmic, affected different tissues that were investigated in both the patient and relatives and changes a highly conserved amino acid. In addition, this mutation caused a defect in complex I activity, which was associated with an increase in both ROS levels and mitochondrial mass. Interestingly, this mutation affects the nucleotide directly next to the m.11778G>A mutation, which is the most common mutation associated with LHON [254]. However, none of the patients with the m.11777C>A mutation presented signs of optic neuropathy which are the main clinical phenotypes of LHON patients [482]. In addition, patients with the m.11777C>A mutation showed different clinical phenotypes, with severity, from patients with 11778G>A mutation. The ND4 subunit in complex I binds to ubiquinone during oxidative phosphorlation and this binding is stabilized by the presence of positively charged amino acids such as arginine. A change of amino acid charge can cause instability of the binding resulting in a defect in the electron transport chain [483, 484]. The m.11778A>G mutation changes the amino acid at position 340 from arginine to histidine but with similar charge, the m.11777C>A mutation changes the arginine to serine,

which results in a loss of charge [482]. This could explain the increase in phenotype severity in patients with the m.11777C>A mutation.

In addition, the m.11777C>A mutation was described previously as a disease-causing mutation in patients with Leigh syndrome [357] late-onset encephalopathy [482] and Leigh-like syndrome [359]. More recently, the m.11777C>A mutation was reported in an infant with Leigh syndrome [485]. Similar results between patients with the m.11778G>A mutation and the m.11777C>A mutation, i.e. defect in complex I activity and increase in mitochondrial mass [399], suggest they were affected by a similar mechanism.

Patient #4 presented with a clinical phenotype related to Leigh syndrome. The m.13051G>A mutation was identified in the subunit ND5 of complex I. It affected all investigated tissues, affected a highly conserved amino acid in the ND5 subunit and was not found in healthy individuals. It was homoplasmic in patient's samples and heteroplasmic in relatives. However, being homoplasmic does not exclude its role in pathogenicity since the m.13051G>A mutation has been previously reported in a few patients with Leigh syndrome or Leigh-like disease and associated with isolated complex I deficiency [486] [315]. Moreover, this mutation caused a statistically significant increase in both ROS levels and mitochondrial mass in fibroblasts from the patient.

The m.13051G>A mutation was firstly reported as a pathogenic mutation in a Dutch pedigree, which included two LHON affected brothers and their visually affected maternal aunt, all of whom were negative for the primary LHON mutations [487]. More recently, the m13051G>A mutation was identified in two brothers, who were referred to the diagnostic lab because they developed phenotypes consistent with a mitochondrial disorder. The first patient (deceased) presented with seizures, pigmentary retinal degeneration and optic atrophy, while the second patient had very acute onset of blurred vision. Based on clinical presentations they were suspected to have LHON, however, full genome sequencing from patients' samples showed they were negative for all primary LHON mutations and the m.13051G>A mutation was the only mtDNA mutation identified (Figure 7-1).

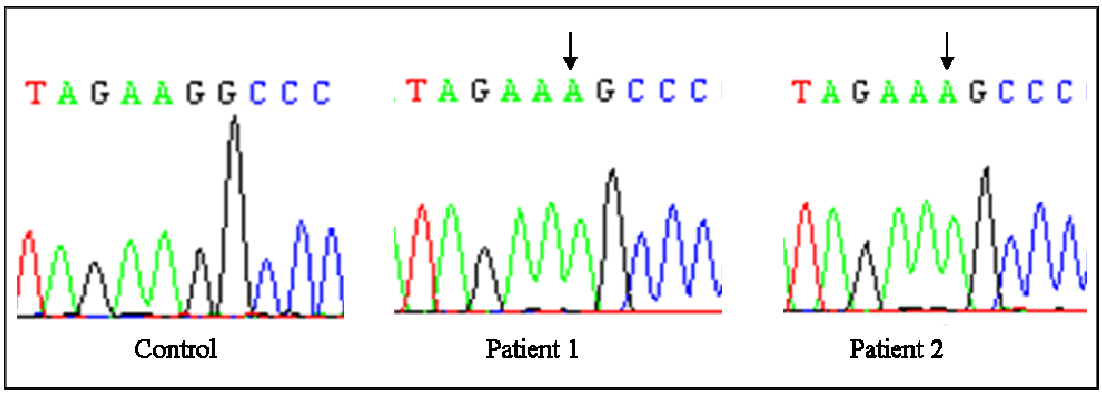

Figure 7-1 Sequence chromatogram showing the m.13051G>A transition in the two brothers.

Arrows indicate to the position of the m.13051G>A in the two patients as compared to control.

Histochemical and histological analyses of muscle biopsies from both patients revealed normal COX/SDH staining except for one COX-deficient fibre (Figure 7-2-A & 7-2-B) and some COX-positive fibres, which showed an unusual increase in activity in the periphery and pale staining in the center. In addition, immunohistochemistry revealed normal staining with antibodies against complex I subunit (Figure 7-2-C, D, E, F), consistent with the biochemical investigations, which revealed no defect in respiratory chain complexes. Although this mutation is believed to be pathogenic in both patients, further investigations are still required to support the role of this mutation in pathogenicity. These include quantifying the mutation load in muscle and other affected tissues from the second patient and relatives, where available. This approach will also help to determine whether this mutation is inherited or sporadic.

In addition to being a hot spot for MELAS mutations [340], *MTND5* harbours a number of other pathogenic mutations, which have been shown to cause Leigh syndrome [488], a Leigh-MELAS overlap syndrome [486] and MELAS-MERRF syndrome [338]. However, because the ND5 subunit of complex I is involved in proton translocation machinery [84] and/or ubiquinone binding [85], this may explain why the m.13051G>A mutation did not affect complex I activity in these patients. However, both the increase of ROS levels and mitochondrial mass in the main patient makes the m.13051G>A mutation a strong candidate to cause the disease in these patients.

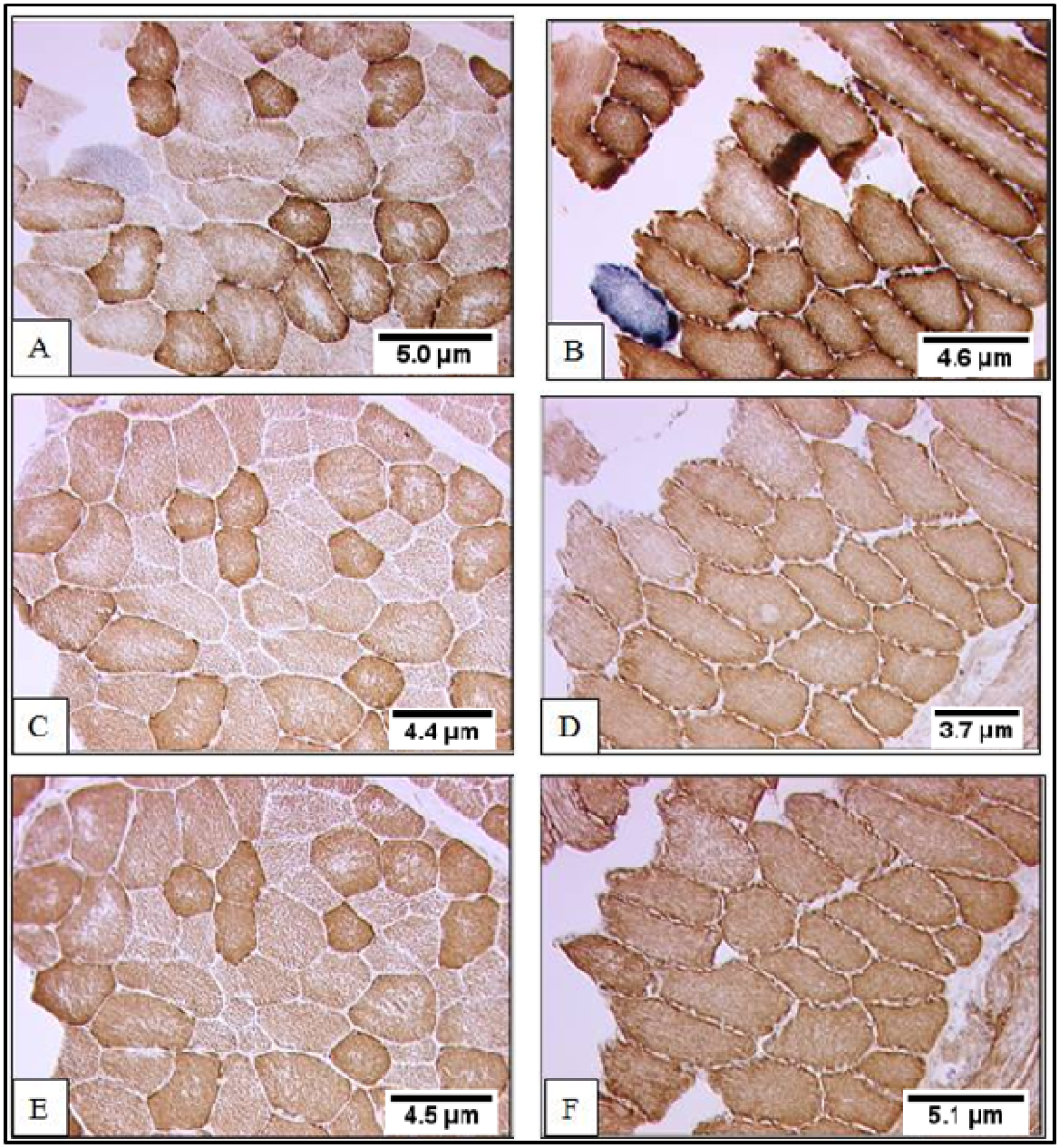

Figure 7-2 Histochemical and immunohistochemical analyses of the two brothers with the m.13051G>A mutation.

COX/SDH staining showing ~ 1% COX negativity in muscle biopsies from patient 1 (A) and patient 2 (B). Immunohistochemistry analysis using antibody against Complex I (subunit-19 kDa) showed no defect in complex I activity neither in the COX-deficient nor COX-positive fibres in patient 1 (C) and patient 2 (D) when compared to same sections probed with antibody against complex II (subunit-70 kDa) as a control (E) and (F).

The m.13513G>A mutation was identified in patient #5 who presented with Leigh syndrome. This mutation was heteroplasmic, affected a highly conserved amino acid in ND5 and caused a biochemical defect only in muscle. Unlike most pathogenic mutations, which may only cause diseases when present at high mutation loads, the 13513G>A

mutation was shown to be pathogenic even when present at low or intermediate levels of heteroplasmy [315]. However, it is difficult to correlate between the m.13513G>A mutation heteroplasmy levels and complex I activity since different levels of heteroplasmy seem to affect complex I activity differently in previously published cases. High levels of the m.13513G>A mutation affected complex I activity [392], intermediate levels gave normal complex I activity [489] but low levels of heteroplasmy have been reported to cause a defect in complex I [315, 393]. This difference can be attributed to several factors such as nuclear genetic background, mtDNA haplotypes, age and environment [393].

Finally, patient #6 who presented with spasms, pigmentary retinopathy, encephalopathy, increased blood lactate, changes in basal ganglia and defect in complex I activity in muscle, was found to harbor the pathogenic m.14453G>A mutation in *MTND6* subunit of complex I. This change is heteroplasmic, it changes the highly conserved amino acid at position 47 from alanine to valine and it was found to affect all investigated tissues from the patient.

Several pathogenic mutations have been identified in the *MTND6* subunit, which is known to be a hotspot for LHON disease [397, 490, 491], LHON/encephalopathy [492] and LHON/dystonia [493, 494]. The majority of MELAS syndromes are associated with the mtDNA m.3243G>A point mutation in the mt-tRNA$^{Leu(UUR}$ gene, the m.14453G>A mutation is the first *MTND6* mutation to be associated with MELAS [343]. In addition, a previous study showed that mutation in the *MTND6* subunit caused a defect in complex I assembly and sharp decrease in activity [495]. It is possible the m.14453G>A mutation may cause pathogencity in this patient by similar mechanism.

7.2. Identification of two novel, pathogenic mt-tRNA mutations

mtDNA mutations may affect mitochondrial protein synthesis such as mtDNA deletions or single nucleotide substitutions, which predominantly affect mitochondrial transfer RNA (mt-tRNA) genes [1, 400]. [402]. Although mt-tRNA genes represent ~10% of the mtDNA genome, almost 75% of mtDNA–related diseases are caused by mutations in these genes [406].

Patient NCL-1 was described with CPEO, muscle weakness and COX negativity in muscle fibres with ragged red fibres, which suggest a mitochondrial accumulation. The m.618T>G

mutation was the only pathogenic mutation identified in this patient within mt-tRNA^{Phe}. It is not a reported neutral polymorphic variant, it is heteroplasmic, and affects a highly conserved base pairing within the mt-tRNA^{Phe} anticodon stem. Also, higher levels of mutation were observed in COX-deficient fibres as compared to COX-positive fibres confirming segregation with the biochemical defect.

Unlike other species, the human mt-tRNA^{Phe} has no paired bases in the anticodon stem which results in a bulge (Figure 7-3). The previously reported m.618T>C mutation, which resides next to the anticodon bulge destabilised and destroyed anticodon stem formation. Therefore, it may severely affect the secondary and tertiary structure of mt-tRNA^{Phe} and its function [422]. The patient with the m.618T>C mutation had a clinical phenotypes almost similar to that seen in our patient, in terms of muscle weakness and COX deficiency with ragged red fibres, which suggests both mutations, which reside in the same position within mt-tRNA^{Phe}, have the same role in pathogenicity. In addition, the m.582T>C is another novel mutation in mt-tRNA^{Phe}, within the aminoacyl acceptor stem was reported in a patient with mitochondrial myopathy [419]. Moreover, the m.606A>G mutation in mt-tRNA^{Phe}, which affects the same base pair within the anticodon stem was pathogenic [496].

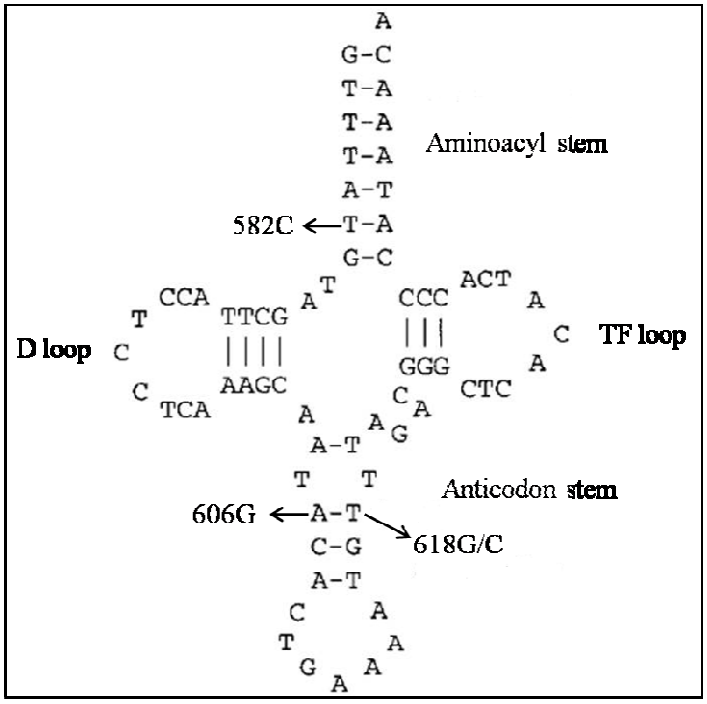

Figure 7-3 Proposed secondary structure of the human mt-tRNA^{Phe}.

This figure shows the bulge structure and position of other reported mtDNA mutations within the mt-tRNA^{Phe} (taken and modified from [422]).

However, it is still not known what is causing COX negativity in the second daughter (patient NCL-2) who had neither evidence of mtDNA deletions nor the m.618T>G mutation. Full genome sequence of single COX-deficient fibre from the patient revealed no significant change. This raises the possibility that the COX-deficient fibres a secondary phenomenon to defect in other nuclear encoded genes leading to a depletion of mtDNA copy number in these cells.

Patient Portland-4 was described with a clinical phenotype consistent with mitochondrial defect, with COX negativity in muscle and a mild defect of respiratory chain complex I. The m.12261T>C mutation within the mt-tRNA$^{Ser(AGY)}$ gene was the only pathogenic mutation identified. It is not a reported neutral polymorphism, it is a heteroplasmic change with higher levels in postmitotic muscle than mitotic cells and it affects a highly conserved nucleotide within the tRNA structure. Also, it showed higher mutation loads in COX-deficient fibres as compared to COX-positive fibres confirming segregation with the biochemical defect.

Another unrelated patient, who was described with mitochondrial phenotypes similar to those seen in our patient, was identified with a novel heteroplasmic mtDNA mutation (the m.12207G>A mutation) within the same gene [423]. In addition, retinitis pigmentosa and progressive sensorineural hearing loss, which were described in our patient, were identified in another patient harbouring the pathogenic m.12258C>A mutation within mt-tRNA$^{Ser(AGY)}$ [497]. Although, these mutations affect different positions within the same gene, they give rise to similar phenotypes, which suggests that they may affect mt-tRNA$^{Ser(AGY)}$ function by a similar mechanism. The m.12207G>A mutation is thought to affect processing of the precursor RNA and amino acid charging of the tRNA, consequently affecting protein translation [423].

Generally, the mt-tRNA mutations are considered functionally recessive and give a biochemical defect when they affect most mtDNA molecules in a cell (70–90%) [207]. However, this concept was challenged after the identifications of two mt-RNA mutations that give a biochemical defect with low mutation loads [402, 413].

A patient was also described (Chapter 5) with three distinct genetic diseases caused by three mutations: a dominant *PMP22* gene duplication, an X-linked recessive *HPRT* gene mutation and the m.12283G>A mutation within the tRNA$^{Leu(UCN)}$. The m.122831G>A

mutation was the only mitochondrial mutation identified and was thought to have a pathogenic role for several reasons. It is not a reported neutral polymorphism, it is not present in control individuals and other patients with mitochondrial disorder and it affects a highly conserved nucleotide, which resides within the variable DHU loop of mt-tRNA$^{Leu(UCN)}$. Interestingly, there was a very clear skewing of the segregation of mutant mtDNA with the biochemical defect in the COX deficient fibres as compared to the COX-positive fibres, which showed very low levels of the mutation. This pattern is different from those seen in the majority of pathogenic mt-tRNA mutations, where mutation levels in COX-positive fibres can approach the critical threshold, and may often exceed 90% mutant mtDNA [317, 425, 426]. Although the molecular mechanisms controlling this process in humans are poorly understood, they are known to be under the control of the nuclear genome [498].

Finally, the identification of a patient with three genetic defects due to mutations in two genomes is a very rare case. This case and the recent finding of the first, dominant mt-tRNA mutation [402] further highlights a problem with identifying pathogenic mtDNA mutations present at low levels, which may easily escape the established screening methodologies such as direct DNA sequencing. The m.12283G>A mutation is not behaving in a dominant fashion, but was only identified in this patient by sequencing the entire mitochondrial genome of laser microdissected COX-deficient fibres. If this is a common phenomenon, data indicate that the prevalence of pathogenic mtDNA mutations might be higher in the population than currently predicted [232], which reinforces the importance of pursuing a mitochondrial genetic diagnosis in patients with clear mitochondrial phenotypes [499].

7.3 GeneChip resequencing array 2.0

MtDNA is known to be a polymorphic [463] and prone to mutations [238]. To facilitate the identification and quantification of pathogenic mtDNA mutations, accurate and rapid techniques are required. Currently, several techniques have been used and offered advantages and both advantages as described in Chapter 6.

The GeneChip, human mitochondrial resequencing array 2.0, is one of these techniques has been used to investigate the entire mitochondrial genome. This approach has been widely used for several reasons. It amplifies the entire mitochondrial genome using three

reactions reducing time, labor and cost for sample preparation. A quarter of the patients with OXPHOS disease can be genetically diagnosed by this technique [500]. It gives overall accuracy, reproducibility and call rates greater than 90%. It is able to detect as low as 2% of heteroplasmy [501]. Not only can MitoChip be used in identifying mtDNA mutations, but it can also be used in different fields such as disease genetics, forensics, and population genetics. Although all previous features make the MitoChip a great tool in research, it still has disadvantages. It is unable to detect mtDNA deletion and insertion mutations. Although the version (2.0) of Mitochip has been improved for detecting D-Loop region mutations, the MitoChip version (2.0) cannot detect mutations from Asian mtDNA because it is based on the revised Cambridge reference sequence [467], which belongs to the European haplogroup H2 [463]. It may give miscalls and often results need to be validated by conventional sequencing. In conclusion, with the increased identification of mtDNA mutations, the human MitoChip is a high-throughput tool for mutation detection with some limitations.

7.4 Concluding remarks

In this work, different mutations in the mtDNA were identified. Some of these mutations were novel and others were recurrent. In addition to previous investigations, the biochemical and molecular genetic techniques have helped us to better understand the role of these mutations in causing the disease in the investigated patients. Also, my investigations have revealed that not all pathogenic mtDNA mutations have been identified as the number of cases being described continues to increase.

Interestingly, the identification of the m.12283G>A, within mt-tRNA$^{Leu(UCN)}$ with low mutation loads, has broadened our knowledge about the behaviour of mt-tRNA mutations, challenging the general dogma that mt-tRNA mutations are pathogenic only when they have high mutation loads. In addition, this finding has led us to rethink about the way of screening pathogenic mtDNA mutations as mutations present at low levels may easily escape the established screening methodologies such as direct DNA sequencing. Moreover, this finding highlights that mt-RNA with low mutation loads may function by different mechanisms than other mt-tRNA mutations with high mutation loads.

The comparison study between conventional sequencing and the MitoChip (V.2.0) revealed that the second is a high-throughput especially when investigating large

populations but it is still not the ultimate tool to detect all mtDNA mutations because it is not able to detect mtDNA insertion and rearrangement mutations. This favors the use of conventional sequencing, which is more preferred in diagnostic labs to avoid missing simple insertion and small-scale mtDNA mutations. In addition, this shows the need of next generation sequencing techniques with ultimate features to overcome disadvantages associated with old generation sequencing techniques which will provides a great promise in diagnostics.

Finally, more effort is required to increase our knowledge in this field to help us to solve unexplained issues related to mitochondrial biology and diseases to contribute effectively to mitochondrial DNA disease management.

Chapter 8

References

Chapter 8 : References

1. Taylor, R.W. and D.M. Turnbull, Mitochondrial DNA mutations in human disease. Nat Rev Genet, 2005. 6(5): p. 389-402.
2. Sicheritz-Ponten, T., C.G. Kurland, and S.G. Andersson, A phylogenetic analysis of the cytochrome b and cytochrome c oxidase I genes supports an origin of mitochondria from within the Rickettsiaceae. Biochim Biophys Acta, 1998. 1365(3): p. 545-51.
3. Gray, M.W. and W.F. Doolittle, Has the endosymbiont hypothesis been proven? Microbiol Rev, 1982. 46(1): p. 1-42.
4. Margulis, L., Origin of Eukaryotic Cells. Yale Univ. Press, 1970.
5. Margulis, L., Symbiosis in Cell Evolution. W.H.Freeman & Co Ltd 1981.
6. Andersson, S.G., et al., On the origin of mitochondria: a genomics perspective. Philos Trans R Soc Lond B Biol Sci, 2003. 358(1429): p. 165-77; discussion 177-9.
7. Dyall, S.D., M.T. Brown, and P.J. Johnson, Ancient invasions: from endosymbionts to organelles. Science, 2004. 304(5668): p. 253-7.
8. Lang, B.F., M.W. Gray, and G. Burger, Mitochondrial genome evolution and the origin of eukaryotes. Annu Rev Genet, 1999. 33: p. 351-97.
9. van der Giezen, M. and J. Tovar, Degenerate mitochondria. EMBO Rep, 2005. 6(6): p. 525-30.
10. Lithgow, T. and A. Schneider, Evolution of macromolecular import pathways in mitochondria, hydrogenosomes and mitosomes. Philos Trans R Soc Lond B Biol Sci, 2010. 365(1541): p. 799-817.
11. Tovar, J., A. Fischer, and C.G. Clark, The mitosome, a novel organelle related to mitochondria in the amitochondrial parasite Entamoeba histolytica. Mol Microbiol, 1999. 32(5): p. 1013-21.
12. Clark, C.G. and A.J. Roger, Direct evidence for secondary loss of mitochondria in Entamoeba histolytica. Proc Natl Acad Sci U S A, 1995. 92(14): p. 6518-21.
13. Clemens, D.L. and P.J. Johnson, Failure to detect DNA in hydrogenosomes of Trichomonas vaginalis by nick translation and immunomicroscopy. Mol Biochem Parasitol, 2000. 106(2): p. 307-13.
14. Muller, M., The hydrogenosome. J Gen Microbiol, 1993. 139(12): p. 2879-89.
15. Scheffler, I.E., Mitochondria. second ed. 2008: WILEY.

16. Foschini, M.P., et al., Identification of mitochondria in liver biopsies. A study by immunohistochemistry, immunogold and Western blot analysis. Virchows Arch, 1998. 433(3): p. 267-73.
17. Chen, X., et al., Rearranged mitochondrial genomes are present in human oocytes. Am J Hum Genet, 1995. 57(2): p. 239-47.
18. Ankel-Simons, F. and J.M. Cummins, Misconceptions about mitochondria and mammalian fertilization: implications for theories on human evolution. Proc Natl Acad Sci U S A, 1996. 93(24): p. 13859-63.
19. Mason, P.A., et al., Mismatch repair activity in mammalian mitochondria. Nucleic Acids Res, 2003. 31(3): p. 1052-8.
20. Pfaff, E., et al., [Correlation of the unspecific permeable mitochondrial space with the "intermembrane space"]. Eur J Biochem, 1968. 5(2): p. 222-32.
21. Blachly-Dyson, E. and M. Forte, VDAC channels. IUBMB Life, 2001. 52(3-5): p. 113-8.
22. Ernster, L. and G. Schatz, Mitochondria: a historical review. J Cell Biol, 1981. 91(3 Pt 2): p. 227s-255s.
23. LaNoue, K.F. and A.C. Schoolwerth, Metabolite transport in mitochondria. Annu Rev Biochem, 1979. 48: p. 871-922.
24. Hsia, J.C., et al., Existence of phospholipid bilayer structure in the inner membrane of mitochondria. Proc Natl Acad Sci U S A, 1972. 69(11): p. 3412-5.
25. Stoffel, W. and H.G. Schiefer, Biosynthesis and composition of phosphatides in outer and inner mitochondrial membranes. Hoppe Seylers Z Physiol Chem, 1968. 349(8): p. 1017-26.
26. Gray, G.M. and M.G. Macfarlane, Separation and composition of the phospholipids of ox heart. Biochem J, 1958. 70(3): p. 409-25.
27. Bobyleva, V., et al., Effect of cardiolipin on functional properties of isolated rat liver mitochondria. Biochem Mol Biol Int, 1997. 41(3): p. 469-80.
28. Klingenberg, M., and E. Pfaff., BBA (Biochem. Biophys. Acta) Libr., 1966. 7: p. 180-200.
29. Nelson, D.R., C.M. Felix, and J.M. Swanson, Highly conserved charge-pair networks in the mitochondrial carrier family. J Mol Biol, 1998. 277(2): p. 285-308.
30. Hatefi, Y., Ragan, C. I . , Galante, Y. M . The Enzymes of Biological Membranes. 2nd ed. ed. Vol. 4. 1985, New York:: Plenum.

31. Hatefi, Y., The mitochondrial electron transport and oxidative phosphorylation system. Annu Rev Biochem, 1985. 54: p. 1015-69.
32. King, A., M.A. Selak, and E. Gottlieb, Succinate dehydrogenase and fumarate hydratase: linking mitochondrial dysfunction and cancer. Oncogene, 2006. 25(34): p. 4675-82.
33. Palade, G.E., The fine structure of mitochondria. Anat Rec, 1952. 114(3): p. 427-51.
34. Palade, G.E., An electron microscope study of the mitochondrial structure. J Histochem Cytochem, 1953. 1(4): p. 188-211.
35. Ernster, L., and B. Kuylenstierna, In Membranes of Mitochondria and Chloroplasts . 1970, New York.: Van Nostrand Reinhold,.
36. Carrodeguas, J.A., et al., Crystal structure and deletion analysis show that the accessory subunit of mammalian DNA polymerase gamma, Pol gamma B, functions as a homodimer. Mol Cell, 2001. 7(1): p. 43-54.
37. Chen, H., et al., Mitofusins Mfn1 and Mfn2 coordinately regulate mitochondrial fusion and are essential for embryonic development. J Cell Biol, 2003. 160(2): p. 189-200.
38. Greaves, L.C. and R.W. Taylor, Mitochondrial DNA mutations in human disease. IUBMB Life, 2006. 58(3): p. 143-51.
39. Hollenbeck, P.J. and W.M. Saxton, The axonal transport of mitochondria. J Cell Sci, 2005. 118(Pt 23): p. 5411-9.
40. Youle, R.J. and M. Karbowski, Mitochondrial fission in apoptosis. Nat Rev Mol Cell Biol, 2005. 6(8): p. 657-63.
41. Benard, G., et al., Mitochondrial bioenergetics and structural network organization. J Cell Sci, 2007. 120(Pt 5): p. 838-48.
42. Kowaltowski, A.J., Alternative mitochondrial functions in cell physiopathology: beyond ATP production. Braz J Med Biol Res, 2000. 33(2): p. 241-50.
43. Nicholls, D.G. and R.M. Locke, Thermogenic mechanisms in brown fat. Physiol Rev, 1984. 64(1): p. 1-64.
44. Foster, D.O. and M.L. Frydman, Brown adipose tissue: the dominant site of nonshivering thermogenesis in the rat. Experientia Suppl, 1978. 32: p. 147-51.
45. Smith, R.E., J.C. Roberts, and K.J. Hittelman, Nonphosphorylating respiration of mitochondria from brown adipose tissue of rats. Science, 1966. 154(749): p. 653-4.

46. Nicholls, D.G., The bioenergetics of brown adipose tissue mitochondria. FEBS Lett, 1976. 61(2): p. 103-110.
47. Gunter, T.E. and D.R. Pfeiffer, Mechanisms by which mitochondria transport calcium. Am J Physiol, 1990. 258(5 Pt 1): p. C755-86.
48. Gunter, K.K. and T.E. Gunter, Transport of calcium by mitochondria. J Bioenerg Biomembr, 1994. 26(5): p. 471-85.
49. Boveris, A., N. Oshino, and B. Chance, The cellular production of hydrogen peroxide. Biochem J, 1972. 128(3): p. 617-30.
50. Beyer, R.E., An analysis of the role of coenzyme Q in free radical generation and as an antioxidant. Biochem Cell Biol, 1992. 70(6): p. 390-403.
51. Takeshige, K. and S. Minakami, NADH- and NADPH-dependent formation of superoxide anions by bovine heart submitochondrial particles and NADH-ubiquinone reductase preparation. Biochem J, 1979. 180(1): p. 129-35.
52. Vercesi, A.J.K.A.E., Mitochondria in Pathogenesis. 2000, New York: Plenum Publishing Corporation.
53. Boveris, A. and B. Chance, The mitochondrial generation of hydrogen peroxide. General properties and effect of hyperbaric oxygen. Biochem J, 1973. 134(3): p. 707-16.
54. Boveris, A., E. Cadenas, and A.O. Stoppani, Role of ubiquinone in the mitochondrial generation of hydrogen peroxide. Biochem J, 1976. 156(2): p. 435-44.
55. Cino, M. and R.F. Del Maestro, Generation of hydrogen peroxide by brain mitochondria: the effect of reoxygenation following postdecapitative ischemia. Arch Biochem Biophys, 1989. 269(2): p. 623-38.
56. Liu, Y., G. Fiskum, and D. Schubert, Generation of reactive oxygen species by the mitochondrial electron transport chain. J Neurochem, 2002. 80(5): p. 780-7.
57. McLennan, H.R. and M. Degli Esposti, The contribution of mitochondrial respiratory complexes to the production of reactive oxygen species. J Bioenerg Biomembr, 2000. 32(2): p. 153-62.
58. Turrens, J.F. and A. Boveris, Generation of superoxide anion by the NADH dehydrogenase of bovine heart mitochondria. Biochem J, 1980. 191(2): p. 421-7.
59. Adam-Vizi, V. and C. Chinopoulos, Bioenergetics and the formation of mitochondrial reactive oxygen species. Trends Pharmacol Sci, 2006. 27(12): p. 639-45.

60. Brand, M.D., et al., Mitochondrial superoxide: production, biological effects, and activation of uncoupling proteins. Free Radic Biol Med, 2004. 37(6): p. 755-67.
61. Lambert, A.J., J.A. Buckingham, and M.D. Brand, Dissociation of superoxide production by mitochondrial complex I from NAD(P)H redox state. FEBS Lett, 2008. 582(12): p. 1711-4.
62. Hirst, J., M.S. King, and K.R. Pryde, The production of reactive oxygen species by complex I. Biochem Soc Trans, 2008. 36(Pt 5): p. 976-80.
63. Green, D.R. and J.C. Reed, Mitochondria and apoptosis. Science, 1998. 281(5381): p. 1309-12.
64. Susin, S.A., N. Zamzami, and G. Kroemer, Mitochondria as regulators of apoptosis: doubt no more. Biochim Biophys Acta, 1998. 1366(1-2): p. 151-65.
65. Susin, S.A., et al., Mitochondrial release of caspase-2 and -9 during the apoptotic process. J Exp Med, 1999. 189(2): p. 381-94.
66. Krajewski, S., et al., Release of caspase-9 from mitochondria during neuronal apoptosis and cerebral ischemia. Proc Natl Acad Sci U S A, 1999. 96(10): p. 5752-7.
67. Du, C., et al., Smac, a mitochondrial protein that promotes cytochrome c-dependent caspase activation by eliminating IAP inhibition. Cell, 2000. 102(1): p. 33-42.
68. Wang, C. and R.J. Youle, The role of mitochondria in apoptosis*. Annu Rev Genet, 2009. 43: p. 95-118.
69. Ruiz-Pesini, E., et al., An enhanced MITOMAP with a global mtDNA mutational phylogeny. Nucleic Acids Res, 2007. 35(Database issue): p. D823-8.
70. Janssen, A.J., J.A. Smeitink, and L.P. van den Heuvel, Some practical aspects of providing a diagnostic service for respiratory chain defects. Ann Clin Biochem, 2003. 40(Pt 1): p. 3-8.
71. Dudkina, N.V., et al., Structure of a mitochondrial supercomplex formed by respiratory-chain complexes I and III. Proc Natl Acad Sci U S A, 2005. 102(9): p. 3225-9.
72. Lazarou, M., et al., Assembly of mitochondrial complex I and defects in disease. Biochim Biophys Acta, 2009. 1793(1): p. 78-88.
73. Carroll, J., et al., Bovine complex I is a complex of 45 different subunits. J Biol Chem, 2006. 281(43): p. 32724-7.
74. Grigorieff, N., Three-dimensional structure of bovine NADH:ubiquinone oxidoreductase (complex I) at 22 A in ice. J Mol Biol, 1998. 277(5): p. 1033-46.

75. Radermacher, M., et al., The three-dimensional structure of complex I from Yarrowia lipolytica: a highly dynamic enzyme. J Struct Biol, 2006. 154(3): p. 269-79.
76. Peng, G., et al., Isolation, characterization and electron microscopic single particle analysis of the NADH:ubiquinone oxidoreductase (complex I) from the hyperthermophilic eubacterium Aquifex aeolicus. Biochemistry, 2003. 42(10): p. 3032-9.
77. Friedrich, T. and B. Bottcher, The gross structure of the respiratory complex I: a Lego System. Biochim Biophys Acta, 2004. 1608(1): p. 1-9.
78. Sazanov, L.A., et al., A role for native lipids in the stabilization and two-dimensional crystallization of the Escherichia coli NADH-ubiquinone oxidoreductase (complex I). J Biol Chem, 2003. 278(21): p. 19483-91.
79. Hinchliffe, P. and L.A. Sazanov, Organization of iron-sulfur clusters in respiratory complex I. Science, 2005. 309(5735): p. 771-4.
80. Sazanov, L.A. and P. Hinchliffe, Structure of the hydrophilic domain of respiratory complex I from Thermus thermophilus. Science, 2006. 311(5766): p. 1430-6.
81. Potluri, P., N. Yadava, and I.E. Scheffler, The role of the ESSS protein in the assembly of a functional and stable mammalian mitochondrial complex I (NADH-ubiquinone oxidoreductase). Eur J Biochem, 2004. 271(15): p. 3265-73.
82. Janssen, R.J., et al., Mitochondrial complex I: structure, function and pathology. J Inherit Metab Dis, 2006. 29(4): p. 499-515.
83. Yano, T., The energy-transducing NADH: quinone oxidoreductase, complex I. Mol Aspects Med, 2002. 23(5): p. 345-68.
84. Friedrich, T., Complex I: a chimaera of a redox and conformation-driven proton pump? J Bioenerg Biomembr, 2001. 33(3): p. 169-77.
85. Fisher, N. and P.R. Rich, A motif for quinone binding sites in respiratory and photosynthetic systems. J Mol Biol, 2000. 296(4): p. 1153-62.
86. Lazarou, M., et al., Analysis of the assembly profiles for mitochondrial- and nuclear-DNA-encoded subunits into complex I. Mol Cell Biol, 2007. 27(12): p. 4228-37.
87. Hall, R.E. and J.F. Hare, Respiratory chain-linked NADH dehydrogenase. Mechanisms of assembly. J Biol Chem, 1990. 265(27): p. 16484-90.

88. Bourges, I., et al., Structural organization of mitochondrial human complex I: role of the ND4 and ND5 mitochondria-encoded subunits and interaction with prohibitin. Biochem J, 2004. 383(Pt. 3): p. 491-9.
89. Vogel, R.O., et al., Investigation of the complex I assembly chaperones B17.2L and NDUFAF1 in a cohort of CI deficient patients. Mol Genet Metab, 2007. 91(2): p. 176-82.
90. Ugalde, C., et al., Human mitochondrial complex I assembles through the combination of evolutionary conserved modules: a framework to interpret complex I deficiencies. Hum Mol Genet, 2004. 13(20): p. 2461-72.
91. Dunning, C.J., et al., Human CIA30 is involved in the early assembly of mitochondrial complex I and mutations in its gene cause disease. Embo J, 2007. 26(13): p. 3227-37.
92. Vogel, R.O., et al., Identification of mitochondrial complex I assembly intermediates by tracing tagged NDUFS3 demonstrates the entry point of mitochondrial subunits. J Biol Chem, 2007. 282(10): p. 7582-90.
93. Scheffler, I.E., Mitochondria. second ed. 2007: WILEY.
94. Anderson, R.F., et al., Electron transfer within complex II. Succinate:ubiquinone oxidoreductase of Escherichia coli. J Biol Chem, 2005. 280(39): p. 33331-7.
95. Chinnery, P.F., et al., The inheritance of mitochondrial DNA heteroplasmy: random drift, selection or both? Trends Genet, 2000. 16(11): p. 500-5.
96. Battersby, B.J. and E.A. Shoubridge, Selection of a mtDNA sequence variant in hepatocytes of heteroplasmic mice is not due to differences in respiratory chain function or efficiency of replication. Hum Mol Genet, 2001. 10(22): p. 2469-79.
97. Battersby, B.J., M.E. Redpath, and E.A. Shoubridge, Mitochondrial DNA segregation in hematopoietic lineages does not depend on MHC presentation of mitochondrially encoded peptides. Hum Mol Genet, 2005. 14(17): p. 2587-94.
98. Porter, M.H. and C.D. Berdanier, Oxidative phosphorylation: key to life. Diabetes Technol Ther, 2002. 4(2): p. 253-4.
99. Trumpower, B.L., The protonmotive Q cycle. Energy transduction by coupling of proton translocation to electron transfer by the cytochrome bc1 complex. J Biol Chem, 1990. 265(20): p. 11409-12.
100. Khalimonchuk, O. and G. Rodel, Biogenesis of cytochrome c oxidase. Mitochondrion, 2005. 5(6): p. 363-88.

101. Collman, J.P., et al., Catalytic reduction of O2 by cytochrome C using a synthetic model of cytochrome C oxidase. J Am Chem Soc, 2009. 131(14): p. 5034-5.
102. Poyton, R.O. and J.E. McEwen, Crosstalk between nuclear and mitochondrial genomes. Annu Rev Biochem, 1996. 65: p. 563-607.
103. Carr, H.S. and D.R. Winge, Assembly of cytochrome c oxidase within the mitochondrion. Acc Chem Res, 2003. 36(5): p. 309-16.
104. Tsukihara, T., et al., Structures of metal sites of oxidized bovine heart cytochrome c oxidase at 2.8 A. Science, 1995. 269(5227): p. 1069-74.
105. Kirichenko, A., et al., Specific cation binding site in mammalian cytochrome oxidase. FEBS Lett, 1998. 423(3): p. 329-33.
106. Lee, A., et al., Ca(2+)-binding site in Rhodobacter sphaeroides cytochrome C oxidase. Biochemistry, 2002. 41(28): p. 8886-98.
107. Rahman, S., et al., A missense mutation of cytochrome oxidase subunit II causes defective assembly and myopathy. Am J Hum Genet, 1999. 65(4): p. 1030-9.
108. Lemaire, C., S. Robineau, and P. Netter, Molecular and biochemical analysis of Saccharomyces cerevisiae cox1 mutants. Curr Genet, 1998. 34(2): p. 138-45.
109. Meunier, B. and J.W. Taanman, Mutations of cytochrome c oxidase subunits 1 and 3 in Saccharomyces cerevisiae: assembly defect and compensation. Biochim Biophys Acta, 2002. 1554(1-2): p. 101-7.
110. Haltia, T., M. Saraste, and M. Wikstrom, Subunit III of cytochrome c oxidase is not involved in proton translocation: a site-directed mutagenesis study. EMBO J, 1991. 10(8): p. 2015-21.
111. Capaldi, R.A., Structure and function of cytochrome c oxidase. Annu Rev Biochem, 1990. 59: p. 569-96.
112. Wallace, D.C., Diseases of the mitochondrial DNA. Annu Rev Biochem, 1992. 61: p. 1175-212.
113. von Ballmoos, C., A. Wiedenmann, and P. Dimroth, Essentials for ATP synthesis by F1F0 ATP synthases. Annu Rev Biochem, 2009. 78: p. 649-72.
114. Ferguson, S.J., ATP synthase: what dictates the size of a ring? Curr Biol, 2000. 10(21): p. R804-8.
115. Bowler, M.W., et al., How azide inhibits ATP hydrolysis by the F-ATPases. Proc Natl Acad Sci U S A, 2006. 103(23): p. 8646-9.
116. Gibbons, C., et al., The structure of the central stalk in bovine F(1)-ATPase at 2.4 A resolution. Nat Struct Biol, 2000. 7(11): p. 1055-61.

117. Le Bras, M., et al., Chemosensitization by knockdown of adenine nucleotide translocase-2. Cancer Res, 2006. 66(18): p. 9143-52.
118. H.Swalwell, Mitochondrial DNA Mutations in Human Disease. 2007, Newcastle University.
119. Byrne, E. and I. Trounce, Oxygen electrode studies with human skeletal muscle mitochondria in vitro. A re-appraisal. J Neurol Sci, 1985. 69(3): p. 319-33.
120. Acin-Perez, R., et al., Respiratory active mitochondrial supercomplexes. Mol Cell, 2008. 32(4): p. 529-39.
121. Stroh, A., et al., Assembly of respiratory complexes I, III, and IV into NADH oxidase supercomplex stabilizes complex I in Paracoccus denitrificans. J Biol Chem, 2004. 279(6): p. 5000-7.
122. Schagger, H., Respiratory chain supercomplexes of mitochondria and bacteria. Biochim Biophys Acta, 2002. 1555(1-3): p. 154-9.
123. Schagger, H. and K. Pfeiffer, Supercomplexes in the respiratory chains of yeast and mammalian mitochondria. EMBO J, 2000. 19(8): p. 1777-83.
124. Lenaz, G., et al., Mitochondrial respiratory chain super-complex I-III in physiology and pathology. Biochim Biophys Acta.
125. Lee, H.C. and Y.H. Wei, Mitochondrial biogenesis and mitochondrial DNA maintenance of mammalian cells under oxidative stress. Int J Biochem Cell Biol, 2005. 37(4): p. 822-34.
126. Attardi, G. and G. Schatz, Biogenesis of mitochondria. Annu Rev Cell Biol, 1988. 4: p. 289-333.
127. Moyes, C.D. and D.A. Hood, Origins and consequences of mitochondrial variation in vertebrate muscle. Annu Rev Physiol, 2003. 65: p. 177-201.
128. Falkenberg, M., N.G. Larsson, and C.M. Gustafsson, DNA replication and transcription in mammalian mitochondria. Annu Rev Biochem, 2007. 76: p. 679-99.
129. Scarpulla, R.C., Nuclear control of respiratory chain expression in mammalian cells. J Bioenerg Biomembr, 1997. 29(2): p. 109-19.
130. Temperley, R., et al., Hungry codons promote frameshifting in human mitochondrial ribosomes. Science, 2010. 327(5963): p. 301.
131. Clayton, D.A., Transcription of the mammalian mitochondrial genome. Annu Rev Biochem, 1984. 53: p. 573-94.

132. Clayton, D.A., Replication and transcription of vertebrate mitochondrial DNA. Annu Rev Cell Biol, 1991. 7: p. 453-78.
133. Larsson, N.G. and D.A. Clayton, Molecular genetic aspects of human mitochondrial disorders. Annu Rev Genet, 1995. 29: p. 151-78.
134. Reyes, A., et al., Bidirectional replication initiates at sites throughout the mitochondrial genome of birds. J Biol Chem, 2005. 280(5): p. 3242-50.
135. Bowmaker, M., et al., Mammalian mitochondrial DNA replicates bidirectionally from an initiation zone. J Biol Chem, 2003. 278(51): p. 50961-9.
136. Fish, J., N. Raule, and G. Attardi, Discovery of a major D-loop replication origin reveals two modes of human mtDNA synthesis. Science, 2004. 306(5704): p. 2098-101.
137. Holt, I.J., Mitochondrial DNA replication and repair: all a flap. Trends Biochem Sci, 2009. 34(7): p. 358-65.
138. Wanrooij, S., et al., Expression of catalytic mutants of the mtDNA helicase Twinkle and polymerase POLG causes distinct replication stalling phenotypes. Nucleic Acids Res, 2007. 35(10): p. 3238-51.
139. Maier, D., et al., Mitochondrial single-stranded DNA-binding protein is required for mitochondrial DNA replication and development in Drosophila melanogaster. Mol Biol Cell, 2001. 12(4): p. 821-30.
140. Shutt, T.E. and M.W. Gray, Twinkle, the mitochondrial replicative DNA helicase, is widespread in the eukaryotic radiation and may also be the mitochondrial DNA primase in most eukaryotes. J Mol Evol, 2006. 62(5): p. 588-99.
141. Ruhanen, H., et al., Mitochondrial single-stranded DNA binding protein is required for maintenance of mitochondrial DNA and 7S DNA but is not required for mitochondrial nucleoid organisation. Biochim Biophys Acta, 2010. 1803(8): p. 931-9.
142. Wang, Y. and D.F. Bogenhagen, Human mitochondrial DNA nucleoids are linked to protein folding machinery and metabolic enzymes at the mitochondrial inner membrane. J Biol Chem, 2006. 281(35): p. 25791-802.
143. Kienhofer, J., et al., Association of mitochondrial antioxidant enzymes with mitochondrial DNA as integral nucleoid constituents. FASEB J, 2009. 23(7): p. 2034-44.
144. Clayton, D.A., Structure and function of the mitochondrial genome. J Inherit Metab Dis, 1992. 15(4): p. 439-47.

145. Taylor, R.W. and D.M. Turnbull, Mitochondrial DNA transcription: regulating the power supply. Cell, 2007. 130(2): p. 211-3.
146. Ojala, D., J. Montoya, and G. Attardi, tRNA punctuation model of RNA processing in human mitochondria. Nature, 1981. 290(5806): p. 470-4.
147. Gaspari, M., N.G. Larsson, and C.M. Gustafsson, The transcription machinery in mammalian mitochondria. Biochim Biophys Acta, 2004. 1659(2-3): p. 148-52.
148. Park, C.B., et al., MTERF3 is a negative regulator of mammalian mtDNA transcription. Cell, 2007. 130(2): p. 273-85.
149. Shoubridge, E.A., Something old, something new, something borrowed. Cell Metab, 2009. 9(4): p. 307-8.
150. Haque, M.E. and L.L. Spremulli, ICT1 comes to the rescue of mitochondrial ribosomes. EMBO J. 29(6): p. 1019-20.
151. Saada, A., et al., Antenatal mitochondrial disease caused by mitochondrial ribosomal protein (MRPS22) mutation. J Med Genet, 2007. 44(12): p. 784-6.
152. McGregor, A., et al., Absence of expression from RNA internalised into electroporated mammalian mitochondria. Mol Genet Genomics, 2001. 265(4): p. 721-9.
153. Shine, J. and L. Dalgarno, Terminal-sequence analysis of bacterial ribosomal RNA. Correlation between the 3'-terminal-polypyrimidine sequence of 16-S RNA and translational specificity of the ribosome. Eur J Biochem, 1975. 57(1): p. 221-30.
154. Temperley, R.J., et al., Human mitochondrial mRNAs-like members of all families, similar but different. Biochim Biophys Acta. 1797(6-7): p. 1081-5.
155. Tarun, S.Z., Jr. and A.B. Sachs, Association of the yeast poly(A) tail binding protein with translation initiation factor eIF-4G. EMBO J, 1996. 15(24): p. 7168-77.
156. Jones, C.N., et al., Lack of secondary structure characterizes the 5' ends of mammalian mitochondrial mRNAs. RNA, 2008. 14(5): p. 862-71.
157. Koc, E.C. and L.L. Spremulli, Identification of mammalian mitochondrial translational initiation factor 3 and examination of its role in initiation complex formation with natural mRNAs. J Biol Chem, 2002. 277(38): p. 35541-9.
158. Liao, H.X. and L.L. Spremulli, Initiation of protein synthesis in animal mitochondria. Purification and characterization of translational initiation factor 2. J Biol Chem, 1991. 266(31): p. 20714-9.

159. Woriax, V.L., W. Burkhart, and L.L. Spremulli, Cloning, sequence analysis and expression of mammalian mitochondrial protein synthesis elongation factor Tu. Biochim Biophys Acta, 1995. 1264(3): p. 347-56.
160. Hammarsund, M., et al., Identification and characterization of two novel human mitochondrial elongation factor genes, hEFG2 and hEFG1, phylogenetically conserved through evolution. Hum Genet, 2001. 109(5): p. 542-50.
161. Davies, S.M., et al., Pentatricopeptide repeat domain protein 3 associates with the mitochondrial small ribosomal subunit and regulates translation. FEBS Lett, 2009. 583(12): p. 1853-8.
162. Rorbach, J., et al., The human mitochondrial ribosome recycling factor is essential for cell viability. Nucleic Acids Res, 2008. 36(18): p. 5787-99.
163. Zhang, Y. and L.L. Spremulli, Identification and cloning of human mitochondrial translational release factor 1 and the ribosome recycling factor. Biochim Biophys Acta, 1998. 1443(1-2): p. 245-50.
164. Serero, A., et al., An unusual peptide deformylase features in the human mitochondrial N-terminal methionine excision pathway. J Biol Chem, 2003. 278(52): p. 52953-63.
165. Soleimanpour-Lichaei, H.R., et al., mtRF1a is a human mitochondrial translation release factor decoding the major termination codons UAA and UAG. Mol Cell, 2007. 27(5): p. 745-57.
166. Miller, C., et al., Defective mitochondrial translation caused by a ribosomal protein (MRPS16) mutation. Ann Neurol, 2004. 56(5): p. 734-8.
167. Coenen, M.J., et al., Mutant mitochondrial elongation factor G1 and combined oxidative phosphorylation deficiency. N Engl J Med, 2004. 351(20): p. 2080-6.
168. Valente, L., et al., Infantile encephalopathy and defective mitochondrial DNA translation in patients with mutations of mitochondrial elongation factors EFG1 and EFTu. Am J Hum Genet, 2007. 80(1): p. 44-58.
169. Smeitink, J.A., et al., Distinct clinical phenotypes associated with a mutation in the mitochondrial translation elongation factor EFTs. Am J Hum Genet, 2006. 79(5): p. 869-77.
170. Jones, C.N., et al., A disease-causing point mutation in human mitochondrial tRNAMet rsults in tRNA misfolding leading to defects in translational initiation and elongation. J Biol Chem, 2008. 283(49): p. 34445-56.

171. Wiedemann, N., A.E. Frazier, and N. Pfanner, The protein import machinery of mitochondria. J Biol Chem, 2004. 279(15): p. 14473-6.
172. Schatz, G. and B. Dobberstein, Common principles of protein translocation across membranes. Science, 1996. 271(5255): p. 1519-26.
173. Pfanner, N. and A. Geissler, Versatility of the mitochondrial protein import machinery. Nat Rev Mol Cell Biol, 2001. 2(5): p. 339-49.
174. Koehler, C.M., et al., Import of mitochondrial carriers mediated by essential proteins of the intermembrane space. Science, 1998. 279(5349): p. 369-73.
175. Geissler, A., et al., The mitochondrial presequence translocase: an essential role of Tim50 in directing preproteins to the import channel. Cell, 2002. 111(4): p. 507-18.
176. Hoppins, S.C. and F.E. Nargang, The Tim8-Tim13 complex of Neurospora crassa functions in the assembly of proteins into both mitochondrial membranes. J Biol Chem, 2004. 279(13): p. 12396-405.
177. Wiedemann, N., et al., Biogenesis of the protein import channel Tom40 of the mitochondrial outer membrane: intermembrane space components are involved in an early stage of the assembly pathway. J Biol Chem, 2004. 279(18): p. 18188-94.
178. Bogenhagen, D.F., et al., Protein components of mitochondrial DNA nucleoids in higher eukaryotes. Mol Cell Proteomics, 2003. 2(11): p. 1205-16.
179. Nass, M.M., Mitochondrial DNA. I. Intramitochondrial distribution and structural relations of single- and double-length circular DNA. J Mol Biol, 1969. 42(3): p. 521-8.
180. Albring, M., J. Griffith, and G. Attardi, Association of a protein structure of probable membrane derivation with HeLa cell mitochondrial DNA near its origin of replication. Proc Natl Acad Sci U S A, 1977. 74(4): p. 1348-52.
181. Wei, Y.H. and H.C. Lee, Oxidative stress, mitochondrial DNA mutation, and impairment of antioxidant enzymes in aging. Exp Biol Med (Maywood), 2002. 227(9): p. 671-82.
182. Harman, D., Aging: a theory based on free radical and radiation chemistry. J Gerontol, 1956. 11(3): p. 298-300.
183. Harman, D., The biologic clock: the mitochondria? J Am Geriatr Soc, 1972. 20(4): p. 145-7.
184. Harman, D., The aging process. Proc Natl Acad Sci U S A, 1981. 78(11): p. 7124-8.

185. Geromel, V., et al., Superoxide-induced massive apoptosis in cultured skin fibroblasts harboring the neurogenic ataxia retinitis pigmentosa (NARP) mutation in the ATPase-6 gene of the mitochondrial DNA. Hum Mol Genet, 2001. 10(11): p. 1221-8.
186. Brandon, M., P. Baldi, and D.C. Wallace, Mitochondrial mutations in cancer. Oncogene, 2006. 25(34): p. 4647-62.
187. Park, J.S., et al., A heteroplasmic, not homoplasmic, mitochondrial DNA mutation promotes tumorigenesis via alteration in reactive oxygen species generation and apoptosis. Hum Mol Genet, 2009. 18(9): p. 1578-89.
188. Dasgupta, S., et al., Mitochondrial cytochrome B gene mutation promotes tumor growth in bladder cancer. Cancer Res, 2008. 68(3): p. 700-6.
189. Koshikawa, N., et al., Reactive oxygen species-generating mitochondrial DNA mutation up-regulates hypoxia-inducible factor-1alpha gene transcription via phosphatidylinositol 3-kinase-Akt/protein kinase C/histone deacetylase pathway. J Biol Chem, 2009. 284(48): p. 33185-94.
190. Tuppen, H.A., et al., Mitochondrial DNA mutations and human disease. Biochim Biophys Acta. 1797(2): p. 113-128.
191. de Souza-Pinto, N.C., et al., Novel DNA mismatch-repair activity involving YB-1 in human mitochondria. DNA Repair (Amst), 2009. 8(6): p. 704-19.
192. Bohr, V.A., T. Stevnsner, and N.C. de Souza-Pinto, Mitochondrial DNA repair of oxidative damage in mammalian cells. Gene, 2002. 286(1): p. 127-34.
193. Larsen, N.B., M. Rasmussen, and L.J. Rasmussen, Nuclear and mitochondrial DNA repair: similar pathways? Mitochondrion, 2005. 5(2): p. 89-108.
194. Sawyer, D.E. and B. Van Houten, Repair of DNA damage in mitochondria. Mutat Res, 1999. 434(3): p. 161-76.
195. Bogenhagen, D.F., K.G. Pinz, and R.M. Perez-Jannotti, Enzymology of mitochondrial base excision repair. Prog Nucleic Acid Res Mol Biol, 2001. 68: p. 257-71.
196. Bohr, V.A., Repair of oxidative DNA damage in nuclear and mitochondrial DNA, and some changes with aging in mammalian cells. Free Radic Biol Med, 2002. 32(9): p. 804-12.
197. LeDoux, S.P., et al., Repair of mitochondrial DNA after various types of DNA damage in Chinese hamster ovary cells. Carcinogenesis, 1992. 13(11): p. 1967-73.

198. Manfredi, G., et al., The fate of human sperm-derived mtDNA in somatic cells. Am J Hum Genet, 1997. 61(4): p. 953-60.
199. DiMauro, S. and E.A. Schon, Mitochondrial DNA mutations in human disease. Am J Med Genet, 2001. 106(1): p. 18-26.
200. Sutovsky, P., et al., Degradation of paternal mitochondria after fertilization: implications for heteroplasmy, assisted reproductive technologies and mtDNA inheritance. Reprod Biomed Online, 2004. 8(1): p. 24-33.
201. Gyllensten, U., et al., Paternal inheritance of mitochondrial DNA in mice. Nature, 1991. 352(6332): p. 255-7.
202. Shitara, H., et al., Maternal inheritance of mouse mtDNA in interspecific hybrids: segregation of the leaked paternal mtDNA followed by the prevention of subsequent paternal leakage. Genetics, 1998. 148(2): p. 851-7.
203. Schwartz, M. and J. Vissing, New patterns of inheritance in mitochondrial disease. Biochem Biophys Res Commun, 2003. 310(2): p. 247-51.
204. Schwartz, M. and J. Vissing, Paternal inheritance of mitochondrial DNA. N Engl J Med, 2002. 347(8): p. 576-80.
205. Danan, C., et al., Evaluation of parental mitochondrial inheritance in neonates born after intracytoplasmic sperm injection. Am J Hum Genet, 1999. 65(2): p. 463-73.
206. Marchington, D.R., et al., No evidence for paternal mtDNA transmission to offspring or extra-embryonic tissues after ICSI. Mol Hum Reprod, 2002. 8(11): p. 1046-9.
207. Rossignol, R., et al., Mitochondrial threshold effects. Biochem J, 2003. 370(Pt 3): p. 751-62.
208. Hayashi, J., et al., Introduction of disease-related mitochondrial DNA deletions into HeLa cells lacking mitochondrial DNA results in mitochondrial dysfunction. Proc Natl Acad Sci U S A, 1991. 88(23): p. 10614-8.
209. Bender, A., et al., High levels of mitochondrial DNA deletions in substantia nigra neurons in aging and Parkinson disease. Nat Genet, 2006. 38(5): p. 515-7.
210. Jeppesen, T.D., et al., Muscle phenotype and mutation load in 51 persons with the 3243A>G mitochondrial DNA mutation. Arch Neurol, 2006. 63(12): p. 1701-6.
211. Horvath, R., et al., A tRNA(Ala) mutation causing mitochondrial myopathy clinically resembling myotonic dystrophy. J Med Genet, 2003. 40(10): p. 752-7.

212. Ballhausen, D., et al., Mitochondrial tRNA(Leu(UUR)) mutation m.3302A > G presenting as childhood-onset severe myopathy: threshold determination through segregation study. J Inherit Metab Dis.
213. Knott, A.B. and E. Bossy-Wetzel, Impairing the mitochondrial fission and fusion balance: a new mechanism of neurodegeneration. Ann N Y Acad Sci, 2008. 1147: p. 283-92.
214. Alberts B., J.A., Lewis J., Raff M., Roberts K.,Walter P., Molecular Cell of The Biology. fourth ed. 2002: garland science.
215. Labrousse, A.M., et al., C. elegans dynamin-related protein DRP-1 controls severing of the mitochondrial outer membrane. Mol Cell, 1999. 4(5): p. 815-26.
216. Smirnova, E., et al., Dynamin-related protein Drp1 is required for mitochondrial division in mammalian cells. Mol Biol Cell, 2001. 12(8): p. 2245-56.
217. Chan, D.C., Mitochondrial fusion and fission in mammals. Annu Rev Cell Dev Biol, 2006. 22: p. 79-99.
218. Ingerman, E., et al., Dnm1 forms spirals that are structurally tailored to fit mitochondria. J Cell Biol, 2005. 170(7): p. 1021-7.
219. Lee, S., et al., Mitochondrial fission and fusion mediators, hFis1 and OPA1, modulate cellular senescence. J Biol Chem, 2007. 282(31): p. 22977-83.
220. Ishihara, N., Y. Eura, and K. Mihara, Mitofusin 1 and 2 play distinct roles in mitochondrial fusion reactions via GTPase activity. J Cell Sci, 2004. 117(Pt 26): p. 6535-46.
221. Koshiba, T., et al., Structural basis of mitochondrial tethering by mitofusin complexes. Science, 2004. 305(5685): p. 858-62.
222. Cipolat, S., et al., OPA1 requires mitofusin 1 to promote mitochondrial fusion. Proc Natl Acad Sci U S A, 2004. 101(45): p. 15927-32.
223. Olichon, A., et al., Loss of OPA1 perturbates the mitochondrial inner membrane structure and integrity, leading to cytochrome c release and apoptosis. J Biol Chem, 2003. 278(10): p. 7743-6.
224. Hudson, G., et al., Mutation of OPA1 causes dominant optic atrophy with external ophthalmoplegia, ataxia, deafness and multiple mitochondrial DNA deletions: a novel disorder of mtDNA maintenance. Brain, 2008. 131(Pt 2): p. 329-37.
225. Duvezin-Caubet, S., et al., OPA1 processing reconstituted in yeast depends on the subunit composition of the m-AAA protease in mitochondria. Mol Biol Cell, 2007. 18(9): p. 3582-90.

226. Griparic, L., T. Kanazawa, and A.M. van der Bliek, Regulation of the mitochondrial dynamin-like protein Opa1 by proteolytic cleavage. J Cell Biol, 2007. 178(5): p. 757-64.
227. Song, Z., et al., OPA1 processing controls mitochondrial fusion and is regulated by mRNA splicing, membrane potential, and Yme1L. J Cell Biol, 2007. 178(5): p. 749-55.
228. Michaels, G.S., W.W. Hauswirth, and P.J. Laipis, Mitochondrial DNA copy number in bovine oocytes and somatic cells. Dev Biol, 1982. 94(1): p. 246-51.
229. Bereiter-Hahn, J. and M. Voth, Dynamics of mitochondria in living cells: shape changes, dislocations, fusion, and fission of mitochondria. Microsc Res Tech, 1994. 27(3): p. 198-219.
230. Chinnery, P.F. and D.C. Samuels, Relaxed replication of mtDNA: A model with implications for the expression of disease. Am J Hum Genet, 1999. 64(4): p. 1158-65.
231. Schaefer, A.M., et al., The epidemiology of mitochondrial disorders--past, present and future. Biochim Biophys Acta, 2004. 1659(2-3): p. 115-20.
232. Schaefer, A.M., et al., Prevalence of mitochondrial DNA disease in adults. Ann Neurol, 2008. 63(1): p. 35-9.
233. Elliott, H.R., et al., Pathogenic mitochondrial DNA mutations are common in the general population. Am J Hum Genet, 2008. 83(2): p. 254-60.
234. Bitner-Glindzicz, M., et al., Prevalence of mitochondrial 1555A-->G mutation in European children. N Engl J Med, 2009. 360(6): p. 640-2.
235. Kirby, D.M., et al., Biochemical Assays of Respiratory Chain Complex Activity. Methods Cell Biol, 2007. 80C: p. 93-119.
236. DiMauro, S. and E.A. Schon, Mitochondrial respiratory-chain diseases. N Engl J Med, 2003. 348(26): p. 2656-68.
237. Bogenhagen, D.F., Repair of mtDNA in vertebrates. Am J Hum Genet, 1999. 64(5): p. 1276-81.
238. Lightowlers, R.N., et al., Mammalian mitochondrial genetics: heredity, heteroplasmy and disease. Trends Genet, 1997. 13(11): p. 450-5.
239. Wallace, D.C., Mitochondrial diseases in man and mouse. Science, 1999. 283(5407): p. 1482-8.
240. Taylor, R.W., et al., The diagnosis of mitochondrial muscle disease. Neuromuscul Disord, 2004. 14(4): p. 237-45.

241. Mitchell, A.L., et al., Sequence variation in mitochondrial complex I genes: mutation or polymorphism? J Med Genet, 2006. 43(2): p. 175-9.
242. McFarland, R., et al., De novo mutations in the mitochondrial ND3 gene as a cause of infantile mitochondrial encephalopathy and complex I deficiency. Ann Neurol, 2004. 55(1): p. 58-64.
243. Ivanov, P.L., et al., Mitochondrial DNA sequence heteroplasmy in the Grand Duke of Russia Georgij Romanov establishes the authenticity of the remains of Tsar Nicholas II. Nat Genet, 1996. 12(4): p. 417-20.
244. Wallace, D.C., M.D. Brown, and M.T. Lott, Mitochondrial DNA variation in human evolution and disease. Gene, 1999. 238(1): p. 211-30.
245. McFarland, R., et al., Multiple neonatal deaths due to a homoplasmic mitochondrial DNA mutation. Nat Genet, 2002. 30(2): p. 145-6.
246. McFarland, R., et al., Familial myopathy: new insights into the T14709C mitochondrial tRNA mutation. Ann Neurol, 2004. 55(4): p. 478-84.
247. Taylor, R.W., et al., A homoplasmic mitochondrial transfer ribonucleic acid mutation as a cause of maternally inherited hypertrophic cardiomyopathy. J Am Coll Cardiol, 2003. 41(10): p. 1786-96.
248. McFarland, R., et al., Assigning pathogenicity to mitochondrial tRNA mutations: when "definitely maybe" is not good enough. Trends Genet, 2004. 20(12): p. 591-6.
249. Sue, C.M., et al., Maternally inherited hearing loss in a large kindred with a novel T7511C mutation in the mitochondrial DNA tRNA(Ser(UCN)) gene. Neurology, 1999. 52(9): p. 1905-8.
250. Prezant, T.R., et al., Mitochondrial ribosomal RNA mutation associated with both antibiotic-induced and non-syndromic deafness. Nat Genet, 1993. 4(3): p. 289-94.
251. Helm, M., et al., Search for characteristic structural features of mammalian mitochondrial tRNAs. RNA, 2000. 6(10): p. 1356-79.
252. Ingman, M. and U. Gyllensten, mtDB: Human Mitochondrial Genome Database, a resource for population genetics and medical sciences. Nucleic Acids Res, 2006. 34(Database issue): p. D749-51.
253. Holt, I.J., et al., Deletions of muscle mitochondrial DNA. Lancet, 1988. 1(8600): p. 1462.
254. Wallace, D.C., et al., Mitochondrial DNA mutation associated with Leber's hereditary optic neuropathy. Science, 1988. 242(4884): p. 1427-30.

255. Bardosi, A., et al., Myo-, neuro-, gastrointestinal encephalopathy (MNGIE syndrome) due to partial deficiency of cytochrome-c-oxidase. A new mitochondrial multisystem disorder. Acta Neuropathol (Berl), 1987. 74(3): p. 248-58.
256. Mazziotta, M.R., et al., Fatal infantile liver failure associated with mitochondrial DNA depletion. J Pediatr, 1992. 121(6): p. 896-901.
257. Manouvrier, S., et al., Point mutation of the mitochondrial tRNA(Leu) gene (A 3243 G) in maternally inherited hypertrophic cardiomyopathy, diabetes mellitus, renal failure, and sensorineural deafness. J Med Genet, 1995. 32(8): p. 654-6.
258. Trounce, I., E. Byrne, and S. Marzuki, Decline in skeletal muscle mitochondrial respiratory chain function: possible factor in ageing. Lancet, 1989. 1(8639): p. 637-9.
259. Cortopassi, G.A. and N. Arnheim, Detection of a specific mitochondrial DNA deletion in tissues of older humans. Nucleic Acids Res, 1990. 18(23): p. 6927-33.
260. Rowland, L.P., et al., Clinical syndromes associated with ragged red fibers. Rev Neurol (Paris), 1991. 147(6-7): p. 467-73.
261. Finnila, S., Phylogenetic analysis of mitochondrial DNA: Detection of mutations in patients with occipital stroke, in Neurology. 2000, Oulu University Oulu.
262. Lowell, B.B. and G.I. Shulman, Mitochondrial dysfunction and type 2 diabetes. Science, 2005. 307(5708): p. 384-7.
263. Wilson, F.H., et al., A cluster of metabolic defects caused by mutation in a mitochondrial tRNA. Science, 2004. 306(5699): p. 1190-4.
264. Maassen, J.A., et al., Mitochondrial diabetes: molecular mechanisms and clinical presentation. Diabetes, 2004. 53 Suppl 1: p. S103-9.
265. McFarland, R., R.W. Taylor, and D.M. Turnbull, The neurology of mitochondrial DNA disease. Lancet Neurol, 2002. 1(6): p. 343-51.
266. Old, S.L. and M.A. Johnson, Methods of microphotometric assay of succinate dehydrogenase and cytochrome c oxidase activities for use on human skeletal muscle. Histochem J, 1989. 21(9-10): p. 545-55.
267. Fromenty, B., et al., Efficient and specific amplification of identified partial duplications of human mitochondrial DNA by long PCR. Biochim Biophys Acta, 1996. 1308(3): p. 222-30.
268. Taylor, R.W., et al., Succinate-cytochrome c reductase: assessment of its value in the investigation of defects of the respiratory chain. Biochim Biophys Acta, 1993. 1181(3): p. 261-5.

269. Taylor, R.W., et al., A novel mitochondrial DNA point mutation in the tRNA(Ile) gene: studies in a patient presenting with chronic progressive external ophthalmoplegia and multiple sclerosis. Biochem Biophys Res Commun, 1998. 243(1): p. 47-51.
270. Pinkert, C.A., et al., Mitochondria transfer into mouse ova by microinjection. Transgenic Res, 1997. 6(6): p. 379-83.
271. Jenuth, J.P., et al., Random genetic drift in the female germline explains the rapid segregation of mammalian mitochondrial DNA. Nat Genet, 1996. 14(2): p. 146-51.
272. Jenuth, J.P., A.C. Peterson, and E.A. Shoubridge, Tissue-specific selection for different mtDNA genotypes in heteroplasmic mice. Nat Genet, 1997. 16(1): p. 93-5.
273. Sligh, J.E., et al., Maternal germ-line transmission of mutant mtDNAs from embryonic stem cell-derived chimeric mice. Proc Natl Acad Sci U S A, 2000. 97(26): p. 14461-6.
274. Marchington, D.R., D. Barlow, and J. Poulton, Transmitochondrial mice carrying resistance to chloramphenicol on mitochondrial DNA: developing the first mouse model of mitochondrial DNA disease. Nat Med, 1999. 5(8): p. 957-60.
275. Inoue, K., et al., Generation of mice with mitochondrial dysfunction by introducing mouse mtDNA carrying a deletion into zygotes. Nat Genet, 2000. 26(2): p. 176-81.
276. Larsson, N.G., et al., Mitochondrial transcription factor A is necessary for mtDNA maintenance and embryogenesis in mice. Nat Genet, 1998. 18(3): p. 231-6.
277. Silva, J.P., et al., Impaired insulin secretion and beta-cell loss in tissue-specific knockout mice with mitochondrial diabetes. Nat Genet, 2000. 26(3): p. 336-40.
278. Wredenberg, A., et al., Increased mitochondrial mass in mitochondrial myopathy mice. Proc Natl Acad Sci U S A, 2002. 99(23): p. 15066-71.
279. Wang, J., et al., Dilated cardiomyopathy and atrioventricular conduction blocks induced by heart-specific inactivation of mitochondrial DNA gene expression. Nat Genet, 1999. 21(1): p. 133-7.
280. Martin, G.M. and L.A. Loeb, Ageing: mice and mitochondria. Nature, 2004. 429(6990): p. 357-9.
281. Trifunovic, A., et al., Premature ageing in mice expressing defective mitochondrial DNA polymerase. Nature, 2004. 429(6990): p. 417-23.
282. Wallace, D.C., Mouse models for mitochondrial disease. Am J Med Genet, 2001. 106(1): p. 71-93.

283. Trifunovic, A., Mitochondrial DNA and ageing. Biochim Biophys Acta, 2006. 1757(5-6): p. 611-7.
284. Trifunovic, A., et al., Somatic mtDNA mutations cause aging phenotypes without affecting reactive oxygen species production. Proc Natl Acad Sci U S A, 2005. 102(50): p. 17993-8.
285. Thompson, L.V., Oxidative stress, mitochondria and mtDNA-mutator mice. Exp Gerontol, 2006. 41(12): p. 1220-2.
286. Vermulst, M., et al., Mitochondrial point mutations do not limit the natural lifespan of mice. Nat Genet, 2007. 39(4): p. 540-3.
287. Akman, H.O., et al., Thymidine kinase 2 (H126N) knockin mice show the essential role of balanced deoxynucleotide pools for mitochondrial DNA maintenance. Hum Mol Genet, 2008. 17(16): p. 2433-40.
288. Zhou, X., et al., Progressive loss of mitochondrial DNA in thymidine kinase 2-deficient mice. Hum Mol Genet, 2008. 17(15): p. 2329-35.
289. Fan, W., et al., A mouse model of mitochondrial disease reveals germline selection against severe mtDNA mutations. Science, 2008. 319(5865): p. 958-62.
290. Stewart, J.B., et al., Strong purifying selection in transmission of mammalian mitochondrial DNA. PLoS Biol, 2008. 6(1): p. e10.
291. Pallotti, F., et al., Biochemical analysis of respiratory function in cybrid cell lines harbouring mitochondrial DNA mutations. Biochem J, 2004. 384(Pt 2): p. 287-93.
292. King, M.P. and G. Attardi, Human cells lacking mtDNA: repopulation with exogenous mitochondria by complementation. Science, 1989. 246(4929): p. 500-3.
293. Dunbar, D.R., et al., Different cellular backgrounds confer a marked advantage to either mutant or wild-type mitochondrial genomes. Proc Natl Acad Sci U S A, 1995. 92(14): p. 6562-6.
294. D'Aurelio, M., et al., Heterologous mitochondrial DNA recombination in human cells. Hum Mol Genet, 2004. 13(24): p. 3171-9.
295. Swerdlow, R.H., Mitochondria in cybrids containing mtDNA from persons with mitochondriopathies. J Neurosci Res, 2007. 85(15): p. 3416-28.
296. Behan, A., S. Doyle, and M. Farrell, Adaptive responses to mitochondrial dysfunction in the rho degrees Namalwa cell. Mitochondrion, 2005. 5(3): p. 173-93.
297. Danielson, S.R., et al., Isolation of transcriptomal changes attributable to LHON mutations and the cybridization process. Brain, 2005. 128(Pt 5): p. 1026-37.

298. Finsterer, J., Treatment of mitochondrial disorders. Eur J Paediatr Neurol. 14(1): p. 29-44.
299. Chinnery, P., et al., Treatment for mitochondrial disorders. Cochrane Database Syst Rev, 2006(1): p. CD004426.
300. Jeppesen, T.D., et al., Aerobic training is safe and improves exercise capacity in patients with mitochondrial myopathy. Brain, 2006. 129(Pt 12): p. 3402-12.
301. Taivassalo, T., et al., Endurance training and detraining in mitochondrial myopathies due to single large-scale mtDNA deletions. Brain, 2006. 129(Pt 12): p. 3391-401.
302. Taivassalo, T. and R.G. Haller, Exercise and training in mitochondrial myopathies. Med Sci Sports Exerc, 2005. 37(12): p. 2094-101.
303. Murphy, J.L., et al., Resistance training in patients with single, large-scale deletions of mitochondrial DNA. Brain, 2008. 131(Pt 11): p. 2832-40.
304. Taylor, R.W., et al., Selective inhibition of mutant human mitochondrial DNA replication in vitro by peptide nucleic acids. Nat Genet, 1997. 15(2): p. 212-5.
305. Bacman, S.R., et al., Modulating mtDNA heteroplasmy by mitochondria-targeted restriction endonucleases in a 'differential multiple cleavage-site' model. Gene Ther, 2007. 14(18): p. 1309-18.
306. Minczuk, M., et al., Sequence-specific modification of mitochondrial DNA using a chimeric zinc finger methylase. Proc Natl Acad Sci U S A, 2006. 103(52): p. 19689-94.
307. Rubio, M.A., et al., Mammalian mitochondria have the innate ability to import tRNAs by a mechanism distinct from protein import. Proc Natl Acad Sci U S A, 2008. 105(27): p. 9186-91.
308. Ling, J., et al., Pathogenic mechanism of a human mitochondrial tRNAPhe mutation associated with myoclonic epilepsy with ragged red fibers syndrome. Proc Natl Acad Sci U S A, 2007. 104(39): p. 15299-304.
309. Park, H., E. Davidson, and M.P. King, Overexpressed mitochondrial leucyl-tRNA synthetase suppresses the A3243G mutation in the mitochondrial tRNA(Leu(UUR)) gene. Rna, 2008. 14(11): p. 2407-16.
310. Rorbach, J., et al., Overexpression of human mitochondrial valyl tRNA synthetase can partially restore levels of cognate mt-tRNAVal carrying the pathogenic C25U mutation. Nucleic Acids Res, 2008. 36(9): p. 3065-74.

311. Craven, L., et al., Pronuclear transfer in human embryos to prevent transmission of mitochondrial DNA disease. Nature.
312. DiMauro, S. and E.A. Schon, Mitochondrial disorders in the nervous system. Annu Rev Neurosci, 2008. 31: p. 91-123.
313. Bentlage, H.A. and G. Attardi, Relationship of genotype to phenotype in fibroblast-derived transmitochondrial cell lines carrying the 3243 mutation associated with the MELAS encephalomyopathy: shift towards mutant genotype and role of mtDNA copy number. Hum Mol Genet, 1996. 5(2): p. 197-205.
314. Trounce, I. and D.C. Wallace, Production of transmitochondrial mouse cell lines by cybrid rescue of rhodamine-6G pre-treated L-cells. Somat Cell Mol Genet, 1996. 22(1): p. 81-5.
315. Kirby, D.M., et al., Low mutant load of mitochondrial DNA G13513A mutation can cause Leigh's disease. Ann Neurol, 2003. 54(4): p. 473-8.
316. Kirby, D.M., et al., Mutations of the mitochondrial ND1 gene as a cause of MELAS. J Med Genet, 2004. 41(10): p. 784-9.
317. Deschauer, M., et al., Novel mitochondrial transfer RNA(Phe) gene mutation associated with late-onset neuromuscular disease. Arch Neurol, 2006. 63(6): p. 902-5.
318. Blakely, E.L., et al., A mitochondrial cytochrome b mutation causing severe respiratory chain enzyme deficiency in humans and yeast. Febs J, 2005. 272(14): p. 3583-92.
319. Birch-Machin, M.A., et al., An evaluation of the measurement of the activities of complexes I-IV in the respiratory chain of human skeletal muscle mitochondria. Biochem Med Metab Biol, 1994. 51(1): p. 35-42.
320. Applegarth, Organelle Disease. 1997: Champan & Hall.
321. Zeviani, M., B. Bertagnolio, and G. Uziel, Neurological presentations of mitochondrial diseases. J Inherit Metab Dis, 1996. 19(4): p. 504-20.
322. Skladal, D., J. Halliday, and D.R. Thorburn, Minimum birth prevalence of mitochondrial respiratory chain disorders in children. Brain, 2003. 126(Pt 8): p. 1905-12.
323. Distelmaier, F., et al., Mitochondrial complex I deficiency: from organelle dysfunction to clinical disease. Brain, 2009. 132(Pt 4): p. 833-42.
324. Smeitink, J., L. van den Heuvel, and S. DiMauro, The genetics and pathology of oxidative phosphorylation. Nat Rev Genet, 2001. 2(5): p. 342-52.

325. Saada, A., et al., C6ORF66 is an assembly factor of mitochondrial complex I. Am J Hum Genet, 2008. 82(1): p. 32-8.
326. Moslemi, A.R., et al., Progressive encephalopathy and complex I deficiency associated with mutations in MTND1. Neuropediatrics, 2008. 39(1): p. 24-8.
327. Campos, Y., et al., Bilateral striatal necrosis and MELAS associated with a new T3308C mutation in the mitochondrial ND1 gene. Biochem Biophys Res Commun, 1997. 238(2): p. 323-5.
328. Opdal, S.H., et al., Possible role of mtDNA mutations in sudden infant death. Pediatr Neurol, 2002. 27(1): p. 23-9.
329. Uusimaa, J., et al., Molecular epidemiology of childhood mitochondrial encephalomyopathies in a Finnish population: sequence analysis of entire mtDNA of 17 children reveals heteroplasmic mutations in tRNAArg, tRNAGlu, and tRNALeu(UUR) genes. Pediatrics, 2004. 114(2): p. 443-50.
330. Ugalde, C., et al., Mutated ND2 impairs mitochondrial complex I assembly and leads to Leigh syndrome. Mol Genet Metab, 2007. 90(1): p. 10-4.
331. Brown, M.D., et al., Novel mtDNA mutations and oxidative phosphorylation dysfunction in Russian LHON families. Hum Genet, 2001. 109(1): p. 33-9.
332. Horvath, J., et al., Sequence analysis of Hungarian LHON patients not carrying the common primary mutations. J Inherit Metab Dis, 2002. 25(4): p. 323-4.
333. Crimi, M., et al., A new mitochondrial DNA mutation in ND3 gene causing severe Leigh syndrome with early lethality. Pediatr Res, 2004. 55(5): p. 842-6.
334. Lertrit, P., et al., A new disease-related mutation for mitochondrial encephalopathy lactic acidosis and strokelike episodes (MELAS) syndrome affects the ND4 subunit of the respiratory complex I. Am J Hum Genet, 1992. 51(3): p. 457-68.
335. Abu-Amero, K.K. and T.M. Bosley, Mitochondrial abnormalities in patients with LHON-like optic neuropathies. Invest Ophthalmol Vis Sci, 2006. 47(10): p. 4211-20.
336. Mayorov, V., et al., The role of the ND5 gene in LHON: characterization of a new, heteroplasmic LHON mutation. Ann Neurol, 2005. 58(5): p. 807-11.
337. Santorelli, F.M., et al., Identification of a novel mutation in the mtDNA ND5 gene associated with MELAS. Biochem Biophys Res Commun, 1997. 238(2): p. 326-8.
338. Naini, A.B., et al., Novel mitochondrial DNA ND5 mutation in a patient with clinical features of MELAS and MERRF. Arch Neurol, 2005. 62(3): p. 473-6.

339. Shanske, S., et al., The G13513A mutation in the ND5 gene of mitochondrial DNA as a common cause of MELAS or Leigh syndrome: evidence from 12 cases. Arch Neurol, 2008. 65(3): p. 368-72.
340. Valentino, M.L., et al., The 13042G --> A/ND5 mutation in mtDNA is pathogenic and can be associated also with a prevalent ocular phenotype. J Med Genet, 2006. 43(7): p. e38.
341. Valente, L., et al., Identification of novel mutations in five patients with mitochondrial encephalomyopathy. Biochim Biophys Acta, 2009. 1787(5): p. 491-501.
342. Ferre, M., et al., Molecular screening of 980 cases of suspected hereditary optic neuropathy with a report on 77 novel OPA1 mutations. Hum Mutat, 2009. 30(7): p. E692-705.
343. Ravn, K., et al., An mtDNA mutation, 14453G-->A, in the NADH dehydrogenase subunit 6 associated with severe MELAS syndrome. Eur J Hum Genet, 2001. 9(10): p. 805-9.
344. Tawata, M., et al., A new mitochondrial DNA mutation at 14577 T/C is probably a major pathogenic mutation for maternally inherited type 2 diabetes. Diabetes, 2000. 49(7): p. 1269-72.
345. van den Bosch, B.J., et al., Increased risk for cardiorespiratory failure associated with the A3302G mutation in the mitochondrial DNA encoded tRNALeu(UUR) gene. Neuromuscul Disord, 2004. 14(10): p. 683-8.
346. Dunbar, D.R., et al., Complex I deficiency is associated with 3243G:C mitochondrial DNA in osteosarcoma cell cybrids. Hum Mol Genet, 1996. 5(1): p. 123-29.
347. Ogilvie, I., N.G. Kennaway, and E.A. Shoubridge, A molecular chaperone for mitochondrial complex I assembly is mutated in a progressive encephalopathy. J Clin Invest, 2005. 115(10): p. 2784-92.
348. Vahsen, N., et al., AIF deficiency compromises oxidative phosphorylation. EMBO J, 2004. 23(23): p. 4679-89.
349. Klein, J.A., et al., The harlequin mouse mutation downregulates apoptosis-inducing factor. Nature, 2002. 419(6905): p. 367-74.
350. Joza, N., et al., Muscle-specific loss of apoptosis-inducing factor leads to mitochondrial dysfunction, skeletal muscle atrophy, and dilated cardiomyopathy. Mol Cell Biol, 2005. 25(23): p. 10261-72.

351. Xiao, C., et al., Ecsit is required for Bmp signaling and mesoderm formation during mouse embryogenesis. Genes Dev, 2003. 17(23): p. 2933-49.
352. Kopp, E., et al., ECSIT is an evolutionarily conserved intermediate in the Toll/IL-1 signal transduction pathway. Genes Dev, 1999. 13(16): p. 2059-71.
353. Vogel, R.O., et al., Cytosolic signaling protein Ecsit also localizes to mitochondria where it interacts with chaperone NDUFAF1 and functions in complex I assembly. Genes Dev, 2007. 21(5): p. 615-24.
354. Kussmaul, L. and J. Hirst, The mechanism of superoxide production by NADH:ubiquinone oxidoreductase (complex I) from bovine heart mitochondria. Proc Natl Acad Sci U S A, 2006. 103(20): p. 7607-12.
355. Valentino, M.L., et al., The ND1 gene of complex I is a mutational hot spot for Leber's hereditary optic neuropathy. Ann Neurol, 2004. 56(5): p. 631-41.
356. Brown, M.D., et al., Functional analysis of lymphoblast and cybrid mitochondria containing the 3460, 11778, or 14484 Leber's hereditary optic neuropathy mitochondrial DNA mutation. J Biol Chem, 2000. 275(51): p. 39831-6.
357. Komaki, H., et al., A novel mtDNA C11777A mutation in Leigh syndrome. Mitochondrion, 2003. 2(4): p. 293-304.
358. Lebon, S., et al., Recurrent de novo mitochondrial DNA mutations in respiratory chain deficiency. J Med Genet, 2003. 40(12): p. 896-9.
359. Bugiani, M., et al., Clinical and molecular findings in children with complex I deficiency. Biochim Biophys Acta, 2004. 1659(2-3): p. 136-47.
360. Kirby, D.M., et al., Leigh disease caused by the mitochondrial DNA G14459A mutation in unrelated families. Ann Neurol, 2000. 48(1): p. 102-4.
361. Fernandez-Moreira, D., et al., X-linked NDUFA1 gene mutations associated with mitochondrial encephalomyopathy. Ann Neurol, 2007. 61(1): p. 73-83.
362. Benit, P., et al., Large-scale deletion and point mutations of the nuclear NDUFV1 and NDUFS1 genes in mitochondrial complex I deficiency. Am J Hum Genet, 2001. 68(6): p. 1344-52.
363. Martin, M.A., et al., Leigh syndrome associated with mitochondrial complex I deficiency due to a novel mutation in the NDUFS1 gene. Arch Neurol, 2005. 62(4): p. 659-61.
364. Loeffen, J., et al., Mutations in the complex I NDUFS2 gene of patients with cardiomyopathy and encephalomyopathy. Ann Neurol, 2001. 49(2): p. 195-201.

365. van den Heuvel, L., et al., Demonstration of a new pathogenic mutation in human complex I deficiency: a 5-bp duplication in the nuclear gene encoding the 18-kD (AQDQ) subunit. Am J Hum Genet, 1998. 62(2): p. 262-8.
366. Scacco, S., et al., Pathological mutations of the human NDUFS4 gene of the 18-kDa (AQDQ) subunit of complex I affect the expression of the protein and the assembly and function of the complex. J Biol Chem, 2003. 278(45): p. 44161-7.
367. Kirby, D.M., et al., NDUFS6 mutations are a novel cause of lethal neonatal mitochondrial complex I deficiency. J Clin Invest, 2004. 114(6): p. 837-45.
368. Triepels, R.H., et al., Leigh syndrome associated with a mutation in the NDUFS7 (PSST) nuclear encoded subunit of complex I. Ann Neurol, 1999. 45(6): p. 787-90.
369. Loeffen, J., et al., The first nuclear-encoded complex I mutation in a patient with Leigh syndrome. Am J Hum Genet, 1998. 63(6): p. 1598-608.
370. Procaccio, V. and D.C. Wallace, Late-onset Leigh syndrome in a patient with mitochondrial complex I NDUFS8 mutations. Neurology, 2004. 62(10): p. 1899-901.
371. Gerards, M., et al., Defective complex I assembly due to C20orf7 mutations as a new cause of Leigh syndrome. J Med Genet, 2009.
372. Saada, A., et al., Mutations in NDUFAF3 (C3ORF60), encoding an NDUFAF4 (C6ORF66)-interacting complex I assembly protein, cause fatal neonatal mitochondrial disease. Am J Hum Genet, 2009. 84(6): p. 718-27.
373. Tam, E.W., et al., A novel mitochondrial DNA mutation in COX1 leads to strokes, seizures, and lactic acidosis. Neuropediatrics, 2008. 39(6): p. 328-34.
374. Palace, J., Multiple sclerosis associated with Leber's Hereditary Optic Neuropathy. J Neurol Sci, 2009. 286(1-2): p. 24-7.
375. Estivill, X., et al., Familial progressive sensorineural deafness is mainly due to the mtDNA A1555G mutation and is enhanced by treatment of aminoglycosides. Am J Hum Genet, 1998. 62(1): p. 27-35.
376. Wilson, J., Leber's hereditary optic atrophy: some clinical and aetiological considerations. Brain, 1963. 86: p. 347-62.
377. Newman, N.J., Leber hereditary optic neuropathy: bad habits, bad vision? Brain, 2009. 132(Pt 9): p. 2306-8.
378. Fischel-Ghodsian, N., Mitochondrial mutations and hearing loss: paradigm for mitochondrial genetics. Am J Hum Genet, 1998. 62(1): p. 15-9.

379. Guan, M.X., N. Fischel-Ghodsian, and G. Attardi, Biochemical evidence for nuclear gene involvement in phenotype of non-syndromic deafness associated with mitochondrial 12S rRNA mutation. Hum Mol Genet, 1996. 5(7): p. 963-71.
380. Cock, H.R., et al., The influence of nuclear background on the biochemical expression of 3460 Leber's hereditary optic neuropathy. Ann Neurol, 1998. 44(2): p. 187-93.
381. Wong, A., et al., Differentiation-specific effects of LHON mutations introduced into neuronal NT2 cells. Hum Mol Genet, 2002. 11(4): p. 431-8.
382. Nikoskelainen, E.K., et al., Leber's hereditary optic neuroretinopathy, a maternally inherited disease. A genealogic study in four pedigrees. Arch Ophthalmol, 1987. 105(5): p. 665-71.
383. Pitkanen, S., et al., Familial cardiomyopathy with cataracts and lactic acidosis: a defect in complex I (NADH-dehydrogenase) of the mitochondria respiratory chain. Pediatr Res, 1996. 39(3): p. 513-21.
384. Lee, H.C., et al., Increase in mitochondrial mass in human fibroblasts under oxidative stress and during replicative cell senescence. J Biomed Sci, 2002. 9(6 Pt 1): p. 517-26.
385. Richter, C., et al., Oxidants in mitochondria: from physiology to diseases. Biochim Biophys Acta, 1995. 1271(1): p. 67-74.
386. Lee, H.C. and Y.H. Wei, Mitochondrial role in life and death of the cell. J Biomed Sci, 2000. 7(1): p. 2-15.
387. Li, K., P.D. Neufer, and R.S. Williams, Nuclear responses to depletion of mitochondrial DNA in human cells. Am J Physiol, 1995. 269(5 Pt 1): p. C1265-70.
388. Joseph, A.M., et al., Compensatory responses of protein import and transcription factor expression in mitochondrial DNA defects. Am J Physiol Cell Physiol, 2004. 286(4): p. C867-75.
389. Lu, C.Y., et al., Increased expression of manganese-superoxide dismutase in fibroblasts of patients with CPEO syndrome. Mol Genet Metab, 2003. 80(3): p. 321-9.
390. Wang, S.B., et al., Mutation of mitochondrial DNA G13513A presenting with Leigh syndrome, Wolff-Parkinson-White syndrome and cardiomyopathy. Pediatr Neonatol, 2008. 49(4): p. 145-9.
391. Finsterer, J., Leigh and Leigh-like syndrome in children and adults. Pediatr Neurol, 2008. 39(4): p. 223-35.

392. Chol, M., et al., The mitochondrial DNA G13513A MELAS mutation in the NADH dehydrogenase 5 gene is a frequent cause of Leigh-like syndrome with isolated complex I deficiency. J Med Genet, 2003. 40(3): p. 188-91.
393. Brautbar, A., et al., The mitochondrial 13513G>A mutation is associated with Leigh disease phenotypes independent of complex I deficiency in muscle. Mol Genet Metab, 2008. 94(4): p. 485-90.
394. Pulkes, T., et al., The mitochondrial DNA G13513A transition in ND5 is associated with a LHON/MELAS overlap syndrome and may be a frequent cause of MELAS. Ann Neurol, 1999. 46(6): p. 916-9.
395. Corona, P., et al., A novel mtDNA mutation in the ND5 subunit of complex I in two MELAS patients. Ann Neurol, 2001. 49(1): p. 106-10.
396. Combet, C., et al., NPS@: network protein sequence analysis. Trends Biochem Sci, 2000. 25(3): p. 147-50.
397. Chinnery, P.F., et al., The mitochondrial ND6 gene is a hot spot for mutations that cause Leber's hereditary optic neuropathy. Brain, 2001. 124(Pt 1): p. 209-18.
398. Palmisano, G., et al., The phosphorylation pattern of bovine heart complex I subunits. Proteomics, 2007. 7(10): p. 1575-83.
399. Yen, M.Y., et al., Increase of mitochondrial DNA in blood cells of patients with Leber's hereditary optic neuropathy with 11778 mutation. Br J Ophthalmol, 2002. 86(9): p. 1027-30.
400. Jacobs, H.T., Disorders of mitochondrial protein synthesis. Hum Mol Genet, 2003. 12 Spec No 2: p. R293-301.
401. Chinnery, P.F., et al., Molecular pathology of MELAS and MERRF. The relationship between mutation load and clinical phenotypes. Brain, 1997. 120 (Pt 10): p. 1713-21.
402. Sacconi, S., et al., A functionally dominant mitochondrial DNA mutation. Hum Mol Genet, 2008. 17(12): p. 1814-20.
403. Shoffner, J.M., et al., Myoclonic epilepsy and ragged-red fiber disease (MERRF) is associated with a mitochondrial DNA tRNA(Lys) mutation. Cell, 1990. 61(6): p. 931-7.
404. Goto, Y., I. Nonaka, and S. Horai, A mutation in the tRNA(Leu)(UUR) gene associated with the MELAS subgroup of mitochondrial encephalomyopathies. Nature, 1990. 348(6302): p. 651-3.

405. Kobayashi, Y., et al., A point mutation in the mitochondrial tRNA(Leu)(UUR) gene in MELAS (mitochondrial myopathy, encephalopathy, lactic acidosis and stroke-like episodes). Biochem Biophys Res Commun, 1990. 173(3): p. 816-22.
406. Schon, E.A., E. Bonilla, and S. DiMauro, Mitochondrial DNA mutations and pathogenesis. J Bioenerg Biomembr, 1997. 29(2): p. 131-49.
407. Enriquez, J.A., A. Chomyn, and G. Attardi, MtDNA mutation in MERRF syndrome causes defective aminoacylation of tRNA(Lys) and premature translation termination. Nat Genet, 1995. 10(1): p. 47-55.
408. Hao, H. and C.T. Moraes, A disease-associated G5703A mutation in human mitochondrial DNA causes a conformational change and a marked decrease in steady-state levels of mitochondrial tRNA(Asn). Mol Cell Biol, 1997. 17(12): p. 6831-7.
409. Schon, E.A., et al., The mitochondrial tRNA(Leu)(UUR)) mutation in MELAS: a model for pathogenesis. Biochim Biophys Acta, 1992. 1101(2): p. 206-9.
410. Kirino, Y., et al., Specific correlation between the wobble modification deficiency in mutant tRNAs and the clinical features of a human mitochondrial disease. Proc Natl Acad Sci U S A, 2005. 102(20): p. 7127-32.
411. Yasukawa, T., et al., Modification defect at anticodon wobble nucleotide of mitochondrial tRNAs(Leu)(UUR) with pathogenic mutations of mitochondrial myopathy, encephalopathy, lactic acidosis, and stroke-like episodes. J Biol Chem, 2000. 275(6): p. 4251-7.
412. Chomyn, A., et al., The mitochondrial myopathy, encephalopathy, lactic acidosis, and stroke-like episode syndrome-associated human mitochondrial tRNALeu(UUR) mutation causes aminoacylation deficiency and concomitant reduced association of mRNA with ribosomes. J Biol Chem, 2000. 275(25): p. 19198-209.
413. Al-Dosary, M., et al., Neuromuscular disease presentation with three genetic defects involving two genomes. Neuromuscul Disord, 2009. 19(12): p. 841-4.
414. Helm, M. and G. Attardi, Nuclear control of cloverleaf structure of human mitochondrial tRNA(Lys). J Mol Biol, 2004. 337(3): p. 545-60.
415. Kelley, S.O., S.V. Steinberg, and P. Schimmel, Fragile T-stem in disease-associated human mitochondrial tRNA sensitizes structure to local and distant mutations. J Biol Chem, 2001. 276(14): p. 10607-11.

416. Florentz, C., et al., Human mitochondrial tRNAs in health and disease. Cell Mol Life Sci, 2003. 60(7): p. 1356-75.
417. Marzuki, S., et al., Normal variants of human mitochondrial DNA and translation products: the building of a reference data base. Hum Genet, 1991. 88(2): p. 139-45.
418. Moraes, C.T., et al., A mitochondrial tRNA anticodon swap associated with a muscle disease. Nat Genet, 1993. 4(3): p. 284-8.
419. Moslemi, A.R., et al., A novel mutation in the mitochondrial tRNA(Phe) gene associated with mitochondrial myopathy. Neuromuscul Disord, 2004. 14(1): p. 46-50.
420. Elson, J.L., et al., Pathogenic mitochondrial tRNA mutations--which mutations are inherited and why? Hum Mutat, 2009. 30(11): p. E984-92.
421. He, L., et al., Detection and quantification of mitochondrial DNA deletions in individual cells by real-time PCR. Nucleic Acids Res, 2002. 30(14): p. e68.
422. Kleinle, S., et al., A novel mitochondrial tRNA(Phe) mutation inhibiting anticodon stem formation associated with a muscle disease. Biochem Biophys Res Commun, 1998. 247(1): p. 112-5.
423. Wong, L.J., et al., A novel mutation in the mitochondrial tRNA(Ser(AGY)) gene associated with mitochondrial myopathy, encephalopathy, and complex I deficiency. J Med Genet, 2006. 43(9): p. e46.
424. Servidei, S., Mitochondrial encephalomyopathies:gene mutation. Neuromuscul Disord, 2003. 13(10): p. 848-53.
425. McFarland, R., et al., The m.5650G>A mitochondrial tRNAAla mutation is pathogenic and causes a phenotype of pure myopathy. Neuromuscul Disord, 2008. 18(1): p. 63-7.
426. Blakely, E.L., et al., A new mitochondrial transfer RNAPro gene mutation associated with myoclonic epilepsy with ragged-red fibers and other neurological features. Arch Neurol, 2009. 66(3): p. 399-402.
427. Jukes, T.H., Mitochondrial codes and evolution. Nature, 1983. 301(5895): p. 19-20.
428. Krishnan, K.J., et al., A multiplex real-time PCR method to detect and quantify mitochondrial DNA deletions in individual cells. Anal Biochem, 2007. 370(1): p. 127-9.
429. Tulinius, M., et al., Novel mutations in the thymidine kinase 2 gene (TK2) associated with fatal mitochondrial myopathy and mitochondrial DNA depletion. Neuromuscul Disord, 2005. 15(6): p. 412-5.

430. Durham, S.E., et al., Mitochondrial DNA copy number threshold in mtDNA depletion myopathy. Neurology, 2005. 65(3): p. 453-5.
431. Labarthe, F., et al., Clinical, biochemical and morphological features of hepatocerebral syndrome with mitochondrial DNA depletion due to deoxyguanosine kinase deficiency. J Hepatol, 2005. 43(2): p. 333-41.
432. Rotig, A. and J. Poulton, Genetic causes of mitochondrial DNA depletion in humans. Biochim Biophys Acta, 2009. 1792(12): p. 1103-8.
433. Cardaioli, E., et al., A novel heteroplasmic tRNA(Leu(CUN)) mtDNA point mutation associated with chronic progressive external ophthalmoplegia. Biochem Biophys Res Commun, 2005. 327(3): p. 675-8.
434. Puig, J.G., et al., The spectrum of hypoxanthine-guanine phosphoribosyltransferase (HPRT) deficiency. Clinical experience based on 22 patients from 18 Spanish families. Medicine (Baltimore), 2001. 80(2): p. 102-12.
435. Blakely, E., et al., Novel mutations in the TK2 gene associated with fatal mitochondrial DNA depletion myopathy. Neuromuscul Disord, 2008. 18(7): p. 557-60.
436. Saada, A., et al., Mutant mitochondrial thymidine kinase in mitochondrial DNA depletion myopathy. Nat Genet, 2001. 29(3): p. 342-4.
437. Carrozzo, R., et al., Mutation analysis in 16 patients with mtDNA depletion. Hum Mutat, 2003. 21(4): p. 453-4.
438. Blakely, E.L., et al., Sporadic intragenic inversion of the mitochondrial DNA MTND1 gene causing fatal infantile lactic acidosis. Pediatr Res, 2006. 59(3): p. 440-4.
439. Musumeci, O., et al., Intragenic inversion of mtDNA: a new type of pathogenic mutation in a patient with mitochondrial myopathy. Am J Hum Genet, 2000. 66(6): p. 1900-4.
440. Sunnucks, P., et al., SSCP is not so difficult: the application and utility of single-stranded conformation polymorphism in evolutionary biology and molecular ecology. Mol Ecol, 2000. 9(11): p. 1699-710.
441. Hayashi, K., PCR-SSCP: a method for detection of mutations. Genet Anal Tech Appl, 1992. 9(3): p. 73-9.
442. Glavac, D. and M. Dean, Optimization of the single-strand conformation polymorphism (SSCP) technique for detection of point mutations. Hum Mutat, 1993. 2(5): p. 404-14.

443. Barros, F., et al., Rapid and enhanced detection of mitochondrial DNA variation using single-strand conformation analysis of superposed restriction enzyme fragments from polymerase chain reaction-amplified products. Electrophoresis, 1997. 18(1): p. 52-4.
444. Muyzer, G., E.C. de Waal, and A.G. Uitterlinden, Profiling of complex microbial populations by denaturing gradient gel electrophoresis analysis of polymerase chain reaction-amplified genes coding for 16S rRNA. Appl Environ Microbiol, 1993. 59(3): p. 695-700.
445. Fernandez, E., et al., Use of chemical clamps in denaturing gradient gel electrophoresis: application in the detection of the most frequent Mediterranean beta-thalassemic mutations. PCR Methods Appl, 1993. 3(2): p. 122-4.
446. Nakao, M., J.S. Sutcliffe, and A.L. Beaudet, Advantages of RT-PCR and denaturing gradient gel electrophoresis for analysis of genomic imprinting: detection of new mouse and human expressed polymorphisms. Hum Mutat, 1996. 7(2): p. 144-8.
447. Theru A. Sivakumaran, K.K.a.P.J.O., Denaturing high performance liquid chromatography in the molecular diagnosis of genetic disorders. CURRENT SCIENCE,, 2003. 84(3).
448. Biggin, A., et al., Mutation screening of the mitochondrial genome using denaturing high-performance liquid chromatography. Mol Genet Metab, 2005. 84(1): p. 61-74.
449. Cobb, C.J., et al., Rapid mutation detection by the transgenomic wave analyser DHPLC identifies MYOC mutations in patients with ocular hypertension and/or open angle glaucoma. Br J Ophthalmol, 2002. 86(2): p. 191-5.
450. Xiao, W. and P.J. Oefner, Denaturing high-performance liquid chromatography: A review. Hum Mutat, 2001. 17(6): p. 439-74.
451. White, H.E., et al., Accurate detection and quantitation of heteroplasmic mitochondrial point mutations by pyrosequencing. Genet Test, 2005. 9(3): p. 190-9.
452. Ronaghi, M., M. Uhlen, and P. Nyren, A sequencing method based on real-time pyrophosphate. Science, 1998. 281(5375): p. 363, 365.
453. Unemo, M., et al., Molecular typing of Neisseria gonorrhoeae isolates by pyrosequencing of highly polymorphic segments of the porB gene. J Clin Microbiol, 2004. 42(7): p. 2926-34.

454. Ronaghi, M., Pyrosequencing sheds light on DNA sequencing. Genome Res, 2001. 11(1): p. 3-11.
455. Ronaghi, M., et al., Analyses of secondary structures in DNA by pyrosequencing. Anal Biochem, 1999. 267(1): p. 65-71.
456. Taylor, R.W., et al., The determination of complete human mitochondrial DNA sequences in single cells: implications for the study of somatic mitochondrial DNA point mutations. Nucleic Acids Res, 2001. 29(15): p. E74-4.
457. Greaves, L.C., et al., Mitochondrial DNA mutations are established in human colonic stem cells, and mutated clones expand by crypt fission. Proc Natl Acad Sci U S A, 2006. 103(3): p. 714-9.
458. Wong, L.J., et al., Comprehensive scanning of the entire mitochondrial genome for mutations. Clin Chem, 2002. 48(11): p. 1901-12.
459. Bannwarth, S., et al., Rapid identification of mitochondrial DNA (mtDNA) mutations in neuromuscular disorders by using surveyor strategy. Mitochondrion, 2008. 8(2): p. 136-45.
460. Qiu, P., et al., Mutation detection using Surveyor nuclease. Biotechniques, 2004. 36(4): p. 702-7.
461. Bannwarth, S., V. Procaccio, and V. Paquis-Flucklinger, Surveyor Nuclease: a new strategy for a rapid identification of heteroplasmic mitochondrial DNA mutations in patients with respiratory chain defects. Hum Mutat, 2005. 25(6): p. 575-82.
462. Dunbar, S.A., Applications of Luminex xMAP technology for rapid, high-throughput multiplexed nucleic acid detection. Clin Chim Acta, 2006. 363(1-2): p. 71-82.
463. Nishigaki, Y., et al., Extensive screening system using suspension array technology to detect mitochondrial DNA point mutations. Mitochondrion. 10(3): p. 300-8.
464. Thieme, M., et al., ReseqChip: automated integration of multiple local context probe data from the MitoChip array in mitochondrial DNA sequence assembly. BMC Bioinformatics, 2009. 10: p. 440.
465. Maitra, A., et al., The Human MitoChip: a high-throughput sequencing microarray for mitochondrial mutation detection. Genome Res, 2004. 14(5): p. 812-9.
466. Zhou, S., et al., An oligonucleotide microarray for high-throughput sequencing of the mitochondrial genome. J Mol Diagn, 2006. 8(4): p. 476-82.
467. Andrews, R.M., et al., Reanalysis and revision of the Cambridge reference sequence for human mitochondrial DNA. Nat Genet, 1999. 23(2): p. 147.

468. Zhou, S., et al., Frequency and phenotypic implications of mitochondrial DNA mutations in human squamous cell cancers of the head and neck. Proc Natl Acad Sci U S A, 2007. 104(18): p. 7540-5.
469. Kassauei, K., et al., Mitochondrial DNA mutations in pancreatic cancer. Int J Gastrointest Cancer, 2006. 37(2-3): p. 57-64.
470. Budowle, B., et al., Forensics and mitochondrial DNA: applications, debates, and foundations. Annu Rev Genomics Hum Genet, 2003. 4: p. 119-41.
471. Wall, P.K., et al., Comparison of next generation sequencing technologies for transcriptome characterization. BMC Genomics, 2009. 10: p. 347.
472. Metzker, M.L., Sequencing technologies - the next generation. Nat Rev Genet. 11(1): p. 31-46.
473. Hawkins, R.D., G.C. Hon, and B. Ren, Next-generation genomics: an integrative approach. Nat Rev Genet.
474. Schuster, S.C., Next-generation sequencing transforms today's biology. Nat Methods, 2008. 5(1): p. 16-8.
475. Vasta, V., et al., Next generation sequence analysis for mitochondrial disorders. Genome Med, 2009. 1(10): p. 100.
476. Castle, J.C., et al., DNA copy number, including telomeres and mitochondria, assayed using next-generation sequencing. BMC Genomics. 11: p. 244.
477. Di Donato, S., Multisystem manifestations of mitochondrial disorders. J Neurol, 2009. 256(5): p. 693-710.
478. Edmond, J.C., Mitochondrial disorders. Int Ophthalmol Clin, 2009. 49(3): p. 27-33.
479. Larsson, N.G., et al., Leber's hereditary optic neuropathy and complex I deficiency in muscle. Ann Neurol, 1991. 30(5): p. 701-8.
480. Man, P.Y., D.M. Turnbull, and P.F. Chinnery, Leber hereditary optic neuropathy. J Med Genet, 2002. 39(3): p. 162-9.
481. Brown, M.D., The enigmatic relationship between mitochondrial dysfunction and Leber's hereditary optic neuropathy. J Neurol Sci, 1999. 165(1): p. 1-5.
482. Deschauer, M., et al., Late-onset encephalopathy associated with a C11777A mutation of mitochondrial DNA. Neurology, 2003. 60(8): p. 1357-9.
483. Gray, K.A., P.L. Dutton, and F. Daldal, Requirement of histidine 217 for ubiquinone reductase activity (Qi site) in the cytochrome bc1 complex. Biochemistry, 1994. 33(3): p. 723-33.

484. Fearnley, I.M. and J.E. Walker, Conservation of sequences of subunits of mitochondrial complex I and their relationships with other proteins. Biochim Biophys Acta, 1992. 1140(2): p. 105-34.
485. Hadzsiev, K., et al., Mitochondrial DNA 11777C>A Mutation Associated Leigh Syndrome: Case Report with a Review of the Previously Described Pedigrees. Neuromolecular Med.
486. Crimi, M., et al., A missense mutation in the mitochondrial ND5 gene associated with a Leigh-MELAS overlap syndrome. Neurology, 2003. 60(11): p. 1857-61.
487. Howell, N., et al., Sequence analysis of the mitochondrial genomes from Dutch pedigrees with Leber hereditary optic neuropathy. Am J Hum Genet, 2003. 72(6): p. 1460-9.
488. Taylor, R.W., et al., Leigh disease associated with a novel mitochondrial DNA ND5 mutation. Eur J Hum Genet, 2002. 10(2): p. 141-4.
489. Sudo, A., et al., Leigh syndrome caused by mitochondrial DNA G13513A mutation: frequency and clinical features in Japan. J Hum Genet, 2004. 49(2): p. 92-6.
490. Johns, D.R., M.J. Neufeld, and R.D. Park, An ND-6 mitochondrial DNA mutation associated with Leber hereditary optic neuropathy. Biochem Biophys Res Commun, 1992. 187(3): p. 1551-7.
491. Howell, N., et al., Leber hereditary optic neuropathy: involvement of the mitochondrial ND1 gene and evidence for an intragenic suppressor mutation. Am J Hum Genet, 1991. 48(5): p. 935-42.
492. Howell, N., et al., mtDNA mutations that cause optic neuropathy: how do we know? Am J Hum Genet, 1998. 62(1): p. 196-202.
493. De Vries, D.D., et al., Genetic and biochemical impairment of mitochondrial complex I activity in a family with Leber hereditary optic neuropathy and hereditary spastic dystonia. Am J Hum Genet, 1996. 58(4): p. 703-11.
494. Jun, A.S., M.D. Brown, and D.C. Wallace, A mitochondrial DNA mutation at nucleotide pair 14459 of the NADH dehydrogenase subunit 6 gene associated with maternally inherited Leber hereditary optic neuropathy and dystonia. Proc Natl Acad Sci U S A, 1994. 91(13): p. 6206-10.
495. Bai, Y. and G. Attardi, The mtDNA-encoded ND6 subunit of mitochondrial NADH dehydrogenase is essential for the assembly of the membrane arm and the respiratory function of the enzyme. EMBO J, 1998. 17(16): p. 4848-58.

496. Chinnery, P.F., et al., A novel mitochondrial tRNA phenylalanine mutation presenting with acute rhabdomyolysis. Ann Neurol, 1997. 41(3): p. 408-10.
497. Mansergh, F.C., et al., Retinitis pigmentosa and progressive sensorineural hearing loss caused by a C12258A mutation in the mitochondrial MTTS2 gene. Am J Hum Genet, 1999. 64(4): p. 971-85.
498. Battersby, B.J., J.C. Loredo-Osti, and E.A. Shoubridge, Nuclear genetic control of mitochondrial DNA segregation. Nat Genet, 2003. 33(2): p. 183-6.
499. Schaefer, A.M., et al., Ophthalmoplegia due to mitochondrial DNA disease: the need for genetic diagnosis. Muscle Nerve, 2005. 32(1): p. 104-7.
500. van Eijsden, R.G., et al., Chip-based mtDNA mutation screening enables fast and reliable genetic diagnosis of OXPHOS patients. Genet Med, 2006. 8(10): p. 620-7.
501. Leveque, M., et al., Whole mitochondrial genome screening in maternally inherited non-syndromic hearing impairment using a microarray resequencing mitochondrial DNA chip. Eur J Hum Genet, 2007. 15(11): p. 1145-55.

List of publications arising from the work presented in this thesis

1- **Al-Dosary M**, Whittaker RG, Haughton J, McFarland R, Goodship J, Turnbull DM, Taylor RW, Neuromuscular disease presentation with three genetic defects involving two genomes. Neuromuscul Disord, 2009. 19(12): p. 841-4.

2- Tam, E., W., Feigenbaum, A., Addis, J. B., Blaser, S., Mackay, N., **Al-Dosary**,**M**., Taylor, R.W., Ackerley, C., Cameron, J. M., Robinson, B. H., A novel mitochondrial DNA mutation in COX1 leads to strokes, seizures, and lactic acidosis. Neuropediatrics, 2008. 39(6): p. 328-34.

3- Tuppen, H.A.L., Hogan, V.E., He, L., Blakely, E.L., Worgan, L., **Al-Dosary**, **M**., Saretzki, G., Alston, C.L., Morris, A.A., Clarke, M., Jones, S., Devlin, A.M., Mansour, S., Chrzanowska-Lightowlers, Z.M.A., Thorburn, D.R., McFarland, R. and Taylor, R.W. (2010) The p.M292T NDUFS2 mutation causes complex I-deficient Leigh syndrome in multiple families. Brain, 2010. 133(10): p. 2952-63.